Techno-Economic Assessment of the Need for Bulk Energy Storage in Low-Carbon Electricity Systems With a Focus on Compressed Air Storage (CAES)

Techno-economic assessment of the need for bulk energy storage in low-carbon electricity systems with a focus on compressed air storage (CAES)

A dissertation presented

by

Hossein Safaei Mohamadabadi

to

School of Engineering and Applied Sciences

in partial fulfillment of the requirements

for the degree of

Doctor of Philosophy

in the subject of

Engineering Sciences

Harvard University

Cambridge, Massachusetts

December 2014

Dissertation Advisor: David W. Keith Hossein Safaei Mohamadabadi

Techno-economic assessment of the need for bulk energy storage in low-carbon electricity systems with a focus on compressed air storage (CAES)

Abstract

Increasing electrification of the economy while decarbonizing the electricity supply is among the most effective strategies for cutting greenhouse gas (GHG) emissions in order to abate climate change. This thesis offers insights into the role of bulk energy storage (BES) systems to cut GHG emissions from the electricity sector.

Wind and solar energies can supply large volumes of low-carbon electricity. Nevertheless, large penetration of these resources poses serious reliability concerns to the grid, mainly because of their intermittency. This thesis evaluates the performance of BES systems – especially compressed air energy storage (CAES) technology – for integration of wind energy from engineering and economic aspects.

Analytical thermodynamic analysis of Distributed CAES (D-CAES) and Adiabatic CAES (A-CAES) suggest high roundtrip storage efficiencies (~80% and 70%) compared to conventional CAES (~50%). Using hydrogen to fuel CAES plants – instead of natural gas – yields a low overall efficiency (~35%), despite its negligible GHG emissions.

The techno-economic study of D-CAES shows that exporting compression heat to low-temperature loads (*e.g.* space heating) can enhance both the economic and emissions performance of compressed air storage plants. A case study for Alberta, Canada reveals that the abatement cost of replacing a conventional CAES with D-CAES plant practicing electricity arbitrage can be negative (-$40 per tCO_2e, when the heat load is 50 km away from the air storage site).

A green-field simulation finds that reducing the capital cost of BES – even drastically below current levels – does not substantially impact the cost of low-carbon electricity. At a 70% reduction in the GHG emissions intensity of the grid, gas turbines remain three times more cost-efficient in managing the wind variability

compared to BES (in the best case and with a 15-minute resolution). Wind and solar thus, do not need to wait for availability of cheap BES systems to cost-effectively decarbonize the grid. The prospects of A-CAES seem to be stronger compared to other BES systems due to its low energy-specific capital cost.

Table of contents

List of figures

List of tables

List of symbols

$A\text{-}CAES$	Adiabatic compressed air energy storage
ac	Approach temperature of heat exchanger
BC	Blended cost of capital (%)
BES	Bulk energy storage
BL	Boiler of the district heating system
$boil$	Boiling conditions of water
BOP	Balance of plant equipments
$CAES$	Compressed air energy storage
$CAES\text{-}HTE$	Compressed air energy storage paired with a high-temperature electrolyzer
$CAES\text{-}LTE$	Compressed air energy storage paired with a low-temperature electrolyzer
$CapEx$	Specific capital cost ($/unit capacity)
$Capt$	Capacity (size) of each component (MW or MWh)
CC	Combustor
$CCGT$	Combined cycle gas turbine
Ch	Charge process
CL	Intercooler and aftercooler of compressor
C_{Lnt}	Latent heat of evaporation (kJ/kg)
CM	Compressor
CN	Cavern for air storage
$cold$	Cold stream of heat exchanger
C_P, C_v	Specific heat at constant pressure and volume ($\frac{\text{kJ}}{\text{kg}\times\text{K}}$)
CR	Compression ratio
CSP	Concentrated solar power
ct	Fuel credit gained by D-CAES
D	Diameter of pipeline (mm)
$D\text{-}CAES$	Distributed compressed air energy storage
dch	Discharge process
DH	District heating system
dn	Downstream of pipeline
DZC	Dispatchable-zero-carbon generator
E	Voltage applied to electrolyzer (volts)

EL	Electric load or electricity generated or consumed (MWh)
els	Efficiency of electrolyzer (%)
em	State of depleted cavern
et	Exhaust stream of the storage plant
f	Friction factor of pipeline
F	Flow rate of pipeline at standard conditions (m^3/day)
$feul$	Fuel used by storage plant
FHX	Heat exchanger located at exhaust of the plant
fl	State of full cavern
FOM	Fixed operations and maintenance cost ($/yr/capacity)
G	Gibbs free energy (kJ)
GI	GHG emissions intensity of plant ($kgCO_2e$/MWh)
GIF	GHG emissions intensity of fuel ($kgCO_2e$/GJ)
h	Specific enthalpy (kJ/kg)
Δh_f^0	Standard enthalpy of formation (kJ/kg)
HC	Heat recovery unit of D-CAES
HHV	High heating value (kJ/kg)
HL	Heat load (MWh thermal)
hot	Hot stream of heat exchanger
HP	High-pressure equipment
HR	Heat rate (GJ/MWh)
HTE	High temperature electrolysis of steam
I	Electric current of electrolyzer (Amps)
$I\text{-}CAES$	Isentropic compressed air energy storage
in	Inlet conditions
inl	Initial conditions of cavern
IP	Intermediate-pressure equipment
ist	Isentropic process
IX	Exergy loss (kJ)
L	Length of pipeline (km)
$LCOE$	Levelized cost of electricity ($/MWh)
LHV	Lower heating value (kJ/kg)
LP	Low-pressure equipment

LTE	Low-temperature electrolysis of water
m	Mass of air or fuel (kg)
M	Molar mass (kg/kMole)
$Marg$	Marginal capital cost ($/MWh or $/MW)
n	Molar coefficient
NaS	Sodium sulfur battery
net	Performance parameters of D-CAES once fuel credits are taken into account
NG	Natural gas
out	Outlet conditions
P	Pressure (kPa)
$Pb\text{-}A$	Lead acid battery
PHS	Pumped hydroelectric storage
PP	Pipeline of D-CAES
Q	Thermal energy (kJ)
R	Ideal gas constant ($\frac{\text{kJ}}{\text{kg}\times\text{K}}$)
raw	Performance parameters of D-CAES before fuel credits are included
RP	Recuperator
s	Specific entropy ($\frac{\text{kJ}}{\text{kg}\times\text{K}}$)
s^0	Standard entropy ($\frac{\text{kJ}}{\text{kg}\times\text{K}}$)
S	Entropy (kJ)
$SCGT$	Simple cycle gas turbine
sns	Sensible heat (kJ/kg)
SMR	Small modular nuclear reactor
ST	Electricity stored (MWh)
$stage$	Number of stages of compressor/ turbine
T	Temperature (K)
Tax	Emissions tax ($/t$CO_2$e)
TB	Turbine, expander
TS	Thermal energy storage unit
u	Specific internal energy (kJ/kg)
U	Internal energy (kJ)
UF	Utilization factor of compression heat (% of available heat)

up	Upstream of pipeline
V	Volume of air storage (m3)
VOM	Variable operations and maintenance cost ($/MWh)
VRB	Vanadium redox battery
W	Work (kJ)
WR	Work ratio of storage plant
x	Specific exergy (kJ/kg)
X	Exergy (kJ)
X_E	Energy-specific capital cost of storage plant ($/kWh)
XR	Expansion ratio of turbine
X_P	Power-specific capital cost of storage plant ($/kW)
$X\rho$	Exergy density of cavern (kWh/m^3)
$ZnBr$	Zinc bromine battery
π	Price of fuel ($/GJ) or electricity ($/MWh)
γ	Specific heat ratio of air
η	Efficiency (%)
ψ	Exergy of air stream (kJ/kg)
0	Standard conditions

Simply to my parents, Baba and Maman

Acknowledgements

I am grateful to many individuals for being with and supporting me through the long, mostly fun, sometimes frustrating, but rewarding journey of graduate school!

I am deeply thankful to my adviser, David Keith. Thank you David for setting a fantastic example for how to use academic excellence and freedom to spot and tackle energy and environment problems that really matter in making the world a better place. I could always count on your support and advice, even for going on a geology fieldtrip in the Canadian Rockies or attending an energy-policy summer school in Azerbaijan. And thank you for continuously pushing, challenging, and dazzling me, and taking a chance on me at the first place.

Additionally, I would like to thank my academic committee members Jay Apt, Michael Aziz, and Chad Vecitis for their interest in and time for my research. I was privileged to learn from world-class scholars both at Harvard University and University of Calgary. Michael Aziz, Dan Schrag, Meghan O'Sullivan, John Shaw, and Hamid Zareipour particularly contributed to my intellectual growth as a practical researcher who is passionate about abating climate change. I especially thank Ronald Hugo for serving as my co-supervisor during my tenure at the University of Calgary.

I am grateful to the staff of HUCE, ISEEE, SEAS, Carbon Engineering Ltd., and ARC Financial Corp. for their support and resources. I am extremely thankful to Hollie Roberts, whose care and smiles never ended, who kept (or tried very hard to keep) David's door open to me, and who always found a solution – no matter how complicated Hossein's situation was (factor of H!).

My academic friends, thank you all for sharing the burden and joy of graduate school with me. Ashley Mercer, Geoff Holmes, Hanieh Mohammadi, Farhad Javid, Hamid Shaker, Pedram Hassanzadeh, Ganesh Doluweera, Matt Ceh, Daniel Thorpe, Katie Dagon, Lauren Kuntz and too many others to name here, I have been very lucky to have each of you with me on this journey.

It goes without saying that I could not have preserved 24 years of schooling without the unconditional and enormous love, excitement, and encouragement of my parents. My brothers, Ali and Mohsen, thank you for

giving me the peace of mind that mom and dad were in solid hands while I was thousands of miles away from home.

And my last gratitude is reserved for you, Samaneh. My graduate school started with you and you always let me follow my dreams, no matter how crazy they seemed or turned out to be. I am forever grateful for all the love, care, aspiration, and memories.

And thank you God too, for the countless opportunities and occasional sharp turns and bumps here and there in life.

Funding Acknowledgement

My PhD education became possible through a generous scholarship from the Natural Sciences and Engineering Research Council of Canada (NSERC). My studies were also supported by the Harvard University Center for Environment (HUCE), and Harvard School of Engineering and Applied Sciences (SEAS).

Chapter 1: Introduction

Decarbonizing the electricity supply is a "key component of cost-effective mitigation strategies [for] … stabilization of greenhouse gas concentrations in the atmosphere at a level that would prevent dangerous anthropogenic interference with the climate system (430–530 ppm CO_2e in 2100)", according to the Fifth Assessment Report of the Intergovernmental Panel on Climate Change (IPCC) [1]. The importance of the electricity sector in the climate change discussion is due to its large share of anthropogenic greenhouse (GHG) emissions. In the United States for instance, this sector was responsible for ~32% of the total, or ~40% of the energy-related emissions in 2012 [2]. The Fifth Assessment Report of IPCC calls for an 80% market share for low-carbon electricity technologies (*i.e.* renewables, nuclear, and carbon capture and sequestration) by 2050. This 2.7 fold increase requires global determination and collaboration to urgently transform the electricity sector.

The purpose of this dissertation is to examine the role of bulk energy storage (BES) technologies, especially compressed air energy storage (CAES), from engineering and economic perspectives for managing the intermittency of wind-based electricity, with the ultimate goal of reducing GHG emissions from the electricity supply.

Various policy measures have been proposed to decarbonize the electricity sector due to its substantial GHG emissions and relatively low abatement costs. The Clean Power Plan, proposed by the United States Environmental Protection Agency (EPA) in June 2014, is the newest and most ambitious effort of the federal government to cut the CO_2 emissions from power plants. This EPA proposal provides a mix of four strategies (building blocks) to different states in order to meet their emissions reduction targets for the 2020-30 period. It is estimated that the proposed EPA regulation will reduce the carbon emissions from the United State's electricity sector by ~30% from the 2005 levels by the year 2030 [3].

Wide use of renewable energies (in conjunction with nuclear) is among the four building blocks of the Clean Power Plan. Over the past few decades, there has been a massive growth in renewable-based electricity, both in the United States and around the globe. The Renewable Portfolio Standards (RPS), which are currently in place in 29 states and the District of Columbia, and the federal Production Tax Credit (PCT) program have been key to fostering renewables in the United States.

Low capital costs, widespread resources, small land footprint, and negligible emissions are among the important factors that have made wind energy an attractive renewable source for electricity generation. Wind currently accounts for 2.5% of global electricity production (second to hydro in the renewables category). The International Energy Agency (IEA) calls for a boost in the market share of wind to 15-18% by 2050 to limit the global mean temperature increase to 2 °C. This scenario translates to a global cumulative wind capacity of ~2300 GW, compared to only ~319 GW in 2013 [4].

The need for such high penetrations of wind, an intermittent and uncertain resource, can undermine the resilience of the electric power grid. Currently, the variability in the output of renewables is mostly managed by flexible gas turbines. Deep decarbonization mandates will necessitate the limitation of such fossil-fuel based solutions. Various storage technologies, such as electrochemical batteries and molten salt heat storage, have been under development as pathways to support integration of intermittent renewables without substantial GHG emissions. Electricity storage systems can also limit the curtailment of wind and solar, lower the need for transmission buildup, and reduce cycling of baseload plants and dispatching of peaking fossil fuel plants [5].

Technologies for bulk electricity storage (BES), on the order of 10s of MW-hours, are of particular interest for integration of wind at grid-scale. This is because strong fluctuations in the power output of wind farms – even in the case of interconnected farms – occur over long time scales (on the order of hours to days) [6, 7]. Low energy-to-power capacity ratios and high capital costs disfavor most existing storage systems for bulk storage applications. Compressed air energy storage is a relatively mature technology with attractive economics compared to other BES systems that can potentially support integration of wind at scale [8-10]. Nevertheless, prospect of the conventional CAES technology may be poor if the grid is to be deeply decarbonized. This is due to the need of conventional CAES to combust a heating fuel (often natural gas) in order to heat the compressed air prior to expansion and power generation. Heating the air prevents freezing of the moisture present in the compressed air, which can damage the turbomachinery. Fuel combustion also boosts the work output of the air storage facility in contrast to solely harnessing the mechanical energy stored in the compressed air. A means to reduce or even eliminate the natural gas demand of CAES is recovering and

utilizing the compression heat generated during the air storage phase. This heat is rejected to the ambient environment in the conventional CAES configuration because of its low temperature.

This thesis offers a series of engineering and economic analyses to assess the need for and the competitiveness of bulk storage of electricity to manage the intermittency of wind in low-carbon electricity systems. Chapters 2 through 4 focus on comparisons between selected advanced CAES designs that can potentially achieve a lower GHG emissions intensity and the conventional CAES system. Chapter 5 broadens the scope of the analysis and examines the cost-competitiveness of BES technologies in general, as well as in comparison to selected other decarbonization pathways such as gas turbines and nuclear. This dissertation is a compilation of four papers, three of which are published and one is under the peer-review process. Each chapter is based on one of the papers and begins with a preface, which serves two primary functions: (1) contextualize the chapter within the thesis; and (2) clarifies the key assumptions and resolves inconsistencies between papers as they developed over the course of study.

Chapter 2 assesses the thermodynamics of three strategies, which utilize the heat of air compression to lower/eliminate the natural gas demand of the compressed air storage plants. An analytical model is developed to quantify key figures of merit such as roundtrip exergy efficiency and GHG emissions intensity of these advanced CAES systems and to compare them with the conventional CAES design.

Export of the low-temperature heat of compression to supply an external load (*e.g.* space heating) is the core of Distributed CAES (D-CAES) system, the first advanced design analyzed in Chapter 2. The D-CAES facility is credited for the negated consumption of heating fuel to meet the external load; hence, the net (apparent) fuel consumption of D-CAES is lower than of the mainstream CAES.

The heat of compression can alternatively be stored and utilized to heat the compressed air itself during the discharge process provided that temperature of the stored heat is high enough (*e.g.* 600 °C). Increasing the operating pressure of the compressors and limited or no use of intercooling (*i.e.* adiabatic compression) is the primary method for achieving such high temperatures.

Physical storage of the high-temperature heat of compression is the core of the Adiabatic CAES (A-CAES) concept, the second low-carbon compressed air storage technology investigated in Chapter 2. Chemical

storage of the compression heat in the form of hydrogen and combustion of hydrogen later during the discharge phase is the third strategy analyzed in Chapter 2. Hydrogen can be produced via electrolysis at high temperatures (CAES-HTE) or at ambient (low) temperatures (CAES-LTE). The CAES-HTE concept relies on the fact that electricity demand of electrolysis decreases as the temperature of the reaction is raised. Therefore, utilizing the high-temperature heat of compression can reduce the electricity intensity of hydrogen production. These savings are achieved at the expense of higher electricity demand of the air compressors of the CAES-HTE plant, which now operate at higher pressures with limited or no cooling. The CAES-LTE concept is, however, comparable to the conventional CAES system (diabatic compression). The hydrogen produced by a low-temperature electrolyzer fuels the combustor of CAES-LTE, instead of natural gas in the conventional CAES configuration though. Chapter 2 finds that the D-CAES and A-CAES systems have a higher theoretical roundtrip efficiency (~80% and ~70%, respectively) compared to the conventional CAES (~50%), CAES-HTE (~35%), and CAES-LTE (~35%) designs.

Chapter 3 focuses on GHG emissions and economic performance of D-CAES and evaluates its competitiveness with the conventional CAES and gas turbines to manage intermittency of wind at a systems level. On one hand, the D-CAES concept is more capital intensive compared to conventional CAES, primarily due to the need for a pipeline to transport the compressed air from the generation to the storage site. The compressor of D-CAES is relocated from the storage site (the case for conventional CAES) to the heating load site. On the other hand, the sales of the otherwise-wasted heat of compression bring in revenues for D-CAES, especially under emissions constraints.

The trade-off between higher capital cost, higher revenues, and lower emissions of D-CAES in comparison to conventional CAES is evaluated in Chapter 3 from a systems-level point of view. A green-field analysis is performed in which the size and hourly operations of a hypothetical generation portfolio are optimized to meet a variable load at the minimum total cost. Wind, gas turbines (simple and combined cycle), and either conventional CAES or D-CAES compete for market share of electricity supply while a variable carbon tax is enforced. Results of the analysis suggest that gas turbines manage the intermittency of wind more cost-effectively compared to both CAES and D-CAES below a carbon tax of \$40/tCO_2e (with a gas price of \$5/GJ, a 50 km pipeline, and with the specific wind profiles and electricity and heat loads used in Chapter 3). D-CAES

however, turns out to be more attractive than conventional CAES from both economic and emissions perspectives at higher emissions taxes.

While Chapter 3 assesses the performance D-CAES at a systems level, Chapter 4 investigates a market niche for stand-alone D-CAES plants: performing energy arbitrage in deregulated electricity markets. Chapter 4 addresses two key questions with respect to D-CAES:

1. Can D-CAES be economically superior to conventional CAES for the arbitrage application? And what might be the effects of market conditions (price of electricity and gas) on its performance?
2. How realistic it might be to site a suitable geologic formation in the vicinity of a large, concentrated heating load, which is the inherent requirement of D-CAES in the real world?

The economic attractiveness of merchant D-CAES plants can stimulate research and development (R&D) efforts to prove the concept and improve its effectiveness for wind integration.

Chapter 4 evaluates the economics and GHG emissions of two hypothetical D-CAES and conventional CAES facilities performing electricity arbitrage in the Alberta (Canada) wholesales market. Ten years of historical data for the price of electricity and natural gas are used to analyze the effects of market conditions. In addition, a geological screening of the gas reservoirs within a 100 km radius of the major cities in Alberta is presented to inform the question regarding the likelihood of finding an appropriate geologic formation for air storage and the most binding geological constraints.

The analyses carried out in Chapters 2 through 4 suggest that the D-CAES concept could be both economically and environmentally preferable compared to the conventional CAES design. The core requirement of D-CAES for a suitable geologic formation in close proximity of a large heating load would, however, prevents D-CAES from acting as a scalable technology to support wind integration.

Chapter 5 attempts the fundamental question of how cost-efficient bulk storage technologies are in general to support integration of intermittent renewables (especially wind) and to deeply decarbonize the electricity supply. It also examines the cost-competitiveness of specific bulk storage technologies in this context, both at their current costs and with drastic cost reductions.

The impacts of the capital cost of BES systems on the total cost of electricity supply and on the optimal penetration level of wind are evaluated in Chapter 5. A green-field approach is used to meet a variable electric load at the minimum total cost in a carbon-constraint world. A generation fleet made up of wind, gas turbine (simple and combined cycles), bulk storage, and a generic dispatchable-zero-carbon technology (*e.g.* biomass, nuclear) is sized and dispatched in this simulation. The GHG emissions intensity of the fleet is the key constraint, which is systematically reduced from the "business as usual" scenario (no emissions limit) to a carbon-free case. The primary variables are the specific-energy ($/kWh) and specific-power ($/kW) capital cost of the bulk storage system. Parametric modeling, rather than adopting point estimates for the cost of storage, enables studying the effects of reducing the power- and energy-specific costs of various BES technologies. These parameters are varied significantly to investigate how drastic reductions in the cost of BES technologies might impact the final assessment. The simulation reveals cost-effectiveness of the A-CAES and pumped hydro storage (PHS) technologies for wind integration and bulk storage applications, compared to electrochemical batteries. The economics of conventional CAES turn out to be very poor due to its non-negligible GHG emissions, despite the fact that it has one of the lowest capital cost figures among the BES technologies analyzed.

Taken as a whole, this PhD dissertation uses a series of engineering and economic analyses to shed light on the need for bulk storage technologies to integrate wind energy at scale and substantially curb the emissions from the electricity sector. It also provides solutions to improve the emissions performance of compressed air storage technologies to become a more effective tool in our carbon mitigation toolbox. The results and conclusions of this thesis can inform R&D efforts as well as energy policy debates on the relative importance of various bulk storage systems for the cost-effective management of wind and solar intermittency.

Chapter 2: Thermodynamic analysis of four compressed air energy storage designs: Conventional CAES, D-CAES, A-CAES, and CAES-HTE[1]

[1] A condensed version of the thermodynamic analysis of conventional CAES and D-CAES described here is published as: Safaei, H. and M. J. Aziz. Thermodynamic analysis of a compressed air energy storage facility

Preface

This chapter presents thermodynamic analysis of selected compressed air energy storage systems that have lower greenhouse gas emissions compared to the conventional CAES design. This analytical study quantifies several figures of merit of the conventional CAES, distributed CAES (D-CAES), adiabatic CAES (A-CAES), and CAES fueled by hydrogen produced via electrolysis (CAES-HTE and CAES-LTE systems).

Although it is currently among the cheapest and most mature technologies for storage of electricity at utility scales, prospect of conventional CAES may be poor in low-carbon electricity systems. This shortcoming is due to the need of conventional CAES technology to combust natural gas during its discharge process (at levels of 4 GJ/MWh, which leads to emissions intensities of ~260 $kgCO_2e$/MWh). Several "greener" compressed air storage designs have been proposed to reduce the fossil fuel dependence of this technology in order to increase its environmental and economic competitiveness for decarbonizing the electricity supply.

While the next three chapters mainly concentrate on the economics of bulk energy storage systems, this chapter is solely concerned with the thermodynamic performance of selected low-carbon compressed air storage concepts. The systems analyzed include:

- *Conventional CAES:* This is the basic (mainstream) CAES design and is modeled to benchmark the performance of the advanced CAES systems. The heat of compression is dissipated to the ambient environment during the charging period in the conventional CAES. The plant relies on combustion of fossil fuels (often natural gas) to heat the expanding air during the discharge phase.
- *Distributed CAES (D-CAES):* A new design, which has lower net (apparent) fuel consumption than the conventional CAES system. The otherwise-wasted heat of compression is utilized for district heating applications. The D-CAES plant is credited for the negated consumption of heating fuel in the district heating system, hence, the net emissions intensity of D-CAES is lower than of conventional CAES.
- *Adiabatic CAES (A-CAES):* The high-temperature heat of compression is physically stored onsite to heat the expanding air during the power generation phase in this zero-carbon CAES design. The need for fuel combustion is, therefore, eliminated.

- *CAES fueled by hydrogen generated onsite via electrolysis of steam at high temperatures (CAES-HTE):* Hydrogen can fuel the combustor of compressed air storage plants (instead of natural gas in the conventional CAES) to eliminate GHG emissions of the storage facility. In the CAES-HTE configuration, the high-temperature heat of compression is fed into an electrolyzer along with electricity to produce and store hydrogen at the same time as the compressed air production. CAES-HTE has negligible GHG emissions similar to A-CAES, in contrast to conventional CAES and D-CAES. A simpler version of the hydrogen-fueled CAES system can include generating hydrogen via electrolysis of water (instead of steam in the CAES-HTE system) at the ambient temperature (*i.e.* low-temperature electrolysis, LTE). Thermodynamics of this system are also studied. CAES-LTE has a higher electricity demand for the electrolysis process but lower compression requirements compared to CAES-HTE.

The key parameters of interest – from a thermodynamic point-of-view – are the roundtrip exergy efficiency, work ratio, heat rate, GHG emissions intensity, and exergy density of the storage plant. Quantifying these parameters is integral for any comprehensive techno-economic study assessing the potential and importance of various compressed air storage technologies, as possible building blocks of prospective low-carbon grids.

The thermodynamic modeling of CAES systems is presented in two sections. Section 3 of this chapter compares the D-CAES with conventional CAES. This is because D-CAES is a minor variation of conventional CAES and both systems have fossil fuel dependence and non-negligible GHG emissions. Section 4 of this chapter focuses on the zero-carbon configurations, *i.e.* A-CAES, CAES-HTE, and CAES-LTE.

The analytical study presented in this chapter can provide the foundation for and inform a more thorough assessment of various CAES designs in future. Treating compressed air as an ideal gas with temperature-independent specific heat is a shortcoming of the analysis undertaken. Additionally, heat transfer in the air storage, in the thermal storage units (applicable to A-CAES and D-CAES), and along the pipeline (for D-CAES) are not modeled. These simplifications overestimate the thermodynamic performance of compressed air energy storage systems. Using more complex analytical models or simulation software products can improve the robustness of the results regarding the engineering performance of low-carbon CAES systems.

1- Introduction

The compressed air energy storage (CAES) technology rests on storing electricity in the form of the potential energy of compressed air. As shown in Figure 1, electricity is purchased from the grid during the charging phase to run the compressor of CAES. Compressed air is stored for later use – often in an underground cavern to keep the costs low. During the discharge phase, compressed air is withdrawn, combusted with a fuel, and expanded in a turbine (expander) to generate electricity. A CAES facility is very similar to a simple cycle gas turbine (SCGT) with the difference that its compressor is powered by electricity, instead of by the expander in SCGT. Additionally, the compression and expansion processes are decoupled in time in the CAES system while they occur simultaneously in gas turbines. A generic CAES plant may use ~4.2 GJ of natural gas during the discharge phase and ~0.75 MWh of electricity during the charge phase to generate 1 MWh of electricity [9]. This is while a generic SCGT consumes ~10 GJ of natural gas to generate 1 MWh of electricity (assuming an efficiency of 36%). There are currently two commercial CAES plants in operation (Huntorf facility in Germany and McIntosh plant in the USA). More details on the history of the CAES technology is given in Chapter 3.

A major disadvantage of the conventional CAES concept, especially if to be used in the prospective low-carbon grids, is its fuel demand. Fuel combustion increases the power output of the plant, which would be prohibitively low if the storage facility solely harnessed the mechanical energy stored in the compressed air[2]. The compression heat is rejected to the ambient environment in the conventional CAES design, which results in the need to combust fuel and heat up the compressed air prior to expansion (see Figure 1). Moreover, heating of the compressed air is required to prevent freezing of its moisture content during expansion, which can damage the turbine.

[2] As a case in point, compressed air expanding from 25 °C and 7 MPa releases ~600 kJ of work per kg of air, assuming an isentropic efficiency of 85%. The work output, however, increases ~3.6 times (to 2170 kJ/kg) if air expands from 800 °C instead of 25 °C.

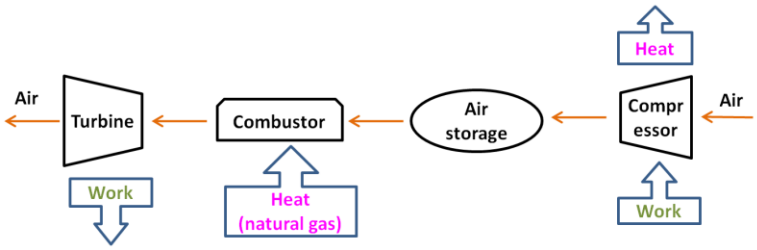

Figure 1: Schematic of a simplified conventional CAES system. Compressor work is supplied by the electricity grid during the charging phase. Natural gas fuels the combustor during the discharging period. The conventional CAES consumes both electricity and heating fuel.

Several variations of compressed air storage have been proposed aiming to reduce its fuel demand. Two main categories are Adiabatic CAES (A-CAES) and Isothermal CAES (I-CAES). A-CAES focuses on physical storage of the compression heat during the charge phase in order to replace fuel combustion during the expansion period and to eliminate direct (*i.e.* inside-the-fence line) GHG emissions. A-CAES needs to compress air to higher pressures compared to the conventional CAES design to generate adequate quantities of heat at high-enough temperatures to fully eliminate the need for fuel combustion. Generating and handling compressed air at such high pressures and temperatures cause various technical challenges. Although A-CAES is still in the R&D phase, it can potentially become an attractive storage technology in carbon-constrained grids. This is due to its zero GHG emissions, moderate roundtrip exergy efficiency (<75% [11-13]), and moderate economics (power-specific and energy-specific capital cost of 1100-1700 $/kW and 10-50 $/kWh, see chapter 5). Figure 2 illustrates a simplified schematic of A-CAES.

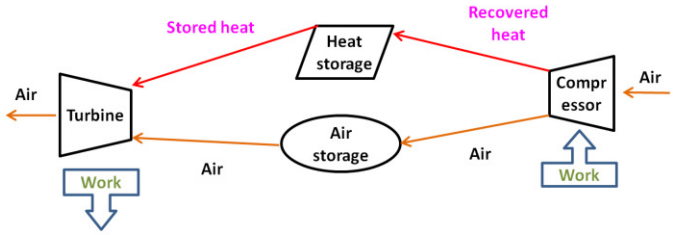

Figure 2: Schematic of a simplified Adiabatic CAES (A-CAES) system. Compression heat is physically stored during the charge phase to later heat the expanding air. Utilization of the compression heat eliminates the need for burning fuel during the discharge phase.

In the Isothermal CAES (I-CAES) design, however, air is compressed and expanded in quasi-isothermal processes (see Figure 3). Theoretically, an isothermal expansion process requires no fuel as long as the

system remains in thermal equilibrium with its surrounding. Additionally, an isothermal compression requires the least theoretical work to compress air. Maintaining thermal equilibrium with the surroundings is nonetheless, impractical at industrial scales as it requires very slow compression and expansion processes (*i.e.* low power rating) or unrealistically large heat transferring surfaces. General Compression Inc., a Massachusetts-based company, is developing this technology for a 10 MW pilot I-CAES facility. Although very little data is publically available, they claim a maximum roundtrip exergy efficiency of ~80% for their "nearly" isothermal technology [14].

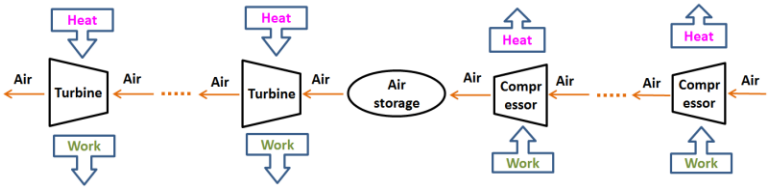

Figure 3: Simplified schematic of Isothermal CAES (I-CAES) system. The compression and expansion processes occur over several stages to maintain a quasi-thermal equilibrium with the ambient environment.

This chapter introduces the concept and assesses the thermodynamics of two newer families of the CAES technology, which can help with reducing the fuel consumption of the compressed air energy storage plants. Thermodynamics of conventional CAES and A-CAES are also assessed here to benchmark the performance of the two proposed advanced CAES concepts.

The first new compressed air storage design analyzed here is Distributed CAES (D-CAES). The otherwise-wasted heat of compression is exported to supply an external low-temperature heating load and gain fuel credits for the compressed air storage facility (see Figure 4). Therefore, the net (apparent) fuel demand of D-CAES (*i.e.* once heating fuel credits from the export of compression heat are accounted for) is lower than of conventional CAES. The presence of a large, concentrated heating load in the vicinity of suitable air storage is essential to the viability of D-CAES in the real world.

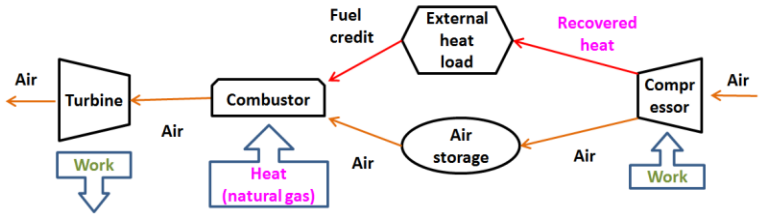

Figure 4: Schematic of a simplified distributed CAES system (D-CAES). Compression heat supplies an external heating load to gain fuel credits equal to the saved heating fuel.

The second new compressed air storage concept studied is CAES fueled by hydrogen produced onsite via electrolysis of steam at high temperatures (called CAES-HTE, see Figure 5). Such a system does not consume any fossil fuel, hence has no GHG emissions. During the charge phase, electricity powers its compressors to charge the air storage and produce high-temperature heat, similar to A-CAES. The compression heat along with electricity and water are supplied to an electrolyzer to produce hydrogen at high temperatures (above 500 °C) from steam. Hydrogen is stored onsite to fuel the combustors and heat the expanding air. The advantage of CAES-HTE compared to A-CAES is elimination of the high-pressure and high-temperature thermal storage system and the associated heat losses. The downsides, however, include the need for a high-temperature electrolyzer, hydrogen store, and hydrogen-compatible combustor.

This chapter also presents the modeling results for a simpler version of CAES fueled by hydrogen. The primary difference of the low-temperature electrolysis design (CAES-LTE) with CAES-HTE is that the electrolysis process occurs at the low (ambient) temperatures; hence the need for handling high pressures and temperatures is eliminated in CAES-LTE. Reducing the temperature of the electrolyzer increases its electricity consumption, though. The rationale for modeling CAES-LTE is to study the effects of increasing the electrolysis temperature on the overall thermodynamic performance of the compressed air storage plant.

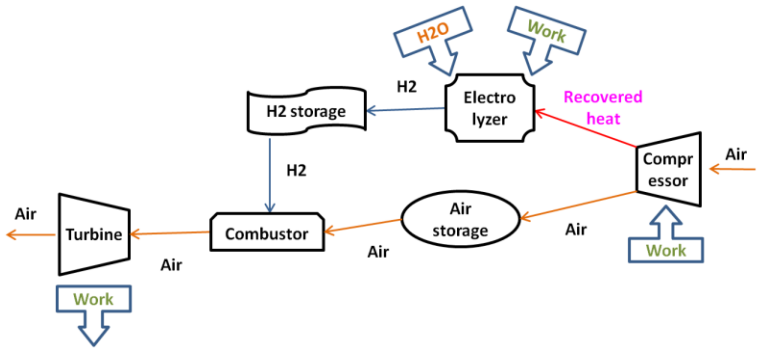

Figure 5: Simplified schematic of CAES coupled with high-temperature electrolyzer (CAES-HTE). Electricity powers both the compressor and electrolyzer. Compressed air and hydrogen are generated and stored during the charge phase. Hydrogen fuels the combustor to heat the expanding air during the discharge phase.

This chapter is composed of three primary parts. Section 2 explains the general methodology and modeling assumptions applied to perform the analytical analysis. Section 3 provides details of the thermodynamic model synthesized to compare the performance of D-CAES with conventional CAES. Section 4 presents the thermodynamic analysis of A-CAES and CAES-HTE (as well as CAES-LTE). The scope of this chapter does not include any economic analysis. The goal is providing a first order analytical estimate of the roundtrip exergy efficiency and other thermodynamic parameters of interest for conventional CAES, D-CAES, A-CAES, and CAES-HTE designs.

2- Methods

The thermodynamics of conventional CAES and A-CAES have been extensively studied in the literature (for example see [12, 15-21]), nevertheless D-CAES and CAES-HTE are new concepts. The primary reason that the conventional CAES and A-CAES systems are modeled here as well is to make a "like-for-like" comparison with D-CAES and CAES-HTE (*i.e.* using similar assumptions and inputs).

An analytical model is presented in this chapter to quantify and compare the thermodynamic performance of the studied compressed air storage systems (*i.e.* conventional CAES, D-CAES, A-CAES, CAES-HTE, and CAES-LTE). The general strategy here is applying the First and Second Laws of thermodynamics to individual system components using the ideal gas approximation for air in order to quantify the mass, energy and exergy flows into and out of the storage facility.

The energy storage literature commonly uses roundtrip efficiency in order to compare the performance of various technologies. This parameter quantifies the electrical energy delivered per unit of electrical energy taken in. Compressed air energy storage systems use both electrical energy (to power the compressor and possibly the electrolyzer) and heating energy (to fuel air combustion) though. Consequently, three key metrics are used in this chapter to fully express the thermodynamics performance of various CAES systems: heat rate, work ratio, and roundtrip exergy efficiency. Heat rate quantifies the heating fuel consumed per unit of electricity generated. This parameter becomes particularly important when the GHG emissions are constrained. This chapter reports heat rate in GJ (lower heating value, LHV) per MWh of electricity generated. Neither A-CAES, CAES-HTE, nor CAES-LTE uses an external fuel therefore; their heat rate and inside-the-fence emissions are zero.

Work ratio expresses the electrical energy consumed by the compressor (and electrolyzer of CAES-HTE and CAES-LTE) per unit of electrical energy generated by the expander. Work ratio is particularly important when the charging electricity is constrained or carbon-intensive.

Roundtrip exergy efficiency combines heat rate and work ratio and characterizes the exergy losses incurred over the full charge and discharge processes. This parameter is the ratio of the exergy delivered (expansion work) to the net exergy provided to the plant. The net exergy used by the plant is the summation of the compression work, the exergy of fuel burned in the combustors (applicable to conventional CAES and D-CAES), and electricity consumed by the electrolyzer (applicable to CAES-HTE and CAES-LTE), minus the exergy credits from sales of waste heat (applicable to D-CAES).

Exergy density of the storage plant is another key variable of interest. One of the critiques against adoption of compressed air storage technologies at scale is the low exergy density of compressed air, especially if no heating fuel is burned to boost the work output of the storage facility (the case for A-CAES). Exergy density is defined as the ratio of the delivered exergy (*i.e.* expansion work) to the volume of the cavern, and is expressed in kWh/m^3. Exergy density is especially important when availability of the storage medium is limited.

This chapter defines GHG emissions intensity of the storage plant as ratio of the GHG emissions of the fuel used by the plant to the work generated by the expander. This parameter has units of $kgCO_2e/MWh$ and only

embraces "inside the fence line" emissions[3]. The GHG emissions intensity of the electricity used to charge the storage plant is not included, unless stated otherwise.

The general assumptions and simplifications used in the thermodynamic analysis are listed below. More specific assumptions are introduced later to model specific systems.

One complete charge and discharge cycle is analyzed, without part-load operation. Air is modeled as an ideal gas with temperature-independent thermodynamic properties. The mass of fuel is assumed negligible compared to air and the mixture of air and fuel is treated as pure air. Equation 1 to Equation 5 list the general ideal gas formulae applied to model air. The ambient environment (subscript 0) is at standard conditions ($P_0 = 101$ kPa, $T_0 = 298$ K). This condition is also the reference state for internal energy, enthalpy, entropy, and exergy calculations.

$m_{air,CN} = \frac{P_{CN} \times V_{CN}}{R_{air} \times T_{CN}}$	Mass of air in cavern	Equation 1
$h = C_{p,air} \times (T - T_0)$	Specific enthalpy of air	Equation 2
$u = \left(C_{v,air} \times T\right) - (C_{p,air} \times T_0)$	Specific internal energy of air	Equation 3
$s = C_{p,air} \times ln\left(\frac{T}{T_0}\right) - R_{air} \times ln\left(\frac{P}{P_0}\right)$	Specific entropy of air	Equation 4
$\psi = (h - h_0) - T_0 \times (s - s_0)$	Specific stream exergy of air	Equation 5

The cavern has a fixed volume and its pressure varies between the minimum pressure of P_{em} and maximum pressure of P_{fl}. In order to maintain its mechanical integrity and to ensure high enough flow rates of withdrawn air, the cavern is not fully depleted. The air mass remaining in the storage at the end of the discharge phase when all the "working air" has been withdrawn to generate electricity is called the "cushion air".

[3] An alternative approach would be dividing GHG emissions associated with fuel used by the storage plant by the net electricity output of the plant, *i.e.* $\frac{HR \times GIF_{NG}}{1 - WR}$.

The cavern and thermal storage units are assumed adiabatic while the pipeline of D-CAES is modeled to be isothermal with the ambient. Raju *et al.* [15], Steta [22], and Xia *et al.* [23] studied heat transfer between the stored air and the cavern wall, which is not in the scope of the present work.

Coolers of the compressors are assumed to have a fixed approach temperature, defined as the difference between temperature of the hot stream leaving the heat exchanger and temperature of the cooling fluid entering: $T_{ac} = T_{out,hot}^{CL} - T_{in,cold}^{CL}$ (see Figure 6). This assumption implies the inlet temperature of the cavern and the output of all the compressor's coolers are fixed through the charging process (Equation 6).

$$T_{in}^{CN} = T_{out,hot}^{CL} = T_{ac} + T_{in,cold}^{CL} = T_{ac} + T_0 \qquad \text{Inlet temperature of cavern} \qquad \text{Equation 6}$$

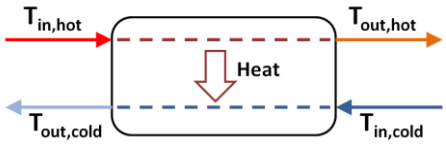

Figure 6: Schematic of the compressor cooler. The hot stream is the exhaust of the preceding compression stage and inlet of the following stage (or the cavern). The cold stream represents an external cooling fluid taking the heat out of the system. The approach temperature is defined as: $T_{ac} = T_{out,hot} - T_{in,cold}$. The cooling fluid is at the ambient temperature ($T_{in,cold} = T_0$).

The discharge temperature of the combustion chambers is maintained at a fixed value (through controlling fuel combustion). The expander (turbine) has two stages; high- (HP) and low-pressure (LP) stages have equal but variable expansion ratios to match the instantaneous cavern pressure (Equation 7).

$$XR_{HP} = XR_{LP} = \sqrt{\frac{P_0}{P_{CN}}} = \sqrt{XR} \qquad \text{Instantaneous expansion ratio of the turbine} \qquad \text{Equation 7}$$

The temperature of the exhaust air stream leaving the storage plant (T_{et}) is assumed to be fixed and constant. Following Osterle [21], an imaginary heat exchanger (HXF) is placed at the exhaust of the storage plant to account for the exergy loss of the exhaust stream to the ambient environment. This heat exchanger cools the air from T_{et} down to the ambient temperature (T_0) (see Figure 7).

The heat flows (Q) are reckoned to be positive if they enter the system (*e.g.* heat added in the combustor, Q_{CC}) and negative if they leave the system (*e.g.* heat dissipated in the coolers of compressor, Q_{HC}). The work (W)

done by the system on the surroundings has a positive sign (*e.g.* expansion work, W_{TB}) whereas the work done on the system has a negative sign (*e.g.* compression work, W_{CM}).

3- Thermodynamic analysis of D-CAES and conventional CAES

An analytical exergy study of conventional CAES and D-CAES is presented in this section with the aim of estimating several thermodynamic figures of merit as a function of selected design parameters (pipeline length, cavern pressure, and throttling the withdrawn air to a fixed pressure prior to power generation).

Thermodynamic analysis of D-CAES in the literature is limited to a recent paper by Bagdanavicius and Jenkins [24]. They performed an energy and exergy simulation of a CAES system paired with a thermal storage (TS) and a district heating (DH) system, so called CAES-TS-DH. That system is similar to the D-CAES configuration studied in this chapter (Figure 8) with the primary difference that Bagdanavicius and Jenkins did not model an air pipeline between the compression train and the air storage. Additionally, they assumed that the withdrawn air was throttled to a fixed pressure prior to generating work.

Bagdanavicius and Jenkins took into account the actual exergy of the recovered heat (not exergy of the heating fuel saved in the DH system) and reported an exergy storage efficiency of ~56%. Work ratio and heat rate of the CAES-TS-DH system were estimated at ~0.82 and 4.0 GJ/MWh (LHV), respectively. Assuming an energy efficiency of 80% for the boilers of the DH system, the net heat rate and roundtrip exergy efficiency of their CAES-TS-DH system would be ~0.6 GJ/MWh and ~100%. Such an optimistic performance is because 93% of the compression work was recovered and supplied to the district heating system in their model.

Bagdanavicius and Jenkins used Cycle-Tempo [25], a thermodynamic simulation software, for the analysis while modeling details of individual components were not discussed. Moreover, the system variables were reported independent of the cavern's instantaneous pressure (*e.g.* 112 MW for the compression power). This study did not justify how the power consumption could remain constant (*i.e.* steady-state operation) while a constant flow rate of air (a modeling assumption) was being injected into the cavern whose pressure was rising.

In Bagdanavicius and Jenkins' model, a four-stage compressor charged a 300,000 m^3 underground reservoir in the pressure range of 50-82 bar. The inlet temperature of the compression stages as well as the cavern was assumed 50 °C. The discharge temperature of the storage plant (*i.e.* exhaust of the recuperator) was kept at 75 °C. Temperature of the thermal storage unit connected to the DH system varied in the range of 40-90 °C. Withdrawn air was throttled to 50 bar prior to combustion with natural gas and power generation in a two-stage expansion.

The following four paragraphs describe the conventional CAES and D-CAES systems studied in this chapter.

In the conventional CAES system (Figure 7), air is compressed in a multi-stage compressor (CM) and stored in an underground reservoir (CN). Each compression stage is followed by a cooler (CL) to reduce the compression work of the succeeding stage and to reduce the volume required for air storage. The compression heat is rejected to the ambient environment.

During the discharge phase, air is first preheated in a recuperator. It is then combusted with fuel (natural gas, NG) and generates work in the expanders (TB). A two-stage expansion train is considered throughout this chapter. The exhaust of the low-pressure (LP) turbine preheats the air entering the high-pressure (HP) combustor in the recuperator. The Huntorf and McIntosh compressed air energy storage plants use this CAES configuration except that the Huntorf facility is not equipped with a recuperator.

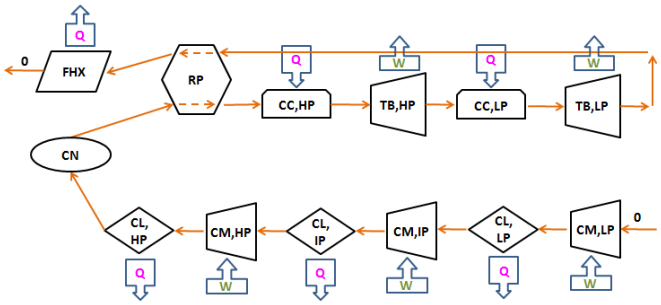

Figure 7: Schematic of the conventional CAES system modeled to benchmark performance of D-CAES. The compression train (CM) is composed of three stages: low-, intermediate-, and high-pressure (LP, IP, and HP). The expansion train (TB) is made of high- and low-pressure stages. "Q" and "W" represent heat and work interactions between the system and the surroundings. "0" indicates ambient condition. CL, CN, CC, RP, and FHX stand for cooler, cavern, combustor, recuperator, and exhaust heat exchanger (respectively).

Figure 8 illustrates the D-CAES system simulated. It recovers and exports the low-exergy compression heat for space and water heating – an application that does not require high-exergy heat, although fuel is often burned for it. The main idea here is to export the otherwise-wasted heat of compression to satisfy an external low-temperature heating load and to be credited for the negated consumption of heating fuel. Note that D-CAES still uses fuel (at levels similar to conventional CAES); nevertheless, it has a lower net heat rate once fuel credits are taken into account.

D-CAES compressor is located within a municipal region to provide its compression heat to a district heating system. The expander is co-located with the cavern, similar to conventional CAES. A pipeline transports air from the compression facility to the storage site. Air needs to be compressed to higher pressures in order to compensate the losses along the pipeline.

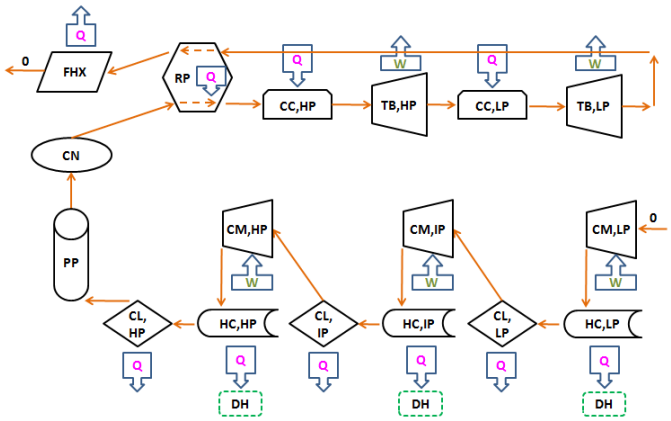

Figure 8: Schematic of the D-CAES system modeled. A portion of the compression heat is recovered by a heat recovery unit (HC) and utilized in a district heating (DH) system to meet an external heating load and to gain fuel credits for the D-CAES plant. Not all the compression heat is suitable for district heating. Heat recovered by the coolers (equal to total compression heat minus heat used by the district heating system) is rejected to the ambient environment due to its low temperature. A pipeline (PP) transports air from the compression to storage site.

3-1- Modeling conventional CAES

The compressor train of the conventional CAES system analyzed to benchmark the performance of D-CAES is assumed to have three stages: low- (LP), intermediate- (IP), and high-pressure (HP). All the stages have variable but equal compression ratios and fixed isentropic efficiencies throughout the charging process. The compression ratio (CR) varies to match the instantaneous pressure of the cavern (see Equation 8).

$$CR_{HP} = CR_{IP} = CR_{LP} = \sqrt[3]{\frac{P_{CN}}{P_0}} = \sqrt[3]{CR}$$ Instantaneous compression ratio of three-stage compressor Equation 8

3-1-1- Charge phase of conventional CAES

At the beginning of each charging period, the initial temperature (T_{inl}^{CN}) and pressure ($P_{inl}^{CN} = P_{em}$) of the cavern are known from the previous cycle. Therefore, the mass of the cushion air is calculated by applying the ideal gas equation of state, as shown in Equation 9.

$$m_{air,inl} = \frac{P_{em} \times V_{CN}}{R_{air} \times T_{inl}^{CN}}$$ Initial mass of air present in the cavern Equation 9

The relationship between changes in the mass of air present in the cavern and the instantaneous pressure of the cavern is found by applying the First Law to the control volume of the cavern:

$$dQ - dW = dU_{CV} - dm_{in} \times h_{in}$$ Equation 10

Because the cavern is adiabatic and at constant volume, $dQ = dW = 0$. Using Equation 1, Equation 2, and Equation 3, the above equation is transformed into Equation 11.

$$dm_{air,ch} = \frac{dP_{ch} \times \mathrm{V_{CN}}}{R_{air} \times \gamma_{air} \times T_{in}^{CN}}$$ Incremental change in mass of air in the cavern during charging Equation 11

Because the inlet temperature of the cavern (T_{in}^{CN}) is known and fixed, Equation 11 is conveniently integrated to find the total mass of air injected (working air), as shown in Equation 12. Once the mass of air in the fully charged cavern is determined (Equation 13), its temperature is calculated by applying the ideal gas equation of state (see Equation 14).

$$m_{air,ch} = \frac{\left(P_{fl} - P_{em}\right) \times V_{CN}}{R_{air} \times \gamma_{air} \times T_{in}^{CN}}$$ Total mass of working air stored Equation 12

$$m_{air,fl} = m_{air,inl} + m_{air,ch}$$ Mass of air in the full cavern Equation 13

$$T_{CN,fl} = \frac{T_{inl}^{CN} \times P_{fl}}{P_{em} + (P_{fl} - P_{em}) \times \frac{T_{inl}^{CN}}{\gamma_{air} \times T_{in}^{CN}}}$$ Temperature of air at the end of charging Equation 14

Compression work required to charge the cavern is quantified by applying the First Law to each compression stage and summing them up (Equation 15). Work of the LP compressor is formulated in Equation 16. A

similar equation is applicable to the IP and HP compressors. The inlet temperature of each stage is fixed and known while the exit temperature is a function of the instantaneous cavern pressure and is determined by applying the isentropic compression formulae (see Equation 17 for the LP compressor).

$W_{CM} = \int_{P_{em}}^{P_{fl}} (dW_{CM,LP} + dW_{CM,IP} + dW_{CM,HP})$	Total work needed to charge the cavern	Equation 15
$dW_{CM,LP} = dm_{air,ch} \times C_{p,air} \times (T_{in}^{CM,LP} - T_{out}^{CM,LP})$	Incremental work of LP compressor	Equation 16
$T_{out}^{CM,LP} = T_{in}^{CM,LP} - \frac{T_{in}^{CM,LP} - T_{out,ist}^{CM,LP}}{\eta_{ist}^{CM,LP}}$	Instantaneous discharge temperature of LP compressor	Equation 17
$T_{out,ist}^{CM,LP} = T_{in}^{CM,LP} \times CR_{LP}^{(\gamma-1)/\gamma}$	Isentropic instantaneous discharge temperature of LP compressor	

Total heat dissipated by the intercoolers and the aftercooler is calculated by applying the First Law to each cooler (Equation 18). As a case in point, Equation 19 quantifies an increment of heat dissipated by the LP intercooler. Note the inlet temperature of each cooler equals the exit temperature of the preceding compression stage. The discharge temperature of the coolers is fixed (Equation 6). Compression heat of the conventional CAES system, which could have been recovered (Q_{CM}) is equal to the heat dissipated by the compressor coolers (Q_{CL}).

$Q_{CL} = \int_{P_{em}}^{P_{fl}} (dQ_{CL,LP} + dQ_{CL,IP} + dQ_{CL,HP})$	Heat rejected by the compressor coolers	Equation 18
$dQ_{CL,LP} = dm_{air,ch} \times C_{p,air} \times (T_{out}^{CL,LP} - T_{in}^{CL,LP})$	Incremental heat rejected by LP cooler	Equation 19
$Q_{CM} = Q_{CL}$	Total compression heat of conventional CAES	Equation 20

Once the initial and final states of the cavern in addition to the compression work are known, the total exergy lost over the charge phase can be calculated by Equation 24.

$\Delta U_{ch}^{CN} = m_{air,fl} \times u_{CN,fl} - m_{air,inl} \times u_{CN,inl}$	Change in internal energy of cavern over the charging process	Equation 21
$\Delta S_{ch}^{CN} = m_{air,fl} \times s_{CN,fl} - m_{air,inl} \times s_{CN,inl}$	Change in entropy of cavern over the charging phase	Equation 22
$\Delta X_{ch}^{CN} = \Delta U_{ch}^{CN} - T_0 \times \Delta S_{ch}^{CN}$	Change in exergy stored in cavern during the charging phase	Equation 23
$IX_{ch} = -\Delta X_{ch}^{CN} - W_{CM} + m_{air,ch} \times \psi_{air,ch}$	Total exergy lost over the charging phase	Equation 24

Note that $\psi_{air,ch} = 0$ since air entering the system is at ambient conditions (see Equation 5).

3-1-2- Discharge phase of conventional CAES

Similar to the charging process, the First Law is applied to the cavern to find the relationship between the instantaneous temperature and changes in the mass and pressure of the air present in the cavern (Equation 25).

$$dm_{air,dch} = \frac{dP_{CN} \times V_{CN}}{R_{air} \times \gamma_{air} \times T_{CN}}$$ Incremental change in the mass of air in cavern during the discharge period — Equation 25

Using Equation 25 and the state equation for ideal gas, the mass of air left in the cavern by the end of the discharge process (cushion air) and total mass of air withdrawn (working air) are calculated as shown in Equation 26 and Equation 27.

$$\frac{dm_{air,dch}}{m_{air,dch}} = \frac{dP_{CN}}{\gamma_{air} \times P_{CN}} \rightarrow$$

$$m_{air,em} = m_{air,fl} \times \left(\frac{P_{em}}{P_{fl}}\right)^{\frac{1}{\gamma}}$$ Mass of air left in the cavern by the end of discharge (*i.e.* cushion air) — Equation 26

$$m_{air,dch} = m_{air,fl} - m_{air,em} =$$

$$\frac{V_{CN}}{R_{air}} \times \left(\frac{P_{em}}{T_{int}^{CN}} + \frac{\left(P_{fl} - P_{em}\right)}{\gamma_{air} \times T_{in}^{CN}}\right) \times \left(1 - \left(\frac{P_{em}}{P_{fl}}\right)^{\frac{1}{\gamma}}\right)$$ Total mass of withdrawn air (*i.e.* working air) — Equation 27

Now that the mass of cushion air is known (Equation 26), the state equation for ideal gas is applied to calculate temperature of the discharging cavern (Equation 28 and Equation 29).

$$T_{CN,dch} = T_{fl} \times \left(\frac{P_{CV}}{P_{fl}}\right)^{(\gamma-1)/\gamma}$$ Instantaneous temperature of air in the cavern during discharge period — Equation 28

$$T_{em} = T_{fl} \times \left(\frac{P_{em}}{P_{fl}}\right)^{(\gamma-1)/\gamma}$$ Temperature of air in the fully depleted cavern (cushion air) — Equation 29

The initial temperature of the fully discharged cavern is set to T_0 (*i.e.* temperature of cavern at the beginning of cycle 1). This temperature eventually reaches asymptotic limits after many cycles, regardless of the initial temperature chosen. Simulation is run until this asymptotic limit is reached and all the results are reported then.

Inlet temperatures of both low- and high-pressure turbines ($T_{in}^{TB,LP}$ and $T_{in}^{TB,HP}$) are fixed and constant in the analysis. However, their exit temperature depends on the instantaneous expansion ratio, which is itself a function of the instantaneous cavern pressure (Equation 7). The First Law is applied to each expander stage to find the work generated (Equation 30 and Equation 31). Discharge temperature of the high-pressure expander is quantified by Equation 32 based on the isentropic expansion formulae. A similar set of equations can be written for the low pressure turbine.

$W_{TB} = \int_{P_{fl}}^{P_{em}} (dW_{TB,HP} + dW_{TB,LP})$	Total expansion work	Equation 30
$dW_{TB,HP} = dm_{air,dch} \times C_{p,air} \times \left(T_{in}^{TB,HP} - T_{out}^{TB,HP} \right)$	Incremental work of the HP expander	Equation 31
$T_{out}^{TB,HP} = T_{in}^{TB,HP} + \eta_{ist}^{TB,HP} (T_{out,is}^{TB,HP} - T_{in}^{TB,HP})$	Instantaneous exit temperature of HP expander	Equation 32
$T_{out,ist}^{TB,HP} = T_{in}^{TB,HP} \times XR_{HP}^{(\gamma-1)/\gamma}$	Isentropic instantaneous exit temperature of HP expander	

Once the instantaneous exit temperature of the HP expander is quantified, total heat added in the LP combustor can be determined by applying the First Law, as shown in Equation 33. Note that $T_{in}^{CC,LP} = T_{out}^{TB,HP}$ and $T_{out}^{CC,LP} = T_{in}^{TB,LP}$.

$Q_{CC,LP} = \int_{P_{fl}}^{P_{em}} dm_{air,dch} \times C_{p,air} \times (T_{out}^{CC,LP} - T_{in}^{CC,LP})$	Heat added in the LP combustor	Equation 33

The instantaneous temperature of air entering the HP combustor from the recuperator can be expressed as a function of the cavern's pressure by applying the First Law to the recuperator (see Equation 34). Similar to the LP combustor, the heat added in the HP combustor is quantified by applying the First Law (see Equation 35). Note that $T_{in}^{CC,HP} = T_{out,cold}^{RP}$ and $T_{out}^{CC,HP} = T_{in}^{TB,HP}$. T_{et} is the fixed temperature of the exhaust stream of the plant, which is leaving the recuperator (RP) and entering the exhaust heat exchanger (FHX).

$T_{in}^{CC,HP} = T_{CN,dch} + T_{out}^{TB,LP} - T_{et}$	Instantaneous inlet temperature of HP combustor	Equation 34
$Q_{CC,HP} = \int_{P_{fl}}^{P_{em}} dm_{air,dch} \times C_{p,air} \times (T_{out}^{CC,HP} - T_{in}^{CC,HP})$	Heat added in the HP combustor	Equation 35

Once the heat added in each combustor is determined, the total mass and exergy of the fuel (natural gas here) consumed are quantified by applying Equation 36 and Equation 37, respectively.

$m_{NG}^{CC} = \frac{Q_{LP,CC} + Q_{HP,CC}}{LHV_{NG}}$	Mass of gas burned by conventional CAES	Equation 36
$X_{NG} = m_{NG}^{CC} \times x_{NG}$	Exergy of gas burned by conventional CEAS	Equation 37

The First Law is again applied to quantify the heat recovered in the recuperator and the heat dissipated in the exhaust heat exchanger, as shown in Equation 38 and Equation 39, respectively.

$Q_{RP} = \int_{P_{fl}}^{P_{em}} dm_{air,dch} \times C_{p,air} \times (T_{et} - T_{out}^{TB,LP})$	Heat recovered in the recuperator	Equation 38
$Q_{FHX} = \int_{P_{fl}}^{P_{em}} dm_{air,dch} \times C_{p,air} \times (T_0 - T_{et})$	Heat rejected to the ambient environment in the exhaust heat exchanger	Equation 39

Finally, the exergy lost over the discharge process is determined by applying Equation 43. The exergy of air stream leaving the storage plant ($\psi_{air,dch}$) is zero similar to the exergy of air entering the plant ($\psi_{air,ch}$). This is because both air streams are at ambient conditions.

$\Delta U_{dch}^{CN} = m_{air,em} \times u_{CN,em} - m_{air,fl} \times u_{CN,fl}$	Change in internal energy of cavern during discharge	Equation 40
$\Delta S_{dch}^{CN} = m_{air,em} \times s_{CN,em} - m_{air,fl} \times s_{CN,fl}$	Change in entropy of cavern over discharge process	Equation 41
$\Delta X_{dc}^{CN} = \Delta U_{dc}^{CN} - T_0 \times \Delta S_{dc}^{CN}$	Change in exergy store of cavern during discharge	Equation 42
$IX_{dch} = -\Delta X_{dch}^{CN} - W_{TB} + X_{NG}^{CC} - m_{air,dch} \times \psi_{air,dch}$	Total exergy lost over the discharge period	Equation 43

3-1-3- Roundtrip analysis of conventional CAES

Once the work, heat, and exergy fluxes during the charge and discharge processes are quantified, the roundtrip exergy efficiency, work ratio and heat rate of conventional CAES are calculated by applying Equation 44 to Equation 46. The GHG emissions intensity and cavern exergy density are determined by Equation 47 and Equation 48.

$\eta_{X,CAES} = \frac{W_{TB}}{-W_{CM} + X_{NG}^{CC}}$	Roundtrip exergy efficiency of conventional CAES	Equation 44
$WR_{CAES} = \frac{-W_{CM}}{W_{TB}}$	Work ratio of conventional CAES	Equation 45
$HR_{CAES} = \frac{m_{fuel}^{CC} \times LHV_{NG}}{W_{TB}} \times 3.6$	Heat rate of conventional CAES	Equation 46

$GI_{CAES} = HR_{CAES} \times GIF_{NG}$	GHG emissions intensity of conventional CAES	Equation 47
$X\rho = \frac{W_{TB}}{V_{CN}}$	Exergy density of conventional CAES	Equation 48

3-2- Modeling D-CAES

As illustrated in Figure 8, the discharge process of the D-CAES facility is identical to that of the conventional CAES system (analyzed in Section 3-1-2). The distinction of these two systems is that a portion of the compression heat is recovered, via three heat recovery units, and utilized in a district heating system in D-CAES. This otherwise-wasted heat of compression brings in fuel credits for the D-CAES plant equal to the heating fuel saved. Therefore, the net (apparent) fuel consumption of D-CAES – defined as fuel directly consumed by the combustors of D-CAES (*i.e.* raw fuel demand) minus fuel saved in the district heating system due to recovery of compression heat – is less than the fuel demand of a similar conventional CAES system. Following are the specific simplifications made to model D-CAES.

Each compressor stage is followed by a heat recovery unit (HC) and a Cooler (CL), as illustrated in Figure 9 for the IP compressor. The heat recovery units cool the compressor's exhaust to a fixed temperature (T_{out}^{HC}). The absorbed heat is utilized by the district heating plant (DH). Compressed air then passes through an intercooler (or aftercooler) to further dissipate its heat. Similar to the conventional CAES model, the exit temperature of the coolers is fixed (Equation 6).

A pipeline transports the compressed air to the storage site. Note that the compression facility and the storage site are located at some distance apart, L_{PP} while the expansion train and cavern are co-located. The compressor pressurizes air enough to compensate pipeline losses so that the cavern pressure can vary between P_{em} and P_{fl}, similar to conventional CAES. The pipeline is assumed to be isothermal ($T_{PP,up} = T_{PP,dn} = T_{out}^{CL,HP} = T_{in}^{CN}$).

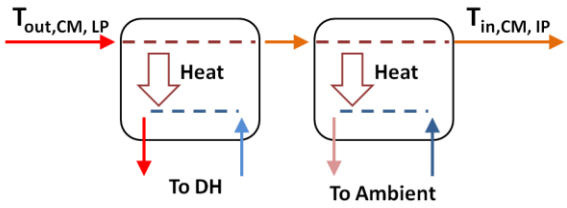

Figure 9: Configuration of the heat recovery unit (HC, on the left) and cooler (CL, on the right) following the low-pressure (LP) compressor. Heat recovered in the HC is utilized in the district heating (DH) system and earns fuel credits. Heat absorbed in the CL is wasted to the ambienet due to its low temperature.

3-2-1- Charge phase of D-CAES

The compressor of D-CAES needs to compensate for the pressure drop along the pipeline ($P_{PP,dp} = P_{PP,up} - P_{PP,dn}$) to reach the same cavern pressure as of conventional CAES. $P_{PP,up}$ is the upstream pipeline pressure (equal to discharge pressure of the high-pressure compressor, $P_{out}^{CM,HP}$) and $P_{PP,dn}$ is the downstream pipeline pressure, which is equal to the instantaneous pressure of cavern (P_{CN}). Note that in the conventional CAES system, $P_{out}^{CM,HP}$ is equal to P_{CN} (*i.e.* no pressure losses between discharge of the high-pressure compressor and inlet of the cavern).

Equation 49 relates the pressure drop to the important pipeline characteristics [26]. The pressure drop ($P_{PP,up} - P_{PP,dn}$) has a nonlinear relationship with the pipeline flowrate, which itself is a function of power consumption of the compressor and the instantaneous compression ratio (see Equation 50). Note that $\dot{W}_{CM}$ and F_{PP} have units of MW and m^3/day (respectively) in these equations.

$$P_{PP,up}^2 - P_{PP,dn}^2 = 9.4 \times 10^4 \times \frac{T_{PP} \times L_{PP} \times f_{PP} \times {F_{PP}}^2}{{D_{PP}}^5}$$ Pressure loss along the air pipeline Equation 49

$$\dot{W}_{CM} = \left(\frac{4.064}{10^9}\right) \times \left(\frac{\gamma}{\gamma - 1}\right) \times \frac{T_{in}^{CM}}{\eta_{ist}^{CM}} \times F_{PP} \times \left(1 - CR^{\frac{\gamma-1}{\gamma}}\right)$$ Power consumption of compressor Equation 50

$$CR = \frac{P_{PP,up}}{P_0}$$ Instantaneous compression ratio of D-CAES Equation 51

The approach used here to calculate the compression work is based on using Equation 49 and Equation 50 to determine the upstream pressure of the pipeline, $P_{PP,up}$ (equal to $P_{out}^{CM,HP}$), over a range of instantaneous

cavern pressures (P_{CN}). The instantaneous compression ratio is given by Equation 51. Similar to the conventional CAES system, Equation 15 to Equation 17 are then applied to determine the compression work.

For a fixed compressor size ($\dot{W}_{CM}$), a series of calculations is performed to find the flow rate (F_{PP}) and discharge pressure (P_{up}) of the compressor that lead to the desired downstream pressure (P_{dn}), which is equal to the cavern pressure and varies between P_{em} and P_{fl}.

Equation 6 and Equation 11 remain valid to quantify temperature of the air stream entering the cavern and the incremental change in mass of the stored air, respectively. Equation 12 to Equation 14 are also used to determine changes in the mass and temperature of the stored air. Equation 15 to Equation 17 calculate the total compression work.

In the D-CAES configuration, compressors are followed by three heat recovery units (HC) and intercoolers/ aftercoolers (CL), which cool the compressed air prior to entering the next stage (or pipeline), as shown in Figure 8 and Figure 9. Heat transferred in the coolers (Q_{CL}) is quantified by applying the First Law. Equation 52 illustrates this for the low-pressure cooler. Equation 53 expresses the total heat released to the environment by the three coolers cumulatively.

$dQ_{CL,LP} = dm_{ch} \times C_{p,air} \times (T_{out}^{CL,LP} - T_{out}^{HC,LP})$	Incremental heat rejected by LP cooler	Equation 52
$Q_{CL} = \int_{P_{em}}^{P_{fl}} (dQ_{CL,LP} + dQ_{CL,IP} + dQ_{CL,HP})$	Heat dumped to the ambient environment	Equation 53

Similarly, the heat absorbed by the heat recovery units is calculated by applying the First Law, as shown in Equation 54 for the LP heat recovery unit. Equation 55 expresses the total recovered heat that is offered to the district heating system. The mass and exergy of the fuel credits are calculated by Equation 56 and Equation 57, respectively. The parameter η_{HC} expresses the percentage of the recovered heat that is consumed by the DH system (*i.e.* utilization factor of the recovered compression heat). The parameter η_{BL} is the efficiency of the boiler of the DH system, which now uses less fuel due to importing waste heat.

$dQ_{HC,LP} = dm_{ch} \times C_{p,air} \times (T_{out}^{HC,LP} - T_{out}^{CM,LP})$	Incremental heat recovered by LP heat recovery unit	Equation 54
$Q_{HC} = \int_{P_{em}}^{P_{fl}} (dQ_{HC,LP} + dQ_{HC,IP} + dQ_{HC,HP})$	Total heat recovered by the heat recovery units of D-CAES	Equation 55

$m_{NG}^{ct} = \frac{Q_{HC}}{LHV_{NG}} \times \frac{\eta_{HC}}{\eta_{BL}}$	Mass of fuel credit to D-CAES	Equation 56
$X_{NG}^{ct} = m_{NG}^{ct} \times x_{NG}$	Exergy of fuel credited to D-CAES	Equation 57
$Q_{CM} = Q_{CL} + Q_{HC}$	Total compression heat available for recovery in D-CAES system	Equation 58

Equation 21 to Equation 24 remain applicable to evaluate the changes in internal energy, entropy, and exergy of the cavern and the total exergy loss over the charging period.

3-2-2- Discharge phase of D-CAES

The discharge process of D-CAES is identical to of the conventional CAES system studied in Section 3-1-2.

3-2-3- Roundtrip analysis of D-CAES

The raw (*i.e.* ignoring fuel credits) roundtrip exergy efficiency, work ratio, and raw heat rate of the D-CAES facility are quantified by Equation 59, Equation 60, and Equation 61, respectively. However, once the fuel credits from heat recovery are taken into account, the adjusted values for the net roundtrip exergy efficiency and net heat rate are determined by Equation 62 and Equation 63, respectively. Heat recovery lowers the net fuel consumption of the D-CAES plant (reduced heat rate), while the pipeline losses increase the compression work (elevated work ratio). Therefore, the net change in the roundtrip exergy efficiency of D-CAES depends on the balance between these two opposing factors. Exergy density of the plant is calculated by Equation 48. The net GHG emissions intensity of D-CAES is expressed by Equation 64.

$\eta_{X,D-CAES,raw} = \frac{W_{TB}}{-W_{CM} + X_{NG}^{CC}}$	Raw roundtrip exergy efficiency of D-CAES	Equation 59
$WR_{D-CAES} = \frac{-W_{CM}}{W_{TB}}$	Work ratio of D-CAES	Equation 60
$HR_{D-CAES,raw} = \frac{m_{NG}^{CC} \times LHV_{NG}}{W_{TB}} \times 3.6$	Raw heat rate of D-CAES	Equation 61
$\eta_{X,D-CAES,net} = \frac{W_{TB}}{-W_{CM} + X_{NG}^{CC} - X_{NG}^{ct}}$	Net roundtrip exergy efficiency of D-CAES	Equation 62
$HR_{D-CAES,net} = \frac{(m_{NG}^{CC} - m_{NG}^{ct}) \times LHV_{NG}}{W_{TB}} \times 3.6$	Net heat rate of D-CAES	Equation 63
$GI_{D-CAES,net} = HR_{D-CAES,net} \times GIF_{NG}$	Net GHG emissions intensity of D-CAES	Equation 64

The utilization factor of the available compression heat (UFQ_{CM}) is also calculated to quantify the portion of the available compression heat (Q_{CM}, Equation 58), which is recovered and utilized (see Equation 65).

$$UF_{CM} = \frac{Q_{HC} \times \eta_{HC}}{Q_{CM}}$$ Portion of available compression heat that is utilized Equation 65

3-3- Numerical example: D-CAES and conventional CAES models

A case study based on the simplified model of the conventional CAES and D-CAES is presented in this section. As discussed earlier, a comprehensive thermodynamic analysis of these systems is beyond the scope of this thesis since the results will be design-specific and the use of sophisticated simulation software such as Aspen Plus would be required to develop a more accurate model.

3-3-1- Base case simulation of D-CAES

Table 1 lists the inputs used in the base case scenario to compare the thermodynamics of conventional CAES and D-CAES. Equation 66 shows the relationship between the cavern pressure (P_{CN}) and the upstream pressure of the pipeline ($P_{PP,up}$, equal to discharge pressure of the high-pressure compressor), using the values from Table 1 and the methodology discussed in Section 3-2-1.

$$P_{PP,up} = 0.764 \times P_{CN} + 2{,}225$$
$$R^2 = 0.99$$ Numerical relationship between pipeline's upstream pressure and cavern's pressure of D-CAES Equation 66

The key thermodynamic outputs of the conventional CAES and D-CAES simulation are listed in Table 2. As expected, compression work of D-CAES is higher than of CAES, for the same storage pressure. It is of note that not all the compression heat is useful to the district heating system due to its too low temperature. This analysis has assumed that the heat recovery unit (HC) has an approach temperature of 30 °C and the hot compressed air is cooled down to $T_{out,hot}^{HC}$= 100 °C (corresponding to an inlet temperature of 70 °C for the cold stream of the heat recovery unit, HC).

Table 1: Input parameters for the numerical example comparing thermodynamics of conventional CAES and D-CAES in the base case scenario.

Parameter	Value	Parameter	Value	Parameter	Value
γ_{air}	1.4	V_{CN}	0.56 Mm^3	L_{PP}	50 km
$C_{p,air}$	1.006 $\frac{kJ}{kg \times K}$	R_{air}	0.287 $\frac{kJ}{kg \times K}$	T_{et}	130 °C
P_{fl}	7 MPa	η_{HC}	100%	η_{is}^{TB}	85%
P_{em}	5 MPa	η_{BL}	80%	x_{NG}	50 MJ/kg
η_{is}^{CM}	85%	$T_{out,hot}^{HC}$	100 °C	GIF_{NG}	66 kg/GJ
T_{ac}	30 °C	T_{PP}	55 °C	LHV_{NG}	50 MJ/kg
$T_{in}^{TB,HP}$	530 °C	$\dot{W}_{CM}$	105 MW	$T_{in,cold}^{CL}$	25 °C
$T_{in}^{TB,LP}$	850 °C	D_{PP}	0.75 m	f_{PP}	0.01

The fuel exergy credit (4,155 GJ) is higher than the recovered heat (3,321 GJ) because of an assumed 80% boiler efficiency of the district heating plant (η_{BL}). Higher compression requirements of D-CAES compared to conventional CAES result in 11% higher exergy losses over the charging process. Nevertheless, the exergy credit from heat recovery (4,155 GJ) is 21 times as large as the additional exergy losses endured to charge the cavern of D-CAES (1,775 GJ) compared to CAES (1,580 GJ). The discharge phases of conventional CAES and D-CAES have the same characteristics.

The simulated D-CAES plant has a higher work ratio (~0.77 versus 0.74) due to pressure losses in the pipeline. It consumes three more units of electrical energy compared to the conventional CAES system to generate 100 units of electricity. Both the conventional CAES and D-CAES plants have moderate values of the raw exergy efficiency (54% and 53%, respectively), which are in the lower spectrum of bulk energy storage technologies. Pumped hydro storage, for example, has a roundtrip storage efficiency of 70-85% [27].

Nevertheless, D-CAES looks substantially more attractive once the fuel credits are taken into account. It reaches a net roundtrip exergy efficiency of 84% and a net heat rate of 1.6 GJ/MWh. This occurs because approximately 70% of the energy consumed by the compressor (W_{CM}=4,730 GJ) is recovered and utilized by

the district heating system (Q_{HC}=3,320 GJ). The GHG emissions intensity of D-CAES (103 $kgCO_2e/MWh$) is 40% of the conventional CAES.

It is of note that this analysis provides an optimistic view of D-CAES performance. This analysis has assumed that all the recovered heat is consumed by the district heating system (*i.e.* η_{HC}=100%). In case of excess recovered heat beyond the instantaneous demand, it may be wasted to the ambient environment or stored in a thermal energy storage system for later use (*i.e.* η_{HC}<100%), both of which lower the storage efficiency of D-CAES.

Table 2: Results of the base case thermodynamics analysis of conventional CAES and D-CAES.

Variable	**CAES**	**D-CAES**	**Variable**	**CAES**	**D-CAES**
W_{CM} (GJ)	-4,560	-4,730	W_{TB} (GJ)	6,180	
Q_{CM} (GJ)	-4,300	-4,480	Q_{CC} (GJ)	6,820	
Q_{HC} (GJ)	0	-3,320	X_{out} (GJ)	6,180	
X_{NG}^{ct} (GJ)	0	4,160	IX_{dch} (GJ)	3,620	
$X_{in,net}$ (GJ)	11,380	7,400	UF_{CM}	0	74%
IX_{ch} (GJ)	1,580	1,760	WR	0.74	0.77
$\eta_{X,raw}$	54.3%	53.4%	$\eta_{X,net}$	54.3%	83.5%
HR_{raw} (GJ/MWh)	4.0		HR_{net} (GJ/MWh)	4.0	1.6
$X\rho$ (kWh/m^3)	3.1		GI_{net} ($kgCO_2$/MWh)	262	103

3-3-2- Sensitivity to length of pipeline

A key parameter in economic viability of D-CAES is the distance between the compressor and the cavern, *i.e.* the length of pipeline (L_{PP}). This distance impacts the thermodynamics of D-CAES as well, due to the dependence of the pressure losses on the pipeline length (see Equation 49). Robustness of the results to the pipeline length is provided in Table 3. A longer pipeline requires more compression work (resulting in higher values for work ratio). At the same time, it provides more heat recovery opportunities (higher Q_{HC}). The work ratio varies from 0.75 to 0.79 when the pipeline length increases from 25 to 100 km, as compared to a value of 0.74 in the conventional CAES model. The net effect of higher compression work (higher work ratio) and higher recovered heat (lower heat rate) is negligible on the roundtrip exergy efficiency of D-CAES.

Table 3: Sensitivity of performance metrics of D-CAES to pipeline length.

Pipeline length (km)	**CAES**	**25**	**50**	**75**	**100**
W_{CM} (GJ)	-4,560	-4,650	-4,730	-4,800	-4,860
X_{NG}^{ct} (GJ)	0	4,060	4,160	4,240	4,320
WR	0.74	0.75	0.77	0.78	0.79
$\eta_{X,net}$ (%)	54.3	83.2	83.5	83.7	83.8
HR_{net} (kJ/kWh)	4.0	1.6	1.6	1.5	1.5

3-3-3- Sensitivity to storage pressure

Another key design parameter is the pressure at which compressed air is stored. To evaluate its effect, the maximum cavern pressure is varied from 7 to 11 MPa while its minimum pressure was fixed at 5 MPa (see Table 4). The work ratio of both conventional CAES and D-CAES systems increases with the storage pressure as the compression losses get larger at higher compression ratios. Nevertheless, the work ratio of D-CAES is less sensitive to increases in the storage pressure. This is because pipeline losses ($P_{up} - P_{dn}$ in Equation 49) are lower at higher pipeline pressures and also because of the decreased flow rates in the pipeline (the size of the compressor is fixed in this simulation; therefore, the flow rate is lower at higher pipeline pressures). Higher compression losses incurred at elevated storage pressures lower the roundtrip exergy efficiency of conventional CAES compared to the base case (P_{fl}=7 MPa and η_X=54%). The net exergy efficiency of D-CAES, however, improves at elevated cavern pressures compared to the base case (P_{fl}=7 MPa and $\eta_{X,net}$=84%), because the additional heat recovery opportunities and lower pipeline losses outweigh increases in the compression losses. The net effect of increasing the storage pressure is to slightly reduce the heat rate of the D-CAES. The heat rate of conventional CAES is not sensitive to this change.

Despite penalties in the roundtrip exergy efficiency, higher storage pressures may be attractive as they increase the exergy density of the storage plant. Raising the maximum cavern pressure from 7 to 11 MPa approximately triples the exergy density. It is of note that higher compression ratios reduce the isentropic efficiency of compressor [28]. Similarly, a wider range for the operating pressure of the expander will likely reduce its efficiency [10]. None of these two negative effects are included in the model. These factors will increase the work ratio of both conventional CAES and D-CAES systems in the real world.

Table 4: Sensitivity of D-CAES thermodynamics to the maximum storage pressure (P_{fl}). All other input parameters are the same as Table 1.

	P_{fl}= 7 MPa		P_{fl}= 9 MPa		P_{fl}= 11 MPa	
Variable	**CAES**	**D-CAES**	**CAES**	**D-CAES**	**CAES**	**D-CAES**
WR	0.74	0.77	0.75	0.77	0.76	0.78
$\eta_{X,net}$(%)	54.3	83.6	54.0	84.2	53.7	84.8
HR_{net}(GJ/MWh)	4.0	1.6	4.0	1.5	4.0	1.4
$X\rho$ (kWh/m^3)	3.1		6.3		9.6	

3-3-4 Sensitivity to expander design and throttling

The base case analysis presented in Section 3-3-1 assumes that the inlet pressures of expanders and consequently, their expansion ratios vary as air is withdrawn from the cavern. An alternative strategy is, however, to throttle the compressed air to a fixed pressure before expanding it the turbines and generating work. Despite the exergy losses associated with throttling and a lower exergy density of the cavern, both the Huntorf and the McIntosh plants utilize this design due to the higher efficiencies of turbines with fixed expansion ratios [10] and in order to keep the power output of the CAES plant constant [29]. The Huntorf plant throttles air to 46 bar (storage pressure of 48-66 bar) whereas the McIntosh plant throttles air to 45 bar (storage pressure of 45-74 bar) [10].

It is reasonable to assume that future compressed air storage plants will avoid throttling losses (to increase the exergy density and to reduce the work ratio) and to assume that this will be facilitated by technological improvements in expander design.

In order to assess the effects of throttling, the simulation is repeated but with constant expansion ratios. Compressed air is throttled to P_{em} prior to entering the recuperator in this case. The throttling process is isenthalpic (constant enthalpy) because it involves no work or heat transfer. Since air is modeled as an ideal gas, an isenthalpic process does not change its temperature (in practice, the temperature of air drops). Therefore, all the previous formulae are still applicable with the difference that a fixed expansion ratio (Equation 67 instead of Equation 7) is now used to determine the work of the expanders.

$$XR_{HP} = XR_{LP} = \sqrt{\frac{P_0}{P_{em}}} = \sqrt{XR}$$ Expander ratio if withdrawn air is throttled prior to work generation Equation 67

Table 5 reports key thermodynamic parameters of conventional CAES and D-CAES with and without throttling, using values of P_{em}= 5MPa, P_{fl}= 7MPa, and L= 50 km (see Table 1). Throttling of compressed air reduces the expansion work of both conventional CAES and D-CAES by 3% (5,980 GJ compared to 6,180 GJ in the base case scenario). The exergy density of the cavern is also decreased by ~3% (3.0 compared to 3.1 kWh/m^3). Throttling lowers the fuel consumption of both storage plants by approximately 3% (6,620 GJ from the base value of 6,820 GJ) because the expansion ratio is lower now (hence, the inlet temperature of the LP combustor is higher). Throttling increases the work ratio of conventional CAES to 0.76 compared to the base case value of 0.74. A similar effect is observed for D-CAES: throttling increases the work ratio from 0.77 to 0.79. The net effect of lower expansion work and fuel consumption is negligible on the heat rate of CAES, whereas it improves the net heat rate of D-CAES by approximately 6% (1.5 compared to 1.6 GJ/MWh). The conventional CAES and D-CAES plants modeled here have roundtrip exergy efficiencies of ~53% and 83%, respectively, when air is throttled to yield a constant inlet pressure for the expanders. These values are marginally lower compared to the scenario without throttling (~54% and 84%). The negative impacts of throttling are likely to be more substantial in the real world as throttling is an exothermic process. Small sensitivity of the results to the pressure of the expanding air also highlights a key shortcoming of CAES: exergy of compressed air is extremely low. Expanding 1 kg of air from 7 MPa and 600 °C generates ~1765 kJ of work, when expanded in a one stage turbine with an isentropic efficiency of 85%. This value is reduced only by 13% (down to ~1535 kJ) when the pressure of expanding air is reduced from 7MPa to 5MPa. To put these numbers in perspective, each kg of natural gas produces ~17.5 GJ of work when combusted in a typical gas turbine with an efficiency of 35%.

Table 5: Effect of throttling on the performance of conventional CAES and D-CAES. "Var. P" represents the turbine design with a variable expansion ratio while "Throttle" indicates that air is throttled to yield a constant expansion ratio for the turbine.

	CAES		**D-CAES**	
	Var. P	**Throttle**	**Var. P**	**Throttle**
W_{CM}(GJ)	-4,560		-4,730	
X_{NG}^{ct}(GJ)	0		4,160	
W_{TB} (GJ)	6,180	5,980	6,180	5,980
Q_{CC} (GJ)	6,820	6,620	6,820	6,620
WR	0.74	0.76	0.77	0.79
$\eta_{X,net}$(%)	54.3	53.5	83.5	83.0
HR_{net}(GJ/MWh)	4.0	4.0	1.6	1.5
$X\rho$ (kWh/m^3)	3.1	3.0	3.1	3.0

3-4- Remarks on thermodynamics of D-CAES

The simulation suggested that utilizing the compression heat to supply an external low-temperature heating need might substantially improve the thermodynamic and GHG emissions of the compressed air energy storage technology. The results revealed that waste heat recovery enhances the storage efficiency from approximately 54% to 84%. In addition, increasing the maximum cavern pressure slightly lowered the roundtrip exergy efficiency of conventional CAES (due to higher compression losses) whereas it improves the D-CAES exergy efficiency (due to increased waste heat recovery in addition to lower pipeline losses).

Despite its attractive thermodynamics, the application of the D-CAES design is limited in the real world due to need for the presence of a suitable air storage cavern in close proximity to a large heat load. Additionally, achieving high storage efficiencies (~80%) calculated here for D-CAES would require storage of the excess recovered heat. Both the capital cost and heat losses from these thermal storage systems would work against the feasibility of D-CAES.

Moreover, the D-CAES design does not solve the fundamental problem that a fossil fuel must be burned during its discharge period. Space and water heating systems will move away from combustion of fossil fuels under emissions constraints (*e.g.* heat pump or solar heating) while the market opportunity for D-CAES is

pairing with a district heating system, which combusts a fossil fuel. Consequently, while D-CAES may become economical and also reduce GHG emissions under certain circumstances, it will not be scalable to substantially help in decarbonizing the electricity grid. The next section of this chapter concentrates on thermodynamics of two zero-carbon compressed air storage technologies that can potentially be adopted at scale.

4- Thermodynamic analysis of A-CAES and CAES-HTE

Despite its higher technical maturity and affordability compared to most other bulk energy storage (BES) systems, prospects of conventional CAES are poor under tight emissions restrictions. This is driven by its fuel demand (heat rate of ~4 GJ/MWh) and the associated GHG emissions (~260 $kgCO_2e$/MWh). Conventional CAES may not be able to compete with more capital-intensive but less polluting technologies such as pumped hydro storage (PHS) and flow batteries, under strict emissions constraints. Some newer designs have aimed to address this issue through replacing the fossil heating fuel of CAES with its compression heat and consequently eliminating its GHG emissions. This section provides thermodynamic analysis of two of these advanced CAES designs: Adiabatic CAES (A-CAES) and CAES fueled by hydrogen produced via electrolysis of steam (CAES-HTE). Thermodynamics of CAES fueled by hydrogen generated via electrolysis of water at the ambient (low) temperature (called CAES-LTE) is also modeled to put the performance of CAES-HTE in perspective.

As shown in Figure 2, the A-CAES system relies on the physical storage of the compression heat, which is later used to heat the expanding air. If enough heat is stored, A-CAES would not require combustion of fuel and could reach a heat rate and GHG emissions rate of zero. Nevertheless, the A-CAES technology calls for generation and storage of high-temperature (exergy) heat in order to increase the temperature of expanding air to around 600 °C. Such high temperatures are desired to boost the power output of the plant (hence higher exergy density) and to prevent freezing of vapor present in the expanding air. This design constraint translates to higher compression ratios and limited intercooling and consequently, higher compression work. General Electric (GE) and five other partners have been collaborating on an A-CAES pilot project called "ADELE" in Germany since 2010. The targeted roundtrip exergy efficiency of this plant is 70% [30].

Thermodynamics of A-CAES has been studied widely in the literature. For example, Steta [22] performed an analytical simulation of the Huntorf plant if it was hypothetically operated in an adiabatic mode. He estimated an exergy efficiency of 57%. Zhang *et al.* [12] also studied the thermodynamics of A-CAES and reported efficiency figures around 75%.

To overcome the technical challenges of high-temperature storage of heat, some researchers have also evaluated A-CAES designs with multi-stage expanders and compressors operating at lower temperatures. Such systems are in fact a combination of the traditional A-CAES (physical storage of heat) and isothermal (several stages of compression and expansion). As a case in point, Buffa *et al.* [17] performed exergy analysis of a seven stage compression and six stage expansion aboveground A-CAES system. The thermal storage system in their model utilized water at the ambient pressure as the working fluid (thus operating below 100 °C). They reported a roundtrip exergy efficiency of ~52%. Similarly, Wolf and Budt [19] analyzed an A-CAES system with a storage temperature of 90-200 °C and estimated an overall exergy efficiency of 52-60%.

An alternative approach to direct storage of heat (A-CAES) is to use it for hydrogen production. In the CAES-HTE configuration, electricity and the high-temperature compression heat are fed into a high-temperature electrolyzer (HTE) to generate carbon-free hydrogen (see Figure 5). Hydrogen is stored onsite to later fuel combustors to heat the expanding air. Basically, CAES-HTE focuses on chemical rather than physical storage of the compression heat.

The CAES-HTE system has few advantages over A-CAES. The thermal storage system is eliminated whose high pressure and high temperature requirements pose various operational and maintenance challenges for A-CAES [11]. Moreover, long idling periods do not degrade the storage efficiency since chemical storage (CAES-HTE) is not prone to energy losses in contrast to physical storage of thermal energy at high temperatures (A-CAES). In addition, CAES-HTE has a higher exergy density since its work output is boosted through hydrogen combustion.

A simpler approach compared to CAES-HTE is to generate hydrogen via electrolysis of water at the low (ambient) temperature (LTE). The CAES-LTE system uses more electricity to generate hydrogen via electrolysis compared to the CAES-HTE configuration. The compression work of CAES-LTE is, however, lower because the need for producing high-temperature compression heat is eliminated (electrolysis of water at ambient temperature instead of the electrolysis of steam at elevated temperatures).

Hydrogen-fueled CAES has its own engineering challenges too. It requires special combustors capable of handling higher flame temperatures and increased NO_x emissions [31, 32]. For instance, integrated

gasification combined cycle (IGCC) designs using syngas with hydrogen contents of 25-40% use diffusion burners and massive inert gas (steam or nitrogen) to dilute the fuel in order to limit NO_x emissions [33]. Therefore, hydrogen combustors need to handle higher flow rates. Moreover, combustion of hydrogen instead of natural gas results in roughly 1.7 more water mass per unit of energy. Higher operating pressures in the CAES-HTE design also impose design and reliability challenges for the combustors compared to gas turbines or conventional CAES [34].

Note that hydrogen can be produced through a variety of pathways: chemical, biological, electrolytic, photolytic and thermo-chemical. Currently, the primary feedstock for hydrogen production is fossil fuels, especially natural gas. Almost all large-scale hydrogen production facilities use steam reforming of methane (SMR) [35]. As shown in Equation 68, methane and steam are converted to hydrogen and carbon monoxide in an endothermic process (700-850 °C and 3-25 bar) [36]. The water-gas shift reaction (Equation 69) is used to convert carbon monoxide to carbon dioxide and hydrogen.

$CH_4 + H_2O \rightarrow CO + 3H_2$	Steam reforming reaction (endothermic)	Equation 68
$CO + H_2O \rightarrow CO_2 + H_2$	Water-gas shift reaction (exothermic)	Equation 69

Two particular pathways are of special interest for producing low-carbon hydrogen. The first one is electrolysis of steam at high temperatures powered by low-carbon electricity. The second pathway is thermo-chemical splitting of water at high temperatures, such as the Iodine-Sulfur (IS) process. These processes are of particular interest of the high-temperature gas-cooled reactor (HTGR) industry because of the availability of very high-temperature heat (~800 °C) [37].

The first process considered by the HTGR industry is electrolysis of steam at high temperatures (HTE) instead of electrolysis of water at low temperatures (LTE). Electrolysis at higher temperatures requires more thermal energy but less electricity per unit of hydrogen produced. Figure 10 illustrates the theoretical energy requirements as a function of the temperature of water/steam being electrolyzed. The HTGR industry is interested in utilizing the HTE technology for hydrogen production due to the availability of high-temperature (~850 °C) and high-pressure (>1 MPa) steam from the Rankine cycle of the nuclear plant [37]. Feeding the high-pressure steam into the HTE generates high-pressure hydrogen, which is desired for

storage. Moreover, high reaction temperatures improve the activity of the electrodes and lower the cathodic and anodic over-voltages. These effects allow for increasing the current density of the electrode and reducing the polarization losses [38]. Therefore, combining HTE with high-temperature reactors is appealing from thermodynamic (reducing electric load and utilizing waste heat), kinetic (lowering polarization losses), and mechanical (producing high-pressure hydrogen for storage) standpoints.

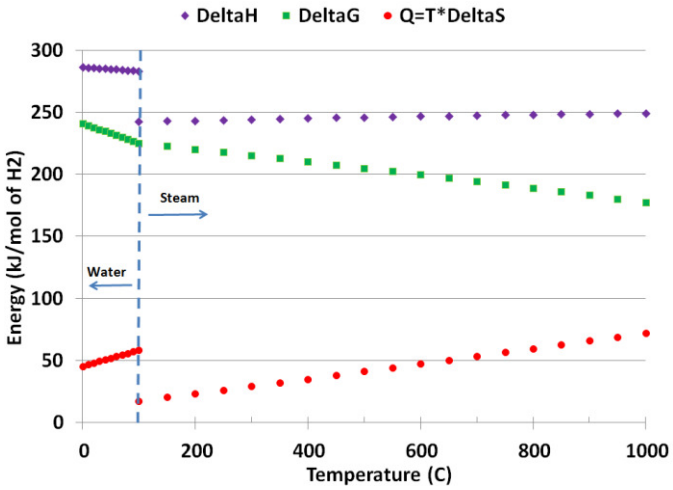

Figure 10: Theoretical energy requirements for electrolysis as a function of the reaction temperature. Electrolysis of steam at higher temperatures requires less electrical work (ΔG, Gibbs free energy) but more heating energy (equal to product of the electrolysis temperature, T_{HTE}, and entropy change, ΔS). The total energy requirements (ΔH) slightly rises as the electrolysis temperature increases. Formulation is given in Section 4-2-2.

The HTE process is the reverse of the solid oxide fuel cell (SOFC), which normally takes place in the temperature range of 700-1000 °C [36]. In a high-temperature electrolyzer, steam is disassociated in the cathode to produce H_2 and O^{2-} while O^{2-} gets oxidized in the anode to produce oxygen (Equation 70 to Equation 72). The theoretical energy demand of electrolysis (ΔH) is equal to the change in the Gibbs free energy (ΔG) plus the heat demand of the reaction ($\Delta S \times T_{HTE}$). The electricity demand (ΔG) has a negative slope with the reaction temperature (-0.05 kJ/mole of H_2 in the 100-1000 °C range). The savings in electricity consumption comes at the expense of higher heat loads (slope of +0.06 kJ/mole of H_2). Therefore, HTE can be a promising option to produce hydrogen when the electricity supply is constrained and high-temperature heat is available.

$H_2O + 2e \rightarrow H_2 + O^{2-}$	Reduction in cathode of electrolyzer	Equation 70
$O^{2-} \rightarrow \frac{1}{2}O_2 + 2e$	Oxidization in anode of electrolyzer	Equation 71
$H_2O \rightarrow H_2 + \frac{1}{2}O_2$	Net electrolysis equation	Equation 72

Energy efficiency of the electrolysis process itself (η_{els}) is a key performance metric of HTE. It is defined as the ratio of theoretical electricity requirement of the cell (ΔG) to the actual power consumed (Equation 73). E and I are the actual voltage and current of the electrolyzer. No commercial large-scale HTE facility currently exists, but the laboratory-scale systems have energy efficiencies of ~50% at operating temperatures around 850 °C [37].

$\eta_{els} = \frac{\Delta G}{E \times I}$	Energy efficiency of the electrolysis cell	Equation 73

The second promising pathway to produce hydrogen with the aim of high-temperature heat is thermo-chemical decomposition of sulfuric and hydriodic acids. Sulfuric acid can be broken through two endothermic processes in the temperature range of ~300-500 and ~800-900 °C (Equation 74). The temperature of helium gas in the HTGR varies in the range of ~400-900 °C, which makes HTGR a proper candidate for implementing this technology to produce hydrogen.

$H_2SO_4(aq) \rightarrow H_2O(g) + SO_3(g)$	300-500 °C, endothermic	
$SO_3(g) \rightarrow SO_2(g) + 0.5O_2(g)$	800-900 °C, endothermic	
$H_2SO_4(aq) \rightarrow H_2O(g) + SO_2(g) + 0.5O_2(g)$	Net reaction of thermo-chemical decomposition of sulfuric acid	Equation 74

The reaction shown in Equation 74 can be paired with the Bunsen reaction (Equation 75) and decomposition of hydriodic acid (Equation 76) to produce hydrogen and oxygen from water (Equation 77), so called the Iodine-Sulfur (IS) cycle.

$2H_2O + I_2 + SO_2 \rightarrow 2HI + H_2SO_4$	Bunsen reaction, 120 °C, exothermic	Equation 75
$2HI \rightarrow H_2 + I_2$	Thermo-chemical decomposition of hydriodic acid, 450 °C, endothermic	Equation 76
$H_2O \rightarrow H_2 + \frac{1}{2}O_2$	Net reaction for thermo-chemical hydrogen production via IS cycle	Equation 77

The Bunsen reaction (Equation 75) occurs at lower temperatures (~120 °C) and is exothermic while decomposition of hydriodic acid (Equation 76) is endothermic and takes place at ~450 °C. Decomposition of hydrogen iodide can be carried out either in gas phase or in liquid phase with the help of a catalyst [39].

Figure 11 illustrates a conceptual design of the IS cycle producing carbon-free hydrogen and oxygen. The overall thermal-to-hydrogen efficiency of this process is estimated around 50% (HHV) [37, 38].

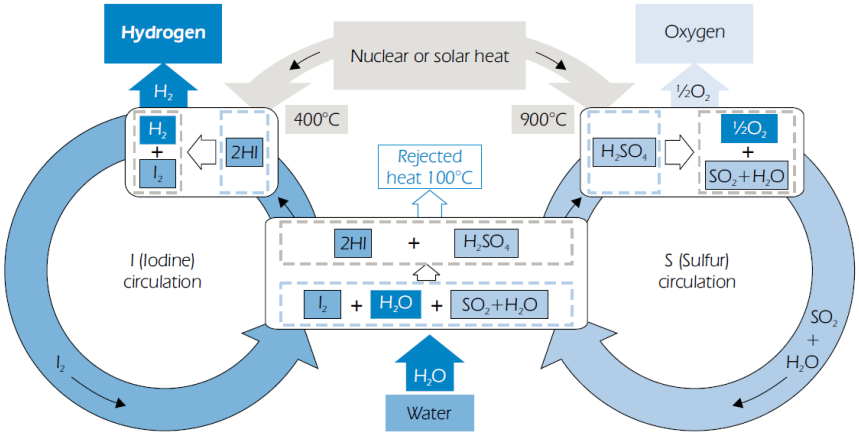

Figure 11: Schematic of the iodine/sulfur thermo-chemical process (IS) to generate hydrogen and oxygen via high-temperature heat. The IS process itself does not consume electricity, heat is the only input. © *OECD/IEA [2006], Hydrogen production and storage: R&D priorities and gaps, IEA Publishing* [36] (permission granted).

Since the IS cycle requires very high-temperature heat (> 800 °C), which is not readily affordable by the compressed air storage plants, this chapter focuses on combining the high-temperature-electrolysis (HTE) concept with conventional CAES as an alternative to A-CAES (physical storage of heat). This process can be done at moderate temperatures (500 °C) [38]. Electricity in addition to the recovered heat of compression is fed to a high temperature electrolyzer to produce hydrogen in the CAES-HTE design (Figure 5). The stored compressed air and hydrogen are used to fuel combustors and generate electricity during the discharge period. Major distinctions of the CAES-HTE design from A-CAES are the elimination of the thermal storage systems (TS) and addition of the HTE unit, hydrogen storage tank, and hydrogen-fueled combustors.

While thermodynamics of hydrogen-fueled (instead of gas-fueled) CAES has been studied earlier (*e.g.* [31]), the concept of CAES supplied by hydrogen generated onsite via HTE is new. This section performs an analytical modeling of CAES-HTE and A-CAES to compare the thermodynamic performance of these two carbon-free advanced CAES designs. The underlying question is whether chemical storage of compression heat in the form of hydrogen produced by a high-temperature electrolyzer (*i.e.* CAES-HTE) is thermodynamically more attractive than the physical storage of heat (A-CAES) or not. A comparable conventional CAES system (*i.e.* with the same number of compression and expansion stages and cavern pressure and volume) is also modeled to benchmark the performance of A-CAES and CAES-HTE. A CAES system paired with a low temperature electrolyzer (CAES-LTE) is also studied in this section to shed light on the pros and cons of producing high-temperature compression heat to generate hydrogen and improve the performance of compressed air storage systems.

Figure 12 illustrates schematics of the A-CAES system simulated here. The compression heat is stored in two thermal energy store units (TS1 and TS2). Intercoolers are eliminated in order to increase the exit temperature of the succeeding compressor stage. A two-stage (LP and HP) compressor is modeled. An aftercooler cools the compressed air prior to storage (between TS2 and cavern).

The expansion train of A-CAES is made up of two stages as well (HP and LP). Withdrawn air is heated by TS1 and TS2 before expansion and power generation (combustors are eliminated in A-CAES). No recuperator is considered here. This is due to the low exit temperature of the LP expander (see Table 10 and Table 11). The exhaust heat exchanger (FHX) cools the discharge stream of the LP expander to the ambient temperature. TS1 absorbs heat from air leaving the low-pressure (LP) compressor and provides heat to air entering the high-pressure (HP) expander. TS2 interacts with the HP compressor and the LP expander.

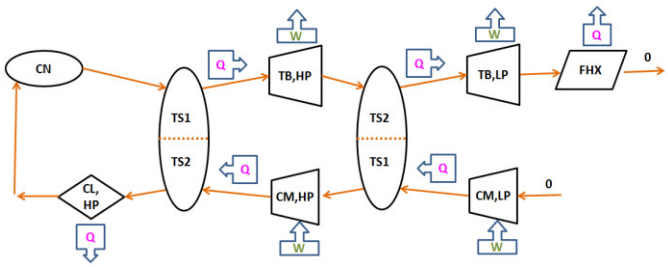

Figure 12: Schematic of the A-CAES system simulated. All of the low-pressure (LP) and a portion of the high-pressure (HP) compression heat are stored in two thermal energy storage facilities (TS1 and TS2). The HP cooler (CL,HP) provides a stream of compressed air at a constant temperature to the cavern (CN). During the discharge phase, TS1 and TS2 heat the compressed air prior to generating work in the high-pressure and low-pressure expanders (TB,HP and TB,LP). No recuperator, intercooler, and combustor are utilized in the A-CAES design. FHX represent the exhaust heat exchanger, which cools the exhaust stream of the LP turbine to the ambient temperature (T_0).

The compressor of CAES-HTE is made up of two stages (Figure 13). An intercooler cools the exhaust of the low-pressure (LP) compressor to a fixed temperature before entering the high-pressure (HP) compressor. Discharge of the HP compressor is fed into a high-temperature electrolyzer to provide the heating energy required for production of steam from water and its electrolysis. Air then passes through the aftercooler before entering the cavern at a constant temperature. The electrolyzer consumes electricity (supplied by the grid) in addition to the thermal energy provided by the hot compressed air leaving the HP compressor. The produced hydrogen and compressed air are stored onsite. The discharge phase of CAES-HTE is identical to that of the conventional CAES system with the difference that the stored hydrogen, instead of natural gas, fuels the combustors. The simulated CAES-LTE system has a similar configuration to CAES-HTE (shown in Figure 13), with the difference that a low-temperature electrolyzer (LTE) is used instead of HTE. Moreover, a three-stage compression train is used since there is no need for producing high-temperature heat in the CAES-LTE system.

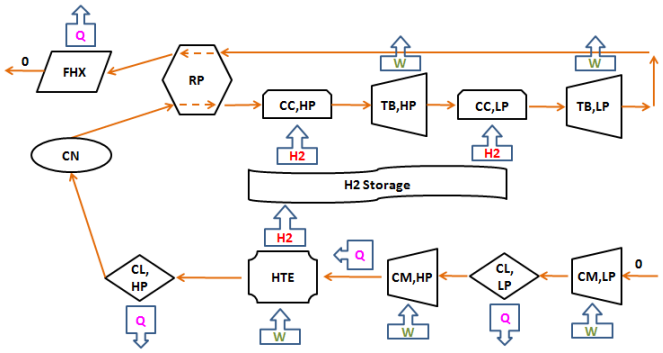

Figure 13: Schematic of the CAES-HTE system. Compression heat lowers electricity demand of the high-temperature electrolyzer (HTE). Heat of the HP compressor (CM, HP) provides both the thermal energy for generating steam (from water supplied at the ambient temperature) and its electrolysis. CL, CN, RP, CC, TB, and FHX stand for compressor's cooler, cavern, recuperator, combustor, expander, and the exhaust heat exchanger. Refer to the nomenclature for the full list of abbreviations.

Finally, Figure 14 shows a conventional CAES system with two stages of compression, instead of the three-stage system shown in Figure 7 and analyzed in Section 3. A two-stage compressor is modeled here so that the performance of A-CAES and CAES-HTE can be benchmarked against conventional CAES.

Increasing the number of compression and cooling stages improves the thermodynamics of compressed air storage plants operating within a specific pressure range. The trade-off analysis between improved thermodynamics, lower operational costs, and higher capital cost of compression and expansion trains made up of several stages is not in the scope of this chapter.

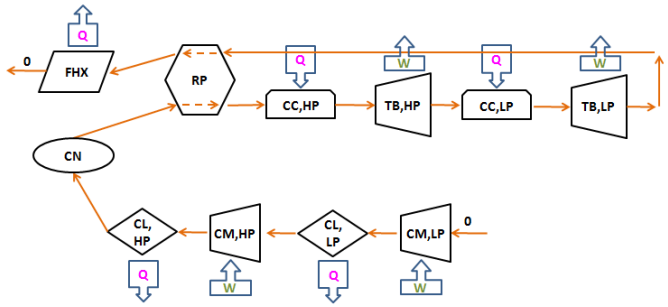

Figure 14: Schematic of the conventional CAES plant modeled to benchmark the performance of A-CAES and CAES-HTE systems shown in Figure 12 and Figure 13. This system is identical to the conventional CAES configuration illustrated in Figure 7 with the distinction that the intermediate-pressure compressor (CM-IP) is eliminated here. Refer to the nomenclature for the full list of the symbols.

The same general assumptions and simplifications listed in Section 2 are applicable to the A-CAES, CAES-HTE, and CAES-LTE models. The compressors have two stages instead of the three stages modeled in Section 3 for

conventional CAES and D-CAES, though. The low- and high-pressure (LP and HP) stages have variable but equal compression ratios. The instantaneous compression ratio is therefore, given by Equation 78 for the simulated two-stage compressors. The compression ratio in the CAES-LTE system is, however, given by Equation 8 since it is assumed to have three stages.

$$CR_{HP} = CR_{LP} = \sqrt[2]{\frac{P_{CN}}{P_0}} = \sqrt[2]{CR}$$ Instantaneous compression ratio of two-stage compressor Equation 78

4-1- Modeling A-CAES

This section provides the specific assumptions made to analyze the A-CAES system shown in Figure 12. The following subsections present the details of the thermodynamic model of A-CAES.

No intercooling is performed in the A-CAES design. The aftercooler of A-CAES is similar to that of conventional CAES; it has a fixed approach temperature (T_{ac}, see Figure 6). Therefore, temperature of the compressed air stream entering the cavern is constant (Equation 6).

The intake temperatures of the expanders (*i.e.* exhaust of TS1 and TS2 during the discharge period) are also assumed constant. However, their values are determined based on the amount of heat stored over the charging phase. Note that the inlet temperatures of expander in the conventional CAES system modeled in Section 3-1 were constant as well but their values were a design parameter (*i.e.* preset). The thermal energy storage units (TS1 and TS2) are modeled isobaric and adiabatic. TS1 absorbs heat from air leaving the low-pressure (LP) compressor and provides heat to air entering the high-pressure (HP) expander. TS2 interacts with the HP compressor and the LP expander.

4-1-1- Charge phase of A-CAES

Equation 6 and Equation 11 are applicable to determine the temperature and mass of compressed air entering the cavern during the charging period. Similarly, Equation 12 to Equation 14 are valid to quantify changes in the mass and temperature of compressed air in the cavern.

The compression work of A-CAES is quantified by applying the First Law to the LP and HP compressors and summing them up (Equation 79). The compression work and discharge temperature of the LP compressor

are quantified by Equation 80 and Equation 81, respectively. Similar formulae can be written for the HP compressor.

$W_{CM} = \int_{P_{em}}^{P_{fl}} (dW_{CM,LP} + dW_{CM,HP})$	Total compression work of A-CAES	Equation 79
$dW_{CM,LP} = dm_{ch} \times C_{p,air} \times \left(T_{in}^{CM,LP} - T_{out}^{CM,LP} \right)$	Incremental work of LP compressor	Equation 80
$T_{out}^{CM,LP} = T_{in}^{CM,LP} - \frac{T_{in}^{CM,LP} - T_{out,ist}^{CM,LP}}{\eta_{ist}^{CM,LP}}$	Instantaneous exit temperature of LP compressor	Equation 81
$T_{out,ist}^{CM,LP} = T_{in}^{CM,LP} \times {CR_{LP}}^{(\gamma-1)/\gamma}$	Isentropic instantaneous exit temperature of LP compressor	

The maximum exit temperature of the HP compressor ($T_{out}^{CM,HP,Max}$) is a preset parameter. The rationale for this design constraint is the following. The exit temperature of the compressor is a key parameter for determining the exergy supplied to and stored in thermal storage (TS), which consequently impacts the temperature of the air entering the expanders. Moreover, there are technical constraints such as the stress on and the fatigue of compressor blades driven by the maximum exit temperature of the compressor.

Thermal storage units (TS1 and TS2) are assumed to have a constant exit temperature during the charging period. The constant exit temperature of TS2 (succeeding the HP compressor) is preset ($T_{out}^{TS2,ch}$). The constant exit temperature of TS1 (preceding the HP compressor) is, however, dictated by the value chosen for maximum discharge temperature of the HP compressor ($T_{out}^{CM,HP,Max}$). Solving the system of equations composed of Equation 82, Equation 83, and Equation 84 finds the fixed inlet temperature of the HP compressor ($T_{in}^{CM,HP}$) that limits the maximum of its exit temperature to the preset value of $T_{out}^{CM,HP,Max}$. Note that $T_{in}^{CM,HP}$ is equal to $T_{out}^{TS1,ch}$.

$CR_{HP,Max} = \sqrt[2]{\frac{P_{fl}}{P_0}} = \sqrt[2]{CR_{Max}}$	Max compression ratio of the two-stage compressor	Equation 82
$T_{out}^{CM,HP,Max} = T_{in}^{CM,HP} + \frac{T_{out,ist}^{CM,HP,Max} - T_{in}^{CM,HP}}{\eta_{ist}^{CM,HP}}$	Relationship between the inlet and exit temperature of HP compressor	Equation 83
$T_{out,ist}^{CM,HP,Max} = T_{in}^{CM,HP} \times \left(CR_{HP,Max}\right)^{\frac{\gamma-1}{\gamma}}$	Relationship between isentropic exit temperature of HP compressor and its inlet temperature	Equation 84

Equation 85 gives the heat stored in TS2 during the charge phase. The inlet temperature of TS2 is equal to the exit temperature of the high-pressure compressor and is a function of the instantaneous compression ratio (see Equation 86 and Equation 87). The exit temperature of TS2 ($T_{out}^{TS2,ch}$) is assumed to be constant throughout the charging process. Equation 88 to Equation 90 show similar formulae for TS1 absorbing heat from compressed air leaving the low-pressure compressor.

$Q_{TS2,ch} = \int_{P_{em}}^{P_{fl}} dm_{air,ch} \times C_{p,air} \times \left(T_{out}^{TS2,ch} - T_{out}^{CM,HP}\right)$	Heat stored in TS2 during charging period	Equation 85
$T_{out}^{CM,HP} = T_{in}^{CM,HP} - \frac{T_{in}^{CM,HP} - T_{out,ist}^{CM,HP}}{\eta_{ist}^{CM,HP}}$	Instantaneous exit temperature of HP compressor	Equation 86
$T_{out,ist}^{CM,HP} = T_{in}^{CM,HP} \times \left(CR_{HP}\right)^{\frac{\gamma-1}{\gamma}}$	Isentropic instantaneous exit temperature of HP compressor	Equation 87
$Q_{TS1,ch} = \int_{P_{em}}^{P_{fl}} dm_{air,ch} \times C_{p,air} \times \left(T_{out}^{TS1,ch} - T_{out}^{CM,LP}\right)$	Heat stored in TS1 during charging	Equation 88
$T_{out}^{CM,LP} = T_{in}^{CM,LP} - \frac{T_{in}^{CM,LP} - T_{out,ist}^{CM,LP}}{\eta_{ist}^{CM,LP}}$	Instantaneous exit temperature of LP compressor	Equation 89
$T_{out,ist}^{CM,LP} = T_{in}^{CM,LP} \times \left(CR_{LP}\right)^{\frac{\gamma-1}{\gamma}}$	Isentropic instantaneous exit temperature of LP compressor	Equation 90

The exergy of the stored heat in TS1 and TS2 can be similarly quantified. The exergy of the air stream (ψ) is calculated according to Equation 2, Equation 4, and Equation 5 since the inlet and outlet temperature and pressure of TS1 and TS2 are all now known.

$\Delta X_{TS1,ch} = \int_{P_{em}}^{P_{fl}} dm_{air,ch} \times \left(\psi_{out}^{TS1,ch} - \psi_{out}^{CM,LP}\right)$	Exergy stored in TS2 during charge	Equation 91
$\Delta X_{TS2,ch} = \int_{P_{em}}^{P_{fl}} dm_{air,ch} \times \left(\psi_{out}^{TS2,ch} - \psi_{out}^{CM,HP}\right)$	Exergy stored in TS2 during charge	Equation 92

Air stream leaving TS2 is cooled in the aftercooler prior to entering the cavern. Equation 93 quantifies the heat rejected in the aftercooler. Equation 94 expresses the total heat that is dissipated by the compressor. This parameter is equal to the heat stored in TS1 and TS2 plus the heat rejected to the ambient environment in the aftercooler of A-CAES.

$Q_{CL} = \int_{P_{em}}^{P_{fl}} dm_{air,ch} \times C_{p,air} \times \left(T_{in}^{CN} - T_{out}^{TS2,ch}\right)$	Heat dissipated by HP aftercooler	Equation 93
$Q_{CM} = Q_{CL} + Q_{TS1,ch} + Q_{TS2,ch}$	Total heat dissipated by the compression train of A-CAES	Equation 94

Equation 21 to Equation 23 remain applicable for quantifying the changes in the internal energy, entropy, and exergy of the air stored in the cavern of A-CAES. Exergy destroyed over the charging period is shown in Equation 95.

$$IX_{ch} = -\Delta X_{ch}^{CN} - W_{CM} + m_{ch} \times \psi_0 - \Delta X_{TS1,ch} - \Delta X_{TS1,ch}$$ Exergy lost during charging phase of A-CAES — Equation 95

4-1-2- Discharge phase of A-CAES

Changes in the mass and temperature of compressed air present in the cavern of A-CAES during the discharge period are expressed by Equation 25 to Equation 29, similar to the conventional CAES model presented in Section 3-1-2.

The analysis assumes perfect storage of heat, *i.e.* all the thermal energy stored during the charging phase is released back to the expanding air. The exit temperature of TS1 and TS2 is assumed to remain constant over the discharge period.

The First Law is applied to perform a series of trials and errors in order to find the fixed (but unknown) exit temperature of TS1 so that the heat released by TS1 during the discharge period becomes equal to the heat previously stored during the charge period (Equation 96 and Equation 97).

$$Q_{TS1,dch} = \int_{P_{fl}}^{P_{em}} dm_{air,dch} \times C_{p,air} \times \left(T_{out}^{TS1,dch} - T_{CN,dch}\right)$$ Heat released by TS1 during discharge phase — Equation 96

$$T_{out}^{TS1,dch} \overset{?}{\Leftrightarrow} Q_{TS1,dch} = Q_{TS1,ch}$$ Finding the exit temperature of TS1 so that the stored and released heats are equal — Equation 97

$T_{CN,dc}$ is the instantaneous temperature of air leaving the cavern (Equation 28). Heat stored in TS1 during the charge phase ($Q_{TS1,ch}$) is already known (Equation 88). Therefore, the exit temperature of ST1 during discharge phase ($T_{out}^{TS1,dch}$) can be determined.

Once the exit temperature of TS1 is calculated, work and discharge temperature of the HP expander are found through applying the First Law to the HP expander (Equation 98 and Equation 99). The instantaneous expansion ratio is expressed by Equation 7.

$W_{TB,HP} = \int_{P_{fl}}^{P_{em}} dm_{air,dch} \times C_{p,air} \times \left(T_{out}^{TS1,dch} - T_{out}^{TB,HP} \right)$	Work generated by HP expander of A-CAES	Equation 98
$T_{out}^{TB,HP} = T_{out}^{TS1,dch} + \eta_{ist}^{TB,HP} (T_{out,is}^{TB,HP} - T_{out}^{TS1,dch})$	Instantaneous discharge temperature of HP expander	Equation 99
$T_{out,ist}^{TB,HP} = T_{out}^{TS1,dch} \times XR_{HP}^{(\gamma-1)/\gamma}$	Isentropic instantaneous discharge temperature of HP expander	

Upon determining the inlet temperature of TS2 (equal to $T_{out}^{TB,HP}$), the First Law is applied to find the exit temperature of TS2 (Equation 100 and Equation 101). The same trial and error procedure explained for TS1 (Equation 96 and Equation 97) is used to pursue this goal.

$Q_{TS2,dch} = \int_{P_{fl}}^{P_{em}} dm_{air,dch} \times C_{p,air} \times \left(T_{out}^{TS2,dch} - T_{out}^{TB,HP} \right)$	Total heat released by TS2 during discharge period of A-CAES	Equation 100
$T_{out}^{TS2,dch} \overset{?}{\Leftrightarrow} Q_{TS2,dch} = Q_{TS2,ch}$	Finding exit temperature of TS2 so that stored and released heats are equal	Equation 101

Similar to the charging phase, the changes in the exergy stock of TS1 and TS2 are quantified with Equation 102 and Equation 103. Since thermal storage systems are modeled as ideal, the exergy released by TS1 and TS2 is equal to exergy previously stored in them during charging.

$\Delta X_{TS1,dch} = \int_{P_{em}}^{P_{fl}} dm_{air,dch} \times \left(\psi_{out}^{TS1,dch} - \psi_{dch}^{CN} \right)$	Exergy released in TS1 during discharge phase of A-CAES	Equation 102
$\Delta X_{TS2,dch} = \int_{P_{em}}^{P_{fl}} dm_{air,dch} \times \left(\psi_{out}^{TS2,dch} - \psi_{out}^{TB,HP} \right)$	Exergy released in TS2 during discharge period of A-CAES	Equation 103

Now that the inlet temperature of the low-pressure turbine is determined (equal to discharge temperature of TS2), the First Law is used to determine the work generated by the LP turbine (Equation 104) and its exit temperature (Equation 105).

$W_{TB,LP} = \int_{P_{fl}}^{P_{em}} dm_{air,dch} \times C_{p,air} \times \left(T_{out}^{TS2,dch} - T_{out}^{TB,LP} \right)$	Total work of LP expander of A-CAES	Equation 104
$T_{out}^{TB,LP} = T_{out}^{TS2,dch} + \eta_{ist}^{TB,LP} (T_{out,ist}^{TB,LP} - T_{out}^{TS2,dch})$	Instantaneous discharge temperature of LP expander	Equation 105
$T_{out,ist}^{TB,LP} = T_{out}^{TS2,dch} \times XR_{LP}^{(\gamma-1)/\gamma}$	Isentropic instantaneous discharge temperature of LP expander	

Finally, heat dissipated in the exhaust heat exchanger is quantified by Equation 106.

$Q_{FHX} = \int_{P_{fl}}^{P_{em}} dm_{air,dch} \times C_{p,air} \times (T_0 - T_{out}^{TB,LP})$	Heat wasted in the exhaust heat exchanger	Equation 106

Equation 40, Equation 41, and Equation 42 remain applicable for calculating changes in the internal energy, entropy, and exergy of cavern over the discharge phase. Equation 107 quantifies the total exergy lost during the discharge phase of A-CAES.

$IX_{dch} = -\Delta X_{dch}^{CN} - W_{TB} - m_{air,dch} \times \psi_{air,dch} - \Delta X_{TS1,dch} - \Delta X_{TS1,dch}$	Exergy lost during discharge of A-CAES	Equation 107

4-1-3- Roundtrip analysis of A-CAES

Once the complete charge and discharge processes of A-CAES are modeled, its overall performance can be evaluated. Equation 45 and Equation 48 remain applicable for expressing the work ratio and exergy density of the plant. Roundtrip exergy efficiency is quantified by Equation 108 (equal to the inverse of work ratio). Since no fuel is consumed, the heat rate and GHG emissions intensity of A-CAES are zero (Equation 109 and Equation 110).

$\eta_{X,AA-CAES} = \frac{W_{TB}}{-W_{CM}}$	Roundtrip exergy efficiency of A-CAES	Equation 108
$HR_{AA-CAES} = \frac{m_{NG}^{CC} \times LHV_{NG}}{W_{TB}} \times 3.6 = 0$	Heat rate of A-CAES	Equation 109
$GI_{AA-CAES} = HR_{AA-CAES} \times GIF_{NG} = 0$	GHG emissions intensity of A-CAES	Equation 110

4-2- Modeling CAES-HTE

In addition to the simplifications and assumptions listed in Section 2, which are applicable to all CAES configurations studied in this chapter, the following specific assumptions are used to simulate the CAES-HTE system illustrated in Figure 13.

An intercooler cools the exhaust stream of the LP compressor to a constant temperature before entering the HP compressor. The maximum discharge temperature of the HP compressor is a design parameter and is preset, similar to the A-CAES model. The exhaust stream of the HP compressor is used to boil water, to heat up the generated steam to the constant temperature of the electrolyzer (T_{HTE}), and to provide the heating energy required for the electrolysis process itself. An aftercooler follows the electrolyzer to lower the

temperature of compressed air to a fixed value ($T_{CN,in}$) before storage. The generated hydrogen is stored onsite to heat the air during the discharge phase. No physical storage of heat is performed, in contrast to the A-CAES design.

The discharge phase of CAES-HTE is identical to that of the conventional CAES with the distinction that hydrogen (produced during charging) fuels the combustors instead of natural gas (an external fuel for conventional CAES).

4-2-1- Discharge phase of CAES-HTE

Since the heating loads of the low- and high-pressure combustors determine the amount of hydrogen fuel needed and consequently the energy demand of the electrolyzer during the charge phase, the discharge phase of CAES-HTE is analyzed first.

Equation 25 to Equation 29 remain applicable for quantifying the changes in the mass and temperature of the compressed air present in the cavern during discharge. Similar to the conventional CAES system, the inlet temperatures of the low-pressure and high-pressure turbines ($T_{in}^{TB,LP}$ and $T_{in}^{TB,HP}$) are preset. Therefore, Equation 30 to Equation 32 quantify the expansion work and the instantaneous exit temperature of HP and LP turbines. The heat load of the LP and HP combustors are determined by applying Equation 33 and Equation 35. Finally, the mass, and exergy of the hydrogen fuel needed are calculated via Equation 112 and Equation 113.

$Q_{CC} = Q_{LP,CC} + Q_{HP,CC}$	Heat load of combustors of CAES-HTE	Equation 111
$m_{H2}^{CC} = \frac{Q_{CC}}{LHV_{H2}}$	Mass of hydrogen fuel needed	Equation 112
$X_{H2}^{CC} = m_{H2}^{CC} \times x_{H2}$	Exergy of hydrogen fuel needed	Equation 113

Equation 40 to Equation 42 remain valid to quantify the changes in the internal energy, entropy, and exergy of the compressed air present in the cavern. The exergy lost during the discharge phase is quantified by Equation 114. Note that the exergy of air stream leaving the plant for the ambient environment ($\psi_{air,dch}$) is zero since the discharge stream of the exhaust heat exchanger is at the ambient conditions.

$I_{dch} = -\Delta X_{dch}^{CN} - \mathrm{W_{TB}} + X_{H2}^{CC} - m_{air,dch} \times \psi_{air,dch}$	Exergy loss of the discharge phase of CAES-HTE	Equation 114

4-2-2- Charge phase of CAES-HTE

Charging process of CAES-HTE (Figure 13) is similar to that of the conventional CAES (Figure 14) with the key difference that exhaust stream of the HP compressor first transfers some of its heat to an electrolyzer and the rest to the aftercooler. As with the A-CAES simulation, the maximum exit temperature of the high-pressure compressor is preset. This parameter dictates the exit temperature of the low-pressure intercooler (a constant but unknown parameter). Note that discharge temperature of the LP intercooler was a preset parameter in the conventional CAES model presented in Section 3-1-1.

Equation 9 to Equation 14 remain applicable to quantify changes in the mass and temperature of compressed air in the cavern during the charge period. Work of the low-pressure compressor and its exit temperature are calculated by applying the First Law to the LP compressor (Equation 115 and Equation 116).

$W_{CM,LP} = \int_{P_{em}}^{P_{fl}} dm_{air,ch} \times C_{p,air} \times (T_{in}^{CM,LP} - T_{out}^{CM,LP})$	Total work of LP compressor	Equation 115
$T_{out}^{CM,LP} = T_{in}^{CM,LP} - \frac{T_{in}^{CM,LP} - T_{out,ist}^{CM,LP}}{\eta_{ist}^{CM,LP}}$	Instantaneous discharge temperature of LP compressor	Equation 116
$T_{out,ist}^{CM,LP} = T_{in}^{CM,LP} \times CR_{LP}^{(\gamma-1)/\gamma}$	Isentropic instantaneous discharge temperature of LP compressor	

The next step after quantifying the inlet temperature of the low-pressure cooler (equal to exit temperature of the low-pressure compressor, Equation 116) is calculating its discharge temperature, which is equal to the inlet temperature of the high-pressure compressor. This temperature is assumed to remain constant during the charging period. Its value, however, is dictated by another design parameter: the maximum exit temperature of the high-pressure compressor. Similar to A-CAES model, solving the system of equations made up of Equation 82, Equation 83, and Equation 84 determines the inlet temperature of the high-pressure compressor ($T_{in}^{CM,HP}$, which is equal to $T_{out}^{CL,LP}$).

Once the inlet temperature of the high-pressure compressor is known, its work and instantaneous exit temperature can be determined by applying Equation 117 and Equation 118.

$W_{CM,HP} = \int_{P_{em}}^{P_{fl}} dm_{air,ch} \times C_{p,air} \times (T_{in}^{CM,HP} - T_{out}^{CM,HP})$	Total work of HP compressor	Equation 117
$T_{out}^{CM,HP} = T_{in}^{CM,HP} - \frac{T_{in}^{CM,HP} - T_{out,ist}^{CM,HP}}{\eta_{ist}^{CM,HP}}$	Instantaneous discharge temperature of HP compressor	Equation 118
$T_{out,ist}^{CM,HP} = T_{in}^{CM,HP} \times CR_{HP}^{(\gamma-1)/\gamma}$	Isentropic instantaneous discharge temperature of HP compressor	

As illustrated in Figure 10, the energy demand of the electrolyzer depends on the reaction temperature. For the sake of simplicity, this analysis assumes a fixed electrolysis temperature, equal to the average exit temperature of the HP compressor during the charging period (see Equation 123).

$CR_{HP,Min} = \sqrt[2]{\frac{P_{em}}{P_0}} = \sqrt[2]{CR_{Min}}$	Minimum compression ratio of the two-stage compressor	Equation 119
$CR_{HP,Max} = \sqrt[2]{\frac{P_{fl}}{P_0}} = \sqrt[2]{CR_{Max}}$	Maximum compression ratio of the two-stage compressor	Equation 120
$T_{out}^{CM,HP,Min} = T_{in}^{CM,HP} - \frac{T_{in}^{CM,HP} - T_{out,ist}^{CM,HP,Min}}{\eta_{ist}^{CM,HP}}$	Minimum instantaneous exit temperature of HP compressor	Equation 121
$T_{out,ist}^{CM,HP,Min} = T_{in}^{CM,HP} \times CR_{HP,Min}^{(\gamma-1)/\gamma}$		
$T_{out}^{CM,HP,Max} = T_{in}^{CM,HP} - \frac{T_{in}^{CM,HP} - T_{out,ist}^{CM,HP,Max}}{\eta_{ist}^{CM,HP}}$	Maximum instantaneous exit temperature of HP compressor	Equation 122
$T_{out,ist}^{CM,HP,Max} = T_{in}^{CM,HP} \times CR_{HP,Max}^{(\gamma-1)/\gamma}$		
$T_{HTE} = 0.5 \times (T_{out}^{CM,HP,Max} + T_{out}^{CM,HP,Min})$	Reaction temperature of electrolysis	Equation 123

Since the instantaneous inlet temperature of the electrolyzer is known as a function of the compression ratio (equal to $T_{out}^{CM,HP}$, Equation 118), one can apply the First Law to the electrolyzer to find its constant exit temperature (T_{out}^{HTE}), which results in the desired heat load of the electrolyzer ($Q_{HTE,total}$, quantified in the next paragraph). The trial-and-error process is again used to find T_{out}^{HTE} as shown in Equation 124 and Equation 125.

$Q_{HTE} = \int_{P_{em}}^{P_{fl}} dm_{air,ch} \times C_{p,air} \times (T_{out}^{HTE} - T_{in}^{HTE})$	Total heat absorbed by HTE from the exhaust of HP compressor	Equation 124
$T_{out}^{HTE} \overset{?}{\Leftrightarrow} Q_{HTE,total} = Q_{HTE}$	Applying trial-and-error to find exit temperature of HTE	Equation 125

Total heat demand of the electrolyzer ($Q_{HTE,total}$) is based on mass of hydrogen needed to fuel the combustors during the discharge process (Equation 112). This heating load is made up of four components: sensible heat load to bring water fed to the electrolyzer at the ambient temperature to 100 °C ($Q_{Sns,water}$), latent heat load to boil water ($Q_{Lnt,water}$), sensible heat load to bring steam from 100 °C to the electrolysis temperature ($Q_{Sns,steam}$), and finally the heat required for the electrolysis of steam itself ($Q_{HTE,steam}$).

As shown in the electrolysis reaction (Equation 72), one mole of hydrogen (2 g) and half a mole of oxygen (16 g) are generated per mole of water (18 g) electrolyzed. The relationship between mass of hydrogen and water can therefore, be expressed by Equation 126

$m_{H_2O}^{HTE} = m_{H2}^{CC} \times \frac{M_{H_2O}}{M_{H_2}} \times \frac{n_{H_2O}}{n_{H_2}}$	Mass of water electrolyzed per mole of hydrogen generated	Equation 126

The sensible heat load of water and steam and the latent heat are quantified based on Equation 127, Equation 128, and Equation 129.

$Q_{Sns,water} = m_{H_2O}^{HTE} \times C_{p,water} \times (T_{boil} - T_0)$	Sensible heat load of HTE to heat up water to boiling temperature	Equation 127
$Q_{Sns,steam} = m_{H_2O}^{HTE} \times C_{p,steam} \times (T_{HTE} - T_{boil})$	Sensible heat load of HTE to heat up steam to the electrolysis temperature	Equation 128
$Q_{Ltn,water} = m_{H_2O}^{HTE} \times C_{Lnt,water}$	Latent heat load of HTE to produce steam	Equation 129

For the electrolysis process itself, the total energy requirement (ΔH), the change in entropy (ΔS), and the electricity demand (change in the Gibbs free energy, ΔG) are determined according to Equation 130 to Equation 132.

$$\Delta H_{HTE}(T) = n_{H_2} \times \Delta h_{H_2}(T) + n_{O_2} \times \Delta h_{O_2}(T) - n_{H_2O} \times \Delta h_{H_2O}(T)$$ Energy demand of HTE process Equation 130

$$\Delta S_{HTE}(T) = n_{H_2} \times \Delta s_{H_2}(T) + n_{O_2} \times \Delta s_{O_2}(T) - n_{H_2O} \times \Delta s_{H_2O}(T)$$ Entropy change of the HTE process Equation 131

$$\Delta G_{HTE}(T) = \Delta H_{HTE}(T) - T_{HTE} \times \Delta S_{HTE}(T)$$ Electric (work) load of HTE process Equation 132

The changes in specific enthalpy (Δh) and entropy (Δs) of the reactant and products are expressed by Equation 133 and Equation 134, respectively. Symbols Δh_f^0 and s^0 represent the standard specific enthalpy of formation and the standard specific entropy. Specific heat (c_p,) is itself a function of temperature. The values for the standard enthalpy of formation, standard entropy, and specific heat of water and steam are tabulated in Table 6.

$$\Delta h(T) = \Delta h_f^0 + \int_{T_0}^{T_{HTE}} C_p(T) \times dT$$ Change in specific enthalpy Equation 133

$$\Delta s(T) = s^0 + \int_{T_0}^{T_{HTE}} \frac{C_p(T)}{T} \times dT$$ Change in specific entropy Equation 134

Therefore, Table 6 and Equation 130 to Equation 134 can be used to quantify the heat and work load of the electrolysis process, as shown in Equation 135 and Equation 136.

$$Q_{HTE,steam} = T_{HTE} \times \Delta S_{HTE}(@T_{HTE})$$ Heat load to electrolysis steam at T_{HTE} Equation 135

$$W_{HTE} = \frac{\Delta G_{HTE}(@T_{HTE})}{\eta_{fd}}$$ Work load of the electrolyzer Equation 136

Table 6: Thermodynamic properties used to quantify energy demand of electrolysis [40, 41].

	Δh_f^0(kJ/mol)	s^0(kJ/kmol/K)	C_p(kJ/kmol/K)	C_{Lnt}(kJ/mol)	n
$H_2(g)$	0	131	$27.28 + 0.00326 \times T + 50000/T^2$	NA	1
$O_2(g)$	0	205	$29.96 + 0.00418 \times T - 167000/T^2$	NA	0.5
$H_2O(l)$	−285.83	70	75.44	40.7	1
$H_2O(g)$	−241.82	189	$30 + 0.01071 \times T + 33000/T^2$	NA	1

Finally, the total heat load of the electrolyzer ($Q_{HTE,total}$) is expressed by Equation 137. As discussed earlier, this variable is plugged into Equation 124 and Equation 125 to find the discharge temperature of the electrolyzer.

$Q_{HTE,total} = Q_{Sns,water} + Q_{Lnt,water} + Q_{Sns,steam} + Q_{HTE,steam}$	Total heat load of the electrolyzer	Equation 137

The First Law is applied to each cooler to determine the heat removed by the LP intercooler and HP aftercooler (Equation 138 to Equation 140). Note that the discharge temperature of the aftercooler is preset to the approach temperature plus the ambient temperature ($T_{ac} + T_0$), same as the conventional CAES model. The intake temperature of the HP compressor ($T_{in}^{CM,HP}$) is equal to the exit temperature of the LP intercooler. The total compression heat available for recovery is equal to the heat dissipated in the coolers (Equation 138) plus the heat load of the electrolyzer (Equation 137), as shown in Equation 141.

$Q_{CL} = \int_{P_{em}}^{P_{fl}} (dQ_{CL,LP} + dQ_{CL,HP})$	Heat dissipated in the compressor coolers	Equation 138
$dQ_{CL,LP} = dm_{air,ch} \times C_{p,air} \times (T_{in}^{CM,HP} - T_{out}^{CM,LP})$	Incremental heat of LP cooler	Equation 139
$dQ_{CL,HP} = dm_{air,ch} \times C_{p,air} \times (T_{CN,in} - T_{out}^{HTE})$	Incremental heat of HP cooler	Equation 140
$Q_{CM} = Q_{CL} + Q_{HTE,total}$	Total compression heat available for recovery in CAES-HTE	Equation 141

Equation 21 to Equation 23 remain valid for quantifying the changes in the internal energy, entropy, and exergy of the compressed air in the cavern. The exergy lost over the charging process of CAES-HTE is calculated by Equation 142.

$IX_{ch} = -\Delta X_{ch}^{CN} - W_{CM} - W_{HTE} + m_{ch} \times \psi_0 + X_{H2}^{CC}$	Exergy lost during charging phase of CAES-HTE	Equation 142

4-2-3- Roundtrip analysis of CAES-HTE

The CAES-HTE system does not use any fossil fuel; therefore, its heat rate and GHG emissions are zero while its roundtrip exergy efficiency is quantified by Equation 143. Work ratio of CAES-HTE is determined by Equation 144. CAES-HTE has a higher work ratio compared to a similar conventional CAES system because of

the work load of the electrolyzer (W_{HTE}). Equation 48 remains applicable to calculate the exergy density of the plant.

$\eta_{X,CAES-HTE} = \frac{W_{TB}}{-W_{CM} - W_{HTE}}$	Roundtrip exergy efficiency of CAES-HTE	Equation 143
$WR_{CAES-HTE} = \frac{-W_{CM} - W_{HTE}}{W_{TB}}$	Work ratio of CAES-HTE	Equation 144
$HR_{CAES-HTE} = 0$	Heat rate of CAES-HTE	Equation 145
$GI_{CAES-HTE} = HR_{CAES-HTE} \times GIF_{H_2} = 0$	GHG emissions intensity of CAES-HTE	Equation 146

The analysis of CAES-LTE system is similar to of the CAES-HTE plant with the difference that the compression heat is fed to a low-temperature electrolyzer (LTE) to produce hydrogen and no constraint is imposed on the maximum discharge temperature of the high-pressure compressor ($T_{out}^{CM,HP,Max}$). Moreover, the exit temperature of the low-pressure cooler ($T_{out,hot}^{CL}$) is constant and preset to the ambient temperature plus the approach temperature ($T_0 + T_{ac}$), similar to the conventional CAES model (see Figure 6 and Equation 6).

4-3- Modeling conventional CAES

A comparable conventional CAES system to the modeled A-CAES and CAES-HTE systems is also considered to benchmark the performance of these two advanced CAES systems. This conventional CAES system is identical to the system analyzed in Section 3-1, with the exception that its compressor has two stages (Figure 14) instead of three stages (Figure 7).

Since the compressor is made up of two stages, Equation 78 is used instead of Equation 8 to quantify the instantaneous compression ratio. The compression work and heat of the intermediate-pressure compressor stage are zero in Equation 15 and Equation 18, as the compression train is composed of only low- and high-pressure stages.

4-4- Numerical example: A-CAES and CAES-HTE models

This section provides a series of numerical examples to compare the thermodynamics of conventional CAES, A-CAES, and CAES-HTE.

The two key design parameters of interest are the storage pressure (5-10 MPa) and the allowable maximum exit temperature of the HP compressor ($T_{out}^{CM,HP,Max}$=600 °C, applicable to CAES-HTE and A-CAES only). The operating pressure of the cavern in the real world is constrained by the geomechanics of the reservoir and mechanical design of the compressor and turbines. The pressure range impacts the exergy density of the storage plant. One of the critiques against adoption of compressed air storage technologies, particularly A-CAES, at scale is their low exergy density and hence the need for large air storage units. Increasing the storage pressure of compressed air will help in relaxing this limitation.

The discharge temperature of the HP compressor determines the exergy available to directly (A-CAES) or indirectly (CAES-HTE) heat the expanding air. Nevertheless, high operating temperatures of the compressor pose technical challenges for their design and also operations of the thermal storage units (*e.g.* higher rates of heat loss). Therefore, the maximum discharge temperature of the HP compressor is treated as the second primary design parameter of interest.

4-4-1- Base case simulation of CAES-HTE and A-CAES

Table 7, Table 8, and Table 9 list the input parameters for thermodynamic analysis of A-CAES, CAES-HTE, and conventional CAES (respectively) performed in the base case. Note that two key optimistic assumptions are included in these simulations. First, the heat losses from TS1 and TS2 are negligible, all the thermal energy and exergy stored are released back to the expanding air. Moreover, energy efficiency of the HTE cell is assumed 100%; therefore, the theoretical and actual work load of the electrolyzer are equal (see Equation 73). Table 10 gives the key simulation results for CAES, A-CAES, and CAES-HTE, based on the input parameters shown in Table 7, Table 8, and Table 9 (*i.e.* base case scenario).

The compression work of A-CAES and CAES-HTE (15,220 GJ) is higher than of conventional CAES (12,110 GJ). This 25% increase is driven by limited intercooling during the charging process; therefore, the work of the HP compressor in A-CAES and CAES-HTE is higher than of conventional CAES. Work load of the LP compressor is equal for the three systems. Elevated compression work can be a potential drawback for A-CAES and CAES-HTE if the electricity used to charge the cavern is scarce or carbon intensive.

Table 7: Input parameters to study the performance of A-CAES system.

Parameter	Value	Parameter	Value	Parameter	Value
γ_{air}	1.4	V_{CN}	0.56 Mm^3	$T_{in,cold}^{CL}$	25 $°C$
$C_{p,air}$	1.006 $kJ/(kg.K)$	η_{is}^{TB}	85%	R_{air}	0.287 $kJ/(kg.K)$
$P_{CN,fl}$	10 MPa	$T_{out}^{CM,HP,Max}$	600 $°C$	$Stage_{CM}$	2
$P_{CN,em}$	5 MPa	T_{ac}	30 $°C$	$Stage_{TB}$	2
η_{is}^{CM}	85%	$T_{out}^{TS2,ch}$	100 $°C$		

Table 8: Input parameters to analyze the CAES-HTE configuration.

Parameter	Value	Parameter	Value	Parameter	Value
γ_{air}	1.4	V_{CN}	0.56 Mm^3	x_{H2}	114 $\frac{MJ}{kg}$
$C_{p,air}$	1.006 $\frac{kJ}{kg\times K}$	R_{air}	0.287$\frac{kJ}{kg\times K}$	LHV_{H2}	120 $\frac{MJ}{kg}$
$P_{CN,fl}$	10 MPa	$T_{out}^{CM,HP,Max}$	600 $°C$	GIF_{H2}	0
$P_{CN,em}$	5 MPa	η_{is}^{TB}	85%	$Stage_{CM}$	2
η_{is}^{CM}	85%	$T_{in}^{TB,LP}$	850 $°C$	$Stage_{TB}$	2
T_{ac}	30 $°C$	T_{et}	130 $°C$	$T_{in,cold}^{CL}$	25 $°C$
$T_{in}^{TB,HP}$	530 $°C$	η_{fd}	100%		

The A-CAES system is the most efficient configuration (UF_{CM}= 96%) with respect to utilizing the available compression heat compared to CAES-HTE (55%) and conventional CAES (zero). Its expander, however, generates 34% less work (10,580 GJ) compared to CAES and CAES-HTE (15,990 GJ), with the same storage pressure and volume. This is because the inlet temperatures of the expanders of A-CAES are lower (no fuel combustion).

A-CAES has the highest storage efficiency (70%) compared to CAES-HTE (53%) and conventional CAES (54%). A-CAES has a moderate work ratio (~1.44) compared to that of CAES-HTE (1.88). Conventional CAES has the lowest work ratio (~0.76) since it burns natural gas at a rate of 4.0 GJ per MWh of electricity generated.

Assessing the competitiveness of these storage technologies in low GHG-intensive grids requires a comprehensive thermodynamic and economic analysis, which is beyond the scope of this chapter. Nevertheless, the simple thermodynamic analysis presented here indicates that prospects of CAES-HTE are lower compared to A-CAES due to its low exergy efficiency and high work ratio, let alone the technical and economic complications of high-temperature electrolyzers, hydrogen storage, and hydrogen-fueled combustors.

Table 9: Input parameters to evaluate the thermodynamics of the conventional CAES used to benchmark performance of A-CAES and CAES-HTE.

Parameter	**Value**	**Parameter**	**Value**	**Parameter**	**Value**
γ_{air}	1.4	V_{CN}	0.56 Mm^3	LHV_{NG}	50 $\frac{MJ}{kg}$
$C_{p,air}$	1.006 $\frac{kJ}{kg \times K}$	R_{air}	0.287$\frac{kJ}{kg \times K}$	GIF_{NG}	66 $\frac{kg}{GJ}$
$P_{CN,fl}$	10 MPa	$T_{out}^{CM,HP,Max}$	600 °C	x_{NG}	50 $\frac{MJ}{kg}$
$P_{CN,em}$	5 MPa	$T_{in}^{TB,HP}$	530 °C	T_{ac}	30 °C
η_{is}^{CM}	85%	$T_{in}^{TB,LP}$	850 °C	T_{et}	130 °C
η_{is}^{TB}	85%	$T_{in,cold}^{CL}$	25 °C		

This analysis also highlights some shortcomings of A-CAES. Exergy density of A-CAES (~5.2 kWh/m^3) is about 65% of that of comparable conventional CAES and CAES-HTE systems (~7.9 kWh/m^3). In other words, A-CAES would require ~50% more cavern volume to generate the same amount of work, everything else being equal. Another shortcoming of A-CAES is the low discharge temperature of its low-pressure turbine. In the base case simulation of A-CAES system, the minimum exit temperature of the LP turbine reaches ~180 °C, which is much less compared to of conventional CAES and CAES-HTE systems (~390 °C). If this temperature reaches below the freezing point, the moisture in the air can freeze and damage the turbine.

The simulation results presented in Table 10 are based on an ideal electrolysis process (with an energy efficiency of 100%) while the experimental literature reports efficiencies around 50% [37]. Moreover, the energy requirements to compress hydrogen for storage purposes are ignored, which will degrade the storage

efficiency of CAES-HTE system even more. Figure 15 illustrates the dependence of the overall exergy efficiency of the storage plant to the energy efficiency of the electrolyzer cell. An energy efficiency of 50% corresponds to a roundtrip exergy efficiency of 36% compared to a storage efficiency of 53% when assuming an ideal electrolyzer for the CAES-HTE system.

The total heat and work load of the high-temperature electrolyzer (HTE) are 7,960 and 14,825 GJ, respectively. Note that only ~40% of this heating load (3,260 GJ) is used for the electrolysis process itself, the rest is consumed to generate steam at the electrolyzer's temperature. The total heat and work load of the HTE are ~125% higher and 15% lower compared to the heat load (3,565 GJ) and work demand (17,395 GJ) if the electrolysis was performed at the ambient conditions ($T_0 = 25\ °C$) instead of at the elevated temperature ($T_{HTE} = 555\ C$). Total energy requirements of HTE (22,785 GJ) is roughly 10% higher than of electrolysis at the ambient temperature (20,960 GJ).

If hydrogen produced via electrolysis of water at the ambient temperature (low-temperature electrolysis, LTE) is used to power the combustors of CAES, the roundtrip exergy efficiency of such a LTE-CAES system would be ~54% (with a pressure range of 5-7 MPa for the cavern). This value is very similar to that of the CAES-HTE system (~53%, assuming an energy efficiency of 100% for the electrolyzer). This indicates that lower electricity demand of the high-temperature electrolyzer is balanced by the higher compression work of CAES-HTE. Therefore, roundtrip exergy efficiency of CAES-LTE is comparable to of CAES-HTE. Electricity demand of HTE is lower than of LTE; therefore, the storage efficiency of CAES-HTE is less sensitive to the energy efficiency of the electrolyzer compared to CAES-LTE (Figure 15).

Table 10: Simulation results for the thermodynamic analysis of AA-CAE and CAES-HTE in the base case scenario (inputs tabulated in Table 7, Table 8, and Table 9). NA stands for Not Applicable.

	CAES	**A-CAES**	**CAES-HTE**
W_{CM} (GJ)	12,110	15,220	15,220
$Q_{HTE,total}$ (GJ)	NA	NA	7,960
$Q_{HTE,steam}$ (GJ)	NA	NA	3,260
W_{HTE} (GJ)	NA	NA	14,825
T_{HTE} (GJ)	NA	NA	555
Q_{TS} (GJ)	NA	13,615	NA
X_{TS} (GJ)	NA	6,250	NA
Q_{CL} (GJ)	11,465	962	6,620
UF_{CM} (%)	0	96	55
W_{TB} (GJ)	15,990	10,580	15,990
Q_{CC} (GJ)	17,590	0	17,590
η_X (%)	53.8	69.5	53.2
WR	0.76	1.44	1.88
HR (GJ/MWh)	4.0	0	0
$X\rho$ (kWh/m^3)	7.9	5.2	7.9
GI (kgCO_2/MWh)	261	0	0
X_{input} (GJ)	29,715	15,220	30,040
IX_{ch} (GJ)	4,295	1,154	5,460
X_{output} (GJ)	15,990	10,580	15,990
IX_{dch} (GJ)	9,430	3,490	8,590
$T_{out}^{TB,\mathrm{LP},Min}$ (°C)	391	181	391
m_{fuel} (kg)	3.52×10^5	0	1.47×10^5
m_{air} (kg)	2.12×10^7		

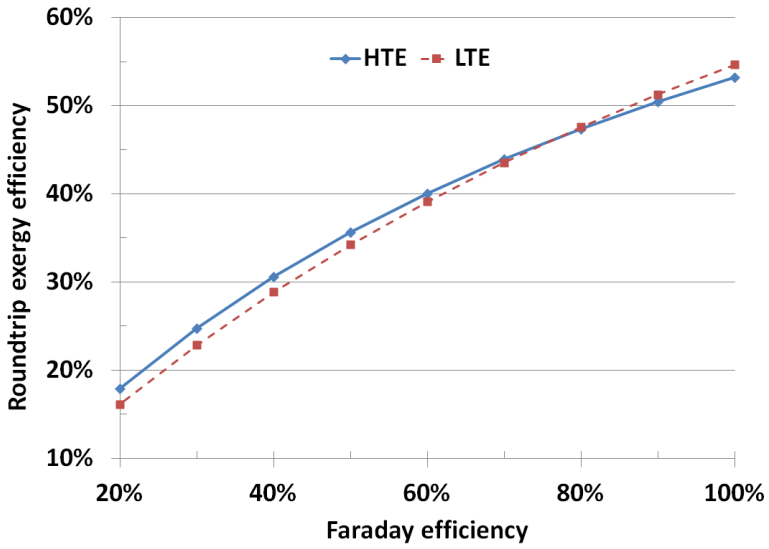

Figure 15: Effect of energy efficiency of the electrolyzer on the roundtrip exergy efficiency of CAES-HTE and CAES-LTE. The electrolysis temperature for the HTE and LTE processes is 555 °C and 25 °C, respectively. Electrolysis efficiencies of 100% and 50% correspond to overall storage efficiencies of 53% and 36%, for the CAES-HTE plant. The corresponding values for the LTE-CAES facility are 55% and 34%.

The economics of A-CAES and CAES-HTE are less attractive compared to conventional CAES unless some emissions restrictions are in place. As shown in Table 10, the inside-the-fence emissions intensity of conventional CAES is ~260 $kgCO_2e/MWh$ while A-CAES and CAES-HTE emit no GHG. The inside-the-fence emissions can be misleading though as the GHG emissions of the electricity consumed to charge these plants are not included. Figure 16 illustrates the adjusted (total) emissions of these three plants, as functions of the GHG emissions intensity of the electricity consumed by the compressor. The emissions intensity of the conventional CAES facility is less sensitive to the emissions intensity of the charging electricity because of its lower work ratio (driven by combustion of natural gas). The breakeven point for CAES and CAES-HTE, defined where the GHG emissions intensity of CAES-HTE exceeds of CAES is ~230 $kgCO_2/MWh$ while this value is ~380 for A-CAES.

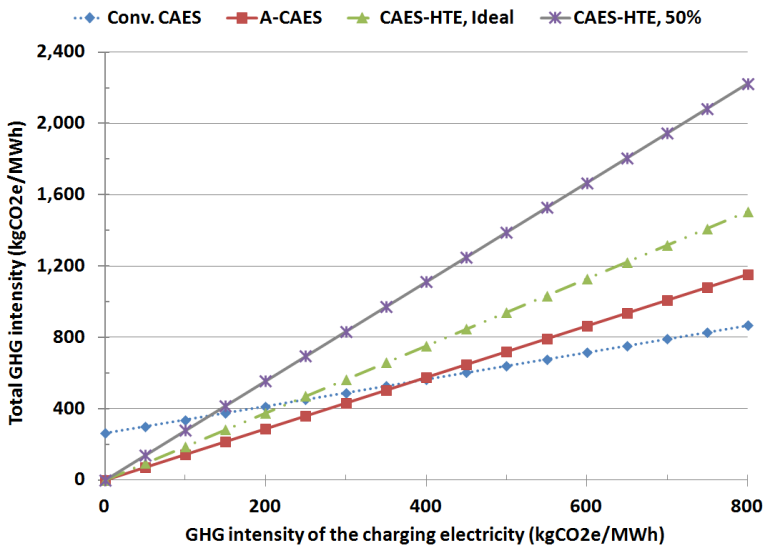

Figure 16: Total GHG emissions of the conventional CAES, A-CAES, and CAES-HTE plants adjusted for the emissions intensity of the electricity used to charge the cavern. Two CAES-HTE systems are modeled: ideal (electrolysis efficiency of 100% for the high-temperature electrolyzer, "CAES-HTE, Ideal") and an electrolyzer with an energy efficiency of 50% ("CAES-HTE, 50%"). All other input parameters are the same as Table 7, Table 8, and Table 9. Performance of the CAES-LTE is similar to of CAES-HTE.

4-4-2- Sensitivity to exit temperature of HP compressor

The maximum allowable exit temperature of the high-pressure compressor ($T_{out}^{CM,HP,Max}$) was chosen as a key design parameter in the simulation of A-CAES and CAES-HTE. Table 11 and Table 12 present the sensitivity of the CAES-HTE and A-CAES performance to this parameter while all other parameters are the same as the base case scenario (provided in Table 8 and Table 7, respectively).

Setting a higher exit temperature for the high-pressure compressor translates to a higher inlet temperature for the HP compressor and to less cooling in the LP intercooler (since the compression ratio is constant). This provides more thermal energy for the electrolysis process and reduces its electricity demand because the electrolysis process takes place at higher temperatures (see Figure 10). Nevertheless, less intercooling increases the work load of the HP compressor, which has a negative impact on the work ratio of the storage plant. As shown in Table 11, the net effect of a higher compression work and a lower electrolysis work is an increase in the exergy consumption of the CAES-HTE to charge the cavern. The total input exergy increases from ~29.4 TJ to 31.9 TJ as the maximum exit temperature of the high-pressure compressor increases from

500 °C to 890 °C. Thermodynamics of the discharge phase is insensitive to these changes (the exergy released by the plant remains ~16.0 TJ).

Storage efficiency of the CAES-HTE system drops from 54% to 50% as the maximum allowable exit temperature of the high-pressure compressor is raised from 500 to 890 °C. Work ratio follows the reverse trend of efficiency; it increases from 1.84 to 1.99. In summary, the simulation results indicate that increasing the maximum discharge temperature of the HP compressor negatively impacts the roundtrip exergy efficiency of CAES-HTE.

As shown in Table 12, raising the exit temperature of the high-pressure compressor ($T_{out}^{CM,HP,Max}$) increases the compression work of the A-CAES system, similar to CAES-HTE. This is because less intercooling is performed and consequently, the inlet temperature to the high-pressure compressor is elevated. At the same time, more heat can be stored and utilized to heat the expanding air. The turbine's total work increases slightly (from ~10.4 to 10.9 TJ) as $T_{out}^{CM,HP,Max}$ is raised from 500 to 890 °C. This small increase (5%) in the expansion work despite much higher (~30%) increase in the thermal energy stored (Q_{TS}) is because the thermal energy recovered and stored in TS1 (Q_{TS1}), and consequently the work generated by the HP turbine ought to decrease to facilitate higher exit temperatures for the HP compressor. Note that TS1 precedes the HP compressor and HP expander.

The net effect of increasing the exit temperature of the high-pressure compressor ($T_{out}^{CM,HP,Max}$) is lowering the storage efficiency of A-CAES. The roundtrip exergy efficiency degrades from 73% to 60% when the maximum discharge temperature of the HP compressor rises from 500 to 890 °C. Exergy density of the cavern improves slightly (by ~5%), which is due to small increases in the work generated by the expanders.

Comparing Table 11 and Table 12 suggests that the storage efficiency of A-CAES is more sensitive to the temperature of air stream leaving the compressor. Raising the maximum exit temperature of the HP compressor from 500 to 890 °C changes efficiency of A-CAES and CAES-HTE in the range of 73-60% and 54-50%, respectively. Increasing the discharge temperature of the HP compressor while keeping the storage pressure the same will degrade the storage efficiency of the plants, especially for A-CAES, while it slightly improves the exergy density.

Table 11: Sensitivity of the thermodynamics of CAES-HTE to the maximum allowable discharge temperature of the high-pressure compressor ($T_{out}^{CM,HP,Max}$). All other input parameters of the simulation are the same as of Table 8.

	$T_{out}^{CM,HP,Max}$ (°C)				
	500	**600**	**700**	**800**	**890**
W_{CM} (GJ)	14,200	15,220	16,235	17,250	18,165
Q_{HTE} (GJ)	7,235	7,960	8,700	9,450	10,145
W_{HTE} (GJ)	15,190	14,825	14,445	14,065	13,720
T_{HTE} (°C)	460	555	650	745	831
W_{TB} (GJ)	15,990				
Q_{CC} (GJ)	17,595				
WR	1.84	1.88	1.92	1.96	1.99
η_X (%)	54.4	53.2	52.1	51.1	50.1
$X\rho_{CN}$ (kWh/m^3)	7.9				
X_{input} (GJ)	29,395	30,040	30,680	31,315	31,885
X_{output} (GJ)	15,990				

A key design constraint in this modeling exercise was the discharge temperature of the expanders. This parameter is desired to remain above the freezing point to avoid damaging the integrity of the expanders. Referring to Table 12, the exit temperature of the HP turbine drops as the maximum exit temperature of the HP compressor ($T_{out}^{CM,HP,Max}$) increases because less heat can be stored in TS1 and then released to the compressed air entering the HP expander. This temperature even drops below the freezing point when the maximum exit temperature of the HP compressor is raised above 700 °C. Designing A-CAES in the real world would need to include a detailed model to optimize the performance of the plant and eliminate freezing concerns. For instance, the HP expander may be designed to have a lower expansion ratio compared to the LP expander. This change will raise and decrease the exit temperature of the HP and LP expanders, respectively.

Table 12: Sensitivity of thermodynamics of A-CAES to the maximum exit temperature of the high-pressure compressor ($T_{out}^{CM,HP,Max}$). All other input parameters are the same as of Table 7.

	$T_{out}^{CM,HP,Max}$ (°C)				
	500	**600**	**700**	**800**	**890**
W_{CM} (GJ)	14,200	15,220	16,235	17,250	18,165
Q_{TS} (GJ)	12,600	13,615	14,630	15,650	16,565
Q_{TS1} (GJ)	4,810	3,790	2,765	1,745	825
Q_{TS2} (GJ)	7,790	9,825	11,865	13,905	15,740
X_{TS} (GJ)	5,235	6,250	7,270	8,285	9,200
W_{TB} (GJ)	10,425	10,575	10,610	10,880	10,915
$W_{TB,HP}$ (GJ)	4,590	4,195	3,725	3,400	2,980
$W_{TB,LP}$ (GJ)	5,830	6,380	6,885	7,480	7,935
WR	1.36	1.44	1.53	1.59	1.67
η_X (%)	73.4%	69.5%	65.4%	63.1%	60.1%
$X\rho$ (kWh/m^3)	5.2	5.2	5.3	5.4	5.4
X_{input} (GJ)	14,200	15,220	16,235	17,250	18,165
X_{output} (GJ)	10,425	10,575	10,610	10,880	10,915
$T_{out}^{TB,HP,Min}$ (°C)	54	26	-8	-31	-61
$T_{out}^{TB,LP,Min}$ (°C)	142	181	217	259	295

4-4-3- Sensitivity to storage pressure

Storage pressure is the second key design parameter whose effects on the thermodynamics of conventional CAES, A-CAES, and CAES-HTE are analyzed here. Table 13 provides the sensitivity of the CAES-HTE model to the maximum storage pressure. All parameters are the same as of Table 8, except the maximum pressure of the cavern, which is varied in the range of 7-12 MPa, compared to 10MPa in the base case. The compression work and hydrogen demand (and consequently, heat and electricity load of the electrolyzer) increase at elevated storage pressures because more air needs to be stored and heated. The operating temperature of the electrolyzer slightly decreases at higher cavern pressures in the CAES-HTE model presented here. This is because the maximum allowable temperature of the HP compressor is assumed to remain constant. Higher cavern pressures translate to higher compression ratios. Keeping the maximum discharge temperature of the

HP compressor ($T_{out}^{CM,HP,Max}$) fixed requires a lower inlet temperature for the HP compressor, hence more heat needs to be absorbed and stored in TS1 (preceding the HP compressor). Therefore, lower discharge temperatures of the HP compressor bring down the average temperature of air entering the electrolyzer, which impacts the reaction temperature of electrolysis (T_{HTE}, see Equation 123). This temperature drops from 578 to 544C as the maximum storage pressure of air ($P_{CN,fl}$) is raised from 7 to 12 MPa.

The expansion work also increases at higher cavern pressures since more compressed air is being handled. The net impact of higher cavern pressures on the roundtrip exergy efficiency and work ratio is negligible (slightly negative) though. This behavior indicates that higher compression work and HTE energy requirements cancel out higher values of expansion work. The exergy density of cavern increases ~2.7 times as the maximum storage pressure varies from 7 to 12 MPa. Therefore, increasing the cavern pressure substantially improves the exergy density of the plant while it marginally degrades its storage efficiency. In the real world, however, the storage efficiency is likely to degrade more compared to the scenario pictured here. For example, this analysis has assumed a fixed isentropic efficiency for the compressors while their efficiency will decrease at very high compression ratios [28].

Increasing the storage pressure has a positive impact on the thermodynamics of A-CAES, as presented in Table 14. Higher cavern pressures translate to higher compression requirements, at the same time more waste heat recovery opportunities become available. The expansion work also increases as a larger mass of air and at a higher pressure is expanded. The net effect of higher compression work, recovered heat, and expansion work is positive on the storage efficiency. It rises from 66% to 71% as the maximum cavern pressure ($P_{CN,fl}$) is lifted from 7 to 12 MPa. The work ratio of A-CAES improves from 1.51 to 1.42. Exergy density of the cavern at 12 MPa is almost 4 times larger compared to 7 MPa (due to the increased expansion work). Finally, the exit temperature of the high-pressure expander is also raised at higher cavern pressures (more stored heat despite higher expansion ratios). This is beneficial in addressing the concerns with freezing of vapor in the expanding air.

Table 13: Sensitivity of the CAES-HTE model to the maximum storage pressure ($P_{CN,fl}$). All other input parameters are the same as of Table 8.

	P_{fl} (MPa)			
	7	**8**	**10**	**12**
W_{CM} (GJ)	5,880	8,930	15,220	21,725
Q_{HTE} (GJ)	3,150	4,745	7,960	21,150
W_{HTE} (GJ)	5,715	8,690	14,820	22,785
T_{HTE} (°C)	578	569	555	544
W_{TB} (GJ)	6,180	9,390	15,990	22,785
Q_{CC} (GJ)	6,820	10,350	17,595	25,030
WR	1.88	1.88	1.88	1.88
η_X (%)	53.3	53.3	53.2	53.1
$X\rho$ (kWh/m^3)	3.1	4.7	7.9	11.3

Table 14: Sensitivity of the A-CAES model to the maximum storage pressure ($P_{CN,fl}$). All other input parameters are the same as of Table 7.

	P_{fl} (MPa)			
	7	**8**	**10**	**12**
W_{CM} (GJ)	5,880	8,930	15,220	21,725
Q_{TS} (GJ)	5,240	7,970	13,615	19,480
W_{TB} (GJ)	3,900	6,000	10,575	15,355
WR	1.51	1.49	1.44	1.41
η_X (%)	66.3	67.2	69.5	70.7
$X\rho$ (kWh/m^3)	1.9	3.0	5.2	7.6
$T_{out}^{TB,HP,Min}$ (°C)	5	11	26	33
$T_{out}^{TB,LP,Min}$ (°C)	195	188	181	173

Table 15 shows the robustness of the conventional CAES model to the air storage pressure. As the maximum cavern pressure ($P_{CN,fl}$) increases from 7 to 12 MPa, the work ratio of conventional CAES increases from 0.74 to 0.77. The impacts on the heat rate and emissions intensity are negligible. The roundtrip exergy efficiency is almost insensitive to changes in the cavern pressure (decreasing from ~54% to 53%). Similar to A-CAES and CAES-HTE models, the exergy density of the cavern increases (by a factor of ~3.5 for conventional CAES).

Table 15: Sensitivity of the thermodynamics of conventional CAES (two-stage compression and expansion design) to the maximum storage pressure of air ($P_{CN,fl}$). All other parameters are the same as of Table 9.

	P_{fl} (MPa)			
	7	**8**	**10**	**12**
W_{CM} (GJ)	4,555	6,990	12,110	17,510
W_{TB} (GJ)	6,180	9,390	15,990	22,785
Q_{CC} (GJ)	6,820	10,350	17,595	25,030
η_X (%)	54.3	54.1	53.8	53.5
WR	0.74	0.75	0.76	0.77
HR (GJ/MWh)	4.0	4.0	4.0	4.0
$X\rho$ (kWh/m^3)	3.1	4.7	7.9	11.3

4-5- Remarks on thermodynamics of A-CAES and CAES-HTE

The simulation results suggest that the A-CAES system has a higher storage efficiency (~70%) compared to conventional CAES (~54%), CAES-LTE (~54%) and CAES-HTE (~53%) (in the base case scenario and assuming an ideal electrolyzer). Using more realistic values for the energy efficiency of the electrolyzer makes CAES-HTE and CAES-LTE even less competitive. An electrolysis efficiency of 50% leads to a roundtrip exergy efficiency of only ~35% for the CAES-HTE and CAES-LTE systems.

Electrolyzing water – instead of steam – to produce hydrogen to fuel the combustors results in similar figures for the roundtrip storage efficiency of a CAES plant paired with an electrolyzer (*i.e.* CAES-HTE and CAES-LTE). The lower electricity demand of the high-temperature electrolysis process (HTE) is offset by higher compression requirements of the CAES plant paired with HTE. Considering the complexity of high-

temperature electrolyzers, the prospect of CAES-HTE seems unattractive compared to A-CAES and even to CAES-LTE.

The design and operation of A-CAES are complicated by the need for high-pressure and high-temperature compressors as well as thermal stores and the need for high-pressure turbines [11]. Additionally, thermal losses degrade the attractiveness of A-CAES. Roundtrip efficiency of hydrogen-based technologies is not impacted by heat losses over long storage periods. Furthermore, CAES-LTE can operate at pressures and temperatures of conventional CAES; thus, its design and operation would be simpler in that perspective. None of these design considerations are included in the thermodynamic analysis presented in this chapter.

Table 16 compares the performance of the CAES, A-CAES, and CAES-HTE systems when the maximum storage pressure is raised from 7 to 12 MPa. Similar to the base case scenario (maximum cavern pressure of 10 MPa), the A-CAES design remains the most attractive. Its efficiency slightly improves (from 66% to 71%) as the storage pressure is raised from 7 to 12 MPa. Roundtrip exergy efficiency of the conventional CAES (~54%) and CAES-HTE (~53%) systems are similar and relatively insensitive to the storage pressure. Despite higher storage efficiencies, the exergy density of A-CAES remain lower (63%-67%) compared to conventional CAES and CAES-HTE systems. Therefore, only emission constraints (in order to beat conventional CAES) and shortage of storage volume (to beat A-CAES) may justify adopting the CAES-HTE system.

Roundtrip exergy efficiency of both A-CAES and CAES-HTE systems degrades as the maximum allowable exit temperature of the high-pressure compressor ($T_{out}^{CM,HP,Max}$) increases, but A-CAES is more sensitive to this change. Work ratio reaches 1.99 for CAES-HTE and 1.67 for A-CAES when $T_{out}^{CM,HP,Max}$= 890 °C compared to the values of 1.36 and 1.84 (respectively) at $T_{out}^{CM,HP,Max}$= 500 °C. The general understanding that neither A-CAES nor CAES-HTE can compete economically with conventional CAES in the absence of high emission constraints is confirmed by the much lower work ratio (0.76) of conventional CAES and its moderate heat rate (~4 GJ/MWh).

Table 16: Effects of increasing the maximum storage pressure ($P_{CN,fl}$) on the thermodynamics of CAES, A-CAES, and CAES-HTE. All other input parameters are the same as Table 7, Table 8, and Table 9.

	$P_{CN,fl} = 7\ MPa$			$P_{CN,fl} = 12\ MPa$		
	CAES	**A-CAES**	**CAES-HTE**	**CAES**	**A-CAES**	**CAES-HTE**
η_X (%)	54.3	66.3	53.3	53.5	70.7	53.1
WR	0.74	1.51	1.88	0.77	1.42	1.88
HR (GJ/MWh)	4.0	0	0	4.0	0	0
$X\rho$ (kWh/m^3)	3.1	1.9	3.1	11.3	7.6	11.3

Table 17: Sensitivity of the thermodynamics of conventional CAES, A-CAES, and CAES-HTE to the maximum discharge temperature of the high-pressure compressor ($T_{out}^{CM,HP,Max}$). All other input parameters are the same as Table 7, Table 8, and Table 9.

		$T_{out}^{CM,HP,Max} = 500C$		$T_{out}^{CM,HP,Max} = 890C$	
	CAES	**A-CAES**	**CAES-HTE**	**A-CAES**	**CAES-HTE**
η_X (%)	53.8	73.4	54.4	60.1	50.1
WR	0.76	1.36	1.84	1.67	1.99
HR (GJ/MWh)	4.0	0	0	0	0
$X\rho$ (kWh/m^3)	7.9	5.2	7.9	5.4	7.9

In summary, this chapter developed and presented a series of analytical models to estimate and compare the thermodynamic performance of four families of compressed air energy storage technologies. Adiabatic CAES (A-CAES) showed the most attractive prospects considering various figures of merit, including roundtrip exergy efficiency (~70%). In comparison, the exergy efficiency of the conventional CAES system was estimated at ~54%. It also had a GHG emissions intensity of ~260 kgCO2e/MWh, and a heat rate of ~4.0 GJ/MWh. The hydrogen-fueled (instead of natural gas) CAES category had the lowest storage efficiency (~35%), partly due to the low exergy efficiency of the electrolyzer cell (assumed 50%). However, none of the hydrogen-based storage systems studied (CAES-HTE and CAES-LTE) generate GHG emissions, which might make them more attractive under tight emissions constraints. The fourth compressed air storage system studied was Distributed CAES (D-CAES). The natural gas credits from export of the heat of compression boosts the net roundtrip exergy efficiency of D-CAES to above 80%. Nevertheless, D-CAES would be practical

only under specific circumstances in the real world; therefore, it cannot be deployed at scale (in contrast to other CAES systems). A closing comment that the analysis presented here was concerned with only thermodynamics and emissions performance. The overall economics (particularly capital cost) and not just storage efficiency will ultimately determine the potential of bulk storage systems. The following three chapters focus on studying the cost-effectiveness of storage technologies to support integration of renewables and curb emissions from the electricity sector.

Chapter 3: Compressed air energy storage (CAES) with compressors distributed at heat loads to enable waste heat utilization[4]

[4] This paper is published as Safaei, H., D.W. Keith, and R.J. Hugo, Compressed air energy storage (CAES) with compressors distributed at heat loads to enable waste heat utilization. *Applied Energy*, 2013. 103: p. 165-179.

Preface

This chapter examines the prospects of a niche application for D-CAES: reducing the cost and greenhouse gas emissions associated with supplying electricity to a municipal region through integrating its electricity and heating infrastructure. While the thermodynamic analysis presented in Chapter 2 revealed a high roundtrip exergy efficiency for D-CAES (~80%) compared to conventional CAES (~50%), this chapter concentrates on the cost and GHG emissions performance of D-CAES in comparison to conventional CAES as well as gas turbines at a systems level.

Capacity and dispatch order of a hypothetical district heating system and an electricity generation portfolio (gas turbine, wind farm, and either D-CAES or conventional CAES) are optimized in a green-field setup to meet time-varying heating and electricity loads of a municipal region at the least cost. Since the compressed air energy storage technology is too capital-intensive to compete with gas turbines at the current low gas prices and emissions regulations, a variable emissions tax (0-80 $/tCO$_2$e) is added to a base gas price of $5.0/GJ. Economics and GHG emissions of the generation fleet equipped with conventional CAES or D-CAES are compared at various emissions taxes and distances between the heat load and the air storage site (*i.e.* length of the air pipeline in the D-CAES configuration).

The results suggest that neither D-CAES (with a 50 km pipeline) nor conventional CAES can outcompete gas turbines in managing the variability of wind below an emissions tax of $40/tCO$_2$e (equivalent to an effective fuel cost of $7.6/GJ). Beyond this threshold, the generation fleet equipped with D-CAES can meet the load at a lower cost and also achieve a lower emissions intensity. The break-even gas price for attractiveness of D-CAES over conventional CAES would depend on the distance between the heat load and air storage site: $7.0 and $8.3/GJ with pipeline lengths of 25 and 100 km, respectively.

The findings of this chapter are based on few simplifying assumptions and limited modeling capabilities. The main simplifications include absence of thermal energy storage for D-CAES, performing a copper-plate analysis, and ignoring forecast errors and the intra-hour and inter-annual variations in the heat and electricity loads as well as wind availability. Future work could build on the existing model to strengthen the

conclusions with respect to the niche markets for D-CAES to cost-effectively contribute to the efforts for GHG emissions mitigation in the electricity sector.

The first modeling simplification is that the heat of compression can supply only the instantaneous heating load. Storage of excess recovered heat could improve the economics of D-CAES provided that sales of the stored heat outcompete the capital and operation cost of the thermal storage system.

The second major simplification is the copper-plate modeling, which ignores capital costs of transmission lines and congestions in the grid. Since the compressor of D-CAES would be located closer to the electric load (inside the municipal region), grid congestions would likely limit the ability of the D-CAES plant to store electricity less compared to a conventional CAES system. Additionally, if the expander of D-CAES is moved from the air storage site to the compression site (*i.e.* compression and expansion trains co-located inside the city), the need for a transmission line between these two locations would be eliminated, which could bring in large cost savings for the D-CAES system.

Another modeling simplification is ignoring forecast errors in wind availability and the electric and heating loads. In other words, an ex-post (perfect foresight) rather than an ax-ante analysis is performed. This modeling approach overestimates the economic value of both D-CAES and conventional CAES. Heat load forecasts are, however, more certain compared to electric load and wind profiles. Therefore, performing an ex-post analysis is unlikely to exaggerate the relative economic value of D-CAES compared to that of conventional CAES. A temporal resolution of one hour over a simulation period of one year is used for the sake of simplicity. The analysis is also based on the load profile of and wind availability in Alberta (Canada). Incorporating the intra-hourly and inter-annual variations in load and wind profiles and forecast errors would enhance robustness of the results and conclusions. Expanding the simulation to other geographical locations could be other areas for future work.

The results suggest attractiveness of D-CAES compared to conventional CAES for reducing both the cost (to a lower extent though) and GHG emissions of supplying electricity and heating loads at a systems level. Nonetheless, D-CAES cannot become a major player in the real-world electricity systems. Its inherent need for a suitable geologic formation (for air storage) in proximity to a large, low-temperature, concentrated heating

load, which is supplied by a district heating system, limits the feasibility of D-CAES projects. Other compressed air storage systems (*e.g.* adiabatic CAES) and most other electricity storage technologies (*e.g.* electrochemical batteries) benefit from a much higher siting flexibility.

1- Introduction

Electricity demand has substantial hourly, daily, and seasonal variations, resulting in the need for peaking plants that operate only during peak-demand periods, and base load power plants that operate below their optimum output during low-demand periods. These effects lead to a reduction in overall system efficiency, shortened plant lifespans, greater requirements of financial investment, and higher greenhouse gas (GHG) emissions.

Renewable energies, especially solar and wind have the potential to provide substantial fractions of electricity supply and to reduce GHG emissions and air pollution from the electricity sector at large scale. Although GHG emissions of nuclear plants and hydroelectric dams are also low, large-scale expansion of these energies is facing difficulty. USA and Canada haven't built a new nuclear plant for more than fifteen years [42, 43] and hydroelectric dams are challenged by environmental and siting concerns [44]. Renewable energies in general, and wind energy in particular, have experienced significant expansion in the past decade. The installed wind capacity in the USA by the end of 2010 (40.2 GW) was approximately 15 times higher than its value at the beginning of the year 2000 [45]. Similarly, the installed wind capacity in Canada has increased more than 30 fold at the end of 2010 (4.0 GW) compared to its levels at the beginning of the year 2000 [46]. In spite of this impressive growth, wind energy still composes a small portion of the total installed capacity in these countries. Integration of wind energy into the electricity grid is complicated by the additional costs raised by its intermittent nature, the challenge that periods of high production do not necessarily coincide with periods of high demand, and sometimes the far distances between sites with good wind resources and high electric loads that mandate construction of capital-intensive transmission lines. As a case in point, Denmark can generate up to 30% of its electric power by offshore wind farms; nevertheless, almost all of its excess wind-based electricity is sold to its neighboring countries with hydroelectric capacities for virtual storage as a means to cope with wind intermittency [44, 47]. Even if periods of peak production and demand coincide, grid congestion may prevent delivery of wind-based electricity to the customers of the grid. In fact, the uncertain production of wind-based electricity has the potential to create or worsen grid congestion problems and grid stability issues [48].

The grid operator can choose any of the following approaches to deal with the intermittency of wind energy and to provide reliable and dispatchable wind-based electricity and thus facilitate higher wind penetration into the grid. These include utilization of fast-response thermal plants, geographically dispersed production sites, and energy storage[5].

a) Fast-ramping thermal plants: These plants, such as gas turbines and diesel generators, can engage as necessary to fill the gap between the generation and demand of electricity. They can quickly ramp up and down to accommodate changes in electricity production and consumption; however, their intermittent (as needed) operation causes them to have low capacity factors. Therefore, their capital, maintenance, and operation costs should be compensated by their limited operational period leading to an increase in the overall cost of wind-based electricity. The transient and partial-load operation of these plants also leads to lower thermal efficiencies and higher emissions of pollutants. In recent years, some new gas turbine designs have been introduced to the market that are claimed to be able to "chase-wind" without significant performance degradation when operated at partial load (*e.g.* Langage CCGT plant in the UK by Alstom [49]). Therefore, compensating inherent fluctuations in wind-based electricity through fast-response thermal plants involves the associated cost of cycling fast ramping thermal plants and/or building specially-designed fast ramping thermal plants.

b) Spatial distribution of generation sites: Another option to cope with intermittency of wind energy is to geographically disperse wind farms over a large area, overcoming localized wind patterns and resulting in smoother overall energy production [50]. However, this arrangement has the disadvantage of increased overall capital cost due to the need for longer transmission lines between distributed production centers and the load and it may not be feasible for some wind projects. Furthermore, this approach may necessitate large-scale planning over a large area, which may include different utility owners and electricity markets, further complicating the market dynamics of wind-based electricity.

[5] Utilizing demand response (interruptible load) and curtailing wind (if transmission resources are insufficient) are among other strategies to achieve reliable operation of the grid.

c) Energy storage: These systems can partially mitigate fluctuations in supply and demand of electricity through storing the excess energy generated during low-demand or high-congestion periods for later use (energy arbitrage application). Storage systems can improve the performance of power plants, *e.g.*, coal and nuclear, by allowing them to operate closer to their optimal design points. More importantly, energy storage systems can convert an intermittent wind farm into a firm capacity that can be dispatched based on the market price of electricity and reliability requirements of the grid (firming application). Strategically sited storage facilities can also prevent or delay the need for new transmission lines through relaxing grid congestions. Storage plants can also provide a variety of other ancillary services (*e.g.* frequency control and black start) essential for ensuring reliability of the grid [51]. Electricity storage systems can be characterized based on their discharge duration and power production capacity. Only compressed air energy storage (CAES), pumped hydro storage (PHS), and emerging flow batteries can presently provide utility-scale storage capacities (hundreds of MW-hours, bulk energy storage application) that may be required for large-scale integration of wind energy into the electricity grid. Although PHS has approximately 40 and 20 GW of installed capacity in Europe and USA respectively [44], development of PHS projects is geographically limited due to the necessity for two large natural or artificial water reservoirs with sufficient elevation difference. Environmental licensing and long construction time (in 10 years scale) are among other factors limiting large expansion of PHS capacities [10, 51].

CAES facilities can use a variety of both underground and aboveground storage facilities and can be constructed in a relatively short time (around three years). CAES systems use inexpensive off-peak electricity to compress air into underground or aboveground storage reservoirs, which are later used to power modified gas turbines and generate electricity. CAES technology was extensively investigated in the 1970s to provide load following services and to gain a high capacity factor for base load power plants (especially nuclear) by storing off-peak electricity. The first CAES plant was commissioned in Huntorf, Germany in 1978 to provide black-start services to nuclear plants as well as provide relatively inexpensive peak power [52]. The Huntorf plant, which is still in operation, stores up to 310,000 m^3 of compressed air at a pressure range of 48-66 bar in two salt caverns and can produce up to 290 MW of electricity at full capacity for 4 hours at an air discharge flow rate of 417 kg/sec [10].

The second utility-scale CAES plant was commissioned in 1991 in McIntosh, Alabama. The McIntosh plant can generate 110 MW of electricity at full capacity for 26 hours at an air discharge rate of 154 kg/sec. It stores up to 540,000 m^3 of compressed air at the pressure range of 45-74 bar in a salt cavern [5]. The Alabama plant consumes up to 25% less fuel than the Huntorf plant as waste heat from the exhaust of the low pressure expander is recuperated to preheat discharge air from the cavern prior to entering the high pressure combustor [5].

Despite the successful operation of these two CAES plants, a series of events slowed down the development of CAES technology in the late 1980s and the 1990s. These events included the loss of momentum in the nuclear industry, the development of efficient and low capital-intensive single and combined cycle gas turbines, drop in natural gas prices, and an overbuilt generation capacity [10, 44]. However, the desire for higher penetration of clean but intermittent wind and solar energy sources into the electricity grid has renewed interest in CAES as a method to overcome their intermittency and thus lower the GHG emissions from electricity generation [10].

Conventional CAES plants are not pure energy storage facilities since their operation requires combustion of fuel during the generation phase. Compressed air is heated during the generation phase (to prevent water vapor from freezing) and then electricity is generated through expansion of heated compressed air in expanders. The Huntorf plant for instance, uses ~5.8 GJ of natural gas per kWh of peak electricity that it generates[6] [5].

A variety of newer CAES designs have been proposed to improve the storage efficiency of conventional CAES plants. One design introduced by Energy Storage and Power Corporation in the 1990s is based on pairing CAES plants with conventional gas turbines. The main idea of this approach is eliminating the combustor in the CAES facility and utilizing the exhaust stream from the gas turbine instead of the combustor of CAES to heat the compressed air and thus improving the overall efficiency [51, 53].

[6] Each kWh of energy equals to 3.6 GJ. Therefore, the thermal efficiency of the Huntorf plant would be 62% solely based on its "inside-the-fence" fuel consumption. This CAES plant also uses 0.82 kWh of electricity during the compression phase for each kWh of electricity that it delivers during the generation phase (work ratio of 0.82).

In contrast to this approach, which focuses on waste heat recovery during the discharging process, the adiabatic CAES (A-CAES) design is based on storing the heat of compression in a thermal energy storage facility. This stored heat then heats compressed air during the generation process and thus lowers (or even eliminates) the fuel consumption of the CAES plant [54]. This concept was introduced in the 1980s and the interest in this concept is recently renewed both in Europe and the United States [11, 51]. However, the A-CAES concept is still in the research and development phase and its development is challenged by few major technical issues including design of high pressure, high temperature, large scale and economically attractive thermal energy storage systems, high pressure and high temperature compressors, and high pressure expanders [20, 55].

This paper introduces and evaluates a different approach to improve the efficiency of conventional CAES plants. This approach focuses on utilizing the otherwise-wasted heat of compression for heating needs and thus improving the overall thermal efficiency of the CAES plant. This new configuration, which is called Distributed CAES (D-CAES), is realized by distributing air-compression stations near heat loads such as district heating facilities instead of siting the compression train at the storage facility (as the case for conventional CAES). An integrated compressed air pipeline network, supplied by these distributed compressors located near high heat-load facilities (*e.g.* hospitals and office towers), would use off-peak electricity to compress air. The heat produced by air-compression would then be utilized or stored for heating needs, and thus lower the overall cost of the D-CAES system by negating the demand for heating fuel usage within these high heat-load regions. The compressed air from this system would be pipelined to favorable geological sites for underground storage. The expander of the D-CAES system located at the storage site would generate electricity via combustion and expansion of stored compressed air, similar to the conventional CAES designs. Further details on different variations of the D-CAES concept may be found in Hugo *et al.* [56].

The D-CAES concept is based on improving the economics of the conventional CAES facilities through the use of the low quality (exergy) heat of compression for space and water heating demands. Waste heat recovery from industrial compressors is a mature technology and therefore introduces less technical complexity compared to the A-CAES design, which requires heat recovery and storage at high pressures and

temperatures. Nevertheless, D-CAES requires a pipeline between the compression site (in a region with high density of heat load) and the storage site (*e.g.* cavern). In the admittedly unrealistic case where the heat load and the CAES storage facility are co-located, then D-CAES would always be preferred to CAES since it provides heat "for free". The essence of our analysis is to explore how the relative competitiveness of CAES and D-CAES depends on pipeline length. The trade-off between the increased capital cost of the D-CAES system compared to conventional CAES (mainly due to the air pipeline) and savings on fuel (used for heating purposes) can make the D-CAES system cheaper compared to the conventional CAES in certain situations.

The intensity and fluctuations of the heat load, size and fluctuations of the electric load, distance between the heat load and storage facility, and the fuel and construction costs are the major players in this trade-off. As mentioned earlier, ambitious plans for higher penetration of wind energy into the electricity grid is one of the main drivers for the renewed interest in the CAES systems in the twenty first century. Therefore, this paper focuses on economic evaluation of D-CAES concept, as an alternative to conventional CAES systems, to provide economic and dispatchable wind-based electricity. To the knowledge of the authors this idea has not been discussed in literature before and this paper is the first to investigate the opportunities in enhancing the economics of CAES through recovery of the otherwise-wasted heat of compression from CAES plants to satisfy heating loads (instead of wasting the heat to the ambient in conventional CAES plants or storing it to later heat the compressed air during the power generation phase as proposed in the A-CAES design). The primary contribution of this paper is providing insight into the potential financial gains through waste heat recovery from the compression trains of CAES for municipal heating applications in order to facilitate R&D work on detailed engineering design of such plants.

It bears mentioning that a different concept of distributed (decentralized) compressed air energy storage has been introduced and discussed in the literature, which is based on replacing the generator of individual wind turbines with compressors to directly store mechanical energy of wind in the form of potential energy of compressed air [57, 58]. The main advantage of this concept is eliminating the energy losses during the process of converting mechanical energy of wind to electricity and then to potential energy of compressed air. Nevertheless, distributing the compressors near heat loads to enable the use of compression heat for space and water heating applications, as proposed in the D-CAES configuration, has not been studied before.

2- Methodology

Although the economic performance of CAES depends on the nature of the electricity market and grid that they participate in, some recent studies have concluded that conventional CAES plants may not be able to compete economically with other alternatives, especially conventional gas turbines, to support of wind-based electricity [52, 59, 60]. This phenomenon is driven by relatively high capital cost of CAES in comparison to gas turbines. However, at elevated fuel prices or in the case of high emissions taxes, CAES technology would become more attractive because of its better fuel economy. In a carbon-constrained world, technologies with high carbon footprints would be phased out and the electricity generation mix would move towards cleaner technologies, which would make the already complicated market dynamics more difficult and uncertain to model. Moreover, compressed air energy storage plants should ideally be designed and operated as independent entities in the electricity market to maximize their economic performance [61]. These plants would buy and store off-peak electricity from a variety of sources and sell electricity back to the grid during periods of peak demand and also provide ancillary services to the grid to maximize their competitiveness and profit in the electricity market.

Because of the complexities associated with forecasting and modeling this real world scenario with higher fuel costs, we study a simplified system to investigate the economics of D-CAES and CAES plants in supporting wind-based electricity. In order to avoid the complex dynamics of the electricity market but at the same time provide insight into the performance of the D-CAES configuration in a close-to-real world scenario, a hypothetical scenario which represents a high-level policy making approach was used in this study. This hypothetical scenario represents a planning firm designing the electricity and heating infrastructure of a portion of a city in a carbon-constrained world. It is assumed that good wind resources are available; therefore the planning firm is considering harnessing this clean energy resource to satisfy a portion of the electric load. Natural gas-based power plants (simple cycle gas turbine, SCGT, and combined cycle gas turbine, CCGT) and natural gas-based compressed air energy storage plants (either conventional CAES or D-CAES) are also considered as candidates for electricity generation because of their relatively low GHG emissions. In addition, the firm plans to utilize district heating technology to satisfy the heat load of a portion of the city with a high load intensity (*e.g.* downtown core) because of the potential of the district heating

technology in supplying cleaner and more efficient heating energy compared to individual heating facilities. The heating energy of this district heating facility could be supplied through either direct combustion of natural gas in heat-only-boilers (HB) or heat recovery from the D-CAES plant. The overall objective of the planner is to satisfy both the electric and heat load at the lowest levelized cost (or maximizing the net social welfare). It is also assumed that the electric load of the city has to be satisfied by its own generation fleet and import and export of electricity are ignored. One should note that in the real world, cities are not normally isolated from the electricity grid and can buy/sell electricity from/to other grids. The authors acknowledge this simplification in the model presented but decide to use this assumption for the sake of simplicity and to evaluate the conditions under which the D-CAES design might be economically preferable to CAES at a high level policy making approach.

The operational performance (*i.e.* revenues) of D-CAES depends most strongly on the size and diurnal and seasonal fluctuations of the heat load profile. In other words, if the heat load is too small then the economic gains from waste heat recovery would not be sufficient to justify the D-CAES system (mainly due to the requirement for capital-intensive air pipelines and the effect of economy of scale on this cost). However, in the real world the magnitude of heat load supplied by district heating networks is limited by increased heat losses in geographically-dispersed networks. In order to build a close to real world scenario, the size of the heat load connected to the district heating network was chosen so that it represented a concentrated municipal heat demand center. The D-CAES system might be chosen over the conventional CAES configuration only when it can be paired with a district heating network. Therefore, instead of modeling the heat demand of an entire city, the authors only focused on satisfying a concentrated heat load (a portion of the city) supplied by a district heating network.

2-1- System of study

As mentioned, two different configurations can be considered to evaluate the performance of conventional CAES and D-CAES systems in meeting the electric and heat loads.

2-1-1- System with a conventional CAES plant

As shown in Figure 17, a wind farm, a conventional CAES plant located outside a city at a favorable geological storage site, and conventional gas turbine plants (SCGT and CCGT) could be utilized to meet the electric demand. The heat load would be satisfied by large scale boilers connected to district heating networks. Since this study focuses on providing reliable and dispatchable wind-based electricity, it is assumed that the CAES facility can only be charged by the wind farm while SCGT and CCGT can provide electricity only for instantaneous use and not for compression in the CAES plant.

2-1-2- System with a D-CAES plant

The major difference between this configuration (Figure 18) and the CAES system (Figure 17) is that the compressor of the compressed air storage facility is located within the city and close to a concentrated heat load. A heat recovery unit (HC) recovers the heat of compression, thereby negating the fuel consumption of the heat-only-boiler (HB) of the district heating system. The generated compressed air is transported via a pipeline network to a suitable geological storage site outside of the city for storage. The expander of the compressed air storage plant is located at this site similar to the conventional system. A low pressure, low temperature thermal energy storage (TS) unit could also be used to store the excess compression heat for later use. This additional component is, however, not considered in this paper for the sake of simplicity.

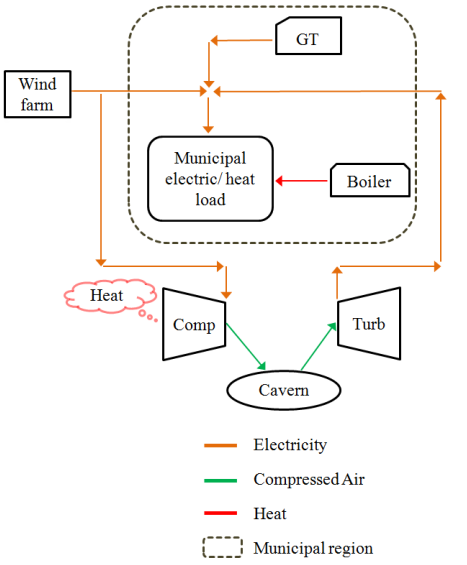

Figure 17: Schematic of the CAES system. Conventional CAES, wind farm, and combined and simple cycle gas turbines (GT) are utilized to meet the electricity demand. Natural gas-based boilers are utilized to satisfy the heat load of a district heating network. Wind-based electricity is the sole energy source to charge the underground compressed air storage facility. Comp and Turb stand for compression and expansion trains of the compressed air energy storage plant.

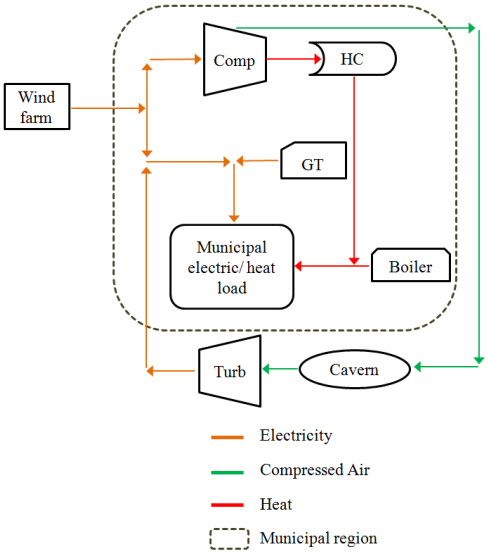

Figure 18: Schematic of the D-CAES system. The compression train (Comp) of the compressed air energy storage facility is located within the city. The generated compressed air is pipelined to the storage facility outside the city where both the underground storage (Cavern) and expansion train (Turb) are located. The heat of compression is recovered by a heat recovery unit (HC) to satisfy the concentrated heat load in conjunction with the boilers of the district heating network.

2-2- Inputs and simulation model

We model a planner who aims to minimize the total (capital and fuel) cost of satisfying a variable electric and heat load over the period of one full year. Following is a description of various inputs and assumptions made to establish this optimization problem.

2-2-1- Simulation resolution and period

High penetration of intermittent wind energy affects the electricity grid in three different time scales: minute-to-minute, intra-hour, and hour- to day-ahead [59]. Since the primary application of compressed air energy storage plants is bulk energy storage (arbitrage and load leveling applications), an hourly resolution was chosen for this study. This approach is in agreement with some of other studies in the field of economic assessment of compressed air energy storage systems to support wind energy [52, 59, 60]. One should note that CAES plants can provide a range of ancillary services in electricity markets in addition to the primary duty of energy arbitrage and load leveling. CAES plants can provide frequency and voltage control services (in seconds time scale) and ramping services (in minutes time scale) in addition to the load following application considered in this study [62]. However, the economic value of these services highly depends on the market in which they are offered; therefore, these services were not included in this study and only energy arbitrage was considered as the primary role of energy storage plants.

In order to capture the diurnal, weekly, and seasonal changes in wind energy, electric load, and heat load, the system was modeled over a period of one full year. Both the heat and electric loads are to be satisfied at each hour over the entire simulation period.

2-2-2- Heat load

District heating networks have the ability to supply heat to different types of heat loads (single houses, office towers, hospitals, etc.). However, an ideal heat load for district heating networks would be a concentrated load (*e.g.* a university) because of the higher capital costs associated with heating pipelines in district heating systems with low heat intensity. Therefore, a large concentrated heat load (three times as the heat load of the University of Calgary, Alberta, Canada) was chosen for this study. The heat load of this university experienced a peak and average hourly value of 48.4 and 21.4 MW thermal in the year 2011. Since the heat load of the

University of Calgary is currently satisfied with a district heating network, this load can be a good representation of a municipal heat load supplied by a district heating network.

2-2-3- Electric load

The electric load profile used in this study is based on the peak electric load profile of the province of Alberta in the year 2011 reported by the Alberta Electric System Operator (AESO) [63]. Alberta's hourly peak load was scaled down to simulate a large electric load with an hourly peak and average load of 1000 MW and 516 MW, respectively. The size of the electric load was chosen arbitrary to represent a real world load. One should note that system of study was assumed to be "congestion free" (copper plate assumption) and the only geographical constraint in the model was the distance between the heat load and the geologic formation for air storage.

2-2-4- Wind profile

Hourly generation data from existing wind farms in Alberta reported by AESO [63] for the period of 2008 to 2011 were used in this study. The hourly capacity factor of wind (ratio of the hourly generation to the name plate capacity of the wind farm) was calculated to represent the quality of wind resources to be exploited for electricity generation during the simulation period.

2-2-5- Compressed air pipeline

A pipeline is required to transport the generated compressed air from the compressor/heat-load site to the underground storage facility. The economics of D-CAES are strongly dependent on the capital cost of the pipeline. A pipeline length of 50 km was used in the base case system and the sensitivity of the results to this value was then assessed through running the simulation with 25 and 100 km long pipelines. Furthermore, an unrealistic scenario with a pipeline length of 0 km is considered to provide better insight into the trade-off between the capital cost of the pipeline and revenues of waste heat recovery. One should note that this study focuses on Calgary, Alberta as a case study. Calgary is in close proximity to depleted gas reservoirs that could be used for underground storage of compressed air.

Due to the relatively short length of the pipeline (50 km) and to maximize waste heat recovery benefits in the D-CAES configuration, no boosting compression stations were considered. In other words, the maximum

downstream pressure of the pipeline was fixed (equal to the maximum cavern pressure, 74 bar) and the upstream compression facility was sized to be able to compensate for the pressure drop along the pipeline.

Equation 147 relates the flow rate of the compressed air to the pipe diameter and length and the upstream and downstream pressures (see nomenclature for definition of symbols) [26].

$$P_{PP,up}^2 - P_{PP,dn}^2 = 9.4 \times 10^4 \times \frac{T_{PP} \times L_{PP} \times f_{PP} \times {F_{PP}}^2}{{D_{PP}}^5} \quad \text{Equation 147}$$

The maximum allowable pressure drop along the compressed air pipeline was set to 35 kPa per km, a typical value for natural gas pipelines [64]. By fixing downstream pressure (P_{dn}) and knowing the maximum air flow rate in the pipeline given compressor size, Equation 147 was used to calculate the pipe diameter. Once the pipe diameter was determined, its length and diameter were used to estimate the capital cost of the pipeline based on a regression model developed for industrial gas pipelines by Sean McCoy [65].

2-2-6- Storage facility

Compressed air energy storage facilities can use both above- and underground storage [15, 66, 67]. Both high pressure storage tanks and pipelines can be utilized in aboveground CAES systems; however, aboveground CAES systems are not economically feasible for utility-scale (bulk) storage due to the significantly higher capital costs of aboveground storage [51]. Underground CAES can utilize a variety of geologic formations (salt caverns, hard rock and porous rock formations, and depleted gas reservoirs) to store compressed air in large quantities [10]. The selection of the proper formation is subject to various factors such as its availability, geological characteristics, and development costs. Porous rock formations were considered as the storage for this study since Calgary is in the proximity to porous rock geologic formations. As explained in the previous section, this formation was assumed to be located at a distance of 50 km from the heat load (equal to the length of the air pipeline) in the base case analysis.

2-2-7- Operation of CAES and D-CAES

A compressed air storage facility is very similar to a conventional gas turbine power plant with the major difference that the air compression and expansion processes do not happen at the same time. However, in principle a CAES plant can run as a simple cycle gas turbine during the periods that the cavern is short on

stored air [52]. This capability was considered in the optimization model such that the expander could receive compressed air required for its operation from both the cavern (running as a pure CAES) and the compressor (running as a pure SCGT).

2-2-8- Fuel price

A series of recent studies [52, 59, 60] have shown that conventional CAES facilities are too capital-intensive to be economically favorable over conventional gas turbines to support wind-based electricity under the current low natural gas prices (as the primary fuel for CAES and gas turbine plants). However, CAES may become attractive in a carbon-constrained world due to its lower emissions compared to conventional gas turbines. Therefore, a variable emissions tax (Tax) is added to in the market price of natural gas price (π_{NG}^{Market}) here. The effective fuel price (π_{NG}^{Eff}, combination of market price of the natural gas, fixed at \$5.0/GJ[7], and emissions taxes) is calculated based on Equation 148. The effective fuel price concept incorporates both the fluctuations in the market price of fuel and the emissions taxes due to the GHG emissions from the combustion of the fuel. A value of 66 kg CO_2e[8]/GJ was considered as GHG emissions associated with burning natural gas, π_{NG}^{Market}, (including the typical[9] upstream emissions) [60]. As a case in point, a market price of \$5.0/GJ for natural gas and an emissions tax of \$30/tCO_2e[10] would translate to an effective natural gas price of \$7.0/GJ. At low levels of tax, neither a CAES nor a D-CAES system is expected to be superior to gas turbines. However, as the effective fuel price increases, CAES becomes more favorable and at some higher fuel prices D-CAES will outcompete both conventional CAES and gas turbines.

$$\pi_{NG}^{Eff} = \pi_{NG}^{Market} + Tax \times \pi_{NG}^{Market} \qquad \text{Equation 148}$$

[7] All heating values in this paper are expressed in terms of lower heating value (LHV). The higher heating value (HHV) energy content of natural gas is about 11% higher than its LHV. Therefore, a natural gas price of \$5.0/GJ (LHV) corresponds to approximately \$4.5/GJ (HHV).

[8] GHG emissions are expressed in equivalent amounts of carbon dioxide (CO_2e) in this paper.

[9] GHG emissions associated with manufacturing of the components were not included.

[10] One t indicates one metric ton (1000 kg).

2-2-9- Capital cost inputs

Table 18 provides the inputs used in evaluating the cost of various components of the two systems. All costs were converted to 2009 inflation adjusted US dollars according to the Chemical Engineering Plant Cost Index [68, 69]. The capital cost of the heat recovery unit was assumed negligible since this heat has to be removed during inter-stage cooling between compression stages and from the compressed air prior to storage anyways (whether it is utilized for heating applications or dumped to the ambient). Similarly, the capital costs of the district heating network (excluding the boilers) were ignored in the analysis since this network would exist in both CAES and D-CAES configurations. In other words, the district heating system would be utilized to satisfy the heat load, regardless the source of the heating energy (HB or HC). Recovering the heat of compression would shave the peak heating load and a smaller boiler could supply the same heat load. Marginal capital cost of boiler was therefore, included in the objective function to take into account cost savings associated with reduced boiler capacity in the D-CAES configuration. In addition, all fixed and variable operation costs were ignored because of the fact that at the high carbon prices, which would be necessary to justify building capital-intensive CAES and D-CAES plants, these operation costs would be negligible compared to the much higher fuel costs[11]. Therefore, only the capital and fuel costs of various system components were considered in the economic analysis.

Another simplification in this study is capital cost of the transmission lines. These lines are required to transmit electricity from the wind farm to the electric load and to the compression train, and from the expansion train to the electric load. Since our scope was to only model electric load of a portion of a city instead of an entire city, it was rational to assume that large transmission lines would already be built between the wind farm, municipal region, and the geologic formation to integrate the valuable wind energy into the electricity grid for the entire city. Therefore, it is assumed that these lines would exist anyway regardless of the specific CAES and D-CAES facilities modeled. We acknowledge the possible inaccuracies

[11] As a case in point, VOM and FOM costs for a CCGT plant is $1.3/MWh and $10.8/kW/year as reported by Greenblatt *et al.* [23]. Assuming a capacity factor of 80%, heat rate of 7.17 GJ/MWh and a gas price of $5.0/GJ, the levelized VOM, FOM and fuel costs of this plant would be $1.30, $1.54 and $35.85 per MWh of electricity generated, respectively. The VOM and FOM costs of the plant would not vary with the price of gas while the fuel cost would. Therefore, the authors do not expect excluding the VOM and FOM costs would introduce major inaccuracies in the results, especially at high fuel prices required for economic attractiveness of CAES and D-CAES plants over gas turbines.

associated with this intentional simplification. The alternative to this approach was including capital cost of the transmission lines; however, we believe the former approach would be a closer and more accurate approximation of the real world case. Costs of the transmission lines of the gas turbine plants were also ignored since these facilities are normally built in close proximities to the load.

Table 18: Economic inputs for optimization of CAES and D-CAES systems.

Parameter	**Base value**	**Reference**
$CapEx_{Wind}$ (\$/MW)	1.67×10^{6}	[70]
$CapEx_{SCGT}$ (\$/MW)	5.92×10^{5}	[70]
$CapEx_{CCGT}$ (\$/MW)	8.50×10^{5}	[70]
$CapEx_{TB}$ (\$/MW)	5.15×10^{5}	[62][12]
$CapEx_{CM}$ (\$/MW)	4.76×10^{5}	[62][12]
$CapEx_{CN}^{Marg}$ (\$/MWh)	1.5×10^{2}	[5]
$CapEx_{CN}^{Base}$ (\$)[13]	12.22×10^{6}	[9]
$CapEx_{HB}^{Marg}$ (\$/MW)	5.0×10^{4}	[71]
BC (%)	10	[60]
$CapEx_{PP}$ (k\$/mm) (with L_{PP}=50 km and 250<D_{PP}<700 mm	$41.46 \times D_{PP} - 1{,}449$	[65][14]
VOM cost of all components	negligible	
FOM cost of all components	negligible	

[12] Estimates for the specific capital cost of the compressor and the expander are based on the estimates for the total capital cost of the McIntosh CAES plant published by the Electric Power Research Institute (EPRI) [25]. This capital cost was adjusted for the capital cost of the salt cavern utilized in McIntosh plant [13] and the ratio of the capital cost of the expander and the compressor to estimate the specific costs of the expander and the compressor separately. The ratio of the specific capital cost of the expander to compressor is assumed 1.08, the average of the values used by Fertig and Apt [12] and Greenblatt *et al.* [23].

[13] The base case of cavern is for a depleted natural gas reservoir capable of storing enough air for 12 hours of continuous electricity generation at a rate of 131 MW as estimated by Electric Power Research Institute [38].

[14] The capital costs of the pipelines are based on the regression analyses developed by Sean McCoy [29] for 263 on-shore natural gas pipeline projects in US. The values used in this study is for a 25, 50, and 100 km pipeline built in Central Region of the United States, as classified by the US Energy Information Administration for natural gas pipeline regions.

2-2-10- Performance characteristics

Table 19 shows the inputs used to characterize the technical performance of various components in the simulation. The roundtrip storage efficiency of compressed air storage facilities can be expressed through using two parameters: work ratio and heat rate. Work ratio indicates the amount of work (off-peak electricity) that the compressor of the plant consumes per unit of electricity that the expander delivers. Heat rate expresses the amount of fuel burned per unit of electricity generated by the expander. The values used for heat rate and work ratio are for a typical CAES facility as reported by the Electric Power Research Institute (EPRI) [5]. It is of note that these parameters may vary based on the design and operation of the storage facility in the real world. Heat rate of compressed air storage facilities is much lower compared to SCGT and CCGT since all the energy generated by the expander is converted to electricity in a CAES plant while up to two thirds of this energy is consumed by the compressor in conventional gas turbines.

It was assumed that up to 70% of the input energy into the compressor of the D-CAES plant could be recovered and utilized to satisfy the heat load. The authors acknowledge that this value might change the capital cost of the heat recovery system; the higher this value, the more sophisticated HC required and the higher the capital cost. Therefore, a conservative value of 70% was used as the heat recovery efficiency of the HC. In addition, the economics of D-CAES might be enhanced if a thermal energy storage facility is utilized to store the excess waste heat for later use. This option is not considered in this study for the sake of simplicity. A value of 80% (higher heating value) was used for the thermal efficiency of the boilers of the district energy system.

Table 19: Performance characteristics of various components of the CAES and D-CAES systems.

Parameter	**Value**	**Reference**
HR_{CCGT} (GJ/MWh)	7.17	[70]
HR_{SCGT} (GJ/MWh)	11.02	[70]
HR_{TB} (GJ/MWh)	4.19	[5]
WR	0.75	[5]
η_{HB}	80%	
η_{HC}	70%	

2-2-11- Optimization model

A mixed integer linear optimization code was developed in MATLAB to minimize the total cost of satisfying the hourly electric and heat loads over the one year simulation period. Size and dispatch of the various system components (wind farm, compressor, expander, cavern, SCGT, CCGT, compressed air pipeline, HC, and HB) were optimized to minimize the value of the objective function shown in Equation 149. This equation shows the total cost to satisfy the annual electric and heat loads at an hourly resolution. The terms in the first set of curly brackets show the amortized capital cost of various system components while the terms in the second set of curly brackets show the total fuel cost. The savings in fuel and capital costs of the heating boiler (HB) are included in the objective function. At each effective fuel price (π_{NG}^{Eff}), capacity ($Capt$) and dispatch of various components are optimized to satisfy the electric and heat load at the minimal cost over the one year period of simulation. Then the capital and fuel costs are used to calculate the annual levelized cost of electricity supply (LCOE) in $ per MWh of electricity. The capital and fuel costs of the boiler would be lower in the D-CAES system compared to CAES (due to waste heat recovery). The difference between these values is treated as a negative cost (savings) in calculation of LCOE of the D-CAES system. The carbon intensity of natural gas (66 kg CO_2e/GJ) was used to calculate the average carbon intensity of electricity generation (kg CO_2e/MWh electricity) in the two systems. The index "t" presents each dispatching period, *i.e.* one hour.

$$
\begin{aligned}
Minimize \quad & BC \times \{(Capt_{CCGT} \times CapEx_{CCGT}) + (Capt_{SCGT} \times CapEx_{SCGT}) \\
& + (Capt_{TB} \times CapEx_{TB}) + (Capt_{CM} \times CapEx_{CM}) \\
& + (Capt_{Wind} \times CapEx_{Wind}) + \left(Capt_{CN} \times CapEx_{CN}^{Marg}\right) \\
& + (D_{PP} \times CapEx_{PP}) - CapEx_{HB}^{Marg} \times (HL_{Max} - Capt_{BL})\} \\
& + \sum_{t=1}^{365\times24} \pi_{NG}^{Eff} \\
& \times \left\{(EL_{CCGT}^{t} \times HR_{CCGT}) + (EL_{SCGT}^{t} \times HR_{SCGT}) \right. \\
& \left. + (EL_{TB}^{t} \times HR_{TB}) - \left(HL_{HC}^{t} \times \frac{3.6}{\eta_{BL}}\right)\right\}
\end{aligned}
\qquad \text{Equation 149}
$$

The major optimization constraints include:

- Hourly electricity generated by the wind farm, simple and combined cycle gas turbines and the expander of the storage facility should be equal to the hourly electric load.

- Heat provided by the boiler (HB) and heat recovery system (HC) at each hour should be equal to the hourly heat load.
- Hourly generation of each component should be less than or equal to its optimal size.
- Hourly heat provided by the HC should be less than or equal to the compression energy at that hour multiplied by the efficiency of the HC.
- Summation of the hourly wind-based electricity provided to the electric load and to the compressor of the energy storage plant should be less than or equal to the optimal size of the wind farm multiplied by its capacity factor at that hour.
- Conservation of energy should be honored for the energy storage plant at each hour; change in energy level of the cavern should be equal to the difference between energy stored and released during that hour.
- The minimum size of SSCGT, CCGT, compressor, expander, and wind farm is set to either 10 MW or 0 MW to simulate a close to real world scenario. This constraint is imposed to avoid too small optimal sizes for the system components (*e.g.* a 0.2 MW gas turbine), which would have a high specific cost ($/kW) due to economies of scale.
- The air storage facility is sized for a week-long storage period and it is assumed to be depleted by midnight Friday each week. Since the electric load and thus its price would be lower during weekends compared to weekdays, the cavern would most probably be generating during the weekdays and storing electricity during weekends.

3- Results and discussion

In order to compare the performance of the D-CAES with the CAES system, a base fuel price of $5.0/GJ was assumed while the emissions tax was varied from 0 to 80 $/t$CO_2$e at $10/t$CO_2$e intervals. Each $10/t$CO_2$e increase in the emissions tax corresponds to approximately $0.7 increase in the effective fuel price. At each effective fuel price, the optimal size and dispatch strategy of various components were determined by the mixed integer linear optimization code developed in MATLAB.

Prior to detailed presentation of results at various emissions taxes and pipeline lengths, it is beneficial to better understand how the objective function and constraints of the optimization impact the simulation. As a case in point, Figure 19 illustrates the distribution of electricity supply, distribution of available wind energy, distribution of energy supplied to compressor for storage, distribution of heat supply, and the energy level of the cavern over a seven day period at an emissions tax of \$60/tCO_2e in the D-CAES scenario. The time frame is arbitrary chosen as the 48th week of the year (Saturday, November 26 to Friday, December 2, 2011) and as expected, electric load is lower over the weekend. Most of the available wind energy is directly used by the electric load and expander of D-CAES is mainly dispatched during hours with low availability of wind. Not surprisingly, less efficient SCGT is poorly competitive with other three types of generators at such a high emissions tax and is dispatched only for very few hours. Furthermore, waste heat of compression supplies a high portion of the heat load during hours with high availability of wind energy (charging period of cavern). Wind energy is curtailed only when it exceeds the electric load and the storage of this energy is limited by the capacity of the compressor. Finally, the cavern is depleted at the end of week to simulate a weekly cycle of energy storage.

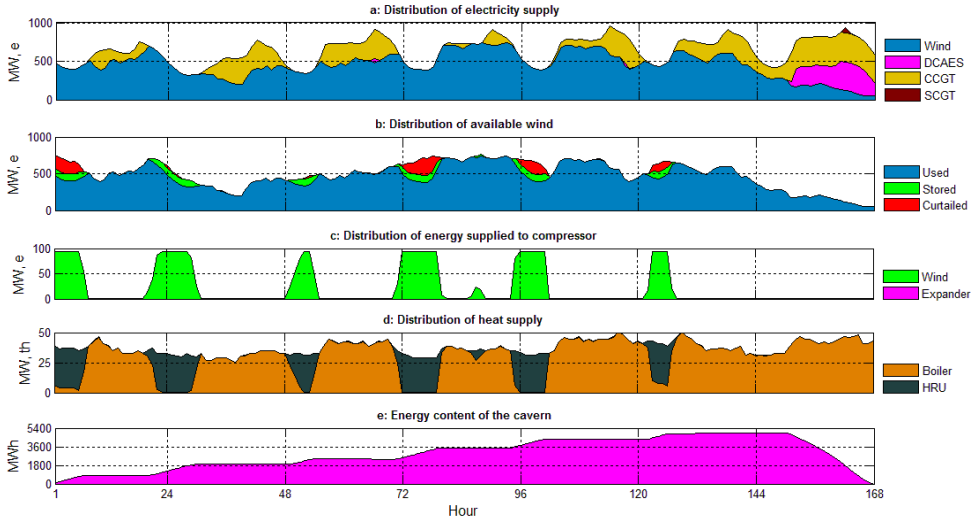

Figure 19: Performance of various components of the D-CAES system over an arbitrary period of one week at an emissions tax of \$60/tCO_2e. Horizontal axis shows the period between Saturday, November 26 and Friday, December 2, 2011. "Used" and "Stored" in subfigure b represent the amount of wind energy that is used by the electric load and by the compressor of D-CAES, respectively. Note wind energy is curtailed only when it exceeds the electric load and its storage is constrained by the capacity of the compressor (94 MW). "MW, e" and "MW, th" stand for MW electric and MW thermal respectively.

3-1- Optimal size of components

An important aspect in determining the cost of electricity supply is the size of various system components. Figure 20 illustrates the optimal size of the single and combined cycle gas turbines, expander, compressor and wind farm as well as the maximum hourly electric load (for comparison) at various values of emissions tax for the CAES configuration. As shown, the generation fleet is composed of only gas turbines in the absence of any emissions tax (*i.e.* an effective fuel price of $5.0/GJ). The optimal size of wind farm increases as emissions tax is introduced while the optimal size of the CAES facility remains zero until a tax of $40/tCO$_2$e. This observation implies that better environmental performance and fuel economy of CAES are not strong enough to justify investing in this capital-intensive technology at low emissions penalties. As the tax (and thus effective fuel price) increases from zero, the size of SCGT (with higher fuel costs but a lower specific capital cost) decreases while the size of the more efficient but more expensive CCGT increases at a mild rate. Once CAES enters the picture at $40/tCO$_2$e, the optimal size of gas turbines declines at a sharp rate while the optimal size of wind farm increases rapidly. Therefore, relatively high emissions taxes would be required for economic competitiveness of the more expensive but less polluting wind farms and CAES facilities with conventional gas turbines. Another interesting observation is the relatively large size of the combined cycle gas turbines even at high emissions tax levels. As a case in point, the size of CCGT is 409 MW while the size of the wind farm and expander reach 1,160 and 397 MW at a high emissions tax of $80/tCO$_2$e. This behavior can be explained by the good thermal efficiency of CCGT technology and low GHG intensity of natural gas as its fuel. The CCGT and SCGT simulated here emit 473 and 727 kgCO$_2$e/MWh. This is while the GHG emissions intensity of the CAES plant is 277 kgCO$_2$e/MWh.

Not surprisingly, the size of the energy storage facility remains zero at tax levels below $40/tCO$_2$e in the D-CAES scenario as well (Figure 21). Utilizing less efficient gas turbines would result in a lower levelized cost of electricity at these low tax levels compared to building more efficient but capital-intensive D-CAES plants. The overall trend is similar to the CAES configuration: rapid increase in the size of the wind farm and expander of D-CAES and decline in the size of the gas turbines at emissions tax of $40/tCO$_2$ and higher. Nevertheless, comparing Figure 20 and Figure 21 leads to an interesting observation: the size of the wind farm, expander, compressor, and simple cycle gas turbines are larger in the D-CAES system compared to the

CAES configuration at the same emissions tax. On the other hand, the optimal size of the combined cycle gas turbine is smaller in the D-CAES system. As a case in point, Table 20 compares these values for the two systems at an emissions tax of \$60/tCO_2e. The larger sizes of the wind farm and energy storage plant (compressor, expander, and cavern) in the D-CAES configuration can be explained by the revenues associated with heat recovery, especially at high emissions taxes. However, the larger size of the less efficient SCGT and smaller size of the more efficient CCGT fleet in the D-CAES system may look strange at the first glance. As will be discusses later in Section 3-2, SCGT has a low capacity factor (dispatched infrequently) at high emissions taxes; therefore, its lower capital cost would favor it over more efficient but more capital-intensive CCGT.

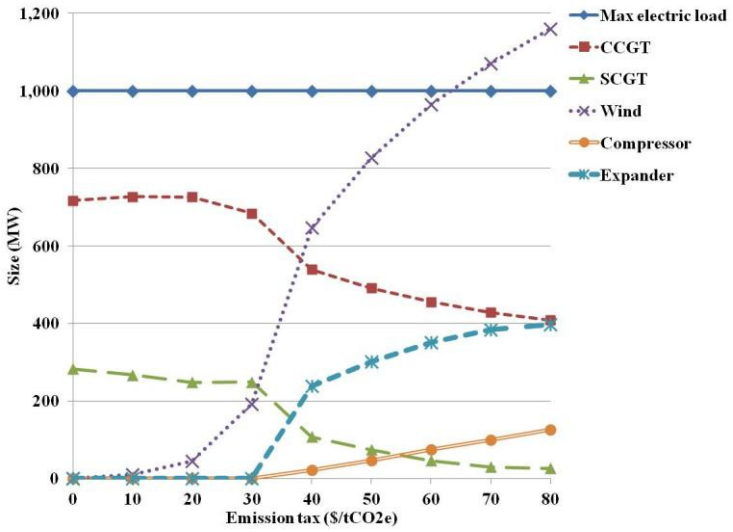

Figure 20: Maximum electric load and the optimal size of electricity generation fleet in the CAES scenario at various levels of emissions tax. Wind and CAES do not enter the electricity market until emissions tax of \$10 and \$40/tCO_2e, respectively. Base price of gas is \$5/GJ. Each \$10 increase in the emissions tax translates to ~\$0.7 increase in the effective price of fuel.

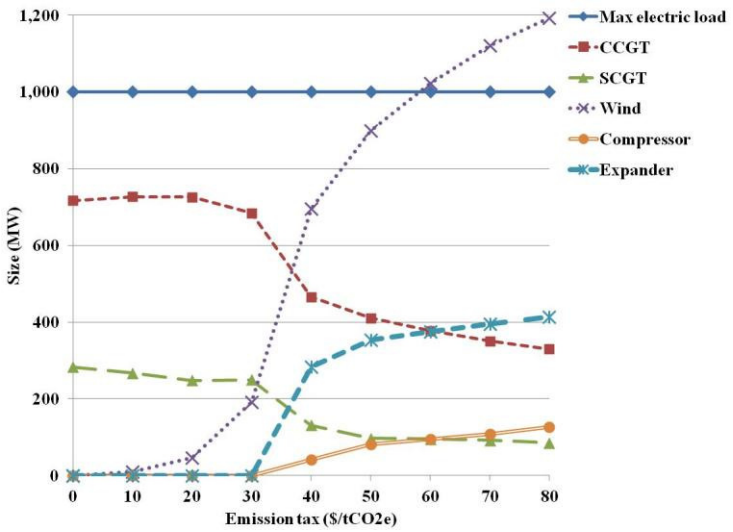

Figure 21: Maximum electric load and the optimal size of electricity generation fleet in the D-CAES scenario at various levels of emissions tax. Similar to the CAES system (Figure 20), wind and D-CAES do not enter the electricity market until emissions tax of \$10 and \$40/tCO_2e, respectively. Base price of gas is \$5/GJ.

Table 20: Optimal size of various system components for the CAES and D-CAES configurations at an emissions tax of \$60/tCO_2e. All values are in MW.

	CCGT	**SCGT**	**Wind farm**	**Expander**	**Compressor**
CAES scenario	456	47	965	351	76
D-CAES scenario	377	95	1,023	375	94

3-2- Distribution of electricity generation

Figure 22 and Figure 23 respectively show the share of the generation fleet of supplying electricity at different values of emissions tax for the CAES and D-CAES configurations.

In the absence of any emissions tax, the entire electric load is supplied by the combined and simple cycle gas turbines (98.0% and 2.0%, respectively). As emissions tax increase to \$30/tCO_2e, wind share increases to 12.1% while the share of CCGT and SCGT decrease to 86.4% and 1.5% in both systems. This level of tax is still not high enough to justify building capital-intensive compressed air energy storage plants and large wind farms. Nevertheless, as more aggressive emissions taxes are enforced, the share of gas turbines sharply decreases because of their less efficient operation and consequently higher emissions intensity compared to CAES, D-CAES and wind. Interestingly, the share of wind energy of the annual electricity generation increases

very fast, the share of CAES remains relatively small, and the share of the CCGT remains intermediate (although declining) at higher emissions taxes. These results reveal that even high emissions taxes ($80/tCO$_2$e at fuel cost of $5/GJ in our case) would not significantly increase the market share of the CAES facilities and most of the wind energy would be directly supplied to the grid rather than stored in the CAES facility due to its high capital costs and the requirement for burning fuel (heat rate of 4.19 GJ/MWh in this study).

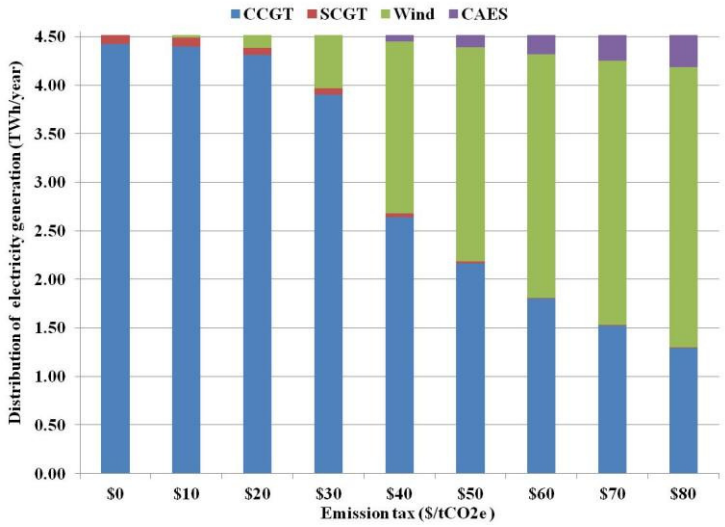

Figure 22: Distribution of annual electricity generation in the CAES configuration at various levels of emissions tax.

Table 21: Share of electricity generation of various components in the CAES and D-CAES configurations at a tax level of $60/tCO$_2$e. All values are expressed as percentage of the annual electric load.

	CCGT	**SCGT**	**Wind farm**	**Expander**
CAES	39.8	0.2	55.5	4.4
D-CAES	35.3	0.6	56.9	7.2

Similar results are observed for the D-CAES system as electric load is supplied solely by gas turbines and wind farm at emissions tax below $40/tCO$_2$e. Nevertheless, a major difference between the D-CAES system and the CAES system is the lower share of CCGT and higher share of wind, expander and SCGT of the annual electricity supply. As tabulated in Table 21, the expander of D-CAES supplies 7.2% of the annual electric load

while this value is 4.4% in the CAES configuration at an emissions tax of $60/tCO$_2$e. In addition, the CCGT share is 35.3% in this configuration while it is 39.8% for the CAES system. This observation is in agreement with the trend of equipment size in Figure 20 and Figure 21 with wind farm and expander replacing a larger market share of the CCGT in the D-CAES system due to revenues from heat recovery. Another observation is the small share of the SSGT of the annual electricity generation. Only 0.6% of the annual load is supplied by the simple cycle gas turbine because of its low thermal efficiency and high fuel costs at high emissions taxes. As discussed in Section 3-1, the size of the SCGT plant is larger in the D-CAES system compared to the CAES system in spite of its low thermal efficiency. However, SCGT has a very low capacity factor (realized annual electricity generation/ maximum possible annual electricity generation) of 3.3% in the D-CAES system; therefore, its lower specific capital cost would justify building a larger SCGT plant in the D-CAES system despite its higher fuel cost per MWh of electricity generated.

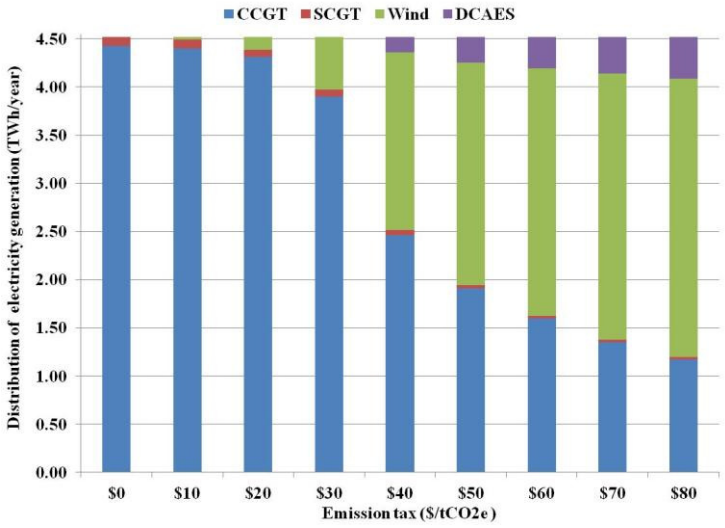

Figure 23: Distribution of annual electricity generation in the D-CAES configuration at various levels of emissions tax.

3-3- Distribution of wind energy

Although higher emissions taxes justify building larger wind farms, the fact that periods with large availability of wind do not necessarily coincide with periods of high electric load necessitates existence of gas turbines and/or storage facilities to fill the gap between the electric load and wind-based electricity generation. Despite the fact that compressed air energy storage plants have a lower heat rate compared to gas

turbines, they still burn fuel during the generation phase, which translates to high fuel costs. To further investigate the role of wind energy in meeting the electric demand, the distribution of the available wind energy (sold to the grid for instantaneous use, stored by the compressed air energy storage plant, or curtailed) at various levels of emissions taxes in the CAES and D-CAES scenarios are illustrated in Figure 24 and Figure 25.

Presence of wind energy is very limited in both systems below emissions taxes of $\$40/tCO_2e$. Interestingly, only a small portion of the available wind energy is stored while a much higher portion is supplied to the grid for instantaneous consumption. This observation is in agreement with the small size of the compressor in both systems as shown in Figure 20 and Figure 21 and is due to the high fuel costs of the storage facilities at high emissions tax. Another observation is the higher availability of wind energy and the portion of it that is stored in the D-CAES scenario, which is driven by revenues gained through waste heat recovery.

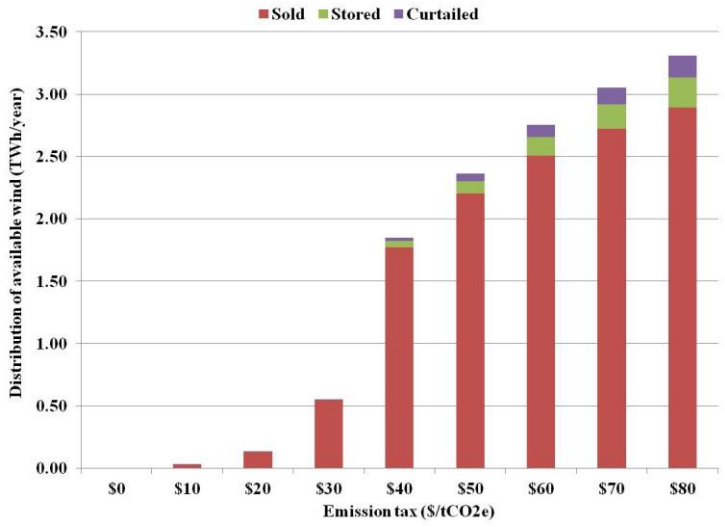

Figure 24: Distribution of available wind energy in the CAES configuration. Sold category represents the portion of available wind that supplies instantaneous electric load. A much smaller portion of the available wind energy is stored for later use (Stored category).

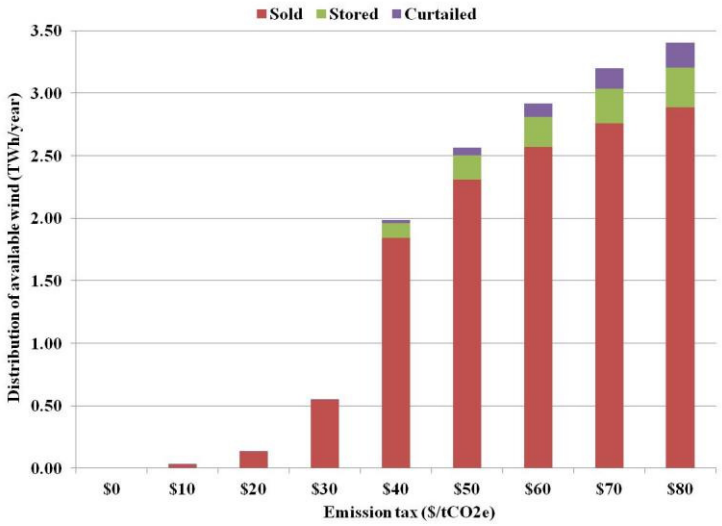

Figure 25: Distribution of available wind energy in the D-CAES configuration at various levels of emissions tax. Note higher penetration of wind energy in this scenario compared to the CAES scenario.

3-4- Distribution of heat supply

The entire heat load is supplied by the conventional boilers at tax levels below \$40/tCO_2e since the size of the compressor and heat recovery unit of D-CAES remains zero. As illustrated in Figure 26, waste heat recovery from the compressor of the D-CAES system negates fuel consumption of the boilers (HB) past this point and consequently reduces their share of annual heat supply so that 16.4% and 35.5% of the annual heat load is supplied by heat recovery (HC) at an emissions tax of \$40 and \$80/tCO_2e, respectively. This figure also illustrates the percentage of available compression heat that is utilized by the heat load (called utilization factor of compression heat). Recovery of waste heat negates consumption of fuel for heating purposes and gains revenues for D-CAES. The utilization factor of waste heat remains very high (above 80%) as the size of compressor increases at higher emissions taxes (see Figure 21 and Figure 26).

One should note that the contribution of the heat recovery system to the heat supply is subjected to the magnitude and fluctuations of both the electric and heat loads. In the system analyzed, the size of the electric load (maximum load of 1000 MW and average annual load of 516 MW electric) is relatively large compared to the heat load (maximum and average hourly heat load of 145.2 and 64.1 MW thermal, respectively). These values inherently make heat recovery from the D-CAES system more economic due to the much larger size of the electric load. This setting is in agreement with real world systems in which the typical size of power

plants are in the range of a few hundred MWs while the size of centralized municipal heat loads are usually in the range of a few tens of MWs. Moreover, a thermal energy storage facility (short- and long-term) might increase the share of heat recovery unit of the annual heat supply (or at least lead to a smaller HC and better economics for the D-CAES system), which is not studied in this paper.

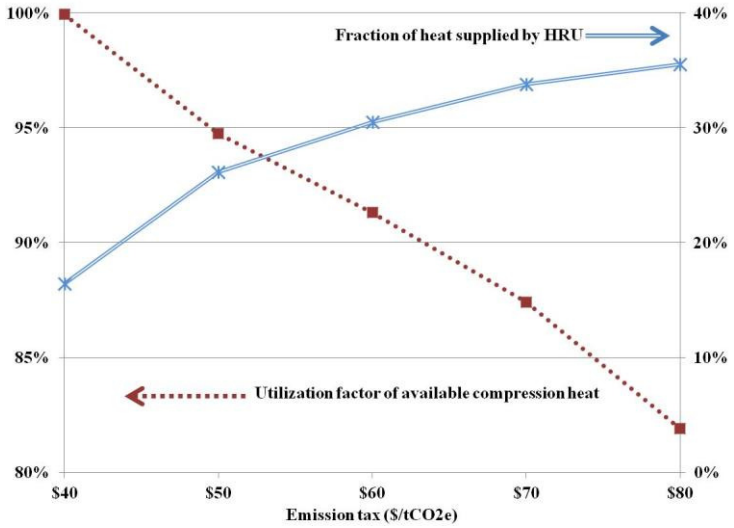

Figure 26: Fraction of the annual heat load supplied by the heat recovery unit (right axis) and percentage of recoverable heat of compression that is utilized by the heat load (left axis) in the D-CAES system. Utilization factor of compression heat decreases at higher emissions taxes since the size of the compressor (and therefore, the available waste heat) increases while the size of heat load is fixed.

3-5- Cost of electricity

Knowing the size and the hourly dispatch of the system components, the average cost of electricity at each effective fuel price was calculated for the two generation fleets considered in this study (one with the conventional CAES and one with the proposed D-CAES system). This cost can be used to determine the cross-over point of emissions tax: the tax level above which the D-CAES system is economically superior to the conventional CAES configuration. The LCOE of the D-CAES system becomes less than the cost of the CAES system ($73.7 and $73.8 /MWh, respectively) at an emissions tax of $40/tCO$_2$e (cross-over point with a pipeline length of 50 km) while the generation fleet is solely composed of wind farm and gas turbine prior to this point in both CAES and D-CAES scenarios. The cost of electricity in the D-CAES system remains lower than the CAES system past this level of emissions tax while their difference grows as the share of wind and

energy storage facilities of the annual electricity supply increases. The annual cost of electricity in D-CAES and CAES scenarios respectively reaches \$81.7 and \$82.6 /MWh at emissions tax of \$80/tCO_2e.

The primary drivers in the trade-off analysis between a D-CAES and a CAES plant are the capital cost of the pipeline and the revenues gained from heat recovery. Furthermore, the heat recovery unit of the D-CAES system would replace some capacity of the boilers of the district heating plant. In order to obtain better insight to this trade-off analysis, the size and capital and fuel costs of various components of the D-CAES system are given at the cross-over carbon price of \$40/tCO_2e in Table 22. The capital and fuel cost of the heat recovery unit are negative since they represent the savings in the capital cost (shaving of peak load of the boilers due to the existence of the HC) as well as the fuel cost of the boilers of the heating system. The capital cost of the air pipeline is approximately 8.5% of the total capital cost of the D-CAES plant (expander, compressor, cavern, and pipeline). However, the annual fuel savings from the heat recovery unit is \$2.86 million per year, more than 50% of the annual fuel consumption of the expander.

Table 22: Optimal size, fuel consumption and the amortized capital cost and fuel cost of the D-CAES plant at a tax of \$40/tCO_2e (the cross-over tax for the scenario with a 50 km long pipeline).

	Size	**Fuel consumption (TJ/year)**	**Capital cost (\$ million/year)**	**Fuel cost (\$ million/year)**
Expander	284 (MW)	734.7	14.62	5.61
Compressor	41 (MW)	NA	1.94	NA
Cavern	4,106 (MWh)	NA	1.26	NA
Pipeline	0.44 m (dia)	NA	1.65	NA
Heat recovery unit	29 (MW)	-374.1	-0.04	-2.86

The exact location of the cross-over point would depend on various system parameters such as the nature of the heat and electricity markets (composition of the generation fleet, value of ancillary services, etc.). The main contribution of this paper is to introduce and investigate the opportunity of the D-CAES system to economically compensate for fluctuations of wind-based electricity in niche markets. Recovery of the low-quality waste heat of compression form a compressed air energy storage facility for heating applications instead of using it to lower fuel consumption of the plant itself (*i.e.* A-CAES design) is a new approach that

could be valuable in a carbon-constrained economy. The authors emphasize that this system does require further evaluation prior to industrial development; however, believe that this model illustrates the potential benefits of D-CAES over conventional CAES technology.

3-6- Sensitivity analysis on the length of pipeline

The cross-over point is sensitive to the inputs and assumptions made in the simulation. Since the major difference between the conventional CAES and D-CAES systems is the air pipeline, the possible effects of the length of the pipeline on the cross-over point and thus the minimum fuel price required for economic competitiveness of D-CAES with CAES is evaluated in this section. In order to investigate the effect of the capital cost of the pipeline in this trade-off analysis, the simulations were repeated with two different pipeline lengths of 100 and 25 km.

D-CAES system with a pipeline length of 100 km: this increased length would not have any impact on the optimal configuration of the CAES system. However, it is expected to increase the LCOE for the D-CAES system (more expensive pipeline). The cross-over emissions tax in this scenario is \$50/tCO_2e as compared to the base case with a threshold tax of \$40/tCO_2e. The optimal values of the system components for the two D-CAES systems with 50 and 100 km pipelines are compared in Table 23. Increasing the length of the pipeline makes wind energy and compressed air storage less favorable and results in lower sizes for the wind farm, expander, compressor, cavern and air pipeline. Since a smaller compressor and wind farm are used, there are fewer opportunities for waste heat recovery and a smaller heat recovery system (HC) and a larger boiler (HB) are required. A longer pipeline, smaller wind farm, smaller HC, and thus higher demand for fuel to meet the electric and heat load would cause an increase of \$0.3/ MWh in the average annual cost of electricity in the D-CAES scenario with a 100 km long pipeline (a value of \$76.6/ MWh). Although this change in LCOE may not seem very high, it indicates that D-CAES systems could compete with conventional CAES systems effectively only under certain circumstances (niche markets) and highlights the importance of custom designing these facilities in accordance to the local parameters and local energy market conditions.

Table 23: Effect of pipeline length on the optimal size of system components and cost of electricity in the D-CAES configuration at an emissions tax of \$50/tCO$_2$e (cross-over point for the D-CAES system with 100 km long pipeline).

L_{PP} **(km)**	**50**	**100**
$Capt_{CCGT}$(MW)	411	416
$Capt_{SCGT}$ (MW)	97	107
$Capt_{Wind}$ (MW)	899	887
$Capt_{TB}$ (MW)	353	339
$Capt_{CM}$ (MW)	81	70
$Capt_{CN}$ (MWh)	7,316	6,362
D_{PP} (mm)	575	520
$Capt_{HC}$ (MW)	56	49
$Capt_{BL}$ (MW)	138	138

Simulation with 25 km pipeline: the cross-over emissions tax for the system with a shorter pipeline length of 25 km is \$30/tCO$_2$e corresponding to an effective fuel price of \$7.0/GJ (at a base natural gas price of \$5.0/GJ). These values are \$40/tCO$_2$e and \$7.6/GJ in the base-case system with a pipeline length of 50 km. The optimal capacity of various components of the two D-CAES systems at the carbon price of \$30/tCO$_2$e is tabulated in Table 24. The high capital cost of the 50 km pipeline leads to the superiority of conventional gas turbines so that the optimal system configuration only includes gas turbines and wind farms in this scenario. In other words, revenues from waste heat recovery would not be high enough to justify building a 50 km pipeline between the compression unit (heat load) and the cavern of the energy storage plant at low emissions taxes. However, these revenues are high enough to justify building a 25 km pipeline. The optimal design of the system with a 25 km pipeline includes a D-CAES facility with a 193 MW expander and a 23 MW compressor. Size of the energy storage plant and wind farms sharply increase past this point and the cost of electricity remains lower in this system compared to the configuration with the pipeline length of 50 km.

Table 24: Effect of pipeline length on the optimal size of system components and cost of electricity in the D-CAES configuration at an emissions tax of \$30/tCO_2e (cross-over point for D-CAES with 25 km long pipeline).

L_{PP} (km)	50	25
$Capt_{CCGT}$(MW)	684	618
$Capt_{SCGT}$ (MW)	249	114
$Capt_{Wind}$ (MW)	192	273
$Capt_{TB}$ (MW)	0	193
$Capt_{CM}$ (MW)	0	23
$Capt_{CN}$ (MWh)	0	2,314
D_{PP} (mm)	0	357
$Capt_{HC}$ (MW)	0	16
$Capt_{BL}$ (MW)	145	134

3-7- Emissions tax and emissions reduction

This study optimizes both the size and the dispatch of the gas turbines, wind farm, and CAES and D-CAES facilities supplying a variable electric load at various emissions taxes. This approach provides insight into the opportunity of reducing the carbon intensity of electricity generation, a major contributor to GHG emissions. The interesting question is how much of an emissions tax would be required to justify investing in more capital-intensive but cleaner technologies (wind and energy storage in this case) and drive the overall emissions of electricity supply below a certain level. The carbon intensity of electricity supply in this model at the natural gas price of \$5.0/GJ (and no emissions tax) is 507 kg CO_2e/MWh and the generation fleet is composed of only gas turbines. As higher emissions taxes are introduced and the effective price of natural gas increases accordingly, this value declines while the average cost of electricity increases.

Figure 27 illustrates the minimum emissions tax (vertical axis on the left) required to lower the emissions intensity from the base case value of 507 kg CO_2e/MWh in the conventional CAES scenario as well as D-CAES scenario with 25, 50, and 100 km long pipelines. This graph also shows an unrealistic scenario of co-located underground storage facility and heat load for the D-CAES system (0 km pipeline), as the most favorable scenario ("free heat" due to the possibility of waste heat recovery at no additional costs compared to the

CAES system). This scenario is presented for the sake of argument and to show the ultimate benefits from heat recovery. The effective price of fuel at each level of emissions tax (based on a fixed market fuel price of $5.0/GJ) is demonstrated on the right-hand side vertical axis. These values are calculated according to Equation 148 and show the total price paid by the plant for each GJ of natural gas consumed (*i.e.* summation of actual market price and emissions taxes).

The GHG intensity of all systems is the same at emissions tax of $0 and $10/t$CO_2$e (absolute values of 507 and 503 kg CO_2e/MWh, respectively) since fuel costs are not high enough to justify investing in either CAES or D-CAES. However, at an emissions tax of $20/t$CO_2$e, D-CAES with 0 km pipeline enters the generation fleet and consequently lowers the GHG intensity of electricity supply (a value of 468 compared to a value of 491 kg CO_2e/MWh for all other scenarios). Similarly, D-CAES with 25 km pipeline, CAES, D-CAES with 50 km pipeline, and D-CAES with 100 km pipeline enter the electricity market at an emissions tax of $30, $40, $40, and $50/t$CO_2$e, respectively. As expected, the D-CAES system with a longer pipeline has a higher emissions intensity compared to the D-CAES system with a shorter pipeline but still lower compared to the CAES scenario. In other words, the same level of emissions reduction would be achieved at a lower emissions tax for the system with a shorter pipeline compared to a system with a longer pipeline (or CAES system). Interestingly, the emissions intensity of all D-CAES systems become similar at very aggressive emissions tax measures so that the difference between GHG intensity of D-CAES systems with 0 km and 100 km pipeline becomes less than 2 kg CO_2e/MWh at an emissions tax of $80/t$CO_2$e (values of 149 and 151 kg CO_2e/MWh, respectively). This can be explained by the fact that the capital costs of the wind farm, expander, compressor, and cavern become much higher compared to the capital cost of the pipeline at such high emissions taxes, hence the total cost and emissions intensities are similar for different pipeline lengths. In other words, the optimal configuration and dispatch of the generation fleet with the D-CAES system for 0, 25, 50, and 100 km pipelines are less affected by the capital cost of the pipelines at aggressive taxes on GHG emissions.

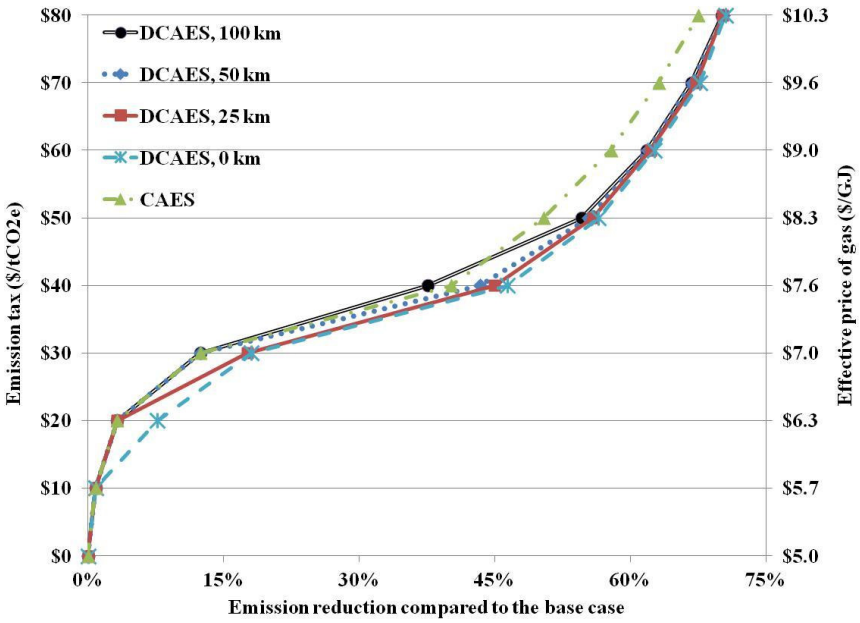

Figure 27: Emissions taxes and corresponding effective fuel prices required to reduce the carbon intensity of the electricity generation fleet compared to the base case of no emissions tax ($5.0/GJ effective fuel price and an average emissions intensity of 507 kg CO_2e/MWh).

4- Conclusions

The potential financial and GHG emissions savings through waste heat recovery in CAES plants to meet heating loads were evaluated in this study. The major additions to the compressed air energy storage facility equipped with waste heat recovery (a D-CAES plant) compared to a conventional CAES plant are a heat recovery unit and a pipeline to transport the generated compressed air from the heat load site to the storage site. A series of hypothetical scenarios with an electricity generation fleet composed of conventional gas turbines (CCGT and SCGT), a wind farm, a conventional CAES or a new D-CAES plant were analyzed. The electricity generation fleet was optimally sized and dispatched at minimum total cost over a period of one year at an hourly resolution. A district heating network equipped with conventional boilers and the heat recovery unit of the D-CAES plant was used to meet a concentrated heat load over the same one year period. The distance between the heat load (compression unit of the D-CAES system) and the underground air storage facility was set as 50 km in the base case.

At emissions tax levels below 40 $/t$CO_2$e, the optimal size of the wind farm and compressed air storage facility were small compared to the size of conventional gas turbines in both CAES and D-CAES configurations.

However, both their size and share of annual electricity generation rapidly increased as more aggressive emissions taxes were introduced. This behavior shows that relatively high taxes on GHG emissions would be required for compressed air energy storage plants (both CAES and D-CAES) to be competitive with conventional gas turbines to be used to compensate for fluctuating output of wind farms. Both the size and share of the wind farm and storage facility were larger in the D-CAES configuration compared to the CAES system revealing the economic gains from the use of otherwise-wasted heat of compression for heating applications. In other words, fuel savings gained from waste heat recovery in the D-CAES system could justify building larger capital-intensive but cleaner wind farms and storage facilities to support wind-based electricity. As a result, the emissions intensity of the generation fleet equipped with D-CAES instead of conventional CAES plant would be lower. The financial gains from heat recovery outweighed the increased capital cost of the D-CAES system past the cross-over point of $\$40/tCO_2e$. The fact that the average cost of electricity in both systems remained close revealed that a D-CAES system could compete economically with conventional CAES plants in certain niche markets but the exact performance would depend on the nature of the electricity market under investigation. It bears mentioning the wide development of D-CAES systems is likely to be firstly limited by the availability of suitable geologic formations in proximity to concentrated heat loads. Considering the size of the electric load (peak of 1 GW), size of simulated heat load (three times the size of University of Calgary), and optimal size of the expander of D-CAES (28% of the peak electric load at an emissions tax of $\$40/tCO_2e$), the size of electric load rather than heat load is expected to be the second limiting factor.

We also evaluated the sensitivity of the results to pipeline length. The cross-over emissions tax price for economic superiority of the D-CAES system with a 100 km pipeline instead of the base-case length of 50 km was increased to the value of $\$50/tCO_2e$. This $\$10/tCO_2e$ increase translates to an increase of $\$0.7/GJ$ of natural gas price. However, the D-CAES system becomes more competitive with the conventional CAES at shorter distances between the heat load (compression facility of the D-CAES plant) and the storage site. The cross-over emissions tax in a system with a shorter pipeline length of 25 km is $\$30/tCO_2e$, corresponding to an effective natural gas price of $\$7.0/GJ$ at a base natural gas price of $\$5.0/GJ$.

Although the complex dynamics of the real world electricity markets were ignored in this study, we believe this assessment provides a high level insight into the possible economic gains from waste heat recovery for heating applications from compressed air storage plants. Due to the higher capital cost intensity of these facilities compared to conventional gas turbines, CAES and D-CAES would not be able to compete economically with gas turbines under normal conditions in the real world. Aggressive GHG taxes or other economic incentives are required to compensate their higher capital costs, which would affect the already complicated market dynamics. Therefore, this simplified approach is not expected to cause significantly higher errors compared to the case in which future market dynamics were forecasted. A macro level approach was chosen in this paper, as the first study to introduce and evaluate D-CAES design, to inform the policy makers and assess the potential of D-CAES in supporting higher penetration of wind energy into the electricity grid in a carbon constraint world. We emphasize the importance of detail engineering and design of D-CAES plants based on the local policies and nature of electricity market to maximize the profit of the plant. In addition, a thermal energy storage unit was not considered in the D-CAES configuration for the sake of simplicity. As a result, the heat of compression could only be used to satisfy the instantaneous heat load. The economics of heat recovery from compressed air energy storage facilities may improve if such thermal energy storage facilities are considered, especially for seasonal storage of waste heat[15]. Finally, a generation fleet with lower pollution levels (*e.g.* NO_x emissions) would benefit the neighboring communities through improved air quality, another benefit of the D-CAES plants that could enhance their competitiveness with conventional CAES systems.

[15] As a case in point, the Drake Landing solar Community in Okotoks, Alberta, Canada utilizes a borehole thermal energy storage facility to store thermal energy collected during the summer months for consumption during the winter months.

Chapter 4: Compressed air energy storage with waste heat export: An Alberta case study[16]

[16] This paper is published as Safaei, H. and D.W. Keith, Compressed air energy storage with waste heat export: An Alberta case study. *Energy Conversion and Management*, 2014. 78: p. 114-124.

Preface

While Chapter 3 explored the economics and emissions performance of D-CAES at a systems level, this chapter concentrates on individual (merchant) D-CAES plants interacting with electricity markets. The core of the analysis presented here addresses the question of how market conditions (price of electricity and gas) and engineering parameters (*e.g.* capacity of air store) may impact the profitability of D-CAES compared to conventional CAES for the electricity arbitrage application. Studying the economic viability of stand-alone D-CAES plants can stimulate R&D on this low-carbon technology to prove the concept and improve its technical characteristics, such as heat exchangers for waste heat recovery and thermal storage systems.

The analysis in Chapter 3 suggested that D-CAES could outperform conventional CAES when sized and operated as a part of the electricity and heating infrastructure. This chapter extends the economic and emissions analysis of D-CAES to deregulated electricity markets, *i.e.* maximizing profitability of the storage plant itself rather than minimizing the total cost of electricity and heat supply. A case study of two hypothetical CAES and D-CAES facilities performing energy arbitrage in the Alberta deregulated electricity market is presented here. A series of sensitivity analyses are performed to evaluate robustness of the results to the key design parameters: distance between cavern and heat load, capacity of cavern, capacity of compressor and turbine, and size of heat load. Moreover, a period of ten years with a variety of electricity and natural gas prices is simulated to assess the relative importance of these two key market factors.

Leaving the thermodynamics, emissions, and economic performance of D-CAES aside, one may ask how realistic it is to find a suitable geologic formation in the vicinity of a large heating load (the inherent requirement of D-CAES). A geological screening of natural gas reservoirs within 100 km radius of the two major cities in Alberta is also performed to shed light into this question.

The results of this chapter are based on a number of modeling assumptions and simplifications. Only one electricity market (Alberta) and one application of storage (arbitrage) are studied. Uncertainties in the price of electricity and natural gas are ignored. The D-CAES plant modeled is incapable of storing any excess recovered heat for future use. Moreover, the operation of the storage plants is assumed not to change the dynamics of the electricity market (*i.e.* price-taker assumption).

The economic performance of any storage facility depends on the dynamics of the electricity market that it operates in. The goal of this chapter is not to single out all possible markets, but to explore the role of two key market factors (*i.e.* wholesale price of electricity and natural gas). Performing the simulation over a ten-year period enables covering a large variety of electricity and gas prices. Moreover, wide spreads in electricity prices, abundance of geologic formations for air storage, and long winter climate make Alberta an appealing candidate for deployment of D-CAES. Since offering energy arbitrage is a primary role of bulk energy storage technologies, this chapter only studies this application of CAES and D-CAES. Including other ancillary services such as load following and firming capacity would strengthen the analysis.

Assuming perfect foresight of electricity and gas prices in the model is not expected to favor D-CAES over CAES in a substantial manner. This is because forecasts of heating loads and gas prices are far more accurate compared to electricity prices over the time scales (few days) that the operations of bulk storage facilities are planned. While the base case scenario presented here allows the recovered heat of compression to be utilized only for instantaneous heating demands, one scenario considers daily storage of thermal energy. The optimal size of the heating load is halved in this case. Performing a more comprehensive thermodynamic analysis of thermal storage could make a stronger case for competitiveness of D-CAES. In addition, D-CAES could offer cooling services (*e.g.* absorption chilling). Incorporating this service in future research can paint a more accurate picture for the economics of heat recovery from compressed air storage plants.

The conclusion that D-CAES may outcompete conventional CAES in the real world electricity markets is promising. The D-CAES plant would earn ~$1.3 million/year more on average compared to the conventional CAES in the 10-year study period (with a relative standard deviation of 119%). Additionally, the GHG emissions intensity of the D-CAES is about half of the CAES facility. Favorable economic as well as emissions performance would lead to a negative abatement cost of -$40 per ton of CO_2e avoided in the base case scenario.

While D-CAES may be more attractive compared to conventional CAES for energy arbitrage applications in certain markets and especially under GHG emissions restrictions, its potential as a cost-effective carbon mitigation tool should not be overstated. Availability of a large heating (or cooling) demand, which is supplied

by a GHG-intensive source and availability of an inexpensive air storage in close proximity are essential for the feasibility of D-CAES projects. These requiems leave limited opportunities for D-CAES compared to CAES, other bulk storage technologies, and low-carbon electricity sources such as biomass.

1- Introduction

Electric system operators dispatch the generation fleet in response to fluctuations in the load and to ensure grid reliability. Baseload power plants are characterized by low marginal costs, low ramp rates and high start up costs. Such inherent properties can lead to their part-load and less efficient operation and also depressed electricity prices during periods of low demand. On the other hand, peaking plants have low start up costs, fast dispatch, and high fuel costs. The variations in load and technical characteristics of the generation fleet cause fluctuations in electricity prices as well as inefficient and more polluting operation of the electricity sector. Penetration of intermittent renewable energies into the electricity grid could worsen the volatility of prices. Low marginal cost of wind and solar-based electricity would depress price of off-peak electricity [72]. At the same time, forecast errors and rapid changes in the output of these plants could increase the price of peak electricity [73, 74].

Price volatility of electricity is a business opportunity for energy arbitrage by energy storage plants. In addition to direct financial gains for the plant itself, an energy storage unit may benefit the electric system (positive externalities) in numerous ways such as increasing the capacity factor of baseload plants and intermittent renewables [10, 60, 67] and reducing grid congestion [5, 61]. Pumped hydro storage (PHS) and compressed air energy storage (CAES) are the two primary technologies for bulk storage of electric energy (hundreds of MW-hours) [59]. Development of PHS is constrained by factors such as the need for sufficient elevation difference between the two reservoirs, large land footprint, relatively high capital costs, and environmental licensing [10, 51].

CAES facilities buy electricity when prices are (relatively) low to run large compressors and store electricity in the form of compressed air, which later is combusted to power modified gas turbines (air expanders) when prices are high. CAES plants can store air in both underground (*e.g.* salt caverns) and aboveground reservoirs (pressure vessels) and thus have more siting flexibility [10]. Furthermore, they have shorter construction time (around 3 years) and are less capital intensive compared to PHS projects [62]. There are currently two operating utility-scale CAES plants in the world. The first one is in Huntorf, Germany with an output of 290

MW over four hours, while the second plant is in McIntosh, Alabama and can generate 110 MW of electricity for 26 hours [10].

Efficiency and economics of CAES have been improved since the commissioning of the Huntorf plant in 1978. Recuperating heat from exhaust of the air expander in order to preheat air prior to entering the combustor reduced fuel demand of the McIntosh plant by 25% [5]. Among various CAES designs, Adiabatic and Distributed CAES are of special interest. They both aim to address energy losses associated with waste heat of the compressor. In adiabatic CAES, air is adiabatically compressed to high pressures and temperatures while its heat is recovered prior to storage. The compression heat is stored in a thermal energy storage facility to reheat compressed air over the discharge phase. Utilization of the compression heat can negate and even eliminate the need for combustion of fuel and consequently increase efficiency of the plant [5]. However, this design is still in the research and development phase as its technical and economic feasibility is challenged by the need for high pressure and high temperature compressors and thermal energy storage facilities as well as high pressure expanders [11, 55].

Distributed compressed air energy storage (D-CAES) aims to enhance efficiency and economics of CAES by utilizing the compression heat for space and water heating applications. The D-CAES concept was first proposed by the authors in an another paper [75] and a patent [56] . Energy used for municipal heating applications could be of low exergy content (low temperature) in contrast to the heating energy required for Adiabatic CAES, which imposes technical difficulties to and cost burdens for this technology. The compressor of D-CAES is located near high heat load centers, such as a hospital. This configuration is different from the conventional CAES in which the compressor is co-located with the expander and air storage. Compression heat would be recovered through a heat recovery unit (HC) and sold to supply a space and water heating load with the aim of supplying a district heating network. Therefore, D-CAES benefits from an additional revenue source compared to CAES. The downside of D-CAES is the need for a pipeline to transport air from the compression facility (co-located with heat load) to the storage site located at favorable geologic formations. Therefore, the capital cost of D-CAES is higher compared to conventional CAES. D-CAES can be only economically feasible where the air storage site is in the vicinity of the heat load, otherwise the cost of pipeline would outweigh revenues from heat recovery. In some markets, the carbon emission reductions that

occur when waste heat displaces heating fuel may have a separate economic value such as a carbon credit, reduction in tax, or other instruments.

Our previous paper [75] evaluated the competitiveness of D-CAES with conventional CAES, simple cycle, and combined cycle gas turbines at a systems level (*i.e.* minimizing the entire cost of electricity supply or maximizing the net social welfare) in a carbon-constrained world. Here we extend our earlier work to examine the performance of D-CAES under real-world market conditions. This paper compares the economics of CAES and D-CAES in a deregulated electricity market based on historical data. Both facilities are dispatched as stand-alone merchant plants performing energy arbitrage to maximize their own profit. They are equipped with a 131 MW expander, a 105 MW compressor and a depleted gas reservoir with 1,572 MWh of generation capacity (enough for discharging at full load for 12 hours) in the base case scenario. The air storage site is located 50 km away from a concentrated heat load (five times larger than the University of Calgary, Canada). Price of natural gas, as a primary fuel for municipal heating would directly impact revenues from waste heat recovery. On the other hand, it can affect the price of electricity and thus the revenues of energy arbitrage. The main contribution of this paper is evaluating the effect of market conditions (gas and electricity prices) and design parameters (*e.g.* length of pipeline) on the economic competitiveness of D-CAES with conventional CAES system in energy arbitrage applications.

The underlying assumption in this paper is that both facilities are price–takers. This implies the storage plants are not sufficiently large so that their operation could affect the dynamics of the market and change the price of electricity or gas. If the capacity of the compressor becomes comparable to the system load, then the price of off-peak electricity would likely rise (due to higher demand). This would be beneficial to the suppliers (higher sales and less cycling) while unfavorable to the consumers (including the storage plant itself due to higher prices). On the other hand, the ability of a large expander to deliver significant volumes would depress the price of peak electricity. This situation would indeed benefit the consumers (lower charges) and the grid (less need to dispatch inefficient plants). However, this would hurt the profitability of the peaking plants, including the storage facility itself. Studying such possible effects is not in the scope of this paper. On the grounds that the size of the modeled compressor and expander are approximately 1% of the

minimum annual load and the total installed generation capacity respectively, we have assumed that operation of the studied storage plants would not impact the dynamics of the market.

2- Methodology

This paper investigates potential financial gains associated with heat recovery for space and water heating applications from the compression train of a CAES plant performing energy arbitrage. The Alberta electricity market is chosen as the market in which energy arbitrage is performed. The dispatch of two hypothetical CAES systems, with and without heat recovery ability, is optimized in various scenarios to maximize the profit of energy arbitrage and heat recovery. We use linear programming in MATLAB to optimize dispatch of the plants at an hourly resolution. A suite of sensitivity analyses is performed to evaluate the robustness of the results to a variety of factors: size of heat load, capacity of air storage, capacity of CAES turbo-machinery, distance between heat load and air storage site, and variations in price of electricity and gas over a period of ten years in Alberta. The size of system components are fixed in each scenario while dispatch of the plants is optimized.

2-1- System of study

CAES can use a variety of geologic formations for air storage. Both Huntorf and McIntosh plants store air in solution-mined salt caverns while Norton facility is to use an abandoned limestone mine [5] and the Iowa Stored Energy Park (ISEP) project was to store air in an aquifer [76]. Depleted gas reservoirs are also attractive for air storage because of their relatively low development costs [5, 10].

A large concentrated heat load over a long time and at a short distance from the air storage site would be ideal for economic attractiveness of D-CAES. This is due to the trade-off between revenues of heat recovery and capital cost of the air pipeline. Because of the relatively cold winter climate of Calgary, Alberta, Canada [77] and abundance of gas reservoirs in its proximity [78], we assess the economics of CAES and D-CAES using depleted gas reservoirs in the vicinity of Calgary, as a case study. Both CAES and D-CAES plants would perform energy arbitrage in the Alberta electricity market while D-CAES would gain extra revenues through sales of its compression heat to a concentrated heat load in Calgary. We do not include capital cost of the base CAES plant and take into account only the cost of additional components required for waste heat recovery (*i.e.*

air pipeline and heat recovery unit). This is because the main goal of this study is quantifying the net value of exporting the otherwise wasted heat of compression from CAES plants. This approach also allows us to avoid the current uncertainties in the true capital cost of conventional CAES technology as only two plants are so far deployed on a commercial scale. The underlying assumption in this paper is that building a merchant conventional CAES facility for energy arbitrage is already justified and our focus is evaluating various circumstances under which heat recovery improves the economics of electric energy storage.

2-2- Electricity market of Alberta

Alberta's deregulated electricity market is managed by the Alberta Electric System Operator (AESO). The Alberta Power Pool is the spot (real time) market of wholesale electricity and there is no day-ahead market. Electricity price is capped at 999.99 $/MWh and negative prices are not allowed [79]. The generation units can voluntary modify their offers up to two hours before the delivery time. After this deadline, “Must Offer/Must Comply” (MOMC) rule is applied to all generators (except wind) implying that they will be penalized if cannot fulfill their commitment. Market participants are dispatched in real time by AESO. The price of the last dispatched unit sets the electricity price, known as system marginal price (SMP). The time-weighted average of SMP determines the wholesale settlement price for each hour, known as the pool price. One distinct characteristic of the Alberta market is lack of a capacity market; it is an "energy only" market. In other words, generators only get paid if they are dispatched. Another important characteristic is the relatively high ratio of average load to peak (load factor of approximately 80%), which is caused by the large share of industrial customers and consequently large market share of baseload plants. The fact that wholesale prices are set in real time, absence of a capacity market, and large market share of baseload plants inherently contribute to the high price of peak electricity in this market. In other words, price of peak electricity needs to be high enough so that the peaking plants (with low capacity factors) are able to recover both their operation and capital costs. Furthermore, wind farms are currently exempted from the MOMC rule and are treated as price takers. The fluctuations in the output of wind farms are managed through the power pool and the balancing services because of their low penetration level into this market (865 MW, 6% of installed capacity in 2011 [80]) without direct cost burdens on wind farms.

The dynamics of this electricity market and relatively high price fluctuations create favorable conditions for energy arbitrage. Therefore, the hypothetical CAES and D-CAES plants are assumed to directly buy and sell electricity from and to the Alberta Power Pool[17]. Natural gas is assumed as the fuel of both storage plants and boilers (BL) of the district heating system. Our model uses historical wholesale electricity price reported by AESO [81] and the weighted average of gas prices traded on the Natural Gas Exchange (NGX) [82].

2-3- Heat load

Compression heat of D-CAES would be supplied to a municipal heat load through a district heating system. While a variety of heat loads can be serviced by district heating networks (single houses, office towers, etc.), a concentrated load would be the ideal candidate due to the relatively high initial and operation costs of long distribution systems. Examples of such ideal loads are downtown core, universities, and shopping malls. Since both the hot water and space heating demands of the University of Calgary are currently supplied through a district heating network, this load is used to represent a typical concentrated municipal heat load that would purchase waste heat from D-CAES. Thermal efficiency and hourly fuel consumption of the heating plant of this university in the year 2011 is used to determine its hourly heat load. This profile has a maximum and average value of 48.4 and 21.4 MW thermal, respectively. Analysis of the profile revealed strong correlation between the average hourly outside temperature and heat load (R^2=0.88). Therefore, we used the historical data for hourly temperature of Calgary reported by Environment Canada [83] to approximate the hourly load of the University of Calgary over the 10 year simulation period. D-CAES plant is assumed to sell its waste heat to a load with the same profile as the University of Calgary but five times larger in the base case system. The effect of heat load size on the economics of D-CAES is examined through sensitivity analysis. The waste heat of D-CAES may satisfy a portion or the entire heat load, depending on its availability. Revenues from heat recovery are assumed equal to the market value of the fuel savings.

A thermal energy storage (TS) unit could store the excess waste heat recovered during periods of low demand for use at a later time with high heating needs, improving the revenues of waste heat recovery. This is because periods of relatively inexpensive electricity price (when the compressor is likely operating) could

[17] Electricity can also be traded in forward markets or through bilateral agreements, which are not in the scope of this work.

coincide with periods of relatively low heating demands. TS systems can store heat over daily, weekly, and even seasonal time scales. In spite of potential economics gains through storage of thermal energy, no such a storage unit is considered in the base case scenario while the impact of daily storage of recovered heat is discussed in Section 3-2.

2-4 Compressed air pipeline

A pipeline would transport compressed air from the compressor to the storage site in the D-CAES configuration. Length of this pipeline is the key factor in economic viability of D-CAES as it impacts initial cost of the pipeline. Where the length of pipeline is zero (heat load and air storage are co-located), D-CAES would always be preferred over conventional CAES.

Although locating a suitable geologic formation for air storage is not in the scope of this paper, we performed a preliminary screening of natural gas reservoirs to investigate the possible availability of such a geologic formation in the vicinity of municipal heating loads in Alberta. We applied a set of geological screening criteria (Table 25) to a database compiled by an engineering firm for gas reservoirs within 100 km radius of Calgary and Edmonton, the two largest cities in Alberta. These criteria are pore volume, porosity, initial pressure, and pay thickness. Although permeability is an important geological characteristic too, it is not included in this screening practice due to the limited availability of rigorous data in the public domain. We recognize that these criteria are only for high level screening and detailed core sampling, reservoir modeling, and air injection tests are required for final selection of a suitable reservoir. The minimum pore volume is set so that enough compressed air (known as cycled air) can be stored to support 12 hours of electricity generation at a rate of 131 MW (capacity of the expander in the base case system), assuming a ratio of 5 for the volume of total stored to cycled air.

The number of gas reservoirs within 100 km radius of Edmonton and Calgary that meet these geological criteria is tabulated in Table 26. As shown, pay thickness is the most limiting factor followed by storage capacity (pore volume), pressure, and porosity of the reservoir and a total of 32 reservoirs met all the criteria. Although the injection and withdrawal rates in CAES facilities are generally higher compared to the rates seen in the natural gas industry, advanced techniques such as horizontal drilling and hydraulic fracturing could

relax the possible constraints imposed by low permeability of gas reservoirs [76, 84]. Therefore, there is a chance that at least one of these 32 identified reservoirs is suitable for storage of compressed air. Based on these results, we assumed a distance of 50 km between the compression and storage site in the base case analysis. The pipeline length is varied between 0 and 100 km in Section 3-5 to evaluate its impact on the economics of D-CAES.

Table 25: Geological criteria for screening of natural gas reservoirs for air storage.

Criterion	**Threshold**	**Notes**	**Reference**
Storage volume	>900,000 m^3	Based on a volumetric ratio of 0.2 for cycled to total stored air	[85, 86]
Porosity	>10%		[87]
Initial pressure	>5,700 kPa	Inlet pressure of expander	[86]
Pay thickness	>15 m		[86]

Table 26: Number of natural gas pools within 100 km radius of Calgary and Edmonton that meet the geological requirements used in this study for air storage.

City	**Total pools**	**Pay thickness**	**Storage volume**	**Initial pressure**	**Porosity**	**All criteria**
Calgary	6,726	187	1,027	3,788	3,793	26
Edmonton	10,039	47	1,625	4,056	7,273	8

The compression unit (located at the heat load site) would pressurize air enough to compensate the pressure losses along the pipeline. Equation 150 is used to estimate the pipeline pressure drop (see nomenclature for definition of symbols) [26].

$$P_{PP,up}^2 - P_{PP,dn}^2 = 9.4 \times 10^4 \times \frac{T_{PP} \times L_{PP} \times f_{PP} \times {F_{PP}}^2}{{D_{PP}}^5} \quad \text{Equation 150}$$

Through fixing the downstream pressure (P_{dn}), maximum pressure drop per unit length of pipeline, and maximum flow rate of pipeline, Equation 150 can be used to calculate the minimum diameter at each pipeline length. The downstream pressure (and hence the storage pressure) is set as 7400 kPa, the average storage

pressure of the ISEP CAES project. The maximum pressure drop is set 25 kPa per km length of pipeline, a typical value for natural gas pipelines [64]. Maximum flow rate of pipeline is calculated based on the capacity of the compressor (105 MW) and storage pressure of 7,400 kPa. The calculated values for the pipeline diameter are shown in Table 27.

Table 27: Diameter and capital cost of the pipeline and work ratio of D-CAES.

Length (km)	Diameter (m)	Capital cost ($ million)	D-CAES work ratio
25	0.74	17.0	0.76
50	0.74	30.6	0.77
75	0.74	43.3	0.77
100	0.74	55.4	0.78

2-5- Performance parameters

Turbo-machinery of CAES is composed of a compressor, expander, and combustor; similar to conventional gas turbines. While about half of energy generated by the expander is used to power the compressor of gas turbine, a CAES compressor is normally powered by electricity. CAES plants use both mechanical energy (electricity to power compressors) and heating energy (fuel to combust air) while gas turbines consume only fuel. Therefore, both the input fuel and electricity must be taken into account to quantify efficiency of a CAES plant. Heat rate represents the amount of fuel consumed per unit of electricity generated and sold. Because no energy is consumed by compressor during the discharge phase, heat rate of CAES is much lower (half to one third) of that for a similar sized gas turbine [5]. Work ratio is the second performance metric of CAES, which expresses amount of electricity purchased to charge the cavern per unit of electricity sold back to the grid. See Table 28 for heat rate and work ratio values used in this study. Work ratio of D-CAES is higher compared to conventional CAES because of the pressure losses in the air pipeline. Table 27 shows values used for work ratio of D-CAES. This parameter is modified for each pipeline length to take into account energy losses in the pipeline according to Equation 150.

It is of note that a CAES plant can operate as a gas turbine when it runs short of stored air [52]. The compressor would consume a portion of the work generated by expander in this case. Therefore, fuel

consumption of CAES would increase from the optimal design point; close or even higher than values seen in gas turbines. A CAES plant is not likely to operate at these elevated heat rates unless high prices of peak electricity outweigh the increase in the fuel costs. Both plants are assumed to have such operational flexibility.

A thermal efficiency of 80% (higher heating value, HHV) is considered for the boilers and distribution pipes of the district heating network. This value is used along with the price of natural gas to estimate the financial revenues of heat recovery for D-CAES. We also used a heat recovery coefficient of 70% indicating that up to 70% of the compression energy can be recovered and supplied to the heat load.

Table 28: Performance characteristics of components of the CAES and D-CAES systems.

Parameter	**Symbol**	**Value**	**Notes**
Expander heat rate	HR_{TB}	4.2 (GJ/MWh)	[9]
CAES work ratio	WR	0.75	[9]
Boiler efficiency	η_{BL}	80%	High heating value
Heat recovery coefficient	η_{Hc}	70%	

2-6- Costing inputs

The underlying assumption in this study is that building a merchant CAES plant is already justified from technical and financial perspectives and the primary question addressed here is whether to build a D-CAES or a conventional CAES facility. Therefore, the capital cost (CapEx) and fixed operation and maintenance costs (FOM) of the base CAES plant are not included in our analysis. The CAES facility is composed of a 131 MW expander, 105 MW compressor and a depleted gas reservoir with 1,572 MWh of storage capacity (equivalent to 12 hours of generation at full capacity), in accordance with a recent study on the design and costing of CAES plants by the Electric Power Research Institute (EPRI) [9]. The major additional equipments in the D-CAES system are the air pipeline and heat recovery unit (HC). Capital cost of the pipeline is estimated for each pipeline length and diameter with the aim of a regression model developed by Sean McCoy [65] (see Table 27). Capital cost of HC is assumed negligible since air has to be cooled down prior to storage anyways, even if the heat is not to be used for heating applications. In other words, the capital cost of the heat

exchanger is already included in the cost of the base CAES plant and no major additional costs are expected for the D-CAES facility[18].

Costs associated with transmission lines to move electricity to/from the plants as well as cost of the gas pipeline required to deliver fuel to the expander are ignored since these components would be common between the two plants. One D-CAES configuration originally proposed by the authors in [56] considers moving both the compression and expansion trains from the storage site to the proximity to heat load. A single pipeline would transport air to the storage site and back to the expander for electricity generation. The advantage of this configuration is eliminating the need for gas pipelines and transmission lines at the storage site. Despite potential cost savings in this scenario, this paper assumes that expander of D-CAES is co-located with the air storage at some distance from the heat load.

Although CapEx and FOM of the base CAES system are excluded from our analysis, marginal capital and FOM cost of the expander, compressor, and air storage are considered in the sensitivity analysis section. These costs are used to evaluate how a different set of equipment size would alter economics of CAES and D-CAES compared to the base case scenario. Marginal costs are derived from a recent report on the design and costing of CAES by EPRI [9] and are shown in Table 29. All CapEx and FOM values are expressed in 2009 inflation adjusted US dollars according to the Chemical Engineering Plant Cost Index [68, 69]. VOM and revenues of energy arbitrage and heat recovery are adjusted for inflation based on Customer Price Indices (CPI) of Alberta reported by Statistics Canada [88] and are reported in 2009 US dollars.

[18] Recovery of the compression heat might reduce the size (and consequently CapEx and FOM cost) of the boilers of the district heating system. A smaller boiler can be utilized since a portion of the heat load is supplied by heat recovery unit (HC) of D-CAES.

Table 29: Costing inputs for assessing the economics of CAES and D-CAES. Capital cost and VOM of the heat recovery unit are negligible.

Parameter	Symbol	Value	Reference
Marginal CapEx of expander	$CapEx_{TB}^{Marg}$	440 ($/kW)	[9, 60]
Marginal FOM of expander	FOM_{TB}^{Marg}	8.0 ($/kW/year)	[9]
VOM of expander	VOM_{TB}	0.87 ($/kWh)	[9]
Marginal CapEx of compressor	$CapEx_{CM}^{Marg}$	415 ($/kW)	[9, 60]
Marginal FOM of compressor	FOM_{CM}^{Marg}	8.0 ($/kW/year)	[9]
VOM of compressor	VOM_{CM}	0.87 ($/kWh)	[9]
Marginal CapEx of air storage	$CapEx_{CN}^{Marg}$	0.15 ($/kWh)	[5]
FOM of pipeline	FOM_{PP}	3,820 ($/km/year)	[89]
Blended cost of capital	BC	10%	

2-7- Optimization model

A linear programming model is developed in MATLAB to determine the optimal dispatch of the CAES and D-CAES plants. The optimal dispatch is defined as the operational strategy which maximizes the annual profit of the energy storage plant through energy arbitrage and heat recovery. The objective function is shown in Equation 151. The first term expresses the financial gains through sales of electricity; the difference between payments from the electricity market and operation cost of the expander (fuel and VOM). The second and third terms represent the costs of running the compressor. The second term shows the cost of powering the compressor by the expander; the fuel consumed by the expander and VOM cost of expander and compressor. The third term calculates the cost of powering the compressor with electricity. The profits of waste heat recovery are calculated in the fourth term. Terms (EL_{Sold}) and (EL_{Pur}) indicate electricity (MWh) sold to and purchased from the grid during time *t*, respectively. Term (EL_{TB_CM}) expresses electricity (MWh) supplied by the turbine of the storage plant to its compressor during time *t*.

$$Maximize \sum_{t=1}^{24\times 8} \Big\{ [EL_{Sold} \times (\pi_{EL} - HR \times \pi_{NG} - VOM_{TB})] - [EL_{TB\_CM} \times (HR \times \pi_{NG} + VOM_{TB} + VOM_{CM})] - [EL_{Pur} \times (\pi_{EL} + VOM_{CM})] + \left[HL_{HC} \times \left(\frac{\pi_{NG} \times 3.6}{\eta_{BL}} - VOM_{HC}\right)\right] \Big\}$$ Equation 151

An hourly resolution is chosen for this study since energy arbitrage is the main application of the plants simulated. This approach is in agreement with other studies in the field of economic assessment of CAES systems dispatched for arbitrage of electric energy [52, 59-61, 90]. A bulk energy storage plant is normally dispatched based on its marginal operation cost and current and expected future price of electricity. This approach requires the plant operator to forecast future price of fuel and electricity. Sioshansi *et al.* [90] evaluated the arbitrage profit of a hypothetical CAES facility in the PJM market with two different planning strategies. In both cases, the operational schedule for the following two weeks was set at the beginning of that period. Arbitrage profits were then summed to estimate the annual profits. The first planning strategy assumed that perfect foresight of market prices over the two week planning horizon was available. This case corresponds to the maximum theoretical profit because of perfect knowledge over future prices. On the contrary, the storage plant was dispatched solely based on the historical prices of the past two weeks in the second case (backcasting method). The simulation results over a period of 6 years revealed that the backcasting method was able to capture about 85% or more of the maximum theoretical value obtained in the first case. This phenomenon is mainly driven by the fact that the diurnal and weekly changes in the electricity prices are relatively predictable and repeated over time. The two scenarios modeled by Sioshansi *et al.* represent two extreme cases for dispatching energy storage plants in the real world. The arbitrage profits of real plants would be in between these extreme cases and sophisticated forecasting models and dispatch algorithms would reduce the gap between actual and the maximum theoretical profits. This paper; therefore, assumes perfect knowledge of electricity and gas prices in each planning period.

We choose a period of eight days as the planning horizon in order to take advantage of fluctuations in electricity prices driven by the diurnal (intra-day) and weekly (weekday and weekend effect) cycles in the demand and prices. This planning horizon is in accordance with sizing of the air storage and operational

strategy of real world CAES plants. As a case in point, the geologic formation of the ISEP CAES project could hold enough air to support 36 hours of electricity generation (week-long storage of energy). Furthermore, each planning period is overlapped one day with the next one to ensure smooth transition (rolling window optimization). This approach ensures that market signals over the next period are taken into account while the dispatch of the energy storage is optimized individually in each period. It is of note that our estimates for arbitrage revenues are more conservative (lower) compared to Sioshansi *et al.* since they used a two week planning horizon versus our 8 day period.

Maximizing profit of the energy storage plants in each eight-day planning horizon is subjected to the following constraints:

- Maximum heat recovered during each hour in the D-CAES configuration is equal to the product of heat recovery coefficient and the compression energy consumed during that hour.
- Heat supplied to the load during each hour is equal to or less than the hourly heat load.
- Output of the expander is less than or equal to its capacity.
- Energy stored in the air storage is less than or equal to its capacity.
- Energy consumption of the compressor in each hour cannot exceed its capacity.
- Conservation of energy is honored for the air storage. The net energy injected in each hour should be equal to the increase in energy level of the cavern during that hour.
- Energy level of air storage at the beginning of each planning period is set based on plant's dispatch in the previous planning period.

Five parameters are determined by the optimization code for each hour: energy level of air storage, electricity purchased from the grid, electricity sold to the market, portion of expander output that is used by the compressor, and finally the amount of compression heat recovered. Figure 28 illustrates a snapshot of optimized dispatch of D-CAES.

Arbitrage profits are calculated over a period of one full year to reflect seasonal changes in the price of electricity and gas as well as the heating load. In order to take the annual fluctuations into account as well, the profits are computed over a period of ten years (2002 to 2011). As illustrated in Figure 29, this period

embraces a wide range of market conditions. Mild prices in early years, significantly higher prices between years 2004 to 2008 (economic boom), depressed prices during the recent economic recession (years 2009 and 2010), and finally high electricity price and very low gas price in 2011 are observed in this decade. This figure also illustrates average of daily standard deviation of electricity prices for each year. As will be shown in next section, the daily fluctuations of electricity prices strongly impact the revenues of electricity arbitrage.

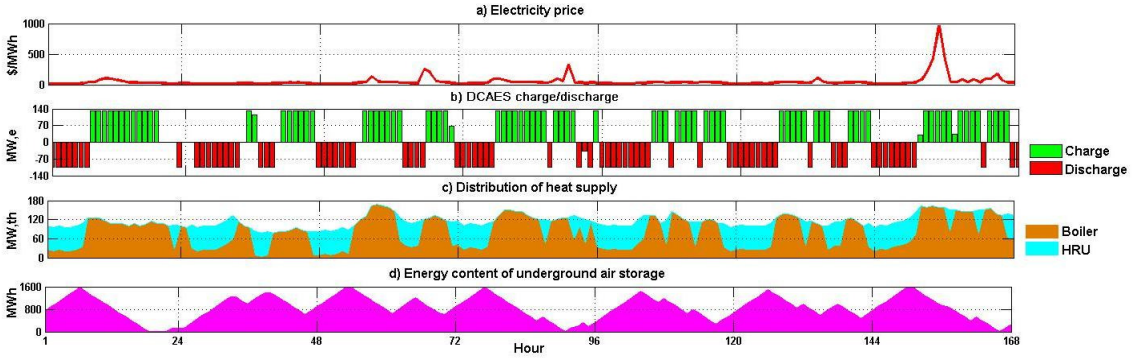

Figure 28: Optimized dispatch of D-CAES system over an arbitrary time period (Saturday, October 29 to Friday, November 4, 2011). "Charge" and "Discharge" in subfigure b represent energy purchased from and sold to the electricity market, respectively.

3- Results and discussions

3-1- Base case scenario

Annual operating (gross) profits of the CAES plant and the additional profits gained by the D-CAES system (profit of D-CAES minus profit of CAES, called "Additional profit of D-CAES" throughout the paper) are presented in Figure 30 . Only the operation costs (electricity, fuel, and VOM) are subtracted from the arbitrage revenues to estimate the operating profit of CAES. Amortized capital and FOM cost of the pipeline are also considered in calculating profits of D-CAES.

The operating profit of conventional CAES experiences large fluctuations with an annual average value of $28.2 million over the decade and a relative standard deviation of 36%. The D-CAES plant earns $1.3 million/year more than CAES on average, with a relative standard deviation of 119%. It is important to note this profit is after taking a 10% blended cost of capital into account to reflect the cost of capital to the owner of the D-CAES plant. In next step, we look into the drivers for such annual fluctuations in profit.

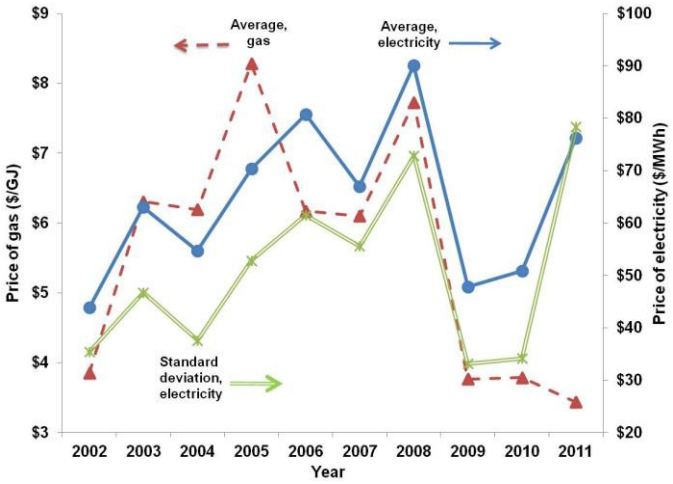

Figure 29: Annual average of gas prices (left axis), electricity prices (right axis) and daily standard deviation of electricity prices (right axis) between 2002 and 2011 in Alberta.

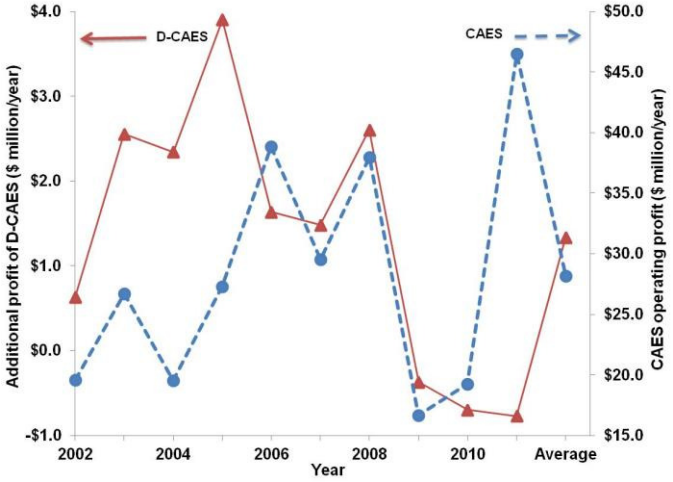

Figure 30: Annual operating profit of the CAES plant (right-hand axis) and the additional profit of D-CAES (defined as profit of D-CAES minus profit of CAES, left-hand axis). Note large variations throughout the ten-year period.

In a perfectly competitive market, all participants should offer electricity at their marginal cost of generation. This may not; however, be the case for real world electricity markets, especially for the Alberta market with a relatively small size (average load of 8.4 GW in 2011). Coal is the price setter for approximately 54% of the year while gas plants are marginal for almost the rest of the time. However, high electricity prices (when sales of stored energy is highly profitable) are weakly impacted by gas prices in this market (R^2= 0.03 for correlation between daily price of electricity and gas over the study period). Periods with high electricity prices might be driven by various factors such as physical constraints or outage of generators and

transmission lines as well as weather conditions. Lack of a capacity market and the ability of market participants to voluntarily modify their offers up to two hours before the delivery time may also contribute to high price of peak electricity. On the other hand, price of gas has a direct impact on the operation cost of the CAES and D-CAES plants and revenues of waste heat recovery. Therefore, variations in price of gas will not change the value of electricity arbitrage while it would directly affect operation cost of both plants and value of heat recovery.

Figure 31 explores the impact of gas prices and fluctuations in electricity prices on the operating profit of CAES over the ten years of simulation. Since compressed air storage plants are sized and dispatched for short-term cycles, we use daily standard deviation of electricity prices, averaged over each year, to quantify volatility in electricity prices. The CAES profits are essentially uncorrelated with gas prices (R^2=0.04), but they have a strong correlation with fluctuation in electricity prices (R^2=0.95). The relative importance of electricity and gas prices on economics of CAES can be further explored through studying their annual fluctuations (see Figure 29). As a case in point, years 2010 and 2011 experienced similar gas prices ($3.8 and $3.4/GJ, respectively) while daily standard deviation of electricity prices was 130% higher in 2011. The arbitrage profit of D-CAES is 140% higher in 2011. Years 2004 and 2010 are good examples of two years with similar daily volatility in electricity prices but wide spreads in gas prices. Gas prices were 64% higher in 2004 while CAES plant has similar arbitrage profits in those two years.

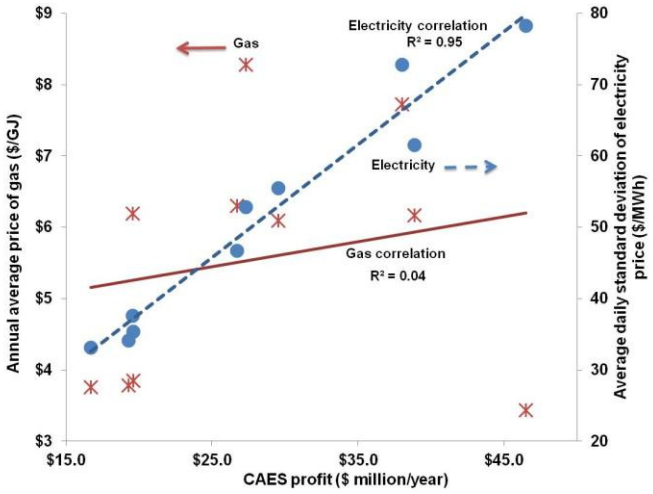

Figure 31: Correlation of CAES operating profit with price of gas and volatility of electricity prices over the ten year simulation period. Profit of CAES is strongly correlated with standard deviation of electricity prices.

While a poor correlation between price of gas and arbitrage profits is observed, gas prices have a strong impact on the revenues of heat recovery. Figure 32 shows the changes in profit difference of D-CAES and CAES with respect to the gas prices and fluctuations of electricity prices. The additional profit of D-CAES is strongly impacted by gas prices (R^2=0.91) and there is no notable dependence on electricity prices (R^2=0.02). Year 2005 experienced the highest profit difference (14%) between D-CAES and CAES, highest price of gas, a moderate volatility in electricity prices and an intermediate profit for CAES. On the contrary, year 2011 with the least additional D-CAES profit experienced the lowest gas price, the most volatile electricity prices, and the highest arbitrage profit for CAES.

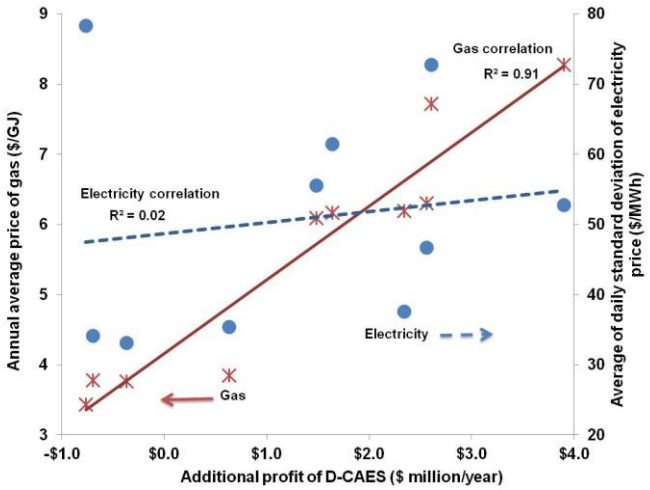

Figure 32: Annual price of gas, price volatility of electricity, and additional profit of D-CAES (with respect to CAES) over the ten-year study period. Note the strong correlation between profit of D-CAES and gas prices.

D-CAES plant purchases 33% more electricity from the market each year on average indicating that revenues from waste heat recovery significantly alter the dispatch of the energy storage plant. The fact that compressor and consequently expander of D-CAES operate more often implies that D-CAES would consume more gas compared to CAES. At the same time, heat recovery negates fuel consumption of the district heating system. To quantify these two opposite effects on the net fuel consumption and emissions, the GHG emissions intensity of both plants are calculated. GHG emissions intensity is defined as the net amount of greenhouse gases emitted per megawatt-hour of electricity sold. A value of 66 kg CO_2e[19]/GJ (lower heating value) is used

[19] GHG emissions are expressed in equivalent amounts of carbon dioxide (CO_2e) in this paper.

for carbon content of natural gas (including the typical[20] upstream emissions) [60]. The fuel savings of the district heating system as a result of recovery of the compression heat is subtracted from the fuel consumption of the D-CAES plant to determine the net fuel consumption and GHG emissions intensity of the D-CAES plant. The annual average emissions intensity of D-CAES turned out 48% lower than CAES (144 and 273 kg CO_2e/MWh, respectively). Compressed air energy storage plants are considered as promising alternatives to gas turbines in providing cleaner peak electricity, especially if the off-peak electricity has a low GHG emissions intensity, such as wind or nuclear. GHG intensity of a gas turbine with an efficiency of 35% would be 680 kg CO_2e/MWh, a much higher value compared to CAES and D-CAES[21]. The superior environmental performance of D-CAES compared to conventional CAES and gas turbines could make this technology more attractive if aggressive measures for emissions reduction are incorporated into the electricity market.

Carbon abatement cost is often used to inform policy making in identifying the most economic ways to reduce GHG emissions among alternative technologies. The fact that the D-CAES facility has stronger economics and at the same time a lower GHG emissions intensity, results in a negative abatement cost of -\$40 /t[22]CO_2e over the study period. In other words, recovery of the otherwise wasted heat of compression would not only lower GHG intensity of the conventional CAES systems, but it also would provide a profit of \$40 per ton of avoided CO_2e in our model.

Finally, it is important to note that the energy storage plants modeled in this study are both stand-alone merchant facilities. This mode of ownership involves some positive externalities, which could be captured by the plants themselves (especially D-CAES) if a utility co-owns such a storage facility with other generators. Following is two examples of scenarios where co-ownership might improve economics of energy storage:

[20] Indirect GHG emissions (e.g. from manufacturing of equipments) are not included.

[21] One should note that net GHG intensity of energy storage plants will depend on the source of electricity used for charging if the life-cycle GHG intensity is to be determined. Only "inside-the-fence" emissions are considered in this paper. The grid-wide GHG emissions intensity of Alberta was ~750 kgCO_2e/MWh in 2011.

[22] One “t” indicates one metric ton (1000 kg).

- A utility could utilize either a conventional CAES or D-CAES facility to lower the cycling cost of its baseload assets. The energy storage plants would have almost the same effect on the operation of baseload units if they were individually operated; however, none of the financial benefits would be collected by the storage plants themselves. As the compressor of D-CAES has a higher capacity factor, the positive externalities would be higher for this plant.
- A utility can provide firming capacity for its wind assets through co-operating a compressed air energy storage plant with its wind farms[23]. If the MOMC rule is to be applied to wind farms, an independent wind farm would be penalized for shortage of delivery and would lose potential revenues if more wind becomes available. A D-CAES facility would have a higher desire to store the otherwise curtailed wind due to the revenues of heat recovery. From a public-policy perspective, wind energy currently has some negative externalities on the electricity market of Alberta since it is exempted from the MOMC rule. Co-operation of wind farms with CAES/D-CAES facilities can partially address this issue.

3-2- Optimal size of heat load

Higher needs for thermal energy would improve the economics of waste heat recovery. The heat load used in this study experiences large variations (relative standard deviation of 42%). Therefore, revenues of heat recovery would fluctuate significantly unless the size of heat load is relatively large compared to the size of compressor and heat recovery unit (HC). In other words, not all the available compression heat would earn revenue for D-CAES unless the size of HC is comparable to the base (minimum) heating load. The size of heat recovery unit is set as 73.5 MW (70% of the size of compressor) while the minimum heating load is 35.8 MW thermal in the base case.

In order to evaluate the impact of heat load size on economics of D-CAES, we varied its value from 0.5 to 10 times the size of the University of Calgary's load. This ratio is set at 5 in the base case scenario[24]. The profit

[23] Wind farms are currently exempted from the MOMC rule in the Alberta market, mainly due to the low penetration of wind.

[24] Note that a heating load scale of 5 in our model corresponds to a value of 2.3 and 1 for the ratio of the peak and average heating load (in year 2011) to the size of compressor, respectively.

difference between D-CAES and CAES systems is averaged over the ten year simulation period for each load size and it varies between -$2.6 million and $1.6 million, as shown in Figure 33. A minimum value of 2.5 for the size of the load yields in positive net profits from heat recovery. A marginal increase in heat load has a significant impact on the profits of heat recovery at load sizes below 5. Figure 33 also shows the percentage of available compression heat that is curtailed. This value is very high (73%) at a load size of 0.5 while it drops to 4% at a size of 5. One should note that a larger heat load generally translates to longer heating pipelines for the district heating network and consequently higher pressure and heat losses (higher operation costs). Therefore, the optimal size of the heat load paired with a D-CAES plant is project-specific and is determined based on the trade-off between revenues of waste heat recovery and capital and operation costs of the district heating network.

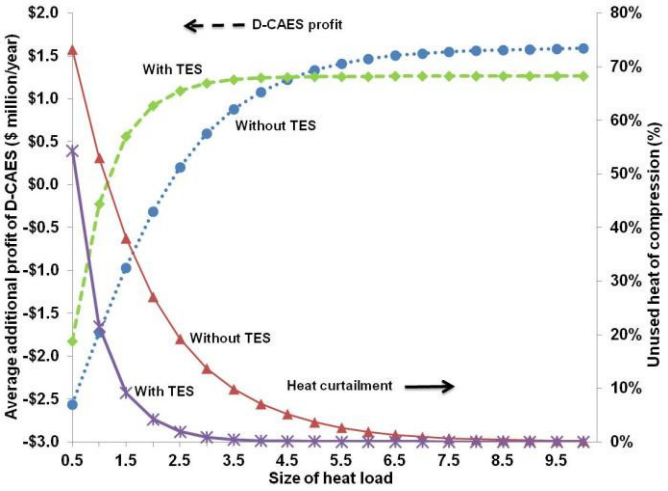

Figure 33: Effect of size of heat load and storage of waste heat (day-long) on profit of D-CAES (left) and curtailment of compression waste heat (right). Size of heat load is expressed in relative terms compared to the University of Calgary (annual average of 21.4 MW thermal).

As discussed earlier, storing the surplus heat of compression for later use could improve both economic and environmental performance of D-CAES. In addition to the base case, we consider a scenario in which hot water tanks can store the excess recovered heat for the same day use. We use a value of $3.37 million for capital cost of such a thermal energy storage (TS) system in consultation with an engineering firm. The hot water tanks are sized to store heat of compression at the heat recovery unit's (HC) full capacity for 12 hours. Figure 33 illustrates the impact of utilizing such a TS system on the profit of D-CAES as well as portion of the

available compression heat that is sold. As observed, the ability of storing the excess heat significantly improves profits of heat recovery up to a load size of 2.5. Cost-effectiveness of TS weakens as the size of load increases and consequently there is a higher instantaneous need for the heat of compression.

3-3- Optimal size of air storage

As discussed in Section 3-1, revenues of heat recovery incentivize D-CAES plant to store more electricity. A larger reservoir would enable storing more energy during periods of high heating demand and low electricity price. A larger storage would also increase the arbitrage revenues of both plants as more electricity could be sold. On the other hand, a storage facility would be more capital intensive. In order to investigate this trade-off, the profit of CAES and D-CAES plants are compared in a range of storage capacities. The lower bound is a plant with a generation capacity of 4 hours (524 MWh) while the upper bound assumes 60 hours of energy discharge. The size of compressor and expander are fixed in all cases at 105 and 131 MW, respectively. It is important to note that our analysis presumes the marginal capital cost of the air storage linearly increases with its size (at a slope of $0.15/kWh, see Table 29).

Figure 34 shows the operating profits of CAES and D-CAES at various cavern capacities. Similar trends are observed for both plants: an incremental increase in the size of reservoir sharply enhances their profits up to a capacity of 12 hours while the rate of change is minimal past this point. Increasing the capacity of the air storage has a stronger impact on the profits of D-CAES since it improves revenues of both energy arbitrage and heat recovery. An increase in the storage size beyond 48 hours has even a negative impact on economics of D-CAES and CAES. This behavior implies that increase in the initial cost of the reservoir overweighs the incremental revenues of energy arbitrage and heat recovery. It is of note that a larger cavern also translates to larger capital cost requirements and higher investment risks, especially due to the small financial gains at storage sizes larger than 12 hours. Therefore, a smaller reservoir might be chosen in the real world projects compared to the optimal sizes shown in Figure 34.

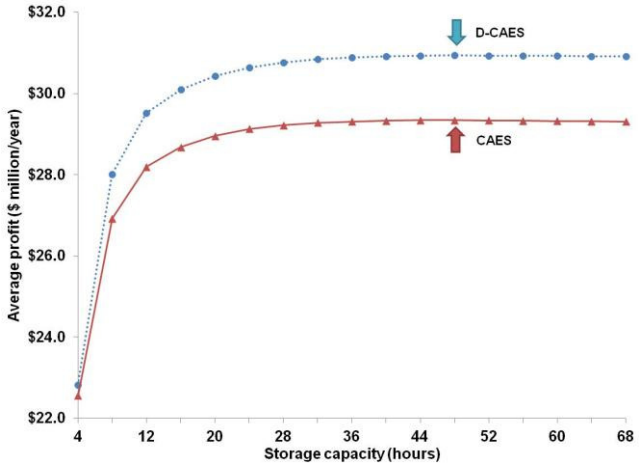

Figure 34: Effect of the size of air storage on operating profits of CAES and D-CAES plants, averaged over the simulation period. Arrows indicate the optimal size of the storage facility.

3-4- Optimal size of turbo-machinery

Capacity (size) of compressor constraints the rate of electricity storage as well as the revenues of heat recovery. Similarly, size of the expander limits sales of stored electricity to the grid. Therefore, compressor and expander should ideally be sized for each electricity market. We vary ratio of the expander to compressor size in a wide range and calculate the profit of CAES and D-CAES plants (see Figure 35). Capacity of the compressor, air storage, and heat load are kept same as the base case system. Capacity of the expander is changed between 52.5 MW and 1,050 MW, half and ten times the size of compressor, respectively.

Increasing the size ratio significantly improves economics of CAES and D-CAES at low ratios and profits of both plants peak at a size ratio of 5.5. As discussed in the methodology section, high market share of baseload plants and infrequent high prices are inherent characteristics of the Alberta electricity market. As a case in point, Figure 36 shows the price duration curves for three arbitrary years during the simulation period. A general observation is depressed prices for most of the time year. Therefore, a larger expander would enable the plant operator to take more advantage of limited periods with high prices. On the other hand, a larger expander would result in faster depletion of air storage and calls for increased capacity factor of compressor. Consequently, the revenues of waste heat recovery would also increase (profit of D-CAES rises faster compared to CAES in Figure 35). Increasing this size ratio past 5.5 has a negative impact for both plants revealing that increased capital costs overweigh marginal revenues of arbitrage and heat recovery. Therefore,

a ratio of approximately 5.5 for the size of expander to compressor would be the optimal ratio for the Alberta electricity market.

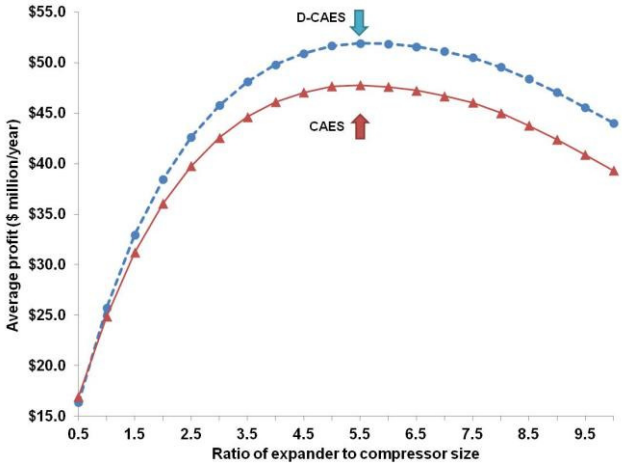

Figure 35: Effect of size ratio of expander to compressor on profits of CAES and D-CAES, averaged over the ten years of study. Arrows indicate the optimal values. Capacity of compressor (105 MW) and air storage (1,572 MWh) are fixed in all case.

It bears mentioning that the optimal size ratio might be lower in the real world caused by other factors not included in this study. As a case in point, a larger expander would necessitate a larger transmission line, which may face technical or siting constraints. Higher initial cost of a larger plant might also present a higher investment risk. Moreover, adding too much peaking capacity would depress the price of peak electricity. A final note is that these results are very market specific and depend on the application of the storage facility. For instance, a CAES facility that is to provide firming capacity or energy arbitrage for a wind farm would likely have a larger compressor so that it can store as much wind energy when it becomes available.

3-5- Effect of pipeline length

While aboveground vessels can also be used for air storage, a utility-scale facility needs to store air in a geological reservoir due to their significantly lower capital cost. Availability of a suitable geologic formation in vicinity of the heat load is crucial for economic viability of D-CAES. Figure 37 shows the result of a sensitivity analysis on the distance between the air storage site and the heat load, as the main parameter impacting the capital cost of the D-CAES pipeline. The pipeline length is varied between 25 km and 100 km and the annual profit difference of D-CAES is calculated in each case. Besides, an unrealistic scenario in which

the air storage and heat load are co-located (pipeline length of 0 km) is considered to further illustrate the effect of pipeline cost on economics of D-CAES.

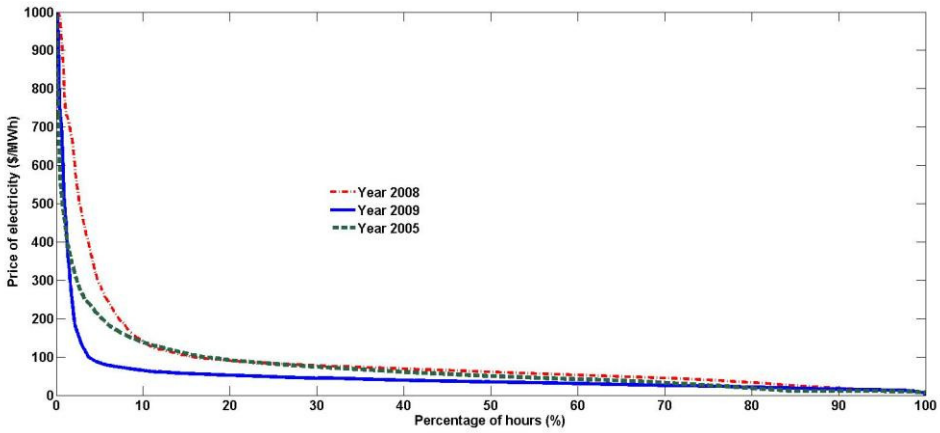

Figure 36: Percentage of hours in various years during which the Alberta electricity prices were higher than a certain value (price duration curves).

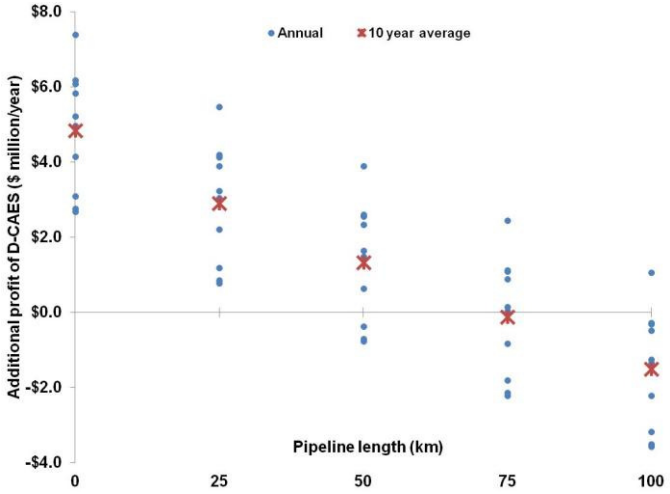

Figure 37: Profit difference between D-CAES and CAES plants at various distances between heat load and air storage site (pipeline length). Note the relatively wide spread of annual profits over the 10 years of study at each pipeline length.

Although the regression model used in this study takes into account the cost of material, labor, right of way, and some miscellaneous costs (*e.g.* surveying, and engineering), the exact cost of the air pipeline to a D-CAES plant would be affected by local parameters, which are unique to each project. However, results of our simulation reveal promising economics of D-CAES with a break-even point of 75 km for pipeline length so that profits of CAES and D-CAES would become equal. Figure 37 illustrates both the additional profit of

D-CAES in each year and the average values over the ten-year simulation period at each pipeline length. The cost of very short pipelines might be higher in the real world due to the fixed project costs (*e.g.* engineering, right of the way). Nevertheless, we are confident in the approximate location of the break-even point since it occurs at a relatively long length of 75 km. In other words, Figure 37 might over estimate the economics of heat recovery at very short distances between heat load and air storage. However, D-CAES is very likely to be economically justified over conventional CAES in the current Alberta market, providing a suitable depleted gas reservoir exists within 75 km of the heat load.

4- Conclusions

We evaluated the possibility of enhancing the economic and environmental performance of CAES through recovery of compression heat for municipal heating applications. The compressor of the D-CAES system is co-located with a concentrated heat load inside the city in contrast to the conventional CAES configuration in which both compressor and expander are at the air storage site. We optimized the profit of two hypothetical merchant CAES and D-CAES plants performing energy arbitrage using ten years of historical data from the Alberta electricity market. Compression heat was recovered to supply a concentrated heat load with an annual average of 107 MW thermal. Capacity of expander and compressor were fixed at 131 and 105 MW in the base case scenario, respectively.

The D-CAES plant earned an additional profit of $1.3 million/year on average, after taking into account a 10% cost of capital. The profit difference of D-CAES and CAES varied between -$0.8 million and $3.9 million, with negative values in only 3 out of the ten years of simulation. Profits of D-CAES showed a strong correlation with gas prices (R^2=0.91) because the economic advantage of D-CAES comes from reduction in gas demand for heating applications. Lower GHG intensity as well as higher profits led to a negative abatement cost of -$40/t$CO_2$e for the D-CAES compared to a CAES plant. Superior emissions performance of D-CAES could further improve its viability if a policy frame is in place to support cleaner technologies. Larger capacity factor of the D-CAES compressor, motivated by revenues of heat recovery might also improve D-CAES attractiveness if the energy storage plant is to provide other services in addition to energy arbitrage, such as firming capacity for intermittent renewable energies.

Economics of both plants showed high sensitivity to the size of cavern at capacities below 12 hours of electricity generation with minor effects afterwards. The optimal turbo-machinery composition had a significantly larger (5.5 times) expander compared to the compressor for both plants. We highlight that this optimal size largely depends on the application and the market environment in which the plants are operating. In electricity markets like Alberta with high share of baseload electricity (load factor of 80%), a merchant stand-alone plant dispatched for energy arbitrage would have a very limited window to sell high value electricity and recover its capital and operation costs. Having a larger expander; therefore, facilitates sales of larger quantities of peak electricity during those short windows.

An essential requirement for economic attractiveness of D-CAES over CAES is availability of suitable geologic formation in the vicinity of a concentrated heat load. Our case study for Alberta, with high heating loads and high price volatility, revealed that revenues from export of waste heat would breakeven with increased capital requirements at a pipeline length of 75 km. D-CAES can also be superior to conventional CAES in electricity markets with high peak prices and cooling loads in summer. Waste heat of compression can supply cooling energy with the aim of technologies such as absorption chilling, adding to financial and environmental profits of energy arbitrage. An example of such a location in North America could be Texas with outstanding wind resources, availability of aquifers and salt formations, and political support for wind energy.

A final remark that although our analysis revealed export of waste heat could be profitable, CAES technology is very unlikely to be economically viable unless the electricity market is carbon constrained [52, 60, 67]. We caution that waste heat recovery will not radically change this situation and some levels of emissions policy will still be required for large-scale deployment of this technology.

Chapter 5: How much bulk energy storage is needed to decarbonize electricity?[25]

[25] A condensed version of this chapter was submitted in October 2014 for publication in *Proceeding of the National Academy of Sciences (PNAS)* as Safaei, H. and Keith, D. How much bulk energy storage is needed to decarbonize electricity?

Preface

The previous three chapters focused on the engineering and economic analyses of selected compressed air energy storage (CAES) designs, which could reduce the carbon emissions intensity of the electricity supply. This chapter examines a broader research question about energy storage: How *significant* are the role of and the need for bulk electricity storage (BES) systems, as a tool in our carbon mitigation toolbox?

The conviction that cheap and mature bulk storage is a prerequisite to integrate intermittent renewables at scale is commonplace. This chapter investigates this claim through quantifying the significance (importance) of bulk electricity storage technologies in a deeply-decarbonized electricity system in future. The importance of storage is measured by two criteria:

1. How much can BES lower the decarbonization costs – the overall cost of supplying the electric load under stringent emissions constraints?
2. What is the optimal deployment of BES relative to the intermittent renewables (wind here) and other clean generators (*e.g*. nuclear and gas turbines)?

Rather than using a point estimate for the capital cost of bulk storage systems, a parametric approach is used. BES is treated as a black box with fixed technical characteristics but a variable capital cost, which is split into power-specific ($/kW) and energy-specific ($/kWh) costs. This strategy allows concentrating on the capital cost of storage, the single most important parameter impacting its economic viability. Varying the cost of bulk storage systems in a wide range and mapping the existing and emerging BES technologies in this range enable identifying the more cost-efficient bulk storage technologies for electricity decarbonization. This approach also guides R&D efforts and informs carbon mitigation policies regarding the role of BES technologies to cost-effectively integrate the intermittent renewables and curb emissions from the electricity sector, even if costs are drastically reduced.

The economics of various BES technologies and their optimal deployment level in carbon-constrained grids have particular implications for the future of compressed air storage systems. Two main critiques of the CAES technology are: non-negligible GHG emissions and the low exergy intensity, despite its low capital cost compared to most BES technologies. A generic CAES plant emits ~280 $kgCO_2e$ per MWh of electricity

generated (assuming a heat rate of 4.2 GJ/MWh). The Adiabatic CAES concept aims to address this shortcoming through eliminating the need for combusting natural gas prior to expansion of air and power generation. Compressed air storage facilities, particularly A-CAES need large air store units due to the very low exergy density of compressed air. For instance, the McIntosh CAES plant uses ~200 m^3 of storage volume per MWh of capacity. Scarcity of suitable geologic formations in desired geographical locations can undermine the viability of this technology if large amounts of BES are required in low-carbon electricity systems.

An important improvement to the model presented here would be to include a more diverse set of renewables, particularly solar, in the generation portfolio. The capital cost of solar-based electricity is currently higher than of wind; however, it has been declining steeply over the past few years. Since this chapter envisions a future electricity system with drastic emissions cuts, solar energy may become more economical compared to wind in that world. Including solar energy at various cost estimates would, therefore be of high priority to expand the current model in order to inform the electricity decarbonization debate.

Performing the simulation for different and wider geographical areas and over finer time resolutions could also strengthen the analysis. The wind and load data in this chapter are from ERCOT at a 15-minute resolution over one year. Different correlations between the electricity load and availability of intermittent renewables could change the need for storage. Moreover, renewable resources, especially wind, can face large inter-annual variations. Incorporating the reliability requirements and transmission constraints could improve the robustness of the conclusions.

Refining the current study to more realistically model the dispatch of various generators could also be an area of future work. All generators are assumed to have a fixed efficiency regardless of their loading. Operational constraints, such as minimum up and down time, are not modeled here for the sake of simplicity. Table 39 at the end of this chapter provides a comprehensive list of the key modeling simplifications and discusses their likely impact of the key conclusions.

1- Introduction

Availability of low cost and scalable bulk electricity storage (BES) technologies is often considered a prerequisite for use of wind and solar energies as a means to gain deep reductions in Greenhouse Gas (GHG) emissions from the electricity sector [53, 91-93]. Examples of such systems are pumped hydroelectric storage (PHS), compressed air energy storage (CAES), and vanadium redox flow batteries (VRB). In current electricity markets with low penetration of renewables and low natural gas prices, BES is not economical, and its technical and economic characteristics are uncertain due to its limited deployment.

Our question is: how important are the emerging BES technologies in enabling the integration of intermittent renewables? We tackle this question by analyzing the optimal deployment of electricity supply and BES technologies that meet specified GHG emissions constraints. We operationalize the *importance* of BES as the amount that it lowers the cost of electricity as the stringency of carbon constraints is increased, or almost equivalently, the amount by which it increases the penetration of renewables under the same constraints. Our analysis aims to inform policy for decarbonizing the electricity supply, and in particular for developing R&D incentives and market support for BES.

We assess the economically desired amount of BES using a simple linear-constrained optimization model that optimizes the size and dispatch of a hypothetical generation fleet under deep carbon reduction mandates (*e.g.* emissions cuts of greater than 50%). Rather than using a point estimate of future BES costs, we work parametrically, exploring how storage capital costs determine the grid-average cost and emissions intensity of electricity. Electricity storage can provide a variety of services such as frequency regulation to support integration of intermittent renewables, but here we limit our analysis to bulk (multi-hour) storage of electricity.

Our primary contribution is to assess the economics of BES as a function of its power- and energy-specific capital cost when it is used to achieve deep decarbonization of electricity supply. Applying a simple model enables us to parametrically evaluate the role of the capital cost which is the single most important determinants of the economic viability of BES. Previous work has examined the economics of specific BES technologies in comparison to gas turbines in low carbon grids [60, 75, 94]. The rationale for focusing on gas

as a rival for BES is low carbon emissions compared to coal, high operational flexibility, and low capital costs. Several studies have examined the competitiveness of a wide array of storage technologies at the grid level. These systems-level assessments use complex utility-grade models (*e.g.* incorporating security-constrained unit commitment) to take into account the specifics of the modeled grid and its reliability requirements. An example is the Pacific Northwest National Laboratory's (PNNL) report on the intra-hour balancing requirements to facilitate a 20% penetration level for wind [94]. But existing literature does not cover the parametric "what if" question we address here: what are the price and performance parameters required for BES to play a significant role in enabling intermittent renewables to achieve deep emissions cuts in the electricity sector.

Our modeling approach allows us to estimate the economically optimal amount of bulk storage—both energy storage and peaking capacity. Estimating storage requirements is a complicated task. An important factor here is the cost of storage, which the literature often underestimates. Barnhart and Benson [95] picked a storage scale equal to 4-12 hours of the average electricity demand in order to evaluate the energetic and material implications of large-scale deployment of storage systems. In a different study however, Pickard [93] used a storage size roughly 5.5 times larger than the average daily primary energy demand, while neither of these authors justified their selection from an economic point of view. Denholm and Hand [96] applied a dispatch model to the ERCOT grid and concluded that wind and solar penetration levels as high as 80% while keeping the curtailment rates below 10% would require a combination of load shifting and storage of one day of demand. Similarly, Denholm and Hand's analysis is not based on any economic metrics such as cost of storage or even wind and solar plants themselves. In another study, Solomon *et al.* [91] estimated the "appropriate" amount of storage to support solar PV in Israel, defined as "neither too small to increase grid penetration of PV in a significant manner nor wastefully large" without any economic considerations. Parametric modeling of the BES capital cost allows us to explore its impact on the overall cost of electricity supply and to assess the economically optimal deployment of BES over a wide range of estimates for the BES capital cost.

2- Data and methods

We use real world wind and load data to build our electricity system model. We optimize the size and dispatch order of the generation fleet to minimize the cost of electricity supply under a range of BES costs and GHG emissions constraints. Our analysis is based on the following key simplifying assumptions. First, since our focus is on deep emissions reductions under which essentially all coal power plants have to retire (or have carbon capture and sequestration, CCS retrofits) and because deep reductions will likely not occur until the existing fleet nears the end of its economic life, we ignore the existing capacity and perform a green-field analysis. Second, transmission costs and constraints are ignored. Third, since we are studying BES, we use a temporal resolution of 15 minutes and ignore short-period reliability requirements. Fourth, we ignore forecast errors in the load and wind profiles. Finally, we limit our time horizon to one year, ignoring inter-annual variations in load and wind. We examine the impact of these assumptions on our policy-relevant conclusions in Section 3-5 to Section 3-7 and in Table 39.

2-1- Modeling energy storage

Variations in the engineering and economic parameters of BES technologies obviously affect their cost effectiveness in supporting renewables. No BES technology, except PHS has been deployed at large scale so far (PHS accounts for 99% of the existing 141 GW global electricity storage capacity [27]). Limited experience and the emergence of new technologies make assessing the importance of BES in low emission grids difficult. As Table 30 illustrates, current literature uses widely different assumptions about the capital cost (CapEx) and efficiency of BES systems.

Elzinga *et al.* [27], Hittinger *et al.* [97], as well as Sundararagavan and Baker [98] studied the significance of selected economic and technical parameters and concluded that CapEx was consistently the single most important parameter undermining the economic feasibility of electricity storage systems. We therefore, focus on CapEx as the main variable of BES throughout our analysis. We first draw general conclusions by treating BES as a black box with fixed technical characteristics but variable CapEx (see Table 32). This approach allows us to perform a systems level analysis to provide a first order estimate of the market share of BES in

low carbon economies. We then study specific BES technologies in a wide range of CapEx estimates to assess their significance in lowering the cost of cutting carbon emissions.

We assume that the total CapEx of a BES facility is the sum of two components, one proportional to the peak power capacity and the other proportional to the stored energy capacity. We further assume that any combination of power and energy capacities is technically feasible. Power-specific capital cost (X_P) has units of $/kW, and the energy-specific capital cost (X_E) has units of $/kWh. In the case of PHS for example, X_P and X_E primarily represent the CapEx of turbomachinery and water reservoir, respectively.

We explore the balance between X_P and X_E in determining the economics of BES and as a means to guide R&D in prioritizing its cost reduction targets. This strategy also helps in assessing the economically optimal ratio of power to energy capacity over a wide range of X_P and X_E. This optimal ratio has implications for the technical feasibility of large-scale adoption of some BES technologies, such as availability of minerals and chemicals for electrodes (power capacity) and electrolytes (energy capacity) of flow batteries.

We map cost estimates for selected BES technologies on the X_E and X_P coordinate system in Figure 38. The basis of our estimates is provided in Table 30. Two distinct regions are observed. Region 1 represents mechanical systems (PHS and CAES) distinguished with low energy capital cost (X_E) but very high values for power cost (X_P). Region 2 embraces electrochemical systems with intermediate values for X_E and X_P. We refer to BES systems situated in regions 1 and 2 as mechanical and electrochemical hereafter.

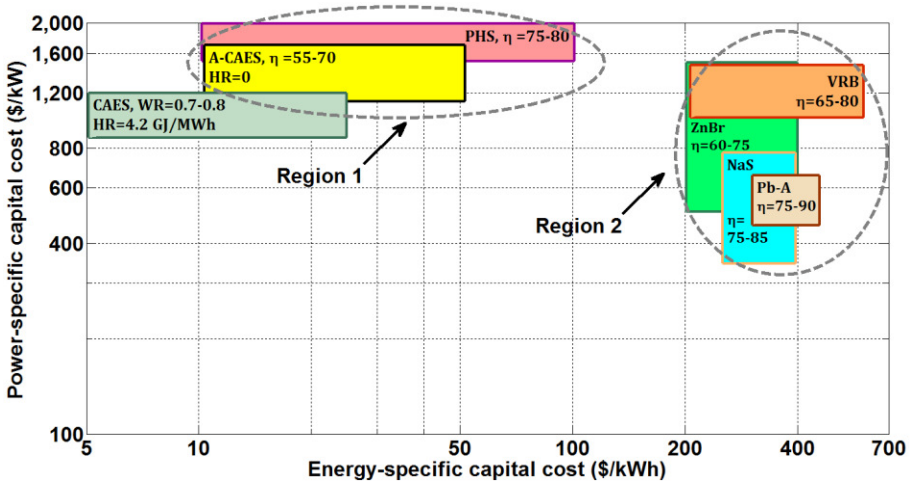

Figure 38: Mapping of selected BES technologies on the X_E and X_P plane. Each box represents a BES technology and its location corresponds to the ranges shown in bold in Table 30 for the energy-specific (X_E) and power-specific (X_P) capital cost of BES. Estimates for the storage efficiency (η), heat rate (HR), and work ratio (WR)[26] are included. Regions 1 and 2 represent mechanical and electrochemical technologies, respectively.

Table 30: Economic and technical characteristics of selected BES technologies. Values in bold represent the authors' best estimates and are used in Figure 38.

BES technology	**X_P ($/kW)**	**X_E ($/kWh)**	**Efficiency (%)**
Pumped hydroelectric storage (PHS)	2300 [94], 1500-2000 [99], 1200 [100], 600-2000[27] [101], 1500-2300 [94], 2000 [98], **1500-2000**	10 [94], 100-200 [99], 75 [100], 0-20 [101], 12 (plus $2/kWh for BOP[28]) [98], **10-100**	70-85 [27, 101, 102], 80 [98], 85 [100], 50-85 [103], **75-80**
Underground diabatic compressed air energy storage (CAES)	655 [53], 850-1140 [94], 740-830 [99], 700 [100], 425-480 [101], 750-1200[29] [9], 835[30] [104], 450 (plus $160/kW for BOP) [98], **850-1200**	7 [53], 3 [94], 5 [100], 3-10 (+$50/kWh for balance of plant equipment, BOP) [101], 5-25[31] [9], 1-2 [99], 20 [104], 10 [98], **5-25**	4.2 and 0.8 [53], 4.2 and 0.75 [9], 4.2 and 0.67 [60], **0.7-0.8 and 4.2** (Values present heat rate in GJ/ MWh and work ratio)

[26] Heat rate (HR) and work ratio (WR) of a compressed air energy storage facility express the heating fuel (GJ) and electricity (MWh) consumed by the plant per unit of electrical energy (MWh) generated, respectively. Heat rate and gas price are expressed based on the lower heating value (LHV) of fuel in this chapter, unless otherwise is stated.

[27] In our opinion, storage costs reported by this source are too optimistic.

[28] BOP: Balance of the plant equipment.

[29] We calculated this range based on the estimates for two different CAES facilities (135 MW and 405 MW with 12 hours of storage).

Table 30 (Continued)

Aboveground diabatic CAES (AD-CAES)	800-900 [99], 517 [101], 835 [104], **850-1200**[32]	200-240 [99], 50 (+$40/kWh for BOP) [101], 220-260[33] [104], **200-250**	**0.7-0.8 and 4.2**[34] (heat rate in GJ/ MWh and work ratio)
Underground adiabatic CAES (A-CAES)	920[35] [53],**1100-1700**	8 [53],**10-50**[36]	77 [53], 50-75 [22], **55-70**
Lead acid battery (Pb-A)	450 (+$100/kW for BOP) [98], 420-660 [99], 400 [100], 200-580 [101], **450-650**	200-400 [98], 330-480 [99], 175-250 (+$50/kWh for BOP) [101], 330 [100], **300-450**	65-85 [27], 75 [98], 75-80 [100], 85 [101], 85-90 [104], 75-90 [105], 60-95 [106], 70-90 [107], 75-86 [101], **75-90**
Sodium sulfur battery (NaS)	3000 (+$100/kW for BOP) [98], 350 [100], 260-810 [101], **350-800**	534 [98], 350 [100], 245 (+$40/kWh for BOP) [101], **250-400**	75-85 [27, 101], 85 [98], 75 [100, 105], 75-80 [104, 108], 75-90 [107], **75-85**
Zinc bromine battery (ZnBr)	2000 (+$100/kW for BOP) [98], 400 [100], 640-1500 [101], **500-1500**	400 [98, 100], 200-400 [101], **200-400**	75 [98, 101, 106, 107], 70 [100], 65-70 [104], 60-65 [105, 108], **60-75**
Vanadium redox battery (VRB)	3200 (+$100/kW for BOP) [98], 942-1280 [94], 400 [100], 1250-1800 [101], **1000-1500**	630 [98], 600 [100], 175-1000 [101], 173-257 [94], **200-600**	65-85 [27], 80 [98], 70-85 [101], 65-75 [104], 65 [100], 75 [94], 75-78 [108], 65-70 [105], 85 [106], **65-80**

[30] Values are based on cost estimates for two different CAES facilities (135 MW with 8 and 20 hours of storage).

[31] Lower and upper bounds represent depleted gas reservoirs and domal salt caverns.

[32] We assume that underground and aboveground CAES have similar specific power capital costs.

[33] We estimated the energy-specific cost (X_E) of aboveground CAES based on the total costs cited for underground and aboveground CAES, assuming comparable values for their power-specific CapEx (X_E).

[34] We assumed underground and aboveground CAES have comparable thermodynamic performance.

[35] We adjusted the limited-publically available cost estimates for A-CAES based on their and our estimates for diabatic CAES.

[36] Energy density of cavern of A-CAES is roughly half of CAES. We therefore, doubled our estimates for CAES to calculate energy-specific cost (X_E) of A-CAES.

2-2- Load and wind data

Wind and load profiles are based on historical data from the Electric Reliability Council of Texas (ERCOT) between May 2012 and April 2013. Load is normalized to its peak and wind is normalized to installed capacity. We choose a temporal resolution of 15 minutes. Power spectrum analysis of wind farms indicates that the majority of high amplitude variations in their output occur at low frequencies (hourly and daily timescales) [109], so a 15-minute resolution over one full year captures requirements for bulk energy storage. Performing the analysis over one full year also enables assessing the need for long duration storage of energy (*e.g.* hydrogen-based BES systems).

Correlations between wind availability and electric load obviously impact storage requirements. ERCOT is a large electricity grid (peak load of 66.5 GW and wind capacity of 10.0 GW in 2012), so the chosen profiles represent an important real world case. The load factor defined as ratio of the average to peak load is 56% for our load profile. There is a slight anti-correlation (coefficient of -0.15) between our load and wind profiles. Cumulative duration curves for load and wind are shown in Figure 39. Note that there are periods with insignificant wind availability while the load does not ever fall below 34% of its peak. Even if wind capacity is 1.6 times of the peak load– the point at which annual average wind production matches the annual average load– wind will still be incapable of supplying all of the load 53% of the time (marked by point “B” on the graph). This value is still non-negligible (17%) even when wind capacity is 5 times larger than peak load (point “C” on “n=5” line).

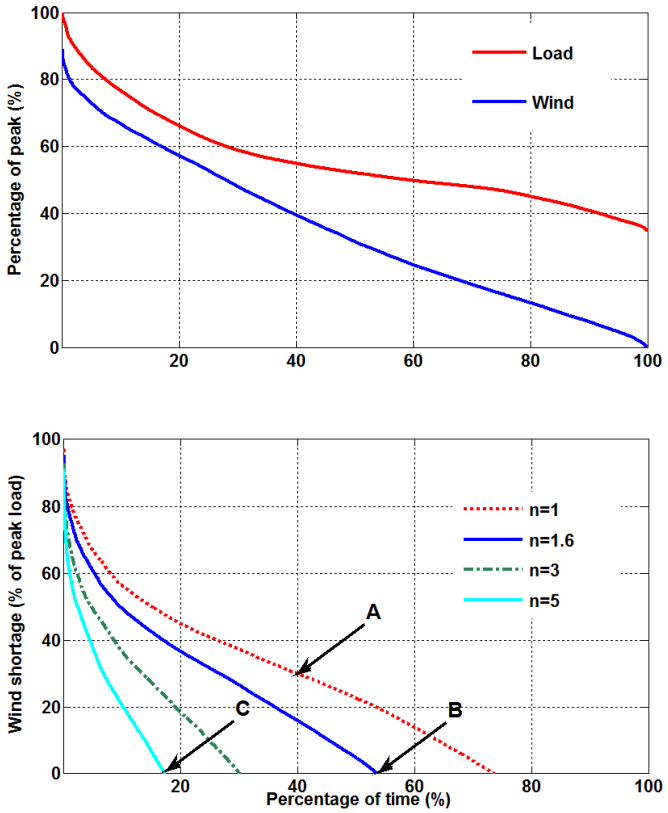

Figure 39: Temporal distribution of wind and load profiles used for the simulation. The top figure illustrates percentage of time (on horizontal axis) during which wind availability or electric load is higher than a certain value shown on the vertical axis (*a.k.a.* duration curve). Wind and load profiles are normalized to peak load and installed wind capacity, respectively. The lower plot shows percentage of time during which wind shortfall in supplying the load is higher than a certain value shown on the vertical axis. Parameter "n" is the ratio of wind capacity to peak load. Point "A" for example, shows that in 40% of the year shortage in wind supply is at least 30% of the annual peak load, when the installed wind capacity is equal to the annual peak load (n=1).

2-3- Electricity system model

We simultaneously optimize installed capacity and dispatch during operation of a generation fleet to meet the load at the minimum cost. We use a set of scenarios defined by a series of imposed constraints on the annual average GHG intensity of electricity ranging from 300 to 0 $kgCO_2e/MWh$ (CO_2e equivalents are used to account for methane emissions as discussed in details below). The power- and energy-specific CapEx of BES are varied to sample the two-dimensional (X_E and X_P) space within each emissions intensity scenario. The system-average levelized cost of electricity (LCOE, $/MWh) is minimized at each emissions intensity and at the sampled values of X_E and X_P. The LCOE includes fixed and variable operating and maintenance costs (FOM

and VOM), fuel costs, and amortized CapEx. The objective function is shown in Equation 152, given the definitions in Table 31.

$$\sum_{y}\left[\left\{Capt_y \times \left(BC \times CapEx_y + FOM_y\right)\right\} + \left\{\sum_{z}\left(EL_{y,z} + ST_{y,z}\right) \times \left(HR_y \times \pi_{NG} + VOM_y\right)\right\}\right] \qquad \text{Equation 152}$$

Where $y \in Y = \{SCGT, CCGT, Wind, BES, DZC\}$ and $z \in Z = \{1,2,3, \dots, 365 \times 24 \times 4\}$

Table 31: List of parameters and variables of the objective function. See Table 32 for the numerical values of the parameters.

$CapEx$	Specific capital cost ($/MW or MWh)	$Capt$	Installed capacity (MW or MWh)
BC	Blended cost of capital (%)	EL	Electricity delivered to load (MWh)
FOM	Fixed operation and maintenance cost ($/MW or MWh/year)	VOM	Variable operation and maintenance cost ($/MWh)
Y, y	Set Y includes the electricity supply technologies, *i.e.* gas turbines, wind, BES, and DZC (index y)	Z, z	Set J includes the planning periods over the entire year at a 15-minute resolution (index j)
π_{NG}	Price of gas ($/GJ)	ST	Electricity stored in BES (MWh)
HR	Heat rate (GJ/MWh)		

This objective function calculates the total annual cost of electricity supply and has two parts (shown in curly brackets). The first section takes into account the amortized capital cost and the fixed operations and maintenance cost of the generation and storage fleet. The second part of the objective function considers the fuel cost and the variable operation and maintenance cost associated with electricity generation (both directly provided to the load and stored in BES) and by the generation fleet. Note that we simultaneously optimize the capacity and dispatch of the generation fleet. We develop a simplified utility planning model, which minimizes the system-wide cost of electricity supply in a green-field setup.

The decision variables include installed capacity (size) of the generation fleet and their dispatch in each 15-minute period over the simulation period (one year). The key constraints include:

- The electricity load must be satisfied in each 15-minute time interval.
- The annual average GHG emissions ($kgCO2_e$/MWh) should be less than a preset value (*e.g.* 0 in the carbon free scenario), except in the BAU scenario.

- Output of each system component cannot exceed its capacity.
- Conservation of energy must hold for BES; the change in the stock of energy in each 15-minute period should be equal to the difference between energy injected and withdrawn, after taking into account the storage efficiency.

This optimization problem is solved in MATLAB using linear programming with the interior-points algorithm. It takes about 500 seconds on a 2012 vintage CPU for each of 320 sample points in the X_E and X_P plane.

We assume that any combinations of simple and combined cycle gas turbines (SCGT and CCGT), wind farms, and BES can be utilized to meet the load. Our model also includes a generic generation source called dispatchable-zero-carbon, DZC. This category represents the (near) zero carbon but dispatchable technologies that are currently too costly but are likely to emerge as more cost effective in a carbon-constrained world. Examples can be gas turbines integrated with CCS, concentrated solar power (CSP) equipped with thermal storage (TS), and nuclear power plants.

We vary X_E and X_P of BES in the range of 5-700 $/kWh and 100-2000 $/kW, respectively to cover 320 sample points. All BES technologies are assumed to have the same efficiency within a given scenario except for diabatic CAES which is modeled separately (because it consumes fuel during the discharging phase). Charge and discharge rates of BES are assumed to be equal.

We consider four scenarios for emissions intensity of the grid; business as usual (BAU) and caps of 300, 150, and 0 $kgCO_2e/MWh$. Note that these values, even BAU (this scenario leads to an emissions intensity of ~448 $kgCO_2e/MWh$) represent sharp emissions reductions compared to the existing grids, mainly because coal is not included in our model. For instance, the average carbon intensity of the entire USA grid and the global average in 2010 were 503 and 536 $kgCO_2/MWh$ [110].

Table 32 summarizes various inputs of our model. Roundtrip efficiency of storage is set at 75%, an average value based on BES technologies in Table 30. The price of gas is fixed at $5/GJ (sensitivity analysis is provided in Section 3-6). Operational considerations such as minimum up and down times, ramp rates, and part-load performance are not included in this modeled.

Our cost estimates for gas turbines and wind farms are based on values reported by the United States' Department of Energy (DoE) [111] and Energy Information Administration (EIA) [112], National Renewable Energy Laboratory (NREL) [113], and Lazard Ltd [114]. We use a value of $9000/kW for DZC. Each specific DZC technology will face some geographical constraints (*e.g.* CSP requires high solar irradiance or CCS needs a suitable geologic formation). DZC, however, represents the least capital-intensive, dispatchable technology— whether CSP, nuclear, CCS, biomass or geothermal—that can be utilized in a given location. Our judgment is that 9000 $/kW is mostly likely an overestimate of this best-case DZC cost (see Section 3-5 for our rationale and the sensitivity analysis on DZC cost).

Table 32: Technical and economic inputs of the model in the base case.

Parameter	**Value**	**Notes**
CapEx of Wind, SCGT, CCGT, DZC	2000, 800, 1100, and 9000 $/kW	Wind and gas turbine data are based on references [111-114]. FOM and VOM of DZC are based on nuclear and CSP [112, 114]
FOM of Wind, SCGT, CCGT, DZC	35, 10, 12, and 100 $/kW/yr	
VOM of Wind, SCGT, CCGT, DZC	0, 10, 3, and 0 $/MWh	
Heat rate of SCGT, CCGT, and CAES	9.8, 6.7, and 4.2 GJ/MWh (LHV)	
Work ratio of CAES	0.75	CAES data from Table 30
Storage efficiency	75%	An average based on Table 30
Price of gas	5 $/GJ (LHV)	
Blended cost of capital	10%	Equivalent to a discount rate of ~8% for 20 years
X_P and X_E of BES	100-2000 $/kW and 5-700 $/kWh	Range used in simulation that cover 320 points in X_P, X_E space

We use a GHG intensity of 66 $kgCO_2e/GJ$ (lower heating value, LHV) [60] for natural gas to account for upstream emissions in addition to combustion emissions[37]. This value leads to a GHG intensity of 647 and 442 $kgCO_2e$/ MWh for the SCGT and CCGT plants in our model. Although estimating life-cycle GHG emissions of

[37] This value exclude emissions associated with building the power plants. In other words, it only concerns with emissions of natural gas itself.

natural gas-based electricity is uncertain (partly due to fugitive methane emissions), our values fit well within the current estimates. For instance, in a 2014 study, O'Donoughue *et al.* [115] applied a meta-analytical process on 250 published references to harmonize estimates of the life-cycle GHG emissions of the electricity fueled by conventionally produced gas. They reported an interquartile range (IQR) of 570-750 with a median of 670 $kgCO_2e/MWh$ for SCGT. The IQR and median values reported for CCGT are 420-480 and 450 $kgCO_2e/MWh$, respectively.

3- Results and Discussions

3-1- Cost of electricity

In our BAU scenario, wind and DZC are not economically viable and gas turbines and storage supply the electric load. CCGT dominates the electricity supply because of the high operating and fuel costs of SCGT compared to CCGT (see Table 32). Even without an emissions constraint, cheap BES reduces the need for peaking plants (SCGT) by increasing utilization of CCGT and thus lowering the cost of electricity. Emissions intensity, however, is insensitive to the storage cost because BES supplies at most 3% of the annual load. CCGT supplies almost all (>97%) of total electricity. Note that the 15-minute resolution may slightly overestimate the share of CCGT as it understates the advantage SCGT should get from its faster ramp rate.

Our central research question is how the capital cost of storage impacts the overall cost of electricity supply under tight carbon constrains. Figure 40 illustrates LCOE at various emission caps over a wide range of X_E and X_P. The most general result is that energy capital cost (X_E) has a stronger influence on LCOE that does power cost (X_P) under all emission scenarios. Comparing Figure 38 and Figure 40, we can see that the existing mechanical BES systems are more likely to cost effectively curb emissions due to their significantly lower X_E compared to electrochemical technologies, despite higher X_P of the mechanical systems.

A second result is that inexpensive BES has a small impact on the LCOE in all scenarios except for the carbon free grid. LCOE differs only 6% (56.6 and 60.3 $/MWh) between the cheapest and most expensive BES system that we model in BAU. As expected, the impact of BES on LCOE rises when a tight cap of 150 $kgCO_2e/MWh$ is

imposed. But even then, BES cuts the costs by only 17% (81.2 versus 97.8 $/MWh) even though emissions are cut by 67% compared to BAU, an even deeper cut when compared with current emissions which include coal.

LCOE is more sensitive to storage cost when emissions are constrained to zero at which point there is a 27% difference between LCOE of the carbon free grid utilizing the cheapest BES system (X_E=5 and X_P=100, LCOE=$143.9/MWh) and the most expensive BES system (X_E=700 and X_P=2000, LCOE=$195.9/MWh).

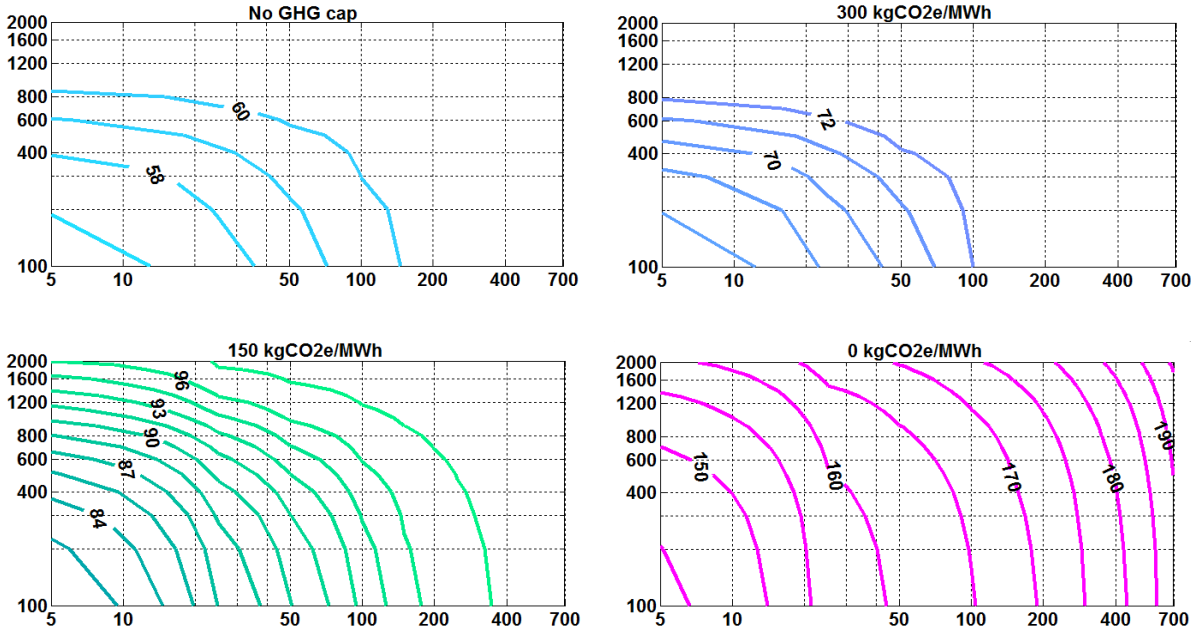

Figure 40: Impact of X_E and X_P and emissions constraints on LCOE. Horizontal and vertical axes show X_E ($/kWh) and X_P ($/kW), respectively. Values on the graphs present LCOE ($/MWh). Subfigures from top left in counter clockwise order correspond to BAU (no emissions constraint), and caps of 300, 150, and 0 $kgCO_2e$/MWh. In all the contour plots, 320 sample points are simulated to cover the range of 5-700 and 100-2000 for X_E and X_P. Contour spacing is constant in each plot; therefore, absence of contour lines in an area indicates no changes larger than the contour spacing.

The strong impact of storage cost on the LCOE in the completely decarbonized system is driven by the absence of gas turbines. Even under the low 150 $kgCO_2e$/MWh scenario, gas can cost-effectively manage the variability of wind, as explored in Section 3-2. Despite their higher fuel and operational cost, the relatively low CapEx of gas turbines allows them to out-compete BES in managing the variability of wind.

3-2- Storage cost and wind penetration

Since emission constraints and availability of affordable BES are often considered as requirements for large-scale adoption of intermittent renewables, we explore effect of these parameters on the economically

optimum level of wind penetration in our model. Because our focus is on deep decarbonization targets, we discuss the results for the 150 $kgCO_2e/MWh$ scenario (~33% of BAU emissions).

The distinct impact of mechanical and electrochemical BES technologies is evident in Figure 41. While electricity cost is almost the same (<5% difference), optimal size of the wind fleet using electrochemical BES is only 60% of the wind fleet using mechanical systems. This indicates that BES systems with low energy capital cost (X_E) facilitate higher penetration of wind energy. If electrochemical rather than mechanical BES systems are utilized, the optimal sizes of the SCGT and DZC fleet get larger to compensate for the smaller wind fleet. The optimal size of CCGT is almost insensitive to the storage cost (approximately 53% for both BES categories).

Note that all power capacity values are expressed as percentage of the peak load (1000 MW) in the contour plots presented in this chapter. The energy capacity of BES is expressed as hours of the average load (556 MW), *i.e.* ratio of the energy capacity (MWh) of the storage fleet to the average load (MW).

These results lead to the conclusion that the optimal wind capacity is very sensitive to the CapEx of BES, especially to its energy capacity cost (X_E). Therefore, mechanical BES systems (region 1 in Figure 38) are better suited for large-scale integration of intermittent renewables, at their current costs.

While lower-cost storage increases wind's share of annual generation, it does little to change the overall electricity cost because it just sifts the balance between wind and DZC. This does not answer a related energy policy question: how important is bulk storage to manage high penetration of intermittent renewables? We explore this by removing DZC from the generation fleet—so intermittent renewables (wind in this case) are the only way to decarbonize—and then enforce a 150 $kgCO_2e/MWh$ emissions cap. We then operationalize the "how important" question by comparing the optimal wind capacity to the capacities of BES and gas.

Table 33 presents the key system parameters when DZC is eliminated from the generation fleet and the same emissions constraint of 150 $kgCO_2e/MWh$ is enforced. A sample BES system from each category (*i.e.* mechanical and electrochemical) was modeled. The energy- and power-specific costs of the mechanical BES system were X_E=30 \$/kWh and X_P=1500 \$/kW while these values were X_E=375 \$/kWh and X_P=550 \$/kW for

the sample electrochemical BES system. We also evaluated the sensitivity of the results to a drastic 50% reduction in both X_E and X_P of these two BES systems.

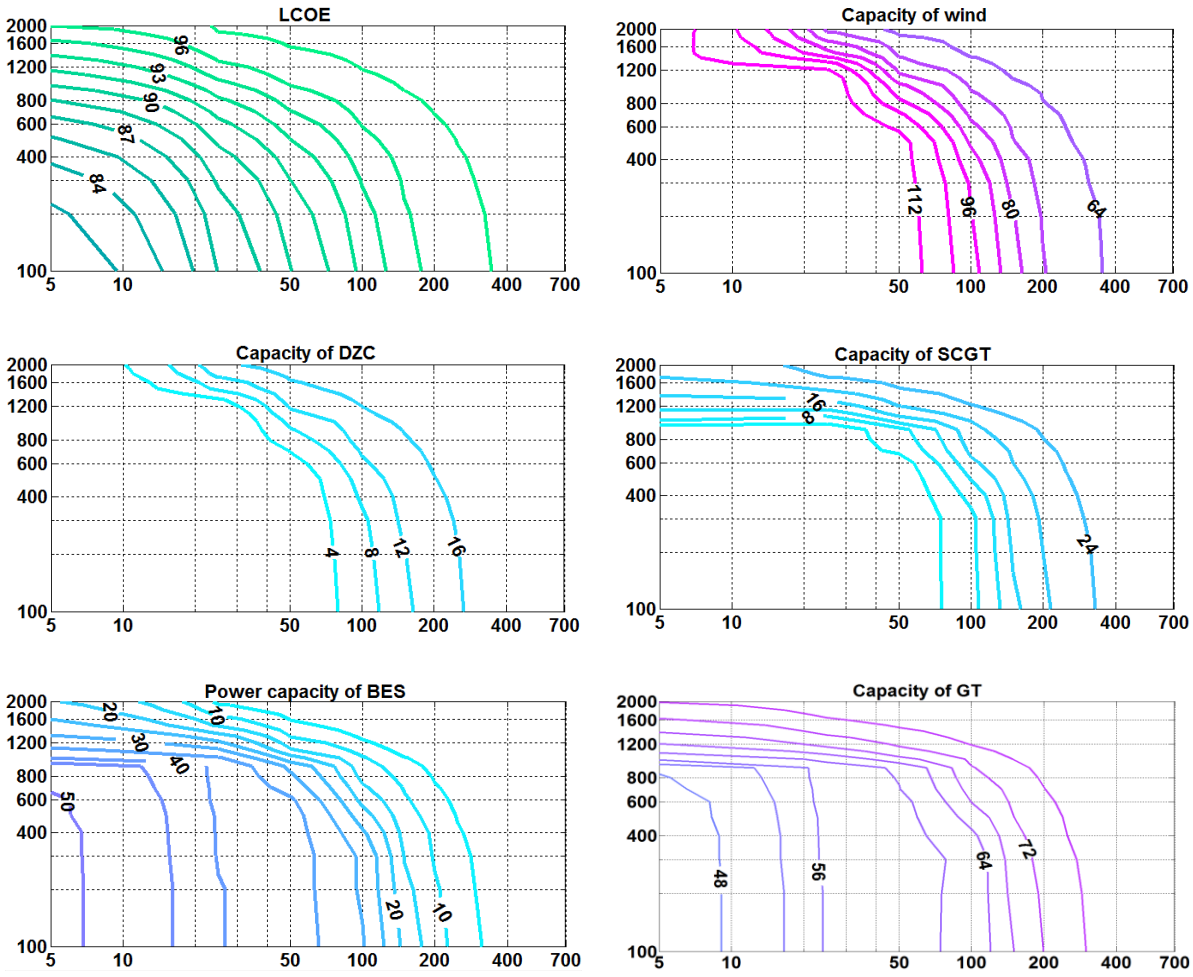

Figure 41: Electricity system characteristics at an emissions cap of 150 $kgCO_2e/MWh$. Subfigures from top left illustrate LCOE, normalized power capacity of wind, DZC, SCGT, BES, and GT (SCGT and CCGT combined). All capacity values are expressed as percentage of the peak electric load. Horizontal and vertical axes show X_E ($/kWh) and X_P ($/kW), respectively.

The required amount of storage remained relatively small (≤22% of peak load, except when the energy and power costs of the mechanical BES system were halved). In contrast, capacity of the gas turbine fleet (aggregate of SCGT and CCGT) remained above 75% of the peak load with the current storage costs of both BES systems and still above ~50% when the costs of the mechanical BES were halved. Moreover, less than 10% of the annual electricity load was supplied by BES in the best case (50% reduced energy and power costs of the mechanical system). Also note the low sensitivity of the overall cost of electricity (LOCE) to reductions

in the capital cost of BES. Halving both the power and energy cost of the mechanical and electrochemical systems reduced LOCE by 7% and 4%, respectively.

Using the example of the mechanical BES system shown in Table 33 (with energy and power costs of X_E=\$30/kWh and X_P=\$1500/kW), we see that capacity of BES and gas are ~20% and 60% (respectively) of the capacity of wind. So one could say that BES is three times less important than gas in providing peaking power under this tight emissions constraint and with current capital cost estimates. Under these conditions, about a third of annual load comes from gas, 6% from BES and the rest from wind.

Table 33: Key characteristics of the generation fleet when DZC is eliminated from the model at an emissions cap of 150 $kgCO_2e$/MWh and gas price of \$5/GJ. The "Reduced CapEx" columns refer to 50% reduction in both the energy (X_E) and power (X_P) capital cost of storage, compared to the current cost estimates. Region 1 and 2 represent a generic mechanical and electrochemical BES system, respectively (see Figure 38). GT refers to the combination of SCGT and CCGT. All other parameters are the same as of Table 32.

	Current CapEx		**Reduced CapEx**	
Storage system	**Region 1**	**Region 2**	**Region 1**	**Region 2**
Energy-specific CapEx (\$/kWh)	\$30	\$375	\$15	\$188
Power-specific CapEx (\$/kW)	\$1500	\$550	\$750	\$275
LCOE (\$/MWh)	\$97.6	\$103.0	\$90.7	\$98.9
BES power capacity (% of peak load)	22	8	42	22
BES energy capacity (hrs of average load)	9	1	18	3
BES market share (% of annual load)	6	1	9	4
GT capacity (% of peak load)	75	88	54	74
GT generation share (% of annual electricity generation)	34	34	34	34
Wind capacity (% of peak load)	120	138	115	127
Ratio of BES power to wind capacity	0.18	0.06	0.37	0.18
Ratio of GT to wind capacity	0.62	0.64	0.47	0.58
Ratio of GT to BES capacity	3.4	10.7	1.3	3.2

The relative importance of BES and GT depends on stringency of the emissions cap too. Here we presented the results at an emissions cap of 150 kgCO2e/MWh – ~70% reduction compared to the current emissions

levels in the United States. With zero or near-zero emissions and no use of DZC, larger storage capacities will be needed to manage wind's intermittency as GT gets too polluting for such extremely low-carbon grids.

Price of gas is another important factor in determining the importance of bulk storage. To explore its effect, we repeat the simulation with a much higher gas price of $20/GJ (Table 34) instead of $5/GJ (Table 33). The optimal ratios of BES and GT to wind capacity do not vary in a substantial manner with $20/GJ gas, except when the cost of the mechanical system is cut by 50%. This indicates that the low capital cost of the gas turbine fleet (Table 32) out-competes its higher operation and fuel costs, hence the GT still supplies one third of the load with $20/GJ gas.

Table 34: Key characteristics of the generation fleet when DZC is eliminated and at an emissions cap of 150 $kgCO_2e/MWh$ and gas price of $20/GJ. The "Reduced CapEx" columns refer to 50% reduction in both the energy (X_E) and power (X_P) capital cost of storage. Region 1 and 2 represent a generic mechanical and electrochemical BES system (see Figure 38). All other parameters are the same as of Table 32.

	Current CapEx		**Reduced CapEx**	
Storage system	**Region 1**	**Region 2**	**Region 1**	**Region 2**
Energy-specific CapEx ($/kWh)	$30	$375	$15	$188
Power-specific CapEx ($/kW)	$1500	$550	$750	$275
LCOE ($/MWh)	$131.7	137.1	124.1	133.0
BES power capacity (% of peak load)	22	8	46	22
BES energy capacity (hrs of average load)	9	1	23	3
BES market share (% of annual load)	6	1	11	4
GT capacity (% of peak load)	75	88	50	74
GT generation share (% of annual electricity generation)	34	34	27	34
Wind capacity (% of peak load)	120	138	130	127
Ratio of BES power to wind capacity	0.18	0.06	0.36	0.18
Ratio of GT to wind capacity	0.62	0.64	0.39	0.58
Ratio of GT to BES capacity	3.4	10.7	1.1	3.2

3-3- Economically optimal deployment of storage

The amount of BES that is technically required for decarbonization with intermittent renewables is (somewhat) independent of the impact of storage on electricity costs. Figure 42 illustrates the power and energy capacity of BES as well as the percentage of annual load supplied by the energy stored in BES (*i.e.* market share of BES), in the 150kgCO_2e/MWh scenario. The portions of the annual generation that comes from wind and DZC are also plotted (called generation share). The generation share of GT (aggregate of SSCGT and CCGT) is ~33% and is insensitive to the storage cost.

Based on the 150 kgCO_2e/MWh scenario, we can make the following comments on the economically efficient penetration level of BES. The power capacity of BES remains below 30% and 10% of the peak load for the mechanical and electrochemical BES systems with their current costs, respectively. Although mechanical technologies have higher X_P, their optimal power capacity is noticeably higher compared to electrochemical systems. This observation again highlights the significance of the energy-specific cost (X_E) in the overall economic viability of BES systems —a major disadvantage of the existing battery systems.

The optimal energy capacity of BES turns out to be small in general, even when we impose ~70% emission reductions compared to BAU. The mechanical storage fleet was sized to supply the average electric load for one full day on its own. This value sharply drops as the energy cost (X_E) increases while the power cost (X_P) simultaneously drops; *i.e.* moving to electrochemical systems.

These relatively low energy capacities signal the unimportance of large-scale storage of electricity over long time horizons (*e.g.* seasonal storage) from an economic point of view. This is driven by the lower competitiveness of BES systems coupled with wind in comparison to low carbon and dispatchable generation facilities, like CCGT and DZC modeled here. Even when we consider the cheapest BES system simulated (X_E=5 and X_P=100, the lower left corner of Figure 38), the BES fleet would be sized to store enough energy to meet the average load for ~40 hours.

The BES share of the total supply of electricity is also small compared to of the rest of the generation fleet. Approximately 6% of the demand is met by the electricity stored in mechanical BES systems (very sensitive to X_E) while this figure becomes marginal for battery technologies with their current capital costs. Even using

the cheapest storage assumptions given above, the contribution of BES remains about 10%. The drop in the share of storage (and consequently the wind fleet) of the electricity supply at elevated storage costs is compensated by DZC.

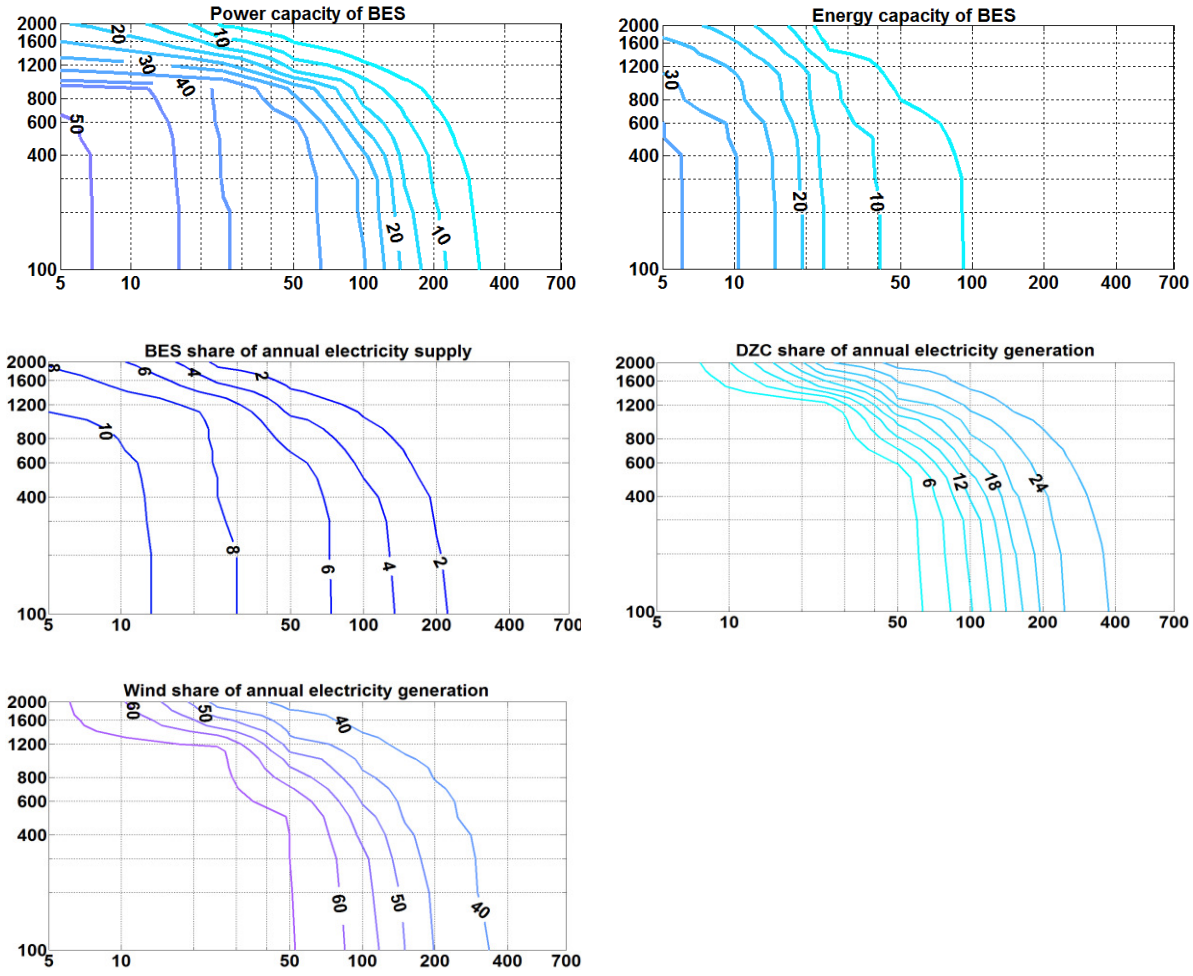

Figure 42: Effect of the cost of storage on its market share at an emissions cap of 150 kgCO2e/MWh. Subfigures from top left in counter clockwise order illustrate normalized power capacity and energy capacity of BES, percentage of annual load supplied by the energy stored in BES, and the portion of the annual electricity generated by DZC and wind. The generation share of GT (~33%) is insensitive to the storage cost. Horizontal and vertical axes show X_E ($/kWh) and X_P ($/kW). Power capacity of BES is normalized to the annual peak load. The energy capacity of BES is expressed in hours and is normalized based on the annual average load (556 MW).

3-4- Implications for specific BES technologies

Which BES technologies are closer to having an impact under carbon constraints and thus would merit a higher priority in R&D efforts directed at decarbonizing the electricity supply? We explore this question through a scenario in which energy- and power-specific costs of each BES technology are cut in half. As a

measure of impact, we use share of the annual load supplied by BES (market share) and the levelized cost of electricity supply. Figure 43 shows results for an emissions cap of 150 $kgCO_2e/MWh$.

None of the existing technologies gain noticeable market share, but when costs are halved PHS and A-CAES make larger gains in market share (7% and 9%, respectively) and make a corresponding impact in reducing the electricity cost. The simulated battery technologies remain prohibitively expensive even when their costs are halved compared to the current estimates.

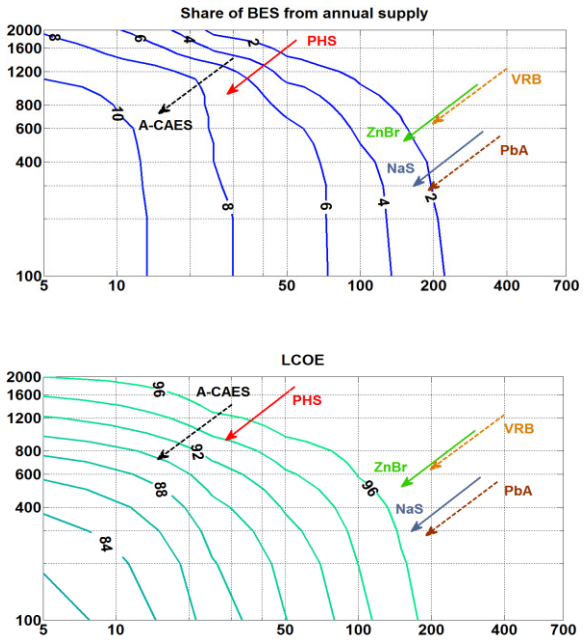

Figure 43: Market share of BES (top, % of load supply) and LCOE (bottom, $/MWh) with a carbon cap of 150 kgCO2e/MWh. Horizontal and vertical axes indicate X_E ($/kWh) and X_P ($/kW). Arrows start from the current cost estimates (average of the range shown for each technology in Figure 38 and Table 30) and end at points with 50% reduction in both X_E and X_P.

We analyzed diabatic CAES separately since unlike all other BES technologies it has non-negligible emissions. The heat rate and work ratio of CAES were set at 4.2 GJ/MWh and 0.75 in our model, respectively. Therefore, the simulated CAES facility emitted 277 $kgCO_2$ per MWh of electricity generated (inside-the-fence lines emissions). We varied X_E and X_P of diabatic underground CAES in the range of 5-25 $/kWh and 850-1200 $/kW, based on the estimates from Table 30. Aboveground CAES was not modeled due to its obvious weaker performance (caused by much higher energy-specific capital cost of >200 $/kWh, refer to Table 30 for details).

We present results from the 150 $kgCO_2e$/MWh cap scenario in Table 35. Availability of diabatic CAES made negligible differences in LCOE. The cheapest CAES system modeled (X_E=5 $/kWh and X_P=850 $/kW) could only store enough electricity to meet the average load for ~1 hour and its power capacity is 7% of the peak load. A higher gas price of $10/GJ instead of $5/GJ did not improve the competitiveness of CAES, as illustrated in Table 35.

For the sake of comparison, we also modeled A-CAES system (heat rate of zero and efficiency of 63%) with the same emissions cap and gas prices. We used the range of 1100-1700 $/kW and 10-50 $/kWh for the power and energy capital cost of A-CAES (refer to Table 30). As seen in Table 35, the role of A-CAES turned out more significant compared to diabatic CAES despite its much higher capital cost. LCOE of the system equipped with A-CAES instead of diabatic CAES was lower (~4% in the base case). Moreover, both the power and energy capacity of A-CAES were much higher compared to of diabatic CAES. The GHG emissions of diabatic CAES severely limit its competitiveness as a BES system under emissions constraints. Note that the significance of diabatic CAES (measured by its impact on LCOE and by its optimal installed capacity) turned out to be even smaller under no emissions constraints (BAU scenario). These results lead to the conclusion that diabatic CAES is too capital intensive for today's grids (no major GHG emissions restrictions) and too polluting for the future low-carbon grids.

Table 35: Key characteristics of underground diabatic CAES and A-CAES at a grid emissions cap of 150 $kgCO_2e$/MWh. All other inputs are the same as Table 32.

Parameter	**Diabatic CAES**		**A-CAES**	
Power CapEx ($/kW)	850-1200		1100-1700	
Energy CapEx ($/kWh)	5-25		10-50	
Efficiency (%)	NA		63	
Work ratio (MWh in/ MWh out)	0.75		1.60	
Heat rate (GJ/MWh)	4.2		0	
Price of gas ($/GJ)	5	10	5	10
LCOE ($/MWh)	97.7-97.8	109.1	93.8-97.8	105.2-109.1
Power capacity (% of peak load)	6-0	6-0	33-1	33-1
Energy capacity (hours of average load)	1-0	1-0	19-0.2	19-0.2

3-5- Sensitivity to capital cost of DZC

Cost figures for DZC are uncertain due to their limited deployment. As a case in point, estimates for the Vogtle AP1000 nuclear plant currently under construction in GA, USA is around 6400 $/kW [116]. The figures for the Korea-UAE nuclear contracts announced in 2009 ($3700/kW [117]) is however, almost half of for the Vogtle project. In a recent study, Abdulla *et al.* [118] used expert elicitations to estimate capital cost of light water reactors, both based on current technology and small modular reactors (SMR). The median of the estimates for a 1 GW reactor ranged from $2600 to $6600/kW while it varied between $4000 and $16300/kW for a 45 MW light water SMR. Cost figures for concentrated solar power plants (CSP) also lay in a wide range. Estimates for the Crescent CSP plant (110 MW, 10 hours of thermal storage, under construction in NV, USA) are about $9000/kW [119, 120] . The price tag of the Solana plant (250 MW, 6 hours of thermal storage, commissioned in 2013 in AZ, USA) is roughly $8000/kW [120]. We used a value of $9000/kW for capital cost of DZC in the base case model.

Figure 44 explores the robustness of our key results and conclusions to the capital cost of DZC. Three scenarios are illustrated in this figure:

a) no BES is allowed (to quantify the economic value of BES at current capital costs in decarbonizing the electricity supply),
b) BES is available at the current costs, and
c) a scenario with 50% reduction in both the energy-specific capital cost (X_E) and power-specific capital cost (X_P) of BES compared to the current levels considered in case b.

We chose one generic BES system from the mechanical (with current costs of X_E=30 $/kWh and X_P=1500 $/kW) and electrochemical (X_E=375 $/kWh and X_P=550 $/kW) BES category to perform this sensitivity analysis. All other simulation inputs have the same values as the base case simulation (listed in Table 32).

The simulated mechanical BES system is much more successful in reducing the LCOE and its power capacity is consistently and considerably (~2-3 times) higher than of the electrochemical system. The optimal BES capacity is almost zero when the cost of DZC is ≤$6000/kW (for the mechanical category) and $9000/kW (for the electrochemical system) with current cost estimates for BES. This is because wind and BES lose their

economic competitiveness as DZC gets less capital intensive. Even cutting both power and energy capital costs of the battery makes marginal changes in the LCOE (≤ $1/MWh) unless capital cost of DZC remains above $9000/kW. As we discussed in Section 2-3, DZC represents the least capital intensive, dispatchable technology—CSP, nuclear, CCS, biomass or geothermal (possibly even with high voltage direct current, HVDC, transmission lines)—that can be utilized in a given location. We believe that the value of 9000 $/kW used in this paper is mostly likely an overestimate of this best-case DZC cost.

Price of gas is an important player in determining the competitiveness of DZC with wind and the required amount of storage. We repeat the simulation with higher gas prices of $10/GJ (Figure 45) and $20/GJ (Figure 46). More expensive gas and DZC bump up the LCOE and optimal capacity of storage. Nevertheless, our general conclusion about higher competitiveness of mechanical BES systems to batteries with their current costs remains valid. The optimal capacity of batteries and particularly their impact on LCOE remain less than of the mechanical systems. Even at the very high gas price of $20/GJ and DZC capital cost of $12000/kW, the power capacity of the simulated electrochemical system remained below 10% of the peak electric load (100 MW). Halving both its power- and energy-specific cost increased this number to below 25% of the peak load. The corresponding figures for the mechanical system modeled here are 20% and 40%.

An interesting observation is that raising the price of gas increases the optimal capacity of BES more at lower DZC costs. This signals that more BES is deployed with cheap DZC to reduce the generation share of now more expensive (higher fuel cost) gas turbines. This is because at very high DZC price tags, the only economical generators would be wind and gas turbine. The optimal capacity of wind and gas turbine (SCGT and CCGT combined) is plotted in Figure 47 and Figure 48 for the simulated mechanical and electrochemical systems with $10/GJ and $20/GJ gas prices, respectively. Considering Figure 45 to Figure 48 reveals that some (although small) BES capacity is deployed despite the absence of wind from the optimal generation fleet at DZC capital costs at or below $6000/kW.

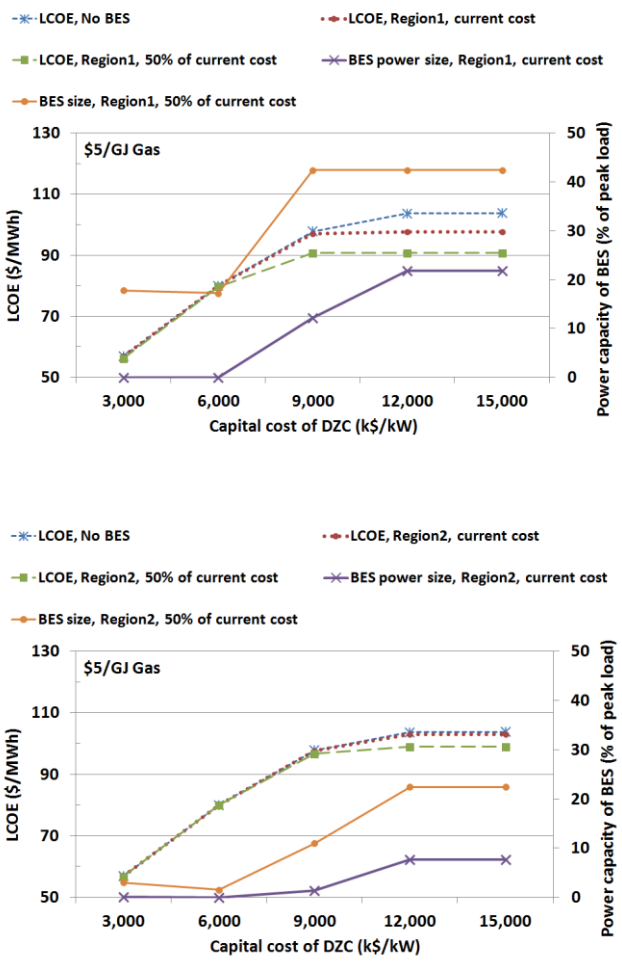

Figure 44: Sensitivity of LCOE and power capacity of BES to capital cost of DZC. Each sub-plot presents three cases: a) no BES is allowed, b) BES at the current capital costs and, c) BES with 50% reduction in both X_E and X_P values considered in case b. The sub-figure on top shows the results for a generic BES system in region 1 with X_E=30 $/kWh and X_P=1500 $/kW as its current costs. The sub-figure at the bottom represents region 2 with X_E=375 $/kWh and X_P=550 $/kW as the current costs. Region 1 and 2 represent mechanical and electrochemical bulk storage systems (see Figure 38). Price of gas is $5/GJ.

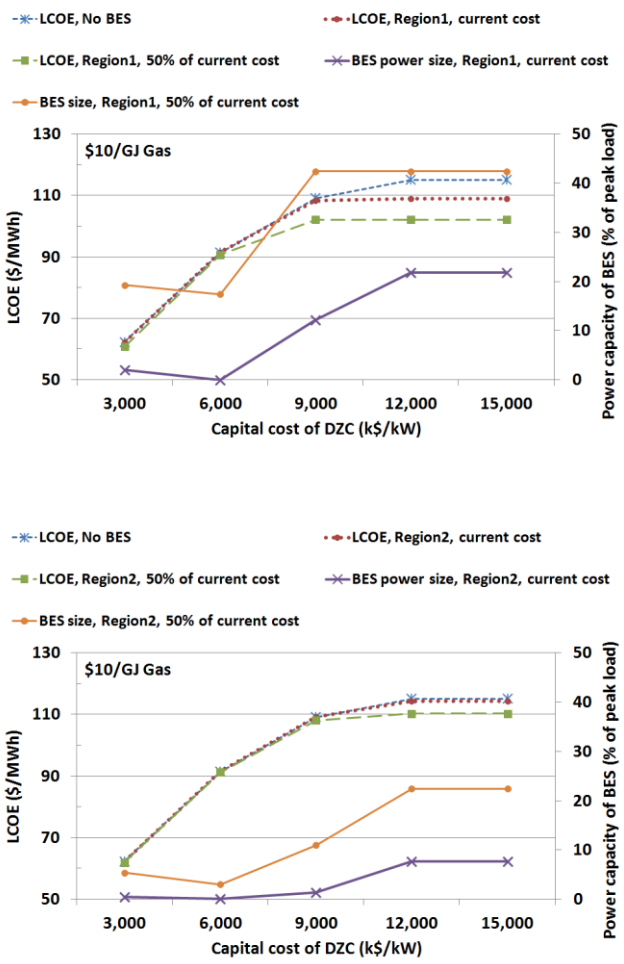

Figure 45: Sensitivity of LCOE and power capacity of BES to the capital cost of DZC. The sub-figure on top shows results for a generic BES system in region 1 with X_E=30 $/kWh and X_P=1500 $/kW as its current costs. The sub-figure at the bottom represents region 2 with X_E=375 $/kWh and X_P=550 $/kW as the current costs. Price of gas is $10/GJ.

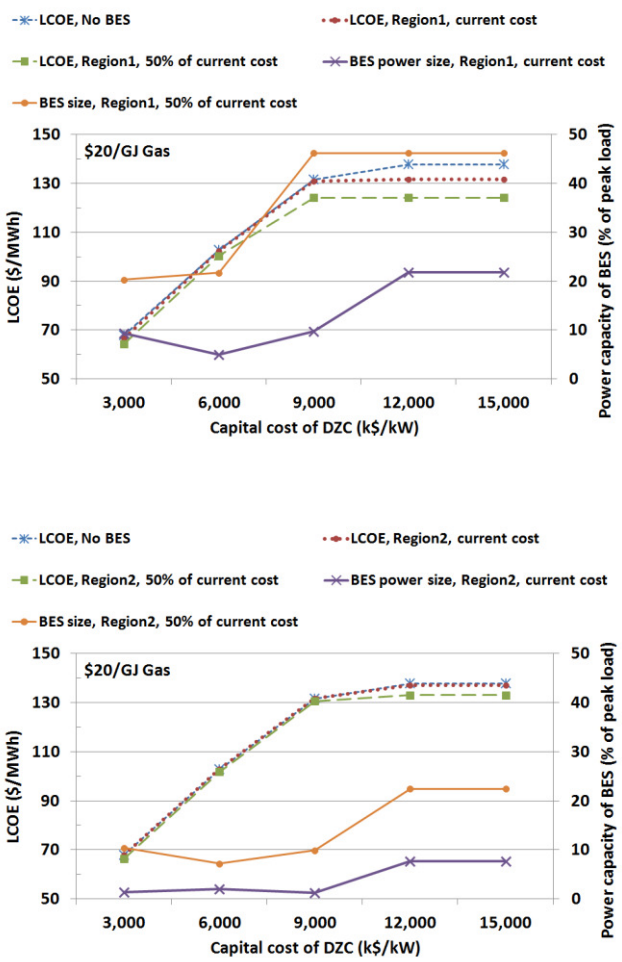

Figure 46: Sensitivity of LCOE and optimal power capacity of BES to the capital cost of DZC. The sub-figure on top shows results for a generic BES system in region 1 with X_E=30 $/kWh and X_P=1500 $/kW as its current costs. The sub-figure at the bottom represents region 2 with X_E=375 $/kWh and X_P=550 $/kW as the current costs. Price of gas is $20/GJ.

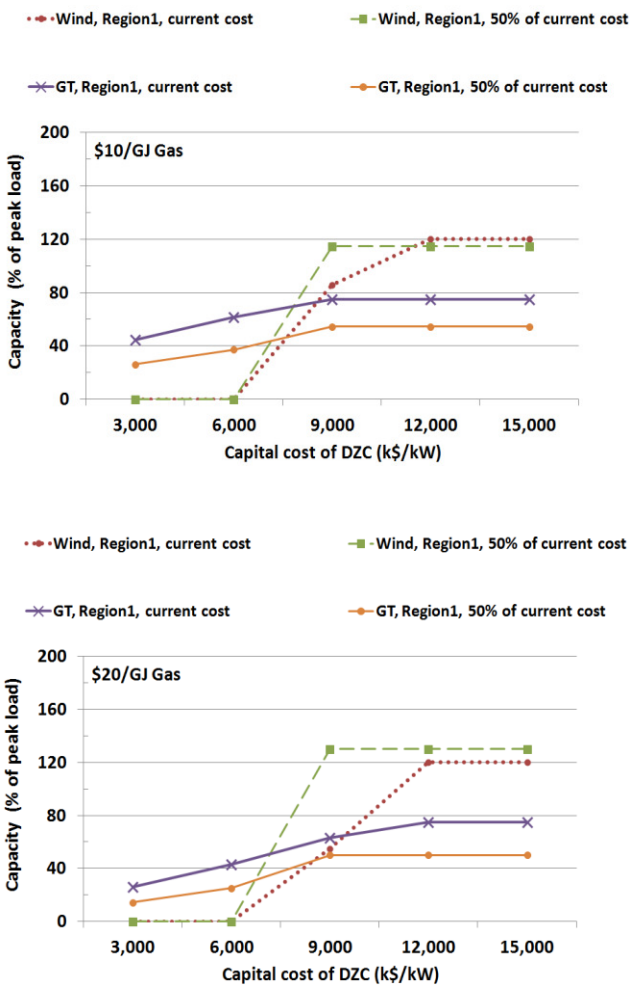

Figure 47: Power capacity of wind and gas turbine fleet with various DZC costs and \$10/GJ (top) and \$20/GJ (bottom) gas prices. The simulation results are for a sample BES system from the mechanical category. Two cost scenarios for BES are considered: current estimates (X_E=30 \$/kWh and X_P=1500 \$/kW) and 50% reduction in both the energy- and power-specific capital cost.

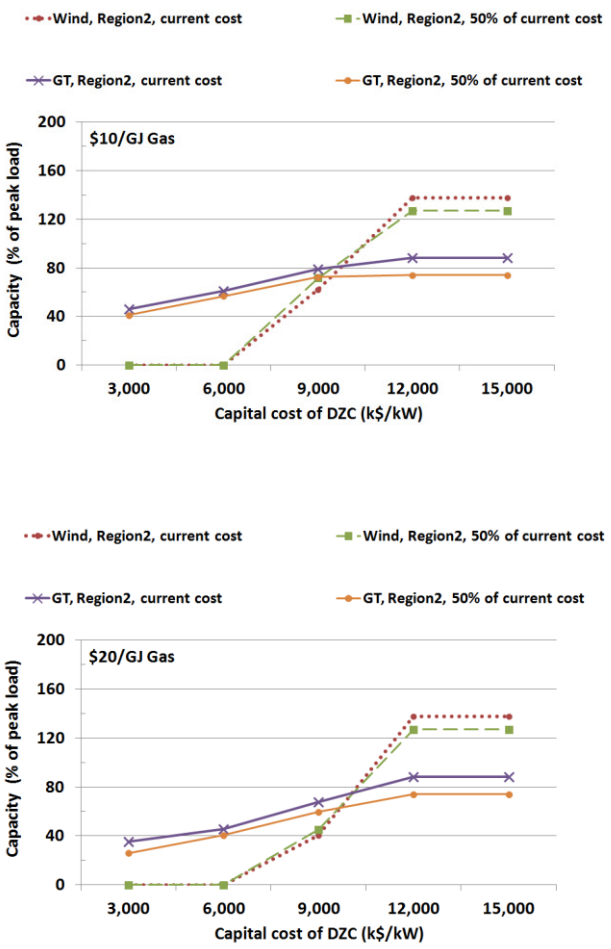

Figure 48: Power capacity of wind and gas turbine fleet with various DZC costs and \$10/GJ (top) and \$20/GJ (bottom) gas prices. The simulation results are for a sample BES system from the electrochemical category. Two cost scenarios for BES are considered: current estimates (X_E=375 \$/kWh and X_P=550 \$/kW) and 50% reduction in both the energy- and power-specific capital cost.

3-6- Sensitivity to price of gas

We used \$5/GJ as the price of natural gas in the base case results presented. This value is comparable to the average price of \$4.8/GJ paid by power plants across the United States between 2009 and 2013 [121]. Due to uncertainties in future gas prices especially under emissions restrictions and in the wake of the unconventional gas revolution, here we evaluate robustness of our key conclusions to this parameter. Similar to Figure 44, Figure 49 illustrates the LCOE and power capacity of a generic mechanical and a battery BES system, but with respect to price of gas instead of DZC CapEx. The GHG emissions intensity is capped at 150 $kgCO_2e/MWh$ and all parameters except price of gas are the same as Table 32.

The availability of BES marginally impacts the overall cost of electricity with the current BES capital costs figures, although the mechanical BES system starts to matter at high gas prices (\$20/GJ). Reducing the energy-specific and power-specific capital costs (X_E and X_P) of the mechanical BES by 50% lowers the LCOE much more (3.5-7.0 \$/MWh compared to LCOE at current X_E and X_P cost figures), particularly with gas prices below \$20/GJ, compared to the generic electrochemical system. There is a maximum of \$2.5/MWh difference between the electricity supply cost of the generation fleet utilizing the electrochemical system with the current capital costs and with 50% cost reduction (occurring at an unrealistically high gas price of \$40/GJ).

The optimal power capacity of BES is far more sensitive because of the reduced optimal capacity of gas turbines at high gas prices and the competition between wind, BES, and DZC to compensate for that. Our conclusion that the optimal capacity of the mechanical BES systems is much (~2-3 times) higher compared to of the battery systems, especially with 50% cost reductions, is also robust to changes in gas prices.

As discussed in Section 3-5, both the capital cost of DZC and price of gas impact the significance of BES in reducing decarbonization costs and supporting wind integration. Figure 50 and Figure 51 show similar results to Figure 49 but for cheaper (\$6000/kW) and more expensive (\$12000/kW) DZC instead of \$9000/kW. Both the overall cost of electricity supply and the optimal capacity of BES (especially for the mechanical system) increase as the capital cost of DZC is raised. Even at the high DZC cost of \$12000/kW, the capacity of the battery system remains below 10% of the peak load. Halving the cost of BES does not increase capacity of the electrochemical BES beyond 20% unless the price of gas gets above \$25/GJ.

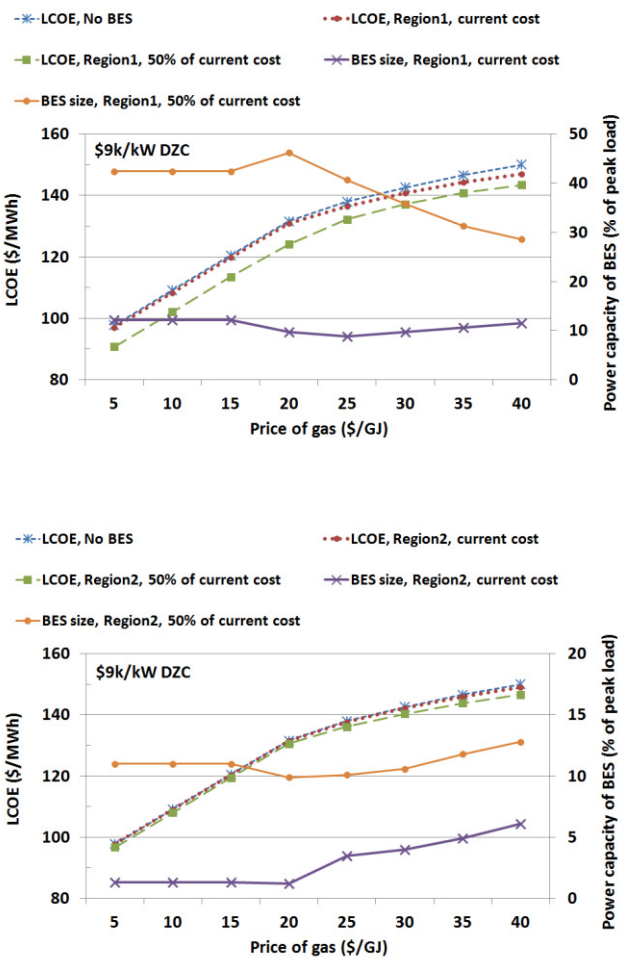

Figure 49: Sensitivity of the LCOE and power capacity of BES to the price of gas. Each sub-plot presets three cases: a) no BES is allowed, b) BES at the current costs, and c) 50% reduction in both X_E and X_P compared to case b. The top sub-figure presents a generic mechanical BES system (from region 1 in Figure 38) with X_E=30 $/kWh and X_P=1500 $/kW as its current costs. The sub-figure at the bottom represents a generic electrochemical technology (from region 2 of Figure 38) with X_E=375 $/kWh and X_P=550 $/kW as the current costs. Capital cost of DZC is $9000/kW in all scenarios.

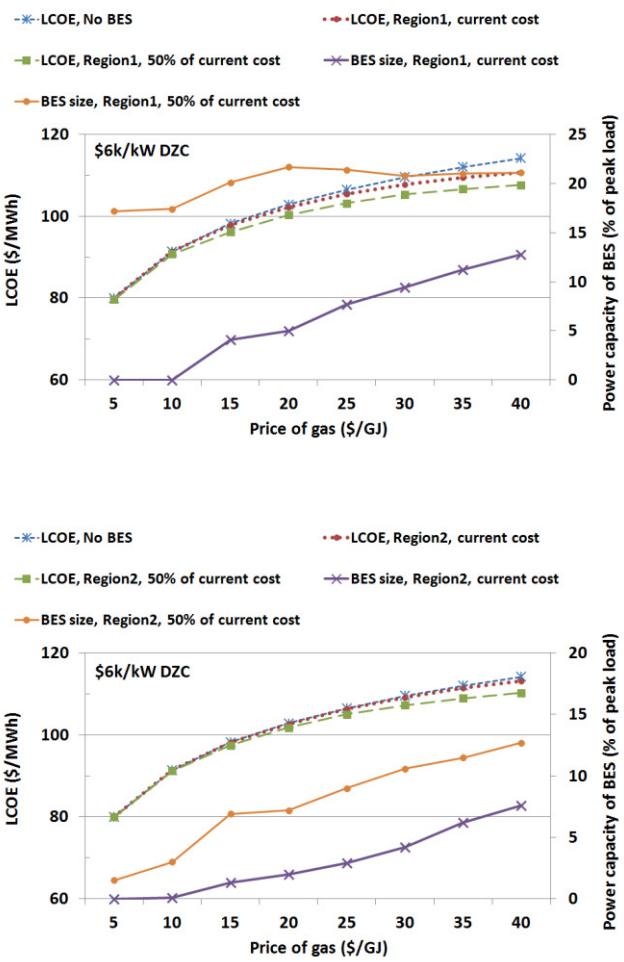

Figure 50: Sensitivity of the LCOE and power capacity of BES to the price of gas at $6000/kW as the CapEx of DZC. The top sub-figure presents a generic mechanical BES system (region 1) with X_E=30 $/kWh and X_P=1500 $/kW as its current costs. The sub-figure at the bottom represents a generic electrochemical technology (region 2) with X_E=375 $/kWh and X_P=550 $/kW as the current costs.

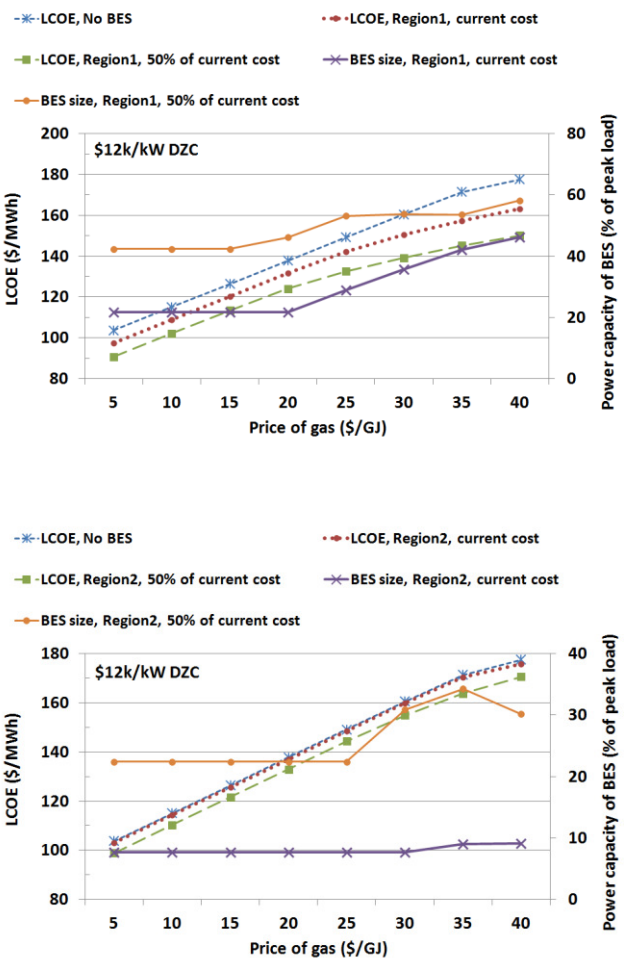

Figure 51: Sensitivity of LCOE and power capacity of BES to the price of gas at $12000/kW as the capital cost of DZC. The top sub-figure presents a generic mechanical BES system (region 1) with X_E=30 $/kWh and X_P=1500 $/kW as its current costs. The sub-figure at the bottom represents a generic electrochemical technology (region 2) with X_E=375 $/kWh and X_P=550 $/kW as the current costs.

3-7- Sensitivity to storage efficiency

The roundtrip efficiency of electricity storage obviously varies among different BES technologies. We focused on the capital cost of storage systems as the dominant parameter impacting the economics of BES throughout the analysis. Nevertheless, A-CAES is among the least efficient BES systems; an average value of 63% compared to 75% for the generic BES system that we modeled (Table 30). In order to assess robustness of the results, we adjusted storage efficiency of the specific BES technologies in two scenarios: 75% (independent of the BES type, similar to Table 32) and the current estimates (according to values listed Table 31). As shown in Table 36, the storage efficiency has insignificant impact on our key results. Even accounting for its low efficiency, A-CAES remains the most cost-effective technology followed by PHS.

Table 36: Sensitivity of the key results to the storage efficiency of specific BES technologies at an emissions cap of 150 $kgCO_2e/MWh$. Average of the values shown in bold in Table 30 are used as the energy- and power-specific capital cost of each storage technology (similar to Figure 43). Two values for storage efficiency are considered: 75% (independent of BES technology) and technology-specific values (see Table 30). All other parameters are similar to Table 32.

Parameter	**PHS**		**A-CAES**		**Pb-A**		**NaS**		**ZnBr**		**VRB**	
Efficiency (%)	75	78	75	63	75	83	75	80	75	68	75	73
X_E ($/kWh)	55		30		375		325		300		400	
X_P ($/kW)	1750		1400		550		575		1000		1250	
LCOE ($/MWh)	97.7	97.7	96.7	97.3	97.7	97.7	97.7	97.7	97.8	97.8	97.8	97.8
BES power (% of peak)	2.6	3.2	14.5	10.0	1.3	1.3	1.6	1.6	0.0	0.0	0.0	0.0
BES energy (hrs of average load)	0.4	0.5	4.6	2.2	0.0	0.0	0.1	0.1	0.0	0.0	0.0	0.0
BES market share (%)	0.8	1.0	4.3	1.9	0.1	0.1	0.2	0.2	0.0	0.0	0.0	0.0

3-8- Upper bound for penetration of storage

What would be the economically optimal deployment of bulk storage provided that storage is free and ideal (without losses)? This question gives the upper bound for the market share that the BES industry could gain. According to Table 37, the ultimate market share of BES would be 31% in the best case (gas price of $10/GJ or higher and with an emissions cap of 150 $kgCO_2e/MWh$). The rest (69%) of the load is directly supplied by

wind in this scenario and the contributions of GT and DZC are zero. The optimal power capacity of BES is 96% of the peak load and its energy capacity is large enough to meet the average electric load for 52 days. In the carbon-free scenario, the optimal capacity of GT and DZC turn out to be zero too, regardless of the gas price.

Table 37: Optimal characteristics of the storage and wind fleet assuming almost free (X_E=X_P=0.001) and almost ideal (efficiency=99.99%) bulk storage with a GHG emissions cap of 150 kgCO_2e/MWh. All other input parameters are similar to Table 32.

Gas price	**LCOE**	**BES power capacity**	**BES energy capacity**	**BES market share**	**Wind capacity**	**Wind gen. share**
$/GJ	$/MWh	% of peak load	Hours of avg. load	% of annual load supply	% of peak load	% of annual generation
5	67.9	78	1027	22	105	66
7.5	73.6	78	1027	22	105	66
≥10	76.9	96	1248	31	159	100

6- Conclusions

We draw two policy-relevant conclusions from this work. First, large-scale adoption of bulk electricity storage compared to variable renewables and gas turbines is neither technically required nor cost effective as a means to reduce carbon emissions even when variable renewables play a large role. In other words, intermittent renewables need not to wait for the availability of cheap bulk storage to become an effective tool for decarbonization. This conclusion breaks down only when emissions must be reduced by more than about 70% *or* when the cost of dispatchable-low-carbon power sources is very high (above $9000/kW with an emissions cap of 150 kgCO_2e/MWh at current BES cost estimates, see Figure 44). Second, at their current costs, adiabatic CAES and PHS show the most appealing prospects in lowering the decarbonization cost among other BES technologies due to their low energy-specific capital costs and despite their much higher power-specific capital costs.

The strength of our analysis, like any other, turns on its assumptions. Our most important simplifications include ignoring transmission, ignoring forecast errors of wind and load, and using a green-field model rather than one that allows dynamic adjustment of capacity over time. We have limited the simulation to 15-minute

time intervals and have not modeled any reliability requirements (*e.g.* reserve margin). We have also used a fixed gas price of $5/GJ and a constant storage efficiency of 75%.

The following paragraphs tease out the quantitative conclusions that underpin each of the high-level claims, and explain why we think the policy-relevant conclusions are robust to our simplifying assumptions. Table 39 provides a systematic overview of all significant assumptions and their likely impact on the conclusions.

Our first conclusion is that availability of inexpensive BES has relatively small effects on the overall cost of electricity generation, unless extremely tight emission mandates are in place *or* dispatchable-low-carbon technologies are very expensive. Under an emissions cap of 150 $kgCO_2e/MWh$ – a ~70% cut in emissions intensity compared to the current USA or world average – a reduction in storage costs by more than an order of magnitude (to X_E=5 $/kWh and X_P=100 $/kW from already optimistic values of X_E=25 and X_P=1500 from the mechanical BES category) cuts the cost of electricity generation by 16%. This is not a significant reduction when compared to the impact of cutting the capital cost of wind or DZC by 50%, which lowers electricity cost by 26% and 29%, respectively (see Table 38 for a complete list of cases and comparative costs and emissions). One should note that assessing the likelihood and the associated costs of cutting the capital cost of different technologies were not in the scope of our analysis. We analyzed only the effects of reducing the capital cost of BES, wind, and DZC on the cost of electricity supply.

The economically optimal deployment of bulk storage was a relatively small fraction of peak capacity, even when we imposed a tight emissions allowance of 150 $kgCO_2e/MWh$ (see Figure 41). It is crucial to note that despite its smaller capacity compared to the wind and gas fleet in our model, the optimal capacity of BES turned out to be substantially large compared to its current deployment level. As a case in point, the ratio of the existing BES power capacity to the peak load in the United States is below 3% (below 0.1% if PHS is excluded) [122]. Therefore, our simulation calls for massive increase in capacity of BES, from the current value of 3% of the peak load to ~10% (for mechanical systems with their current costs, as shown in Figure 41). Our model also shows the need for larger buildup of wind compared to BES capacity. The ratio of the existing wind fleet to peak load is ~8% in the United States while the optimal value for the wind capacity using mechanical BES systems in Figure 41 is ~70%. Therefore, one can argue that the capacity of wind

should increase three times more compared to of BES (with current cost estimates for mechanical systems and with an emissions cap of 150 $kgCO2_e/MWh$).

The energy capacity of our optimally sized storage fleet sufficed to supply the average electric demand continuously for only 2 days with an emissions cap of 150 $kgCO_2e/MWh$, even with the cheapest storage cost system that we simulated (X_E=5 \$/kWh and X_P=100 \$/kW). Other than niche applications that are not captured in this analysis, it is therefore hard to justify the development of storage for significantly longer than a day, especially hydrogen-based technologies which are even more capital intensive and less efficient compared to the systems studied here. The optimal energy capacity of BES in the carbon-free grid also remained small (below one day of average load) when $X_E \geq$ \$25/kWh and $X_P \geq$ \$100/kW. Obviously if the cost of storage is significantly reduced compared to other decarbonization pathways and compared to its current values, BES would capture a larger market share. As shown in Table 37, a free and ideal storage system would be sized to supply the average electric load for ~40-50 days.

In many respects, we use assumptions that are optimistic for BES and therefore we give an upper bound for its cost effectiveness. The economically optimal size of the wind fleet would be lower in the real world once transmission requirements are taken into account (*i.e.* more capital-intensive wind farms). A smaller wind fleet would likely translate to a larger DZC fleet and hence, less variability in electricity supply. Therefore, the need for bulk storage and its impact on the overall cost of electricity would likely be lower than what we have presented here (see Table 39). Imperfect forecasts of wind availability and electric load would also hurt the economics of wind and storage compared to dispatchable generators. Finally, increased geographical dispersion of wind farms in future low carbon grids can lower the variability in the aggregate wind generation and reduce the need for BES.

Table 38: LCOE corresponding to various sensitivity analyses discussed in the conclusion section. All cases assume an emissions cap of 150 $kgCO_2e/MWh$. "W.R.T." stands for "with respect to".

Scenario	**LCOE ($/MWh)**	**% change W.R.T base case**
Base case (Table 32 with X_E=25 $/kWh, X_P=1500 $/kW, and GHG cap= 150 $kgCO_2e/MWh$)	96.8	0%
Base case with X_E=5 $/kWh and X_P=100 $/kW	81.2	-16%
Base case with $1000/kW wind	72.0	-26%
Base case with $4500/kW DZC	68.6	-29%
Base case with $10/GJ gas	108.1	+12%
Base case with X_E=5 $/kWh, X_P=100 $/kW, and $10/GJ gas	92.6	-4%
Base case with $4500/kW DZC and $10/GJ gas	83.4	-14%
Base case with $1000/kW wind and $10/GJ gas	77.7	-20%
Base case with X_E=30 $/kWh and X_P=1400 $/kW (A-CAES cost values)	96.7	~0%
Base case with X_E=30 $/kWh, X_P=1400 $/kW, and efficiency of 63% (A-CAES cost and efficiency values)	97.3	1%
Base case with X_E=30 $/kWh, X_P=1400 $/kW, and efficiency of 70% (A-CAES cost values and 10% improvement in efficiency)	97.0	0%

The price of natural gas in the future is obviously uncertain. Due to the strong performance of gas turbines in our results, especially CCGT, we assessed the effects of higher gas prices on the impacts that availability of cheap BES will have on the cost of electricity generation. Using higher gas prices mildly changes the aforementioned 16% drop in the cost of electricity with $5/GJ gas when the storage cost is reduced by more than an order of magnitude to X_E=5 $/kWh and X_P=100 $/kW (see Table 38). The same order-of-magnitude drop in storage costs but now with 10 $/GJ gas, reduces the electricity cost by only 14%. This saving is again not significant when we compare it with the benefits of lowering the capital cost of wind itself or DZC. Halving the cost of wind and DZC at $10/GJ gas lowers the cost of electricity by 23% and 28%, respectively. (Refer to Figure 49 to Figure 51 for full sensitivity analysis.)

Cost-reduction efforts of various BES technologies should be prioritized, among other goals, according to their effectiveness in decreasing the cost of low-carbon electricity. As a case in point, the California Public Utilities Commission's 2013 decision to exclude PHS plants larger than 50 MW from the California's 1.3 GW

(by 2020) electricity storage mandate may be hard to defend on the basis of cost effectiveness or technical potential. The Commission argues that "the sheer size of PHS projects would dwarf other smaller, emerging technologies; and as such, would inhibit the fulfillment of market transformation goals" [123]. We strongly support the deployment storage technologies to enable learning-induced cost reductions. However, we caution that such technology-favoring policies can delay development of more cost-effective storage technologies such as PHS that seem to play a more significant role in decarbonizing electricity. We acknowledge that this argument also depends on one's judgment about the likelihood of future R&D progress in various BES technologies (*i.e.* reduction in the cost of each BES technology per unit of R&D expenditure).

While electrochemical batteries are currently very far from being cost effective for bulk storage of electricity, they are or may be technically important and cost competitive in two other important applications in a low-carbon economy. First, they can be attractive tools for managing mismatch between supply and demand of electricity at finer temporal resolutions which are not included in our study or ensuring reliability of the grid. These technologies have an economic advantage over other BES systems (*e.g.* PHS) and low carbon generators (*e.g.* DZC): they can be deployed in smaller scales and have higher operational flexibilities (*e.g.* higher ramp rates). Second, the electrochemical battery (and also hydrogen-based) technologies may play a central role in decarbonizing the transportation sector. Finally, note that each BES technology may well find a market niche (*e.g.* small islands with wind and diesel generation); here we examined only the large-scale electricity systems.

Our second high-level conclusion is that the economics of BES are primarily driven by its energy-specific capital cost. Therefore, mechanical storage technologies (characterized with low energy-specific X_E, but high power-specific X_P, capital costs) are currently more competitive compared to electrochemical systems (intermediate X_E and X_P). Even halving the capital costs of batteries makes marginal changes in the overall cost of electricity generation (see Figure 43). Nevertheless, lowering the capital cost of mechanical systems, especially power-specific cost, drives a much steeper drop in decarbonization costs and it also boosts integration of wind and market share of storage. (Note that we have assessed the relative impacts of cutting the cost of various technologies on the cost of supplying low-carbon electricity. We have not, however, studied the relative effects of R&D investment in reducing the capital cost of various technologies.) Therefore,

developing BES technologies with low energy-specific capital costs (*e.g.* A-CAES) deserves a higher priority for bulk storage applications, unless the capital cost of systems with high power-specific costs (*i.e.* flow batteries) can be reduced much faster and cheaper.

We acknowledge that siting of pumped-hydro and underground compressed air energy storage projects is geographically constrained in contrast to electrochemical systems. PHS requires two large water reservoirs with sufficient elevation difference and has a large land footprint. Underground storage of air needs a suitable geologic formation such as a salt dome. Our study did not include such restrictions.

We were surprised by the promise of underground adiabatic CAES in contrast to very poor performance of diabatic CAES. Despite having the lowest energy-specific capital cost (X_E) among all BES technologies we studied, gas combustion of diabatic CAES hurts its competitiveness under emissions constraints. The results points to the importance of developing storage technologies with low cost of energy capacity and low emissions and the more limited importance of roundtrip efficiency and power-specific cost of BES systems in lowering decarbonization costs.

Finally, note that that we simulated the generation fleet under an optimal GHG constraint. Non-economic choices may produce very different outcomes. A region that forgoes nuclear power or other large-scale DZC or restricts gas turbines beyond the carbon constraints simulated here will use more bulk storage.

Table 39: Qualitative comparison of the major assumptions and simplifications of the model to the real world and their likely impact on the key results. The plus (negative) signs indicate the corresponding assumption/ simplification favors (disfavors) BES in our model compared to a given counterfactual.

Assumption	**Counterfactual**	**Implications**	**Impact on BES**
Green-field analysis	A model with temporal evolution and vintaging of generation capacity in which factors costs and emissions constraints gradually approached the values used in our model (*i.e.* brown-field analysis).	The brown-field model would keep much of the existing gas assets, making BES less competitive as the capital cost of gas turbines would be 'free'.	+
Transmission costs and constraints are ignored	A model with transmission constraints which also considers costs of adding new transmission	Transmission costs driven by resource remoteness would increase the net cost of wind. This would make wind a bit less competitive with DZC and gas, slightly decreasing the need for BES. Moreover, siting of some BES systems (*e.g.* PHS) is geographically constrained. Therefore, considering transmission would hurt economics of some BES.	+
		Transmission costs can incent siting BES near generation (especially wind and solar) to allow economic optimization of the transmission capacity. Moreover, strategically siting of BES across the grid can relieve constraints and defer transmission upgrades.	-
Wind data are from ERCOT with a capacity factor of 35%	A model considering a wide range of geographical areas with different wind and load profiles	ERCOT is endowed with relatively strong wind resources. Lower capacity factors would make wind more capital-intensive and give gas and DZC an advantage over wind and BES. System-wide capacity factors significantly beyond 35% seem unlikely to us.	+ (for capacity factors below 35%)
		Correlation between wind and load may vary in different geographical regions. Repeating the simulation for other systems can enhance robustness of results.	-

Table 39 (Continued)

Solar energy is not modeled	A model allowing both wind and solar capacity	Solar farms have lower capacity factors and are currently more expensive (~>1.5 times) compared to wind farms. Therefore, we do not expect considering solar will alter our conclusions about the need for BES, unless cost of solar steeply drops below of wind in future.	nil
		Wind availability is sometimes higher overnight and in winter, in contrast to load. Changes in solar irradiance may follow changes in load better. This may improve economics of solar-based electricity and possibly increase demand for BES	-
15-minute time resolution	A model considering finer resolutions and reliability requirements of the grid (*e.g.* black start)	A high-temporal resolution model would build storage for the short duration load balancing, but this is independent from bulk storage of electricity, the focus of this paper.	nil
1-year simulation period	Taking into account inter-annual variations in wind	Renewable energies, especially wind, can experience large inter-annual variations, which increase their effective cost and reduce their optimal capacity.	+
Static modeling	A model considering future reductions in cost of all technologies (gas, wind, and DZC), not just BES	Using current cost estimates for gas turbine, DZC, and wind can favor BES providing their costs can be reduced faster than BES and vice versa.	nil
Gas price of $5/GJ	A model considering future gas prices across various region and electricity markets	According to Section 3-6, we do not expect major impacts on the key conclusions unless gas prices are above $20/GJ.	- (if price is beyond ~$20/GJ)
Forecast errors in load and wind are ignored	A model considering forecast errors (ax-ante rather than ex-post) and their improvement over time	Utilization factor of wind and BES would be lower in the real world. Our model can build the smallest amount of wind and BES to economically meet the electric load. Therefore, considering forecast errors would make wind and BES more capital intensive and less economical.	+

Chapter 6: Conclusions

The essence of this dissertation is to assess the role and significance of bulk energy storage technologies (BES), especially compressed air storage (CAES) in cutting greenhouse gas emissions from the electricity supply in service of mitigating climate change. In doing so, three primary research questions are tackled:

1. What are the thermodynamics and engineering performance of selected low-carbon CAES technologies? (Chapter 2)
2. How do the emissions and economics of a newer and cleaner CAES design (Distributed CAES, D-CAES) compare to the mainstream CAES technology as well as to gas turbines? (Chapters 3 and 4)
3. How cost effective are bulk storage technologies in general, as one of the building blocks of future low-carbon electricity systems? Specifically, what would be the economically efficient penetration level of bulk storage at various levels of electricity decarbonization? (Chapter 5)

This chapter summarizes the key findings, conclusions, and energy policy implications of previous chapters. It integrates them into a broader picture regarding the need for bulk electricity storage and its potential to address the practical challenges of deeply cutting emissions from the electricity sector. Future work is recommended to refine the results and broaden the scope of the conclusions.

1- Managing GHG emissions of CAES

Although CAES is arguably among the cheapest and most mature technologies for bulk storage of electricity, the conventional CAES technology may be too carbon intensive to play a role in the prospective carbon-constrained grids. The direct emissions of CAES (~280 $kgCO_2e$/MWh with a heat rate of 4.2 GJ/MWh), which are caused by the need for combusting natural gas to heat compressed air prior to expansion and power generation, seem insignificant (about 40-60% of gas turbines). However, large-scale use of CASE would likely be economical only in a world with a very high prenateratoin of intermitent renewables. The most plausible justificatoin for such a high intgeration of renewables is stringent carbon constraints. Nonetheless, under such tights restrictions, the resudiaul emssions of CASE sharply limit it's competetiveness with respect to other carbon-free storage systems, such as electrochemical batteries.

Poor prospect of the conventional CAES technology as a carbon mitigation tool has motivated development of low- or even zero-carbon compressed air storage concepts. A main category of such advanced designs is

based on utilizing the heat of compression (generated during the charging phase) to negate the heating fuel demand of the storage plant during the discharge process.

Chapter 2 provided a first-order estimate of the thermodynamic and emissions performance of four such cleaner CAES designs. An analytical exergy analysis of one full charge and discharge cycle was performed to quantify the key engineering metrics of these advanced CAES systems, such as roundtrip storage efficiency and exergy density. The First and Second Laws of thermodynamics and ideal gas formulae were applied to different system components to study the performance of the storage plants. Moreover, two of these four CAES designs were introduced and analyzed for the first time. A PCT (Patent Cooperation Treaty) patent application was filed based on one of the studied CAES concepts.

Export of the compression heat to supply external low-temperature heating demands (*e.g.* space heating) had the highest overall exergy efficiency (~80%) (see Section 3-3 in Chapter 2). This concept, called Distributed CAES (D-CAES), is based on relocating the compression facility from the air storage site to the heat load site. Though this system is thermodynamically superior to the conventional CAES design (with an exergy efficiency of ~50%), it will not be technically and economically viable unless a suitable heating load and air storage are in close proximity (in 100 km range, see Section 3-5 in Chapter 4).

Physical storage of the high-temperature (*e.g.* 600 °C) heat of compression to heat the expanding air during the discharge process is the core idea of the second advanced CAES system studied, adiabatic CAES (A-CAES). Although its capital cost would be higher than conventional CAES, A-CAES can reach relatively high roundtrip storage efficiencies (~70%) without any fuel combustion and GHG emissions (see Section 4-4 in Chapter 2).

Chemical storage of the compression heat in the form of hydrogen is an alternative strategy to its physical storage (as done in A-CAES). Hydrogen can be generated via electrolysis and stored at the same time as compressed air. Combustion of the stored hydrogen later heats the expanding air during the power generation phase, which eliminates the need for natural gas combustion (conventional CAES) or physical storage of the compression heat (A-CAES). The inside-the-fence line (*i.e.* direct) GHG emissions of hydrogen-based CAES technologies are negligible, comparable to A-CAES.

The third advanced CAES design studied in Chapter 2 is based on the fact that electricity demand of electrolysis decreases at higher reaction temperatures. Feeding the heat of air compression into a high-temperature electrolyzer (HTE) to reduce the electricity-intensity of hydrogen production is the essence of the CAES-HTE design. Nevertheless, providing high-temperature heat hurts the performance of the compressors (due to higher pressures and limited intercooling). The overall exergy efficiency of the CAES-HTE storage system modeled in Chapter 2 is ~50%, assuming an ideal electrolyzer. Using more realistic values for the efficiency of the electrolyzer itself (*e.g.* an efficiency of 50% instead of 100%) lowers the efficiency of CAES-HTE to about 35% (see Figure 15 in Chapter 2).

The simulation revealed that electrolysis of water at the ambient temperature, so called low-temperature electrolysis (LTE) would lead to similar values for the roundtrip storage efficiency of the CAES-LTE system compared to the CAES-HTE configuration. This is because the lower electricity demand of the electrolyzer is offset by the higher work of the compressor in the CAES-HTE design. Therefore, CAES-LTE looks more competitive than CAES-HTE considering the engineering difficulties and higher costs of electrolyzers operating at elevated temperatures.

Excluding D-CAES – which may be practical only in niche markets – A-CAES seems to provide the best trade-off between storage efficiency, GHG emissions and capital cost among the CAES technologies studied. This conclusion is in line with the recent R&D efforts (*e.g.* the pilot ADELE project in Germany [30]) to prove the concept and overcome the technical challenges of A-CAES as a potentially impactful technology for electricity decarbonization.

In many respects, the thermodynamic simulation presented in Chapter 2 paints an optimistic picture of the performance of CAES technologies. This analytical study rests on the ideal gas equation of state with the assumption of temperature-independent specific heats and ignores several inefficiencies such as heat losses in the cavern or the thermal storage. Part-load operation of the storage plant is not modeled either. Future work could build on the model developed in Chapter 2 to perform a more complicated analysis of the various CAES systems with dynamic modeling of heat transfer and thermal energy storage, particularly A-CAES and D-CAES. A thorough analysis using more sophisticated tools and software products (such as Aspen Plus) can

address some of the modeling limitations and uncertainties of the simulation in Chapter 2. Nevertheless, the systematic treatment of all the CAES technologies using the same approximations is likely to give relative performance figures of merit that are more reliable than absolute performance figures for a particular technology. Furthermore, the agreement of the results presented here with the performance of the real world CAES plants (McIntosh and ADELE) and with the literature of CAES suggests the robustness of the conclusions regarding the poor exergy performance of hydrogen-based and conventional CAES technologies compared to A-CAES and D-CAES.

2- CAES and D-CAES under emissions tax

Locating the compressor inside a municipal region (instead of at the air storage site) is the core requirement of the D-CAES system. This enables supplying the otherwise-wasted compression heat to an external space and water heating load. Heat recovery brings in fuel credits (equal to the saved heating fuel) for the D-CAES facility and reduces its effective (apparent) GHG emissions intensity. However, both the capital cost and pressure losses of the pipeline required to transport the compressed air to the storage site undermine the viability of this low-emissions air storage system.

Chapter 3 informed the question of how exporting the compression heat might strengthen the economics of air storage plants against gas turbines for managing the intermittency of wind. Since a substantial body of literature (for instance [52, 59, 60, 124]) has shown the need for some sort of carbon constraints for CAES to be economically viable compared to gas turbines, various levels of carbon tax were considered and a green-field analysis was undertaken.

The model developed in Chapter 3 optimized the capacity and hourly operations of a hypothetical generation fleet with the total cost of supplying an electric load as the objective function. The generation portfolio was made up of wind, simple and combined cycle gas turbines, and either D-CAES or conventional CAES. A variable carbon tax was blended into the base price of $5/GJ for gas. The electricity and heating load data, as well as wind profiles were from Alberta, Canada. The contribution of this analysis was quantifying the environmental and economic value of heat recovery from CAES at the systems level (*i.e.* designing an economically optimal generation portfolio) under an emissions tax regime (0-80 $/t$CO_2$e).

The length of pipeline was identified as the prominent factor for the economic competitiveness of D-CAES with conventional CAES and gas turbines. Assuming a moderate pipeline length of 50 km, neither CAES nor D-CAES entered the generation fleet until an emissions tax of \$40/tCO_2e was applied (see Figure 20 and Figure 21 in Chapter 3). This level of tax on top of the assumed market price of \$5/GJ was equivalent to an effective gas price of ~\$7.6/GJ. Past this price however, D-CAES provided a lower system-wide cost of electricity compared to conventional CAES, although the gap remained very small (~1% with \$80/tCO_2e tax and a 50 km pipeline). This phenomenon was driven by the small market share of both CAES and D-CAES as compared to wind and gas (~8% of the load supply with an emissions tax of \$80/tCO_2e). Interestingly, gas turbines remained very competitive even at high penalties for GHG emissions (~25% of electricity was supplied by gas at \$80/tCO_2e tax; refer to Section 3-2 in Chapter 3 for details.) It is of note that the electricity load profile used in Chapter 3 was based on the peaking load of Alberta (total load minus the base load). If the total load had been used instead, the share of gas turbines would likely have been even higher.

D-CAES not only reduced the overall cost of electricity supply compared to conventional CAES, but it also improved the total emissions intensity of the generation fleet (by about 10% in the best case). As the carbon tax increased and the distance between the heat load and air storage decreased, D-CAES became the more economically and environmentally attractive (see Figure 27 in Chapter 3).

The analysis in Chapter 3 indentified a range of pipeline lengths and emissions taxes under which D-CAES might support more economical integration of wind compared to conventional CAES and gas turbines. It is important, however, to underscore that D-CAES will not become a game changer for supplying low-carbon electricity due to its inherently small market size. First and foremost, its economics are closely linked to the existence of a suitable air storage facility in close proximity to a large, concentrated heating (or cooling) load. Moreover, the size of the electric load (not the heat load) that D-CAES interacts with seems to be a limiting factor. In order to maximize utilization of the recovered heat, the capacity of the D-CAES compressor should be comparable to the base heating load. The consistently small optimal capacity of the D-CAES compressor compared to the peak electric load (below 10%, see Figure 21 in Chapter 3) indicates that the heating load needs to be much smaller relative to the electricity load. Hence, the niche market of exporting low-

temperature heat of compression can saturate quickly, thus hindering deployment of the D-CAES technology at scale.

There are some additional scenarios in which D-CAES may outcompete CAES that Chapter 3 did not evaluate. While a copper-plate analysis was performed in Chapter 3, transmission constraints will limit the operations of D-CAES less compared to conventional CAES in the real world. Since the compression train of D-CAES is co-located with load, its ability to store excess and cheap electricity is more resistant to grid congestions and transmission outages. Moreover, if the expander of D-CAES is also moved to the load site, no transmission line and gas pipeline between the storage site and the load would be needed. Quantify the economic value of these advantages of D-CAES is left for future research. Finally, storing the excess recovered heat (even seasonal storage) or using it for cooling purposes (*e.g.* absorption chilling) could bring in more profits for D-CAES compared to the simple system analyzed in Chapter 3.

3- CAES and D-CAES in deregulated electricity markets

Volatility in electricity prices is essential for the economic viability of compressed air storage plants whose primary applications are energy arbitrage and load shifting. The price of natural gas is also important as it directly impacts the fuel cost of CAES and possibly shifts the spot price of electricity. Gas prices can also strongly influence the heat recovery revenues of D-CAES because natural gas is a relatively clean and accessible fuel for district heating applications. To explore the interplay between these factors, ten years of historical gas and electricity data from a specific deregulated market (Alberta) were used in Chapter 4 to compare the economics of D-CAES and conventional CAES and to possibly build a business case for D-CAES.

Chapter 4 used a profit maximization routine to study the effects of market conditions (spot prices of gas and electricity) and selected design parameters (*e.g.* size of air store) on the cost competitiveness of two hypothetical D-CAES and conventional CAES plants performing electricity arbitrage. Furthermore, a geological screening of the gas reservoirs within a 100 km radius of the major cities in Alberta was performed to investigate how realistic it might be to site a D-CAES facility in the vicinity of a large, concentrated heating load. Although a general model was synthesized in this chapter, the results were specific to Alberta, as a potential niche market for D-CAES.

The revenues of conventional CAES showed a very strong dependence on volatilities in the electricity prices while it was essentially insensitive to gas prices (correlation coefficients of 0.95 and 0.04; see Figure 31 in Chapter 4). The trend was, however, the opposite for the incremental profit of D-CAES over CAES. It was strongly influenced by gas prices (correlation coefficient of 0.91) and independent of volatilities in electricity prices. The results suggested that both high gas prices and a volatile electricity market were required for economic attractiveness of D-CAES.

D-CAES outperformed CAES over the ten-year simulation period if the heating load and air storage were sited closer than 75 km. Based on the results of the geological screening and since this siting breakeven point occurred at a relatively long distance, Chapter 4 concluded that D-CAES might have a competitive advantage over conventional CAES in Alberta. Higher profits as well as lower GHG emissions led to a negative carbon abatement cost of -\$40/tCO_2e for the D-CAES plant over the study period (with a 50 km pipeline).

Another interesting observation was the relatively small optimal capacity of the compressor compared to the expander (~20%) for both storage facilities. A larger generation compared to storage capacity maximized the sales of electricity during the infrequent price spikes. One should note that as more storage and peaking plants are added to any generation fleet, the volatility of prices will reduce, thus hurting the profitability of individual plants. Such market-specific dependencies introduce high uncertainties in generalizing and extrapolating the results to different geographical regions as well as to future grids with possible major changes (*e.g.* larger availability of interruptible loads). The goal of Chapter 4 was developing a model to assess the cost-competitiveness of D-CAES and applying the model to a specific electricity system in which D-CAES might have a market niche.

Both Chapters 3 and 4 evaluated only the electricity arbitrage and load shifting applications. Nonetheless, operational flexibility of compressed air storage plants such as high part-load efficiency and fast ramp rates may increase their competitiveness with other generation and storage technologies. Incorporating these limited and market-specific benefits into future analyses would provide a better and broader understanding of market niches for D-CAES.

A fundamental assumption in Chapter 4 is that the modeled storage plants act as merchant (stand-alone) facilities and are price takers. However, future price structures could significantly change in response to higher penetration of intermittent renewables. For instance, adding solar farms at scale could depress peak prices (peak in both supply and demand in the afternoon hours) and increase off-peak prices (no generation overnight). Taking into account the price uncertainties is extremely complicated, market-dependant, and geographic-specific. Future work remains to characterize such changes in pricing schemes and their impact on the economics of storage systems.

The screening presented in Chapter 4 highlighted the pay thickness as the most limiting factor among the four geological criteria considered. (Less than 2% of the screened natural gas pools passed this filter, see Section 2-4 in Chapter 4). Permeability, however, may be an even tighter constraint that was excluded from the analysis due to the scarcity of rigorous data in the public domain. High permeability (tens of millidarcy) is required for fast charging and discharging of the air storage plant[38]. Rapid developments in the field of horizontal drilling and hydraulic fracturing (fracking) may relax this constraint in a cost-effective manner though [125]. A thorough assessment of suitable geologic formations for air storage is integral for any comprehensive market analysis of compressed air storage. Such a study would have particular importance for both D-CAES and A-CAES. The inherent geographical requirements of D-CAES add another level of complexity to finding a proper geologic formation. A-CAES seems to provide the best combination of storage efficiency and emissions performance among CAES designs analyzed in Chapter 2. The low exergy density of A-CAES caverns, however, mandates larger storage volumes compared to conventional CAES design. This limitation can potentially undermine the viability of deploying A-CAES at scale.

4- Importance of bulk storage for electricity decarbonization

The low exergy density of compressed air-based storage technologies raises legitimate concerns about their practicality if large volumes of such plants are needed in prospective low-carbon electricity systems (*i.e.* physical shortage of suitable reservoirs for air storage). Geographical constraints for siting pumped hydro

[38] In fact, low permeability was cited as one of the key reasons for cancellation of the Iowa Stored Energy Park (ISEP) CAES project in 2011.

storage (PHS) projects and the high price tags of electrochemical batteries are also concerning if large quantities of bulk storage are needed to manage intermittency of wind and solar and deeply cut the GHG emissions from the electricity sector.

Chapter 5 attempts to address the fundamental question of how much bulk storage is economically efficient to drastically (*e.g.* 70%) decarbonize the electricity supply. A key factor here is the capital cost of storage systems themselves, which is very uncertain (see Table 30 in Chapter 5). Rather than using a point estimate for the cost of specific storage technologies, a parametric approach was taken to address cost uncertainties and technological breakthroughs. Splitting the total capital cost of bulk storage technologies into two separate components (energy-specific and power-specific costs, $/kWh and $/kW) allowed interpretation of the results over a wide range of cost estimates for storage, even significantly below the current values. This strategy can inform R&D efforts and energy policy on the relative importance (and the priority) of reducing the power-specific and energy-specific capital costs of various technologies for bulk storage application.

Storage of the excess wind and solar energies is not the only strategy to achieve a low-carbon electricity grid. Low capital cost in addition to good emissions performance make gas turbines cost-effective carbon mitigation candidates. Moreover, a suite of dispatchable-zero-carbon (DZC) generation technologies such as nuclear, geothermal, and biomass can be deployed instead of, or in conjunction with the intermittent renewables. A sound decarbonization policy needs to consider the cost competitiveness of all potential pathways, not just storage technologies in isolation.

Chapter 5 investigated the economically optimal deployment level of BES, wind, gas turbine, and DZC under stringent restrictions on GHG emissions at a systems level, over a broad range of BES costs. A green-field analysis was performed to minimize the overall cost of electricity supply based on historical wind and electricity load data from ERCOT at a 15-minute temporal resolution and over a simulation period of one year. Robustness of the results to the price of natural gas and the capital cost of wind and DZC was evaluated. Additionally, Chapter 5 provided a comprehensive survey of the literature on the cost and roundtrip efficiency of various bulk storage technologies.

In contrast to the common notion, the availability of cheap storage (*e.g.* 50% reduction compared to today's costs) had relatively small effects (<7%, see Figure 43) on the overall decarbonization costs. This key conclusion broke only when the capital cost of DZC or gas was very high (above ~$9000/kW for DZC and $20/GJ for gas, see Sections 3-5 and 3-6 in Chapter 5) or extremely stringent emissions restrictions were in place (carbon-free electricity, see Figure 40 in Chapter 5). Drastically reducing the capital cost of BES by an order of magnitude (to X_E=5 $/kWh and X_P=100 $/kW from already optimistic values of X_E=25 and X_P=1500 from the mechanical BES category) reduced the LCOE by 15%.

Despite its small influence on the cost of low-carbon electricity, the capital cost of BES (particularly its energy-specific cost) impacted the optimal penetration level of the intermittent renewable (wind) in a noticeable manner (see Figure 41 in Chapter 5). The relative importance of BES to gas turbines for wind integration was approximated by calculating the ratio of their optimal power capacities when DZC was deliberately kept out of the generation portfolio. At a sharp carbon cut of 70% compared to today's emissions levels, the role of BES turned out to be three times less important compared to gas turbines in the best case scenario (refer to Table 33 in Chapter 5 for the details). The relatively lower importance of BES for wind integration compared to gas turbines in Chapter 5, however, should not undermine the absolute need for the buildup of bulk storage systems in the future low-carbon electricity systems. As a case in point, the ratio of the existing capacity of gas turbines to storage is about 19 in the United States [122], far above the optimal ratio calculated in Chapter 5 to sharply decarbonize the electricity supply.

Long-term storage of electricity was not economically justified. The optimal energy capacity of BES sufficed to meet the average load for only one day with the current capital cost estimates and under a tight emissions cap of 150 $kgCO_2e/MWh$ for the generation fleet (~70% cut in today's emissions intensity of the grid). Reducing both the power-specific and energy-specific costs of storage to $100/kW and $5/kWh could not increase the optimal energy capacity of BES by more than a factor of two (Section 3-3 in Chapter 5).

Mechanical-based BES technologies, namely adiabatic CAES (A-CAES) and pumped hydro storage (PHS) were consistently more influential in reducing the cost of electricity supply and in supporting integration of wind compared to electrochemical storage systems (*i.e.* batteries), at their current costs. This is due to the

substantially lower energy-specific costs of the mechanical storage systems despite their higher power-specific costs. A-CAES gained the highest market share among other storage technologies studied because of its low energy-specific cost. Finally, the prospect of diabatic (conventional) CAES turned out to be very poor due to its non-negligible residual GHG emissions associated with combustion of natural gas.

It is necessary for R&D efforts and decarbonization policies not to overestimate the urgency and relative importance of reducing the cost of bulk storage systems to reduce the GHG emissions from the electricity sector. This is based on the much lower impact of reducing the capital cost of BES compared to wind and DZC, and because of the strong performance of gas turbines. One should however, note that Chapter 5 did not study the likelihood and the required R&D expenditures to cut the capital costs of various technologies.

Using real-world load and wind data from ERCOT as a relatively large electricity system with abundant wind resources and performing extensive sensitivity analyses supported the strength and generality of the conclusions in Chapter 5. The findings of this chapter were based on few key simplifications and assumptions and limited modeling capabilities. It is essential to consider the impacts of these simplification and modeling assumptions when evaluating the conclusions (see Table 39 in Chapter 5 for a comprehensive list).

A copper-plate assumption was made in Chapter 5. Taking into account the transmissions costs and constraints can both favor and disfavor BES though. On one hand, including cost of transmission lines makes intermittent renewables more capital intensive. This will work against the optimal capacity of wind and the need for bulk storage to manage its intermittency. On the other hand, strategically siting storage systems, in particular batteries, can reduce grid congestion and strengthen the economic value of storage. Therefore, modeling transmission will make the results more accurate for specific grids though it may hurt the generality of the conclusions.

Including other renewable sources, especially solar energy, in the generation portfolio would also strengthen the analysis. Solar farms have lower capacity factors (~50% lower) and higher capital costs (>50% higher [126] – although the gap is rapidly closing) compared to wind farms. The cost of electricity supply from solar is consequently, higher than wind. On the other hand, the diurnal and seasonal intermittency of solar may match the variability in load better than wind, which can shift the need for storage in both directions.

Inclusion of solar energy may lower the need for the peaking capacity (*e.g.* summer peaks) while it can also increase the need for storing electricity produced overnight by the conventional power plants. Therefore, building on the existing model to include a broader set of generation technologies, especially solar is of high importance to refine the conclusions of Chapter 5.

One of the most comprehensive assessments of renewable integration in the United States is the 2012 NREL's Renewable Electricity Futures Study [127]. This group modeled the entire US grid in 2050 at an hourly resolution to evaluate the technical possibility of supplying a substantial portion (*e.g.* 80%) of the load with renewables. The key strengths of the NREL study in the context of this thesis are taking into account transmission infrastructure, geographical distribution of renewables, reliability requirements (although limited), and a broad portfolio of technology pathways (*e.g.* biomass, clean coal, and solar). Nevertheless, the conclusions with respect to the relative insignificance of storage are consistent with those of Chapter 5. In the 80% renewable integration scenario (equivalent to ~80% reduction in GHG emissions intensity of the electricity sector) for instance, the optimal power capacity of storage to peak load was ~15%. This is while the ratio of the combined capacity of wind and solar to peak load was ~88%. Moreover, the capacity of wind was double that of solar, highlighting the relative importance of including wind in Chapter 5. Finally, the NREL report also asserted the higher cost-effectiveness of mechanical storage systems compared to batteries.

The analysis in Chapter 5 used a temporal resolution of 15 minutes because the core objective was assessing the need for *bulk* storage of electricity. Nevertheless, some bulk storage systems can provide a variety of ancillary services to the grid at finer time scales (*e.g.* frequency control). Inclusion of such market opportunities would provide a broader picture of the role of and need for the storage systems to make low-carbon grids a reality. A drastic change in the overall conclusions regarding the marginal significance of bulk storage for electricity decarbonization, however, is not expected since not all ancillary services are additive. For instance, the reliability requirements for providing spinning reserve could constrain the storage plant from performing peak shaving or load following duties.

Furthermore, variations in wind and solar-based electricity are much stronger (higher amplitude) at larger time scales (lower frequencies); diminishing the relevance of modeling finer times scales when assessing the

need for bulk storage systems. For instance, Lueken *et al.* [109] used the frequency domain (power spectrum) method to analyze the power output from wind, solar photovoltaic (PV), and solar thermal farms and concluded that the fluctuations were at least three orders of magnitude smaller at frequencies of $(10\ \text{min})^{-1}$ compared to those at $(12\ \text{h})^{-1}$. Moreover, interconnecting wind farms – even over moderate distances of few hundred kilometers – reduces their output variability across all time scales but it particularly dampens the high frequency variations [6, 128]. As a case in point, Fertig *et al.* [6] studied the effects of interconnecting wind farms over four wide geographical regions in the United States using the power spectra analysis. They found that daily fluctuations were still 3-5 orders of magnitude stronger than at the hourly time scale. In summary, as the penetration of wind and solar increases, the need for balancing variations at small time scales will decrease more per unit of generated electricity. Consequently, including time resolutions finer than 15 minutes at high penetration of intermittent renewables is not expected to cause a major departure from the fundamental conclusions - that relatively high cost and immaturity of bulk storage technologies are not the key hurdles to deeply cutting emissions from the electricity system.

Another simplification in Chapter 5 was using constant heat rates and emissions intensities for all generators, regardless of their loading. In the real world, ramping limits and part-load operation of gas turbines degrade their CO_2 and NO_x emissions compared to the nameplate levels. For example, in a 2008 study Katzenstein and Apt [129] estimated the emissions of two industrial gas turbines operated at a 1 minute resolution to compensate for fluctuations in the output of individual wind and solar PV farms in order to supply baseload power. They concluded that reductions in CO_2 emissions were ~25% lower in reality compared to the nameplate values. Using a fixed emissions intensity for gas turbines, regardless of their load level is therefore, a shortcoming of the analysis presented in Chapter 5. However, there are indications that the principle conclusions of Chapter 5 are robust to this modeling simplification. Firstly, the part-load efficiency and emissions performances of gas turbines have been improving to address these concerns (*e.g.* KA26 design by Alstom [130], Frame H series by Siemens [131], and FlexEfficiency50 design by General Electric GE [132]). It is reasonable to assume that such improvements will intensify under deep emissions cuts considered in Chapter 5. Secondly, only the time scale of 15 minutes and above is the focus of Chapter 5. A suite of strategies other than ramping gas turbines can be undertaken to address the mismatch between supply and demand at

finer time scales, including interconnecting variable renewables and using demand-side management. In fact, deploying electrochemical batteries might be a cost-effective strategy for that application, which is separate from the concentration of Chapter 5.

In summary, this dissertation has provided an engineering and economic analysis of selected compressed air storage technologies for bulk storage of electric energy to manage variability of wind. Adiabatic CAES revealed the most attractive attributes. A simple but very informative framework was also developed to attempt a broader question of how much bulk energy storage would be needed to drastically and cost effectively cut GHG emissions of electricity supply. The results indicated that gas turbines could cost efficiently support a large penetration level of intermittent renewables. Taken as a whole, the intellectual contribution of this PhD work has been to provide insights into efficient decarbonization of the electricity sector, undoubtedly among the top priorities of any comprehensive and effective policy to mitigate climate change.

Bibliography

1. Edenhofer, O., et al., *Summary for policymakers: mitigation of climate change, Contribution of working group III to the Fifth Assessment Report of the Intergovernmental Panel on Climate Change (IPCC)*. 2014, Intergovernmental Panel on Climate Change (IPCC).

2. *Sources of greenhouse gas emissions (EPA)*. 2014 [cited November 02, 2014]; Available from: http://www.epa.gov/climatechange/ghgemissions/sources/electricity.html.

3. *Overview of the Clean Power Plan - cutting carbon pollution from power plants*. 2014, United States Environmental Protection Agency (EPA): Washington, DC.

4. Philibert, C. and H. Holttinen, *Technology roadmap: wind energy - 2013 edition*. 2013, International Energy Agency (IEA): Paris, France.

5. Knoke, S., *Compressed air energy storage (CAES)*, in *Handbook of energy storage for transmission or distribution applications*, S. Eckroad, Editor. 2002, The Electric Power Research Institute (EPRI): Palo Alto, CA.

6. Fertig, E., et al., *The effect of long-distance interconnection on wind power variability.* Environmental Research Letters, 2012. 7(3): p. 034017.

7. Apt, J., *The spectrum of power from wind turbines.* Journal of Power Sources, 2007. 169(2): p. 369-374.

8. Schainker, R., *Compressed air energy storage to support wind integration*. 2008, Electric Power Research Istitute (EPRI): Palo Alto, CA.

9. Wright, S., *Reference design description and cost evaluation for compressed air energy storage systems*. 2011, Electric Power Research Institute (EPRI): Palo Alto, CA.

10. Succar, S. and R.H. Williams, *Compressed air energy storage, theory, resources, and applications for wind power*. 2008, Princeton Environmental Institute, Princeton University: Princeton, NJ.

11. Jakiel, C., S. Zunft, and A. Nowi, *Adiabatic compressed air energy storage plants for efficient peak load power supply from wind energy: the European project AA-CAES.* International Journal of Energy Technology and Policy, 2007. 5(3): p. 296-306.

12. Zhang, Y., et al., *The thermodynamic effect of air storage chamber model on advanced adiabatic compressed air energy storage system.* Renewable Energy, 2013. 57: p. 469-478.

13. *ADELE CAES pilot: site selected but project delayed.* Modern Power Systems, 2012. 32(6): p. 30, 31.

14. Ingersoll, E. 2013: Personal communication with Hossein Safaei, Cambridge, MA.

15. Raju, M. and S. Kumar Khaitan, *Modeling and simulation of compressed air storage in caverns: A case study of the Huntorf plant.* Applied Energy, 2012. 89(1): p. 474-481.

16. Kim, Y.M. and D. Favrat, *Energy and exergy analysis of a micro-compressed air energy storage and air cycle heating and cooling system.* Energy, 2009. 35(1): p. 213-220.

17. Buffa, F., et al., *Exergy and exergoeconomic model of a ground-based CAES plant for peak-load energy production.* Energies, 2013. 6(2): p. 1050-1067.

18. Grazzini, G. and A. Milazzo, *Thermodynamic analysis of CAES/TES systems for renewable energy plants.* Renewable Energy, 2008. 33(9): p. 1998-2006.

19. Wolf, D. and M. Budt, *LTA-CAES: A low-temperature approach to adiabatic compressed air energy storage.* Applied Energy, 2014. 125(0): p. 158-164.

20. Hartmann, N., et al., *Simulation and analysis of different adiabatic compressed air energy storage plant configurations.* Applied Energy, 2012. 93: p. 541-548.

21. Osterle, J.F., *The thermodynamics of compressed air exergy storage.* Journal of Energy Resources Technology, 1991. 113(1): p. 7-11.

22. Steta, F.D.S., *Modeling of an advanced adiabatic compressed air energy storage (AA-CAES) unit and an optimal model-based operation strategy for its integration into power markets*. 2010, Swiss Federal Institute of Technology (ETH): Zurich, Switzerland.

23. Xia, C., et al., *A simplified and unified analytical solution for temperature and pressure variations in compressed air energy storage caverns.* Renewable Energy, 2015. 74: p. 718-726.

24. Bagdanavicius, A. and N. Jenkins, *Exergy and exergoeconomic analysis of a Compressed Air Energy Storage combined with a district energy system.* Energy Conversion and Management, 2014. 77: p. 432-440.

25. *Cycle-Tempo thermodynamic modeling software*. 2014; Available from: http://www.asimptote.nl/software/cycle-tempo/.

26. Menon, S., *Gas pipeline hydraulics*. 2005, Boca Raton, FL: Taylor and Francis Group.

27. Elzinga, D., et al., *Energy technology perspectives 2014: harnessing electricity's potential*. 2014, International Energy Agency (IEA): Paris, France.

28. Boyce, M.P., *Principles of operation and performance estimation of centrifugal compressors.* Proceedings of the Twenty-Second Turbomachinery Symposium, 1993: p. 161-177.

29. Weber, O., *Huntorf air storage gas turbine power plant.* Brown Boveri Review, 1975. 62: p. 332-337.

30. *ADELE – Adiabatic compressed-air energy storage (CAES) for electricity supply* 2013, RWE Corp.

31. Khaitan, S.K. and M. Raju, *Dynamics of hydrogen powered CAES based gas turbine plant using sodium alanate storage system.* International Journal of Hydrogen Energy, 2012. 37(24): p. 18904-18914.

32. Chiesa, P., G. Lozza, and L. Mazzocchi, *Using hydrogen as gas turbine fuel.* Engineering for Gas Turbines and Power, 2005. 127: p. 73-80.

33. Huth, M., et al. *Operation Experiences of Siemens IGCC Gas Turbines Using Gasification Products From Coal and Refinery Residues*. in *ASME Turbo Expo 2000: Power for Land, Sea, and Air*. 2000. Munich, Germany.

34. Marean, J.B., *Compressed air energy storage: engineering and economic study, Final report*. 2009, New York State Energy Research and Development Authority: Albany, NY.

35. Christopher, K. and R. Dimitrios, *A review on exergy comparison of hydrogen production methods from renewable energy sources.* Energy & Environmental Science, 2012. 5(5): p. 6640-6651.

36. Riis, T., et al., *Hydrogen production and storage: R&D priorities and gaps*. 2006, International Energy Agency (IEA): Paris, France.

37. *Hydrogen fuel : production, transport, and storage*, ed. R.B. Gupta. 2009, Boca Raton, FL: CRC Press.

38. Yildiz, B. and M.S. Kazimi, *Efficiency of hydrogen production systems using alternative nuclear energy technologies.* International Journal of Hydrogen Energy, 2006. 31(1): p. 77-92.

39. Onuki, K., et al., *Thermochemical water-splitting cycle using iodine and sulfur.* Energy & Environmental Science, 2009. 2(5): p. 491-497.

40. Mingyi, L., et al., *Thermodynamic analysis of the efficiency of high-temperature steam electrolysis system for hydrogen production.* Journal of Power Sources, 2008. 177(2): p. 493-499.

41. Shin, Y., et al., *Evaluation of the high temperature electrolysis of steam to produce hydrogen.* International Journal of Hydrogen Energy, 2007. 32(10–11): p. 1486-1491.

42. *World nuclear power plants in operation*. 2011 [cited June 10, 2011]; Available from: http://www.nei.org/Knowledge-Center/Nuclear-Statistics/World-Statistics/World-Nuclear-Power-Plants-in-Operation.

43. *U.S. nuclear power plants*. 2011 [cited June 10, 2011]; Available from: http://www.nei.org/Knowledge-Center/Nuclear-Statistics/US-Nuclear-Power-Plants.

44. Robb, D., *Could CAES answer wind reliability concerns?*, in *Power Magazine*. 2010, McGraw-Hill Inc.: USA. p. 58-61.

45. *Statistics of wind energy in USA*. 2011 [cited June 12, 2011]; Available from: http://www.thewindpower.net/country-datasheet-4.php.

46. *Statistics of wind energy in Canada*. 2011 [cited June 12, 2011]; Available from: http://www.thewindpower.net/country-datasheet-14-canada.php.

47. MacKay, D.J., *Sustainable energy - without the hot air* Version 3.5.2. ed. Vol. Version 3.5.2. 2008, Cambridge: UIT Cambridge Ltd.

48. *The economic impact of CAES on wind in TX, OK, and NM*. 2005, Ridge Energy Storage & Grid Services L.P.

49. Peltier, R. *Top plant: Langage combined cycle power plant (Plymouth, Devon, UK)*. 2010 [cited June 14, 2011]; Available from: http://www.powermag.com/issues/cover_stories/Top-Plant-Langage-Combined-Cycle-Power-Plant-Plymouth-Devon-UK_2949.html.

50. DeCarolis, J.F., *The economics and environmental impacts of large-scale wind power in a carbon constrained world*, in *Engineering and Public Policy*. 2004, Carnegie Mellon University: Pittsburgh, PA.

51. *Compressed air energy storage state-of-science*. 2009, Electric Power Research Institute (EPRI): Palo Alto, CA.

52. Fertig, E. and J. Apt, *Economics of compressed air energy storage to integrate wind power: A case study in ERCOT.* Energy Policy, 2011: p. 2330-2342.

53. Schainker, R. and A. Rao, *Compressed air energy storage scoping for California*. 2008, Electric Power Research Institute (EPRI): Palo Alto, CA.

54. Pickard, W.F., N.J. Hansing, and A.Q. Shen, *Can large-scale advanced-adiabatic compressed air energy storage be justified economically in an age of sustainable energy?* Journal of Renewable and Sustainable Energy, 2009. 1(3): p. 033102-1-10.

55. *Compressed air energy storage power plants*. 2007, FIZ Karlsruhe, German Federal Ministry of Economics and Technology: Bonn, Germany.

56. Hugo, R.J., D.W. Keith, and H. Safaei, *Distributed compressed air energy storage system and method, Application number PCT/US12/27415, United States Patent and Trademark Office*. 2012: USA.

57. Ingersoll, E., *Wind turbine system*, United States Patent and Trademark Office, Pub. No.: US 2008/0047271 Al. 2008, General Compression Inc: USA.

58. Madlener, R. and J. Latz, *Economics of centralized and decentralized compressed air energy storage for enhanced grid integration of wind power.* Applied Energy, 2011. 101: p. 299-309.

59. DeCarolis, J.F. and D.W. Keith, *The economics of large-scale wind power in a carbon constrained world.* Energy Policy, 2006. 34: p. 395-410.

60. Greenblatt, J.B., et al., *Baseload wind energy: modeling the competition between gas turbines and compressed air energy storage for supplemental generation.* Energy Policy, 2007. 35(3): p. 1474-1492.

61. Denholm, P. and R. Sioshansi, *The value of CAES with wind in transmission-constrained electric power systems.* Energy Policy, 2009. 37: p. 3149-3158.

62. Schainker, R., *Compressed air energy storage (CAES): executive summary*. 2010, Electric Power Research Institute (EPRI): Palo Alto, CA.

63. *10 minute historical data for total wind power and Alberta internal load*. 2011 [cited February 02, 2011]; Available from: http://www.aeso.ca/.

64. Sondergard, M., *Annual plan of 2009*. 2009, NOVA Gas Transmission Ltd: Calgary, AB.

65. McCoy, S., *The economics of CO2 transport by pipeline and storage in saline aquifers and oil reservoirs*, in *Engineering & Public Policy*. 2008, Carnegie Mellon University: Pittsburgh, PA.

66. Ibrahim, H., et al., *Study and design of a hybrid wind–diesel-compressed air energy storage system for remote areas.* Applied Energy, 2010. 87(5): p. 1749-1762.

67. Succar, S., D.C. Denkenberger, and R.H. Williams, *Optimization of specific rating for wind turbine arrays coupled to compressed air energy storage.* Applied Energy, 2012. 96: p. 222-234.

68. Lozowski, D., *Chemical engineering plant cost index (CEPCI).* Chemical Engineering, 2012. 119(4).

69. Peters, M., K. Timmerhaus, and R. West, *Plant design and economics for chemical engineers*. 5th ed. 2003, New York: Mc Graw Hill.

70. *Annual energy outlook 2010 (electricity market module)*. 2010, U. S. Energy Information Administration (EIA): Washington, DC.

71. Tyler, T. 2012: Personal communication with Hossein Safaei, Calgary, AB.

72. Olsina, F., et al., *Short-term optimal wind power generation capacity in liberalized electricity markets.* Energy Policy, 2007. 35(2): p. 1257-1273.

73. Green, R. and N. Vasilakos, *Market behaviour with large amounts of intermittent generation.* Energy Policy, 2010. 38(7): p. 3211-20.

74. Zareipour, H., K. Bhattacharya, and C.A. Canizares, *Electricity market price volatility: the case of Ontario.* Energy Policy, 2007. 35(9): p. 4739-48.

75. Safaei, H., D.W. Keith, and R.J. Hugo, *Compressed air energy storage (CAES) with compressors distributed at heat loads to enable waste heat utilization.* Applied Energy, 2013. 103: p. 165-179.

76. Hydrodynamics Group, *Iowa stored energy plant compressed air energy storage project: final project report - Dallas Center Mt. Simon structure case system performance analysis*. 2011, Electricity and Air Storage Enterprises: Edmonds, WA.

77. *The atlas of Canada: heating degree days*. 2004, Natural Resources Canada (NRCan): Ottawa, ON.

78. *The atlas of Canada: crude oil and natural gas resources*. 2009, Natural Resources Canada (NRCan): Ottawa, ON.

79. *Alberta wholesale electricity market*. 2010, Market Surveillance Administrator (MSA): Calgary, AB.

80. *Long-term outlook: 2012-2032*. 2012, Alberta Electric System Operator (AESO): Calgary, AB.

81. *Energy trading system*. 2012 [cited April 15, 2012]; Available from: http://ets.aeso.ca/.

82. *Settlement natural gas prices*. 2012 [cited April 15, 2012]; Available from: http://www.ngx.com/.

83. *National climate data and information archive*. 2012 [cited April 15, 2012]; Available from: http://www.climate.weatheroffice.gc.ca/.

84. Lavoie, R. and D. Keith, *Executive summary: Wabamun area CO2 sequestration project (WASP)*. 2009: Calgary, AB.

85. *Evaluation of benefits and identification of sites for a CAES plant in New York state*. 1994, Electric Power Research Institute (EPRI): Palo Alto, CA.

86. Hydrodynamics Group, *Iowa stored energy plant compressed air energy storage project: compressed air energy storage high level reservoir screening evaluation in Iowa*. 2005, Electricity and Air Storage Enterprises: Edmonds, WA.

87. McCafferty, T.W., W.C. Walke, and J.S. Bonk, *Compressed-air energy storage: Preliminary design and site development program in an aquifer*. 1982, Electrci Power Research Institute (EPRI): Palo Alto, CA.

88. *Consumer Price Index (CPI) by province* 2012 [cited April 15, 2012]; Available from: http://www.statcan.gc.ca/.

89. Bock, B., et al., *Economic evaluation of CO2 storage and sink enhancement options*. 2003, TVA Public Power Institute: Muscle Shoals, AL.

90. Sioshansi, R., et al., *Estimating the value of electricity storage in PJM: arbitrage and some welfare effects.* Energy Economics, 2009. 31(2): p. 269-277.

91. Solomon, A.A., D. Faiman, and G. Meron, *Appropriate storage for high-penetration grid-connected photovoltaic plants.* Energy Policy, 2012. 40: p. 335-344.

92. Brandt, A.R., M. Dale, and C.J. Barnhart, *Calculating systems-scale energy efficiency and net energy returns: A bottom-up matrix-based approach.* Energy, 2013. 62: p. 235-247.

93. Pickard, W.F., *A Nation-Sized Battery?* Energy Policy, 2012. 45: p. 263-267.

94. Kintner-Meyer, M., et al., *National assessment of energy storage for grid balancing and arbitrage: phase 1, WECC*. 2012, Pacific Northwest National Laboratory: Richland, WA.

95. Barnhart, C.J. and S.M. Benson, *On the importance of reducing the energetic and material demands of electrical energy storage.* Energy & Environmental Science, 2013. 6(4): p. 1083-1092.

96. Denholm, P. and M. Hand, *Grid flexibility and storage required to achieve very high penetration of variable renewable electricity.* Energy Policy, 2011. 39(3): p. 1817-1830.

97. Hittinger, E., J.F. Whitacre, and J. Apt, *What properties of grid energy storage are most valuable?* Journal of Power Sources, 2012. 206: p. 436-449.

98. Sundararagavan, S. and E. Baker, *Evaluating energy storage technologies for wind power integration.* Solar Energy, 2012. 86(9): p. 2707-2717.

99. Schainker, R., *Lessons learned from over 50 energy storage cost-benefit studies performed for electric utilities by EPRI*, in *2nd Annual Electric Energy Storage Conference*. 2012: Phoenix, AZ.

100. Schoenung, S., *Energy storage systems cost update: a study for the DOE energy storage systems program*. 2011, Sandia National Laboratories: Livermore, CA.

101. Connolly, D., *A review of energy storage technologies for the integration of fluctuating renewable energy*. 2010, University of Limerick: Limerick, Ireland.

102. Lueken, R. and J. Apt, *The effects of bulk electricity storage on the PJM market.* Energy Systems, 2014: p. 1-28.

103. Lott, M.C. and S.-I. Kim, *Technology roadmap: energy storage*. 2014, International Energy Agency (IEA): Paris, France.

104. Rastler, D., *Electricity energy storage technology options: a white paper primer on applications, costs, and benefits*. 2010, Electric Power Research Institute (EPRI): Palo Alto, CA.

105. Dunn, B., H. Kamath, and J.-M. Tarascon, *Electrical energy storage for the grid: a battery of choices.* Science, 2011. 334(6058): p. 928-935.

106. Mahlia, T.M.I., et al., *A review of available methods and development on energy storage; technology update.* Renewable and Sustainable Energy Reviews, 2014. 33: p. 532-545.

107. Chen, H., et al., *Progress in electrical energy storage system: A critical review.* Progress in Natural Science, 2009. 19(3): p. 291-312.

108. Rastler, D., et al., *Energy storage system costs, 2011 update, executive summary*. 2012, Electric Power Research Institute (EPRI): Palo Alto, CA.

109. Lueken, C., G.E. Cohen, and J. Apt, *Costs of solar and wind power variability for reducing CO2 emissions.* Environmental Science & Technology, 2012. 46(17): p. 9761-9767.

110. *CO_2 emissions from fuel combustion*. 2013, International Energy Agency (IEA): Paris, France.

111. Wiser, R. and M. Bolinger, *2012 Wind technologies market report*. 2013, U.S. Department of Energy: Oak Ridge, TN.

112. *Assumptions to the annual anergy outlook: Electricity market module*. 2013, U.S. Energy Information Administration (EIA): Washington, DC.

113.Tegen, S., et al., *2011 Cost of wind energy review*. 2013, National Renewable Energy Laboratory: Golden, CO.

114. *Lazard's Levelized Cost of Energy Analysis v7.0*. 2013, Lazard Global Power, Energy & Infrastructure.

115. O'Donoughue, P.R., et al., *Life Cycle Greenhouse Gas Emissions of Electricity Generated from Conventionally Produced Natural Gas.* Journal of Industrial Ecology, 2014. 18(1): p. 125-144.

116. Crooks, E., *Southern Company's Georgia reactors are most watched in US sector*, in *Financial Times*. 2014.

117. England, A., P. Hollinger, and S.J.-a.i. Seoul, *South Korea wins $20bn UAE nuclear power deal*, in *Financial Times*. 2009.

118. Abdulla, A., I.L. Azevedo, and M.G. Morgan, *Expert assessments of the cost of light water small modular reactors.* Proceedings of the National Academy of Sciences, 2013. 110(24): p. 9686-9691.

119. Prior, B., *Concentrating solar power 2011: technology. cost and markets*. 2011, GMT Research.

120. *Concentrating solar power projects*. 2014 [cited June 24, 2014]; Available from: www.nrel.gov/csp/solarpaces.

121. *Natural gas prices across US*. 2014 [cited June 10, 2014]; Available from: www.eia.gov/dnav/ng/ng_pri_sum_dcu_nus_m.htm.

122. *Electric power monthly: August 2014*. 2014, U.S. Energy Information Administration (EIA): Washington DC.

123. *Decision adopting energy storage procurement framework and design program*. 2013, California Public Utilities Commission (CPUC).

124. Mauch, B., P.M.S. Carvalho, and J. Apt, *Can a wind farm with CAES survive in the day-ahead market?* Energy Policy, 2012. 48(0): p. 584-593.

125. Schulte, R.H. and I. Gyuk, *Lessons from Iowa (LFI) and DOE Responses to February 9, 2012 Webinar Questions*. 2012, Iowa Stored Energy Plant Agency.

126. *Assumptions to the annual anergy outlook: Electricity market module*. 2014, U. S. Energy Information Administration (EIA): Washington, DC.

127. Hand, M.M., et al., *Renewable electricity futures study*. 2012, National Renewable Energy Laboratory (NREL): Golden, CO.

128. Katzenstein, W., E. Fertig, and J. Apt, *The variability of interconnected wind plants.* Energy Policy, 2010. 38(8): p. 4400-4410.

129. Katzenstein, W. and J. Apt, *Air emissions due to wind and solar power.* Environmental Science & Technology, 2009. 43(2): p. 253-258.

130. Peltier, R., *Langage combined cycle power plant, Plymouth, Devon, UK.* Power, 2010. 154(9): p. 28-29.

131. *The SGT5-8000H: proven in commercial operation*. 2011 [cited December 8, 2014]; Siemens AG]. Available from: http://www.energy.siemens.com/us/pool/hq/power-generation/gas-turbines/SGT5-8000H/downloads/SGT5-8000H_brochure.pdf.

132. *FlexEfficiency50: Combined cycle power plant*. 2011 [cited December 8, 2014]; General Electric (GE)]. Available from: http://www.ge-energy.com/content/multimedia/_files/downloads/FlexEfficiency%2050%20Plant%20eBrochure.pdf.